Modeling Potential Liquefaction during an Earthquake under a Breakwater with PM4Sand

MSc-Thesis

by

E.G. van Lent

to obtain the degree of Master of Science
at the Delft University of Technology,
to be defended publicly on Tuesday July 28th, 2020 at 13:00h.

Student number: 4735064

Thesis committee:

Dr. P. J. Vardon,	TU Delft, Geoscience and Engineering, (Chair)
Dr. ir. R. B. J. Brinkgreve,	TU Delft, Geoscience and Engineering
Prof. Dr. M. A. Hicks,	TU Delft, Geoscience and Engineering
Dr. ir. R. C. Lanzafame,	TU Delft, Hydraulic structures and Flood Risk
ir. P. Lubking,	Van Oord, Geotechnical Engineer
ir. F. van Herpen,	Van Oord, Geotechnical Engineer

An electronic version of this thesis is available at http://repository.tudelft.nl/.

TU Delft

Preface

Before you lies the final version of my MSc thesis to obtain my degree of Master of Science for the master programme Civil engineering, track Geo-engineering, at the Delft University of Technology. The research was conducted at both Van Oord and the Delft University of technology. It has been a long ride with ups and down which provided me with a lot of knowledge.

I would like to thank my thesis committee Phil Vardon, Ronald Brinkgreve, Michael Hicks, Robert Lanzafame, Peter Lubking and Frans van Herpen for all there support and feedback. A special thanks to Ronald Brinkgreve, without your help I would not have been able to find as many alternatives and possible solutions for the numerical model made.

I would like to thank everybody who supported me through my studies. Friends and colleagues from my time in Enschede and Delft. As well as my housemates over the last couple of years. I would also like to thank Paul Verheul for helping me get in contact with Van Oord.

Finally, a very big thank you to my parents, Oscar and Hanna van Lent. Thank you for not only for giving up a few days of your vacation to read my thesis, but for all your support throughout the years. I am blessed to have parents like you and could not have done it without you!

E.G. van Lent
Rotterdam, July, 2020

Abstract

The stability of breakwaters in seismically active areas is not always guaranteed. A new approach to model a breakwater subjected to an earthquake is with PM4Sand. The goal of this research is to find if breakwaters subjected to earthquakes can be correctly modelled with PM4Sand.

To investigate PM4Sand a breakwater subjected to an earthquake on centrifuge scale is modelled in Plaxis. The soils of the centrifuge test are modelled with PM4Sand and UBCSand. After calibrating the soil parameters and incorporating the proper earthquake signal results are generated and compared. The investigated results focus on the settlements of the caisson, deformations of the breakwater and generated Excess Pore Water Pressures underneath the breakwater due to the earthquake. Comparing the results from the numerical models with the centrifuge test result show that both the UBCSand model and PM4Sand can give comparable results for the settlements and deformations. However, both UBCSand and PM4Sand were not able to give the correct EPWP development underneath the breakwater.

Due to the incorrect behaviour of the EPWP underneath the breakwater resulting from the numerical models, this research is not able to conclude that PM4Sand can be used for modelling breakwaters subjected to earthquakes. Further research is needed to investigate the development of EPWP underneath the breakwater during an earthquake. Focus points of future research can be: the influence of the amplitude of an earthquake signal on the EPWP, the influence of modelling a centrifuge test on the behaviour of the EPWP and the influence of the initial static shear stress on the EPWP development.

Contents

List of Figures

List of Tables

List of Abbreviations

Term	Definition
CDSS	Cyclic Direct Simple Shear
CRR	Cyclic Resistance Ratio
CSR	Cyclic Shear Ratio
DSS	Direct Simple Shear
EPWP	Excess Pore Water Pressure
PM4Sand	Plasticity model for sand
UBC3D-PLM	Name of the version of UBCSand that is implemented in Plaxis

List of Symbols

Symbol	Unit	Definition
α	-	Static shear stress ratio
c	kPa	Cohesion
c_d	-	Constant with value 46
D_r	-	Relative density
e_{max}	-	Maximum void ratio
e_{min}	-	Minimum void ratio
fac_{hard}	-	Densification Factor
G	GPa	Shear modulus
G_0	-	Shear Modulus coefficient
h_{p0}	-	Contraction rate parameter
K_G^e	-	Elastic Shear Modulus number
K_G^p	-	Elastic Plastic Modulus number
K_B^e	-	Elastic Bulk Modulus number
K_0	-	Coefficient of lateral earth pressure
K	-	Correction factor for the effects of an initial static shear stress ratio
K_σ	-	Overburden correction factor
K	GPa	Bulk modulus
$N1_{60}$	-	SPT values
n^b	-	Bounding surface parameter
N_c	-	Number of cycles
N^d	-	Dilatancy surface parameter
ne	-	Elastic Shear Modulus Index
np	-	Plastic Shear Modulus Index
me	-	Elastic Bulk Modulus Index
ϕ'_{cv}	(°)	Constant volume friction angle
ϕ'_p	(°)	Peak friction angle
Q	-	Critical state line parameter
$q_{cyc}/2$	kPa	Maximum cyclic shear stress
R	-	Critical state line parameter
R_f	-	Failure Ratio
σ'_{3c}	kPa	Isotropic consolidation stress
σ_{vc}	kPa	Effective confining stress
τ_{cyc}	kPa	Uniform cyclic shear stress
v	-	Poisson ratio

1

Introduction

Breakwaters are structures that protect shore areas, harbours, anchorages or basins from wave disturbance. Breakwaters are barriers that are constructed off the coasts to protect against the force of waves, the effects of weather and longshore drift. Breakwaters can also lead to unintended consequences. Due to the dissipation of energy and relative calm water created by breakwaters the deposition of sediments is often occuring. To design a breakwater adequate information is needed. For example, bathymetry, material volume, wave and tidal regime and meteorological information are all key elements when designing a breakwater. There are several types of breakwaters. The most common breakwaters are:

- Rubble mound breakwaters: These breakwaters are constructed as piles of stones, with the smaller stones at the core of the mound and larger stones as an armour layer to protect the core from incoming waves.
- Caisson type breakwaters: The caisson breakwaters usually have vertical sides that reflects the incoming waves. The caisson can be filled with material to resist the overturning forces created by the hitting waves. Sometimes an additional rubble mound is placed in front of the caisson to absorb som of the wave energy.

These types of breakwaters can be designed in various ways while keeping the basics the same. Some examples are shown in figure 1.1. This research will focus on the caisson type on a rock foundation.

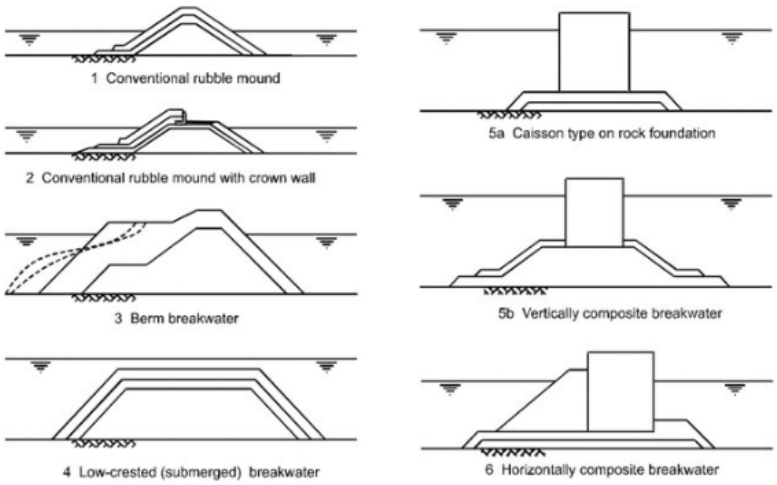

Figure 1.1: Various designs of rubble mound and caisson type breakwaters

When building breakwaters in seismically active areas, the breakwater has to be designed so no liquefaction will occur. Liquefaction is a phenomenon that can occur due to monotonic or cyclic loading. Where monotonic loading means a sudden occurrence of a stress change and cyclic loading is a repeated change in the stress conditions, like an earthquake. Liquefaction mostly occurs in loose to moderate saturated sands with poor drainage possibilities. In case of an earthquake, the pore pressure in the ground increases in such a way that excess pore water pressure is developed. This EPWP pushes the grains from each other and makes them lose contact. When critical excess pore pressure is developed, not enough grains are touching each other and the friction between the grains are lost. Now the ground loses all its strength and liquefaction occurs. This results in sinking structures or large soil deformations. Figure 1.2 shows what happens to the soil particles and structure on top during liquefaction. Looking at the state of the soil before the earthquake figure 1.2 shows the sand particles touch each other which provides the strength of the soil. When the packed structure of the soil breaks down, the separate particles will try to move together into a denser configuration. Figure 1.2 shows that during an earthquake the sand particles become separated from each other, therefore they will try to move together. In case of liquefaction the water cannot be squeezed out of the pores fast enough, which prevents the sand particles to move closer together and liquefaction occurs. This results in a deformed soil after the earthquake as shown in figure 1.2. One of the most well known examples of liquefaction occurred in Niigata, Japan, during a earthquake in 1964. Figure 1.3 shows the result of liquefaction and consequently loss of the foundation his bearing on some apartment buildings during this earthquake.

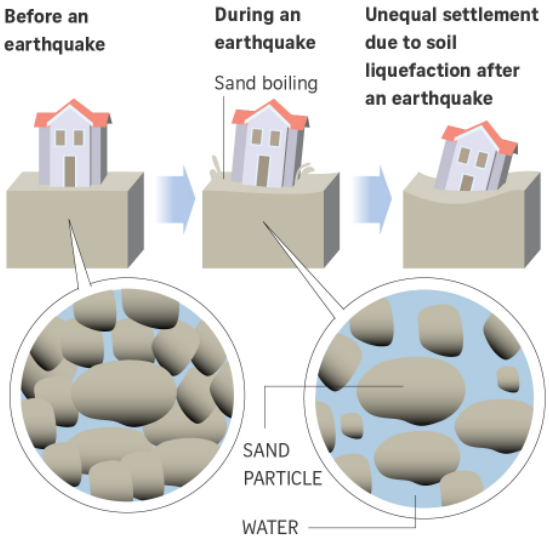

Figure 1.2: The process of liquefaction, where first sand is paced together and after the build up of excess pore pressure the ground loses it strength and the structure sinks

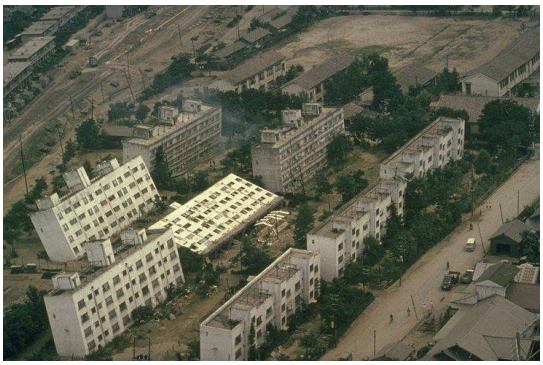

Figure 1.3: Tilting of apartment buildings caused by the Niigata earthquake in 1964

1.1. Problem Definition

An important aspect of breakwaters is stability. There are different ways to check the stability of a breakwater. It can be done analytically, where the stability is checked with, for example, Limit Equilibrium Method (LEM) and simplified seismic displacement analysis. A more advanced way to determine the stability is using numerical models such as the Finite Element Method (FEM). To use FEM, good constitutive models are needed. The most basic standard elasto-plastic soil model is the Mohr-Coulomb model, while the Hardening Soil model is an example of a more advanced model. Some breakwaters will be built on sandy soils in seismically active areas and therefore they need to be designed to withstand the generated forces from the seismic activity. To analyse the effects of dynamic loading, which happens during earthquakes and subsequent liquefaction the UBCSand model is often used. A more recent and advanced model for dynamic calculations is PM4Sand. This performance of PM4Sand are evaluated in this report for the stability and deformations of breakwaters under seismic conditions.

1.2. Goal

The goal of this research is to determine if the effects up to liquefaction in a sandy soil due to an earthquake can be correctly modelled with PM4Sand in Plaxis. The results of PM4Sand are compared with results from the UBCSand model and a centrifuge test.

1.3. Hypothesis

PM4Sand is a good model to use for determining the settlement and excess pore water pressure occurring underneath breakwaters during an earthquake up to liquefaction in sandy soil.

1.4. Research Question

The research question of this report is: *'How does PM4Sand compare to the UBCSand model when used to calculate the stability of a breakwater on a sandy soil in Plaxis that can withstand an earthquake which can induce liquefaction?'*

1.4.1. Sub-Questions

To answer the research question in a structured way, sub-questions have been formulated. The sub-questions are as follows:

1. *What are the strengths and limitations of the UBCSand model and PM4Sand?*
   This question will give an overview of the UBCSand model and PM4Sand. The answer to this question needs to show what the strengths and limitations of both models are and what assumptions are made in these models. Also, the influences of the model parameters will be investigated. Finally, the similarities and differences between the UBCSand model and PM4Sand will be discussed.

2. *How does liquefaction occur in scaled laboratory tests?*
   The goal of this question is to find actual physical data that can be used to verify results given by the model while using PM4Sand in Plaxis.

3. *How does a breakwater react during an earthquake if modelled by the UBCSand model or PM4Sand?*
   For this question a found scaled laboratory test will be modelled in Plaxis with the UBCSand model and PM4Sand. The results generated by the models after an earthquake will be compared with the results from the scaled laboratory test.

4. *How do the results of the UBCSand and PM4Sand model compare?*
   In this question, the results of the models will be compared and differences highlighted.

1.5. Scope

The research will be focused on the settlements, deformations and excess pore water pressure in the breakwater, due to an earthquake that potentially results in a liquefying sand layer under the breakwater.

2

Theoretical Framework

In the Theoretical Framework, the theory and background needed for the rest of the report will be discussed. Firstly liquefaction will be explained. How liquefaction is assessed and what factors are taken into account. Thereafter, the UBCSand model and PM4Sand will be explained. The effects of parameters on the models behaviour will be summarised and what the sensitivity of model outcome to these parameters is. This will answer the first research sub-question: 'What are the strength and limitations of the UBCSand model and PM4Sand'. With this information the similarities and differences between the UBCSand model and PM4Sand will be discussed.

2.1. Definition of Liquefaction during Earthquakes

One of the most damaging causes during an earthquake is liquefaction. During an earthquake, loose sand tends to contract under cyclic loading due to the earthquakes shaking. This increases the Excess Pore Water Pressure (EPWP) if the soil is saturated and unable to dissipate the pore water pressure before another cycle in the earthquake shaking occurs. This leads to a reduction of the effective confining stress within the soil and associated loss of strength and stiffness that contributes to deformation of the soil deposit. This phenomenon is called liquefaction (Idriss & Boulanger, 2008). The way liquefaction previously is described can also be called cyclic (softening) mobility. Another form of liquefaction is called flow (static) liquefaction. Flow liquefaction occurs when the static shear strength is greater than the shear strength of the soil in its liquefied state. This produces flow failures that result in sudden large deformations which can travel over large distances. The term initial liquefaction is also used when discussing liquefaction. This references to the situation where the excess pore pressure ratio, r_u = 1.0 or similarily 100%. After r_u reaches 1.0 the strain deformation of a sample increases significantly (Idriss & Boulanger, 2008).To calculate the r_u from a CDSS test the following equation can be used:

$$r_u = \frac{\Delta u}{\sigma'_{vc}} \tag{2.1}$$

2.2. Influences on the Strength of Sand during Liquefaction

Whether liquefaction in a sand will be triggered depends on several factors, including the number of loading cycles, relative density, confining stress, depositional method, fabric, prior stress-strain history, age, cementation and other environmental factors (Idriss & Boulanger, 2008). The main factors that trigger liquefaction in a sand are the equivalent uniform cyclic shear stress ratio (CSR) and the number of loading cycles. The CSR is the uniform cyclic shear stress (τ_{cyc}) divided by the initial effective confining stress (σ_{vc}) as shown in the following formula:

$$CSR = \frac{\tau_{cyc}}{\sigma'_{vc}} \tag{2.2}$$

It should be noted that this formula is defined for shaking table tests or simple shear tests. The CSR for isotropically consolidated cyclic triaxial tests is defined as:

$$CSR = \frac{q_{cyc}}{2\sigma'_{3c}} \tag{2.3}$$

Where $q_{cyc}/2$ is the maximum cyclic shear stress and σ'_{3c} as the isotropic consolidation stress.

The CSR that is required to reach liquefaction in a specified number of loading cycles is called the cyclic resistance ratio (CRR) (Idriss & Boulanger, 2008). The CRR can be used to compare the cyclic resistance of different sands. A higher relative density results in a higher CRR. The CRR is also dependent on the overburden pressure. Previous research has found that the CRR for a sand with a given density decreases with increasing confining pressure (Somasundaram, 2004). To compensate for this phenomenon H. Seed defined the following correction factor (Seed, 1983):

$$K_\sigma = \frac{CRR_{\sigma'_c}}{CRR_{\sigma'_c=1}} \tag{2.4}$$

where $CRR_{\sigma'_c}$ is the CRR of a soil under a specific value of effective consolidation stress σ'_c, and $CRR_{\sigma'_c=1}$ is the CRR of the same soil when $\sigma'_c = 1atm$ (Idriss & Boulanger, 2008).

Secondly, the CRR is influenced by the initial static shear stress. The initial static shear stress increases or decreases the cyclic resistance depending on the initial relative density. For loose contractive sands, a reduction in cyclic resistance occurs, while dense dilative sands experience an increase in cyclic resistance (Toloza, 2018). If the deformation type is of the 'cyclic mobility' type, the cyclic resistance to liquefaction would increase, while deformations of the 'flow failure' type would result in the cyclic resistance to liquefaction to decrease (Somasundaram, 2004). For the static shear stress effect there is also a empirical correction factor proposed, that is as follows:

$$K_\alpha = \frac{CRR_\alpha}{CRR_{\alpha=0}} \tag{2.5}$$

where α is the ratio of static shear stress to effective consolidation stress, CRR_α is the CRR with sustained static shear stress and $CRR_{\alpha=0}$ is the CRR when $\alpha = 0$ (Idriss & Boulanger, 2008).

Finally, the liquefaction resistance is affected by the state of consolidation stress. A normally consolidated sand specimen that is one-dimensionally consolidated in a cyclic direct shear test will have a coefficient of lateral earth pressure, K_0, that is around 0.5, while a sand specimen in an ICU cyclic triaxial test has a K_0 equal to 1 (Idriss & Boulanger, 2008). Ishihara has done rotational shear tests with different K_0 values that showed that the CRR for anisotropically consolidated specimens ($K_0 \neq 1$) can be approximately related to the CRR for isotropically consolidated specimens ($K_0 = 1$) with the following formula (Ishihara, Yamazaki, & Haga, 1985):

$$CRR_{K_0 \neq 1} = \left(\frac{1 + 2K_0}{3}\right) CRR_{K_0=1} \tag{2.6}$$

This formula can also be written to apply for the cyclic DSS test and cyclic Triaxial tests as follows:

$$CRR_{DSS} = \left(\frac{1 + 2K_0}{3}\right) CRR_{TX} \tag{2.7}$$

2.3. Modelling Liquefaction with UBCSand

In this section, the basics of the UBCSand model will be explained. Since Plaxis is used during the modelling of the breakwater, the explanation will focus on UBC3D-PLM, which is the version of UBC-Sand that is implemented in Plaxis. The UBCSand model is a model with similarities to the Hardening Soil model but uses a different flow rule to allow static liquefaction. Other characteristics of the model are: it accumulates plastic strains upon cyclic loading and it accumulates pore pressure in undrained cyclic loading which may eventually lead to liquefaction (Brinkgreve, 2019).

The elastic behaviour of the model is described by Hooke's law of elasticity, with bulk modulus K and shear modulus G being stress-dependent. The plastic behaviour is defined by the Mohr-Coulomb failure criterion, UBCSand has shear hardening and a non-associated flow rule. Figure 2.1 shows the UBCSand hardening rule. The hardening rule governs the amount of plastic strain as a result of the mobilisation of the shear strength. In figure 2.1 the increment of the sine of the mobilised friction angle to the plastic shear strain increment is shown "PLAXIS Material Models" (2015).

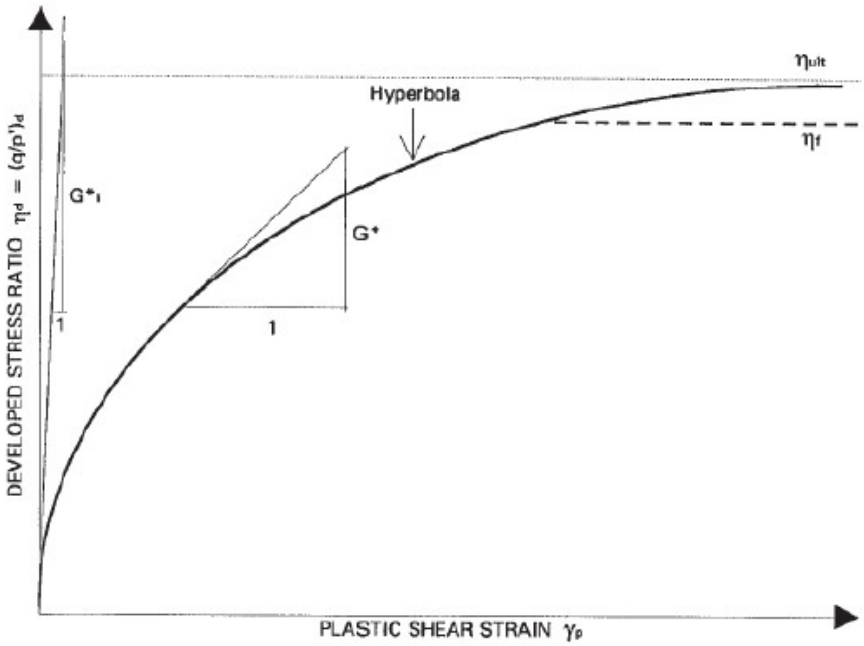

Figure 2.1: Graph showing the UBCSand hardening rule from "PLAXIS Material Models" (2015)

The UBCSand model has the critical state friction angle as a direct input parameter. With this parameter, the transition between contractive and dilative behaviour is given which can be seen in figure 2.2

During cyclic loading, UBCSand starts with elasto-plastic behaviour during the first loading. During unloading, the model will show elastic behaviour until the shear stress is zero. Thereafter the behaviour will be elastoplastic. With continuous cyclic loading, this behaviour is repeated and the amount of plastic volumetric strain may accumulate for every cycle. The hardening yield of the UBCSand model consists of two yield contours. The primary yield contour does not demobilise the mobilised friction angle and the secondary yield contour is based on the mobilised friction angle and therefore can demobilise. The reaction of the yield contours in the p'-q space are shown in figure 2.3.

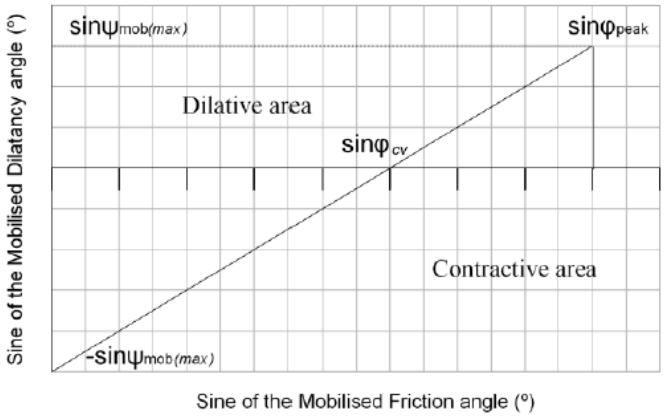

Figure 2.2: Graphical representation of the used flow rule in UBC3D-PLM from “PLAXIS Material Models” (2015)

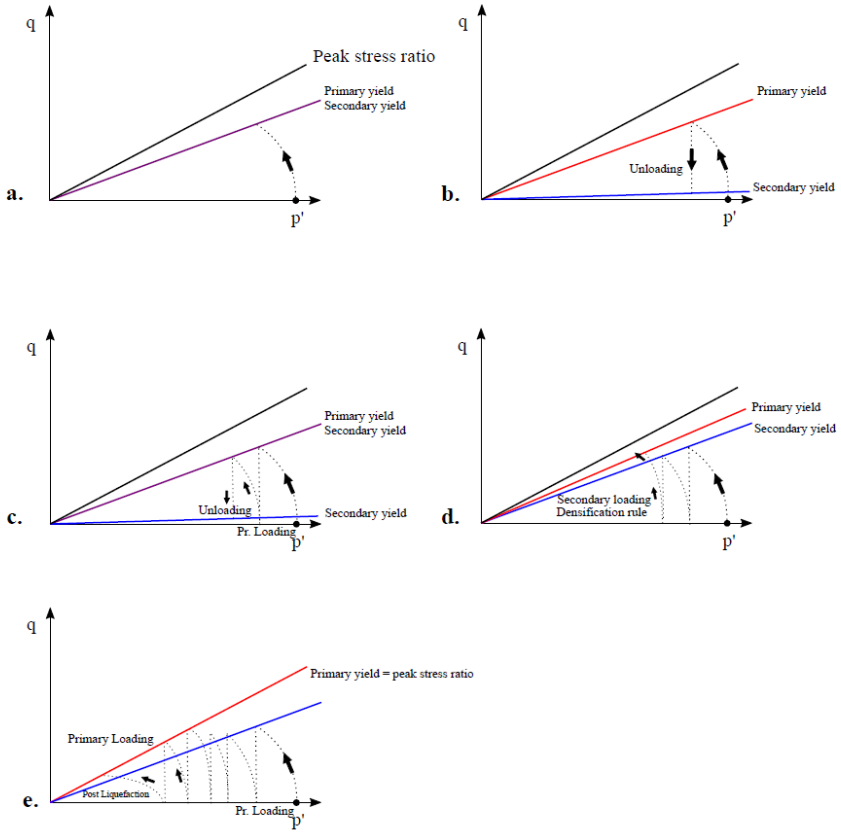

Figure 2.3: The yield contours of UBCSand shown in the p’-q space. From “PLAXIS Material Models” (2015)

2.3.1. UBCSand Parameters

The Plaxis model used for the model with UBCSand is called UBC3D-PLM. The Plaxis report on the UBC3D-PLM model assigns some default values to certain parameters and others have to be determined beforehand. The initial parameters for the UBC3D-PLM are shown in table 2.1. For the remainder of this report, UBC3D-PLM will be referred to as UBCSand. Table 2.1 shows that the following parameters need to be determined:

- Constant volume friction angle, ϕ_{cv}
- Peak friction angle, ϕ_p
- Elastic Shear Modulus number, K_G^e
- Elastic Plastic modulus number, K_G^p
- Elastic Bulk modulus number, K_B^e

Table 2.1: Parameters used in UBCSand from Galavi and Petalas (2013)

Name	Symbol	Unit	Method	Default
Constant volume friction angle	ϕ_{cv}	(°)	CD TxC or DSS	-
Peak friction angle	ϕ_p	(°)	CD TxC or DSS	-
Cohesion	c	kPa	CD TxC or DSS	0
Elastic Shear Modulus	K_G^e	-	Curve Fit	-
Elastic Plastic Modulus	K_G^p	-	Curve Fit	-
Elastic Bulk Modulus	K_B^e	-	Curve Fit	-
Elastic Shear Modulus Index	ne	-	Curve Fit	0.5
Elastic Bulk Modulus Index	me	-	Curve Fit	0.5
Plastic Shear Modulus Index	np	-	Curve Fit	0.5
Failure Ratio	R_f	-	Curve Fit	0.9
Atmospheric Pressure	P_A	kPa	Standard Value	100
Tension Cut-off	σ_t	kPa	-	0
Densification Factor	fac_{hard}	-	Curve Fitting	1
SPT value	$N1_{60}$	-	In-Situ Testing	-
Post Liquefaction Factor	fac_{post}	-	Curve Fitting	0.2-1

As can be seen in table 2.1 the peak and constant volume friction angle need to be determined with a drained triaxial test (CD TxC) or a direct simple shear test (DSS). This can be done by using q-p'graph and determining the ratio $\frac{q}{p'}$ at the critical state or peak in triaxial compression. Using the following formula's it is possible to calculate the ϕ_{cv} or ϕ_p (Idriss & Boulanger, 2008):

$$M_c = (\frac{q}{p'})_{cv} = \frac{6sin(\phi'_{cv})}{3 - sin(\phi'_{cv})} \tag{2.8}$$

Which can be rewritten as:

$$sin(\phi'_{cv}) = \frac{3M_c}{6 + M_c} \tag{2.9}$$

The other parameters need to be determined by curve fitting. Making sure with the help of the Plaxis soil testing tool, SoilTest, that the modelled soil shows similar behaviour in this soil testing tool as during the real tests.

It is also possible to determine the UBCSand parameters with the corrected clean sand equivalent SPT blow-count measurements ($(N_1)_{60}$) (Makra, 2013). The following formula can be used to calculate the peak friction angle and the three different elastic modulus numbers:

For $(N_1)_{60} > 15$:

$$\phi_p = \phi_{cv} + (N_1)_{60}/10.0 + max(0.0, \frac{(N_1)_{60} - 15}{5}) \tag{2.10}$$

For $(N_1)_{60} < 15$:

$$\phi_p = \phi_{cv} + (N_1)_{60}/10.0 \tag{2.11}$$

$$K_G^e = 21.7 \cdot 20.0 \cdot {(N_1)_{60}}^{0.333} \tag{2.12}$$

$$K_B^e = K_G^e \cdot 0.7 \tag{2.13}$$

$$K_G^p = K_G^e \cdot {(N_1)_{60}}^2 \cdot 0.003 + 100.0 \tag{2.14}$$

With the determined peak and constant volume friction angle the $(N_1)_{60}$ can be calculated and with this value the elastic modulus values. When all parameters are determined and the default parameters are put in the model it is possible to calibrate the model. As mentioned before, this can be done by making sure the modelled sand in Plaxis behaves similar to the sand during the experiment. This can be done with the Plaxis SoilTest.

In the following section the parameters that affect liquefaction will be investigated. The most important parameters are (Makra, 2013):

- The relative density D_r and vertical stress σ_{v0}
- The lateral earth pressure coefficient K_0
- Damping ratios
- The static shear stress ratio $\alpha = \frac{\tau_{stat}}{\sigma_{v0}}$

2.3.2. Effect of the Relative Density and Vertical Stress

When looking at the relative density it is clear that an increase in relative density results in an increase of the cyclic resistance ratio (CRR) as can be seen in figure 2.4. Generally it can be seen that the CRR

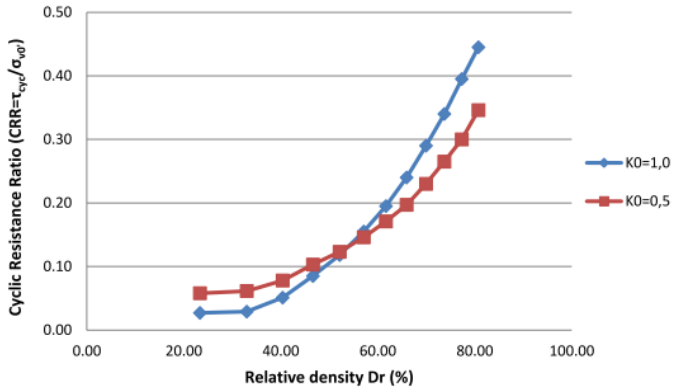

Figure 2.4: Cyclic resistance ratio versus relative density for K_0 = 1 and 0.5 from UBC3D-PLM, graph from Makra (2013)

decreases when the initial vertical stress increases (Makra, 2013). To make an assessment of the liquefaction resistance at different overburden stresses the correction factor K_σ as described in formula 2.4 can be used.

Figure 2.5 shows that an increase in vertical stress results in a lower overburden stress correction factor K_σ and therefore a lower CRR.This figure also shows that the UBCSand model from Plaxis underestimates the strength of the soil at higher overburden pressures. This can be solved by using a suitable densification factor in the model.

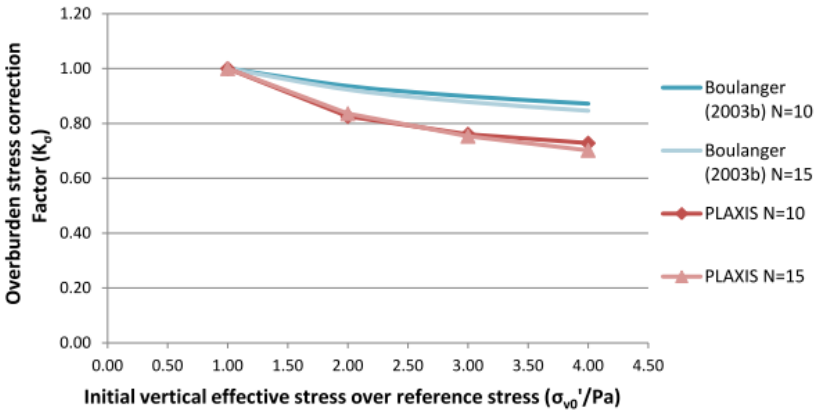

Figure 2.5: Overburden stress correction factor at different stress levels from UBC3D-PLM compared with theoretical values. Graph from Makra (2013)

2.3.3. The Effect of the Lateral Earth Pressure Coefficient

From figure 2.4 it can be seen that the CRR decreases when the K_0 decreases for higher relative densities. This is reasonable since, with the same relative density, overburden stress and an increase in horizontal stress, it becomes more difficult for a soil to liquefy (Makra, 2013). Figure 2.6 shows that the Plaxis model overestimates the cyclic resistance ratio for the corrected clean sand blow count.

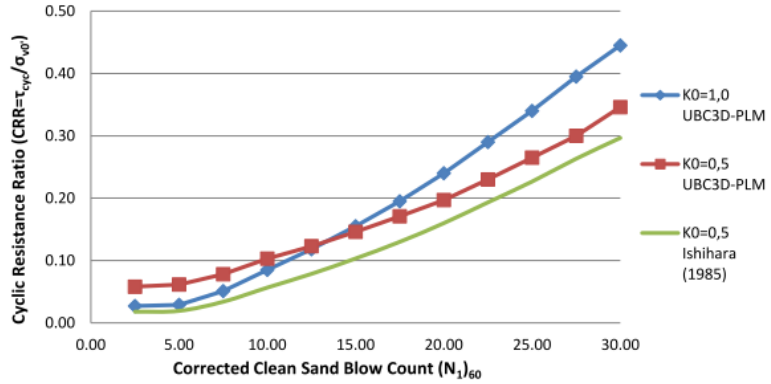

Figure 2.6: Predicted cyclic resistance ratio for $K_0 = 0.5$. Graph from Makra (2013)

2.3.4. The Effect of Damping Ratios

Figure 2.7 shows that UBC3D-PLM overpredicts the damping ratios for different shear strains by quite a bit. This behaviour is expected since in UBCSand unloading is modelled as elastic (Makra, 2013).

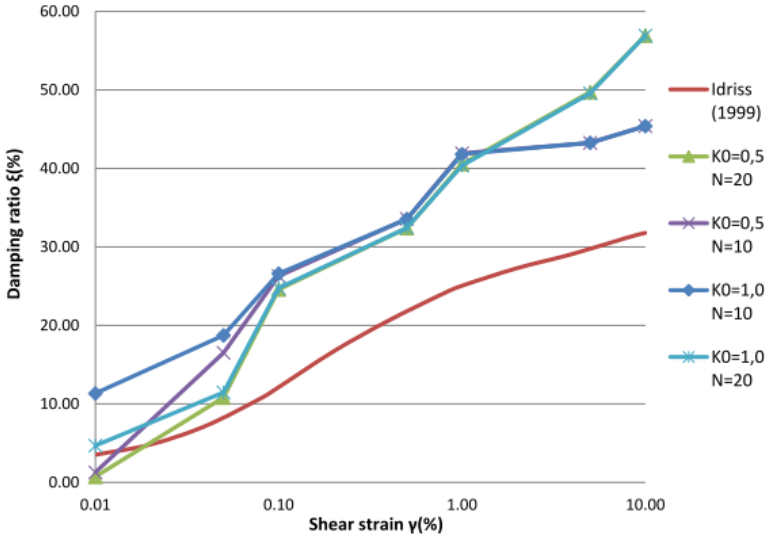

Figure 2.7: Damping ratio at different levels of shear strain from UBC3D-PLM. Graph from Makra (2013)

2.3.5. The Effect of Static Shear Stress

It has been observed that for dense sands an increase in static shear stress ratio results in a larger CRR. For loose sands an increase of the static shear stress ratio results in a lower CRR. To assess this phenomenon the correction factor K_α can be used. K_α adjusts the CRR for the effect of static shear. When looking at figure 2.8 it is clear that UBCSand underestimates the Cyclic Resistance Ratio significantly as the static shear stresses increase. It becomes clear that the model cannot capture the increasing CRR of medium to dense sands as the static shear stress ratio increases (Makra, 2013). Therefore, the UBCSand model is not well suited to be used with initial static shear stress. It leads to an overestimation of the shear strains and therefore overestimates when liquefaction happens. One thing that can be done to improve the results with initial static shear stress is to set the densification factor and liquefaction factor to 1.0.

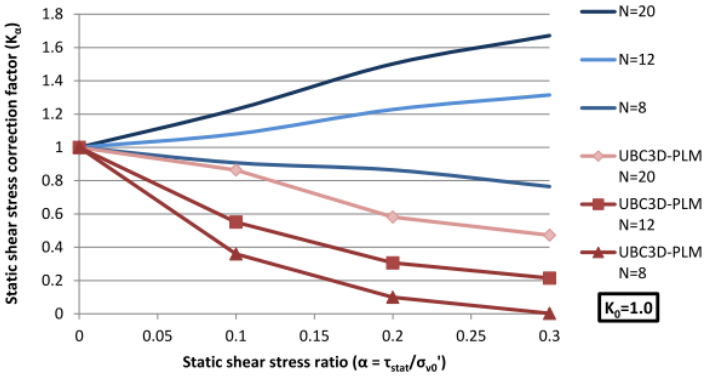

Figure 2.8: Static shear correction factor at different levels of static shear stress ratio with $K_0 = 1.0$. Graph from Makra (2013)

2.4. Modelling Liquefaction with PM4Sand

The plasticity model for sand or PM4Sand has a basic framework of the stress-ratio controlled, critical state compatible, bounding-surface plasticity model for sands that has been elaborated by Dafalias and Manzari (2004). It takes into account elastic and plastic strains increments which are composed by volumetric and deviatoric terms (Toloza, 2018).

PM4Sand follows the critical state soil mechanics framework, with the relative state parameter index as the difference between the current apparent relative density D_r and the relative density at the critical state $D_{r,cs}$. Once the critical state is reached because of shearing, the soil will flow as a frictional fluid.

The model incorporates bounding, dilatancy and critical surface according to Dafalias and Manzari (2004). The bounding ratio controls the ratio between the peak friction angle and the relative state. The bounding surface framework aims to simulate plastic deformations within the yield surface. The dilatancy surface is defined as the location where the transformation from contractive to dilative behaviour occurs (Toloza, 2018). Figure 2.9 shows how the bounding, dilatancy, yield and critical surfaces are schemed.

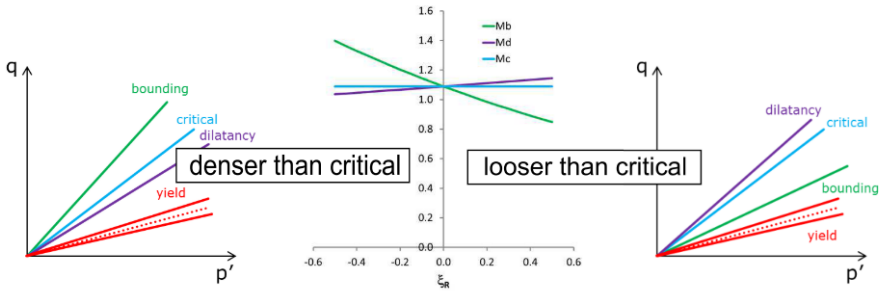

Figure 2.9: Defining the bounding, critical state, dilatancy and elastisity for PM4Sand in the p-q space. Graph from Vilhar et al. (2018) Boulanger and Ziotopoulou (2015)

2.4.1. Fabric Effects in PM4Sand

Cyclic shearing of the soil results in rearrangements and/or destruction of the soil fabric. This effect is called the fabric effect. PM4Sand is designed to also account for the fabric effect.

2.4.2. PM4Sand Parameters

PM4Sand makes use of three main model parameters. These parameters are the relative density D_r, the shear modulus coefficient G_0 and the contraction rate parameter h_{po}.

The relative density controls the dilatancy and stress-strain relation response. It defines if the soil will contract or dilate. The relative density parameter can be defined as an apparent relative density and therefore it can be modified for calibration. The shear Modulus Coefficient G_0 controls the shear modulus at small strains and is affected by factors like cementation and ageing (Boulanger & Ziotopoulou, 2015). The final main model parameter is the contraction rate parameter, h_{po}. This variable adjusts the plastic volumetric strains during contraction and will mostly be adjusted to obtain a target cyclic resistance ratio with respect to cyclic laboratory tests (Toloza, 2018). This calibration will always have to be done.

Finally, the model has some secondary input parameters. These parameters can be used for calibration, but will only be adjusted if changing the main model parameters does not give the desired behaviour. An overview of all PM4Sand parameters can be found in table 2.2

Table 2.2: The input parameters for PM4Sand and the default values if applicable

Name	Symbol	Unit	Method	Default
Apparent relative density	Dr_0	-	$D_r = \frac{e_{max}-e}{e_{max}-e_{min}}$ (2.15) $D_r = \sqrt{\frac{(N_1)_{60}}{C_d}}$ with $C_d = 46$ (2.16)	-
Shear modulus coefficient	G_0	-	$G_0 = \frac{G}{P_A}\sqrt{\frac{P_A}{P}}$ (2.17) $G_0 = 167\sqrt{(N_1)_{60} + 2.5}$ (2.18) $G_0 = 167\sqrt{46 \cdot {D_r}^2 + 2.5}$ (2.19)	-
Contraction rate parameter	h_{p0}	-	Curve fit	-
Atmospheric pressure	ρ_A	kPa	Standard value	101.3
Maximum void ratio	e_{max}	-	$e = \frac{n}{1-n}$	-
Minimum void ratio	e_{min}	-	$e = \frac{n}{1-n}$	-
Bounding surface parameter	n^b	-	Curve fit	0.5
Dilatancy surface parameter	n^d	-	Curve fit	0.1
Constant volume friction angle	ϕ'_{cv}	(°)	Triaxial or DSS test	0.33
Poisson ratio	v	-	Standard value	0.30
Critical state line parameter	Q	-	Standard value	10
Critical state line parameter	R	-	Standard value	1.5
Postshake		-	Standard value	0.0

2.4.3. Sensitivity of PM4Sand Parameters

The sensitivity of the main parameters and two secondary parameters in the PM4Sand model will be assessed. When looking at the reaction of the model in comparison with or without initial shear stress, it can be seen that the model is not able to correctly simulate the effects occurring with initial shear stress. When looking at figure 2.10 and 2.12 it can be seen that PM4Sand can replicate the Fraser Sand results without initial static shear stress much better than with initial static shear stress. In the case of initial shear stress the model significantly overestimates the CRR for the number of cycles to liquefaction (Toloza, 2018).

The Relative Density, D_r
Lowering only the D_r results in lower CRR for the same number of cycles to liquefaction (Toloza, 2018). This makes sense since looser material results in lower cyclic shear resistance and dilative behaviour. However, when the h_{p0} is recalibrated after the D_r is lowered, the CRR for the same number of cycles the liquefaction becomes bigger again. This can be seen in figure 2.10.

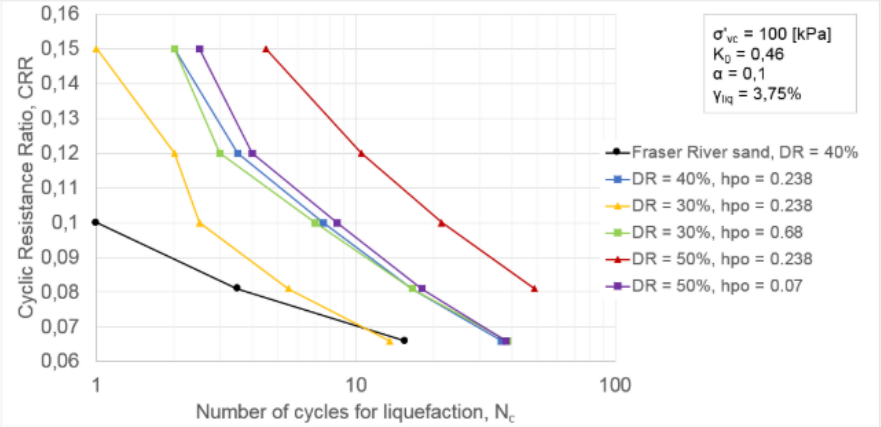

Figure 2.10: CRR vs N_c curves for different apparent relative density D_r, with initial static shear stress. Graph from Toloza (2018)

When looking to the stress-strain relation and stress-path curve, it can be seen that for a lower D_r a lower number of cycles is needed to reach liquefaction. This is explained by looser sands being more susceptible to liquefaction (Toloza, 2018).

After lowering the D_r, the pore pressure ratio also changes over the number of cycles. In case of a lower D_r without calibration h_{p0}, excess pore pressure is generated more quickly and will reach the critical state faster. From figure 2.11 it can be seen that a lower D_r of 30% with calibrated h_{p0} gives the best representation of the pore pressure accumulation.

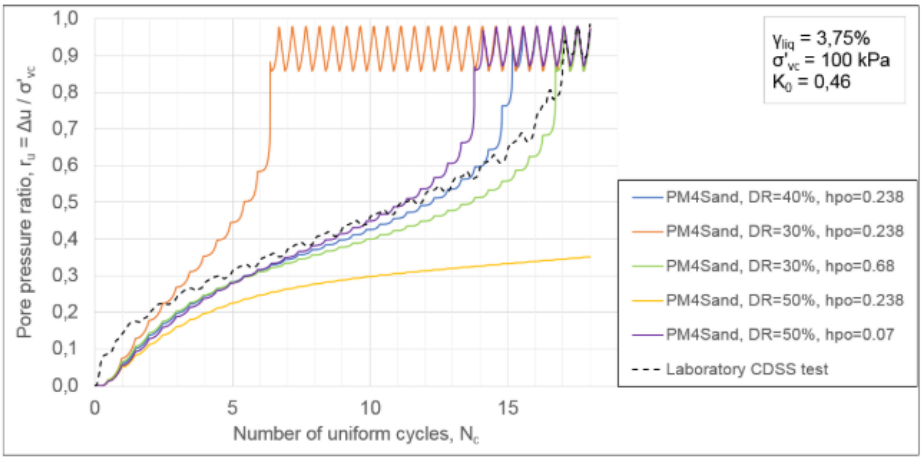

Figure 2.11: Generation of excess pore pressure at different apparent relative density D_r. Graph from Toloza (2018)

Shear Modulus Coefficient, G_0
As expected the shear modulus influences the shear strains increment. A higher G_0 leads to less shear strain. When looking at the stress path with different shear moduli, there is almost no difference when adjusting the shear modulus. From this can be concluded that the shear modulus coefficient has a direct influence on the elastic shear modulus, G, and that the shear modulus influences the model at large strains. When looking at the excess pore pressure, it can be seen that the shear modulus coefficient does not influence it (Toloza, 2018).

Secondary Model Parameters

For PM4Sand two secondary parameters influence the model. These are the bounding surface parameter n^b and the critical state line parameter R.

The bounding surface parameter n^b defines the initial bounding surface of the model and the rate of increment with which the bounding surface approaches the critical surface. As well as the dilatancy tensor which defines the volumetric strains increment. A smaller n^b results in a lower overestimation of the CRR for the number of cycles for liquefaction and a smaller n^b also results in a better stress-strain response than a higher n^b. When using a smaller n^b, the excess pore pressure generation will be slower. The effects of changing the n^b can be seen in figure 2.12

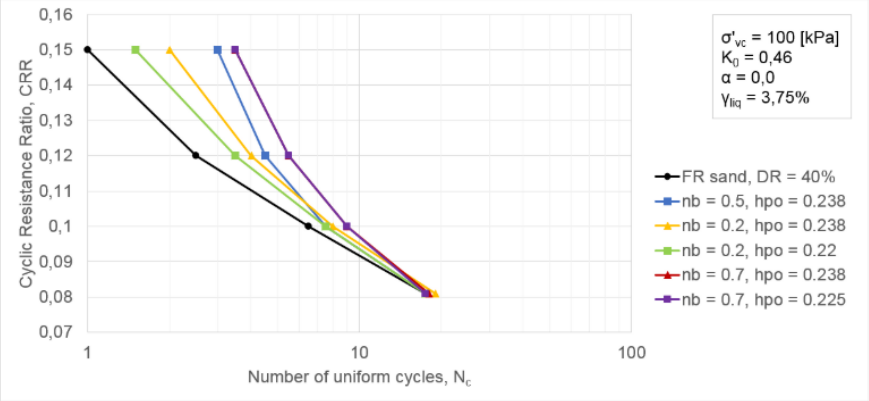

Figure 2.12: CRR curves using different bounding surface parameter n^b, without initial static shear stress. Graph from Toloza (2018)

The critical state line parameter R has a similar effect on the overestimation of CRR for the number of cycles for liquefaction. An increase of R results in a smaller overestimation of the CRR. The excess pore pressure will be generated quicker when using an increased value of R.

Postshake Parameter

It should be noted that during modelling with PM4Sand the Postshake almost always should be zero. The post shake parameter is used to activates the reduction of elastic stiffness that simulates the post-shaking reconsolidation (Vilhar, G. ; Laera, A. ; Foria, F. ; Gupta, A. ; Brinkgreve, 2018). The only situation when this parameter should be 1.0 is at the end of strong shaking. In this case, the parameters of the material should be copied and the post shake should be set to 1.0. For this post-shaking, a new calculation should be performed, with the newly created parameter set.

Effect of Confining Stress

As the confining stress in the ground increases the cyclic shear resistance of the soil decreases. This response is captured in PM4Sand with the correction factor for confining stresses, K_σ. PM4Sand overestimates the confining stress when it is below 1 atm, which resembles the soil close at the surface. While the model underestimates the CRR for confining stresses higher than 1 atm. It can be seen that with a higher relative density D_r and a higher bounding surface parameter n^b, that the over- and underestimation of the overburden effect factor K_σ are higher. This also results in a higher over- and underestimation of the CRR.

2.5. Similarities and Differences between the UBCSand Model and PM4Sand

With the information of the previous sections, it is possible to determine some similarities and differences between the UBCSand model and PM4Sand. The UBCSand model and PM4Sand are similar in the following points:

- Both models make use of a critical state;
- In both models pore water pressure will be accumulated during undrained cyclic loading;
- Both models are not ideal for situations with initial static shear stress, however, UBCSand seems to diverge more.

While the differences between the UBCSand model and PM4Sand are:

- The calibration of the UBCSand parameters should be done cyclic triaxial data, while the calibration of the PM4Sand parameters should be done with Cyclic Direct Simple Shear tests;
- PM4Sand is designed to mainly change one parameter during calibration, while UBCSand has a lot more parameters that need to be adjusted for proper calibration;
- UBCSand uses a critical state friction parameter as input, while PM4Sand uses a relative state parameter.
- The UBCSand model will show elastic behaviour till the shear stress is zero and thereafter the behaviour will be elastoplastic. Where PM4Sand will show more immediate elastoplastic behaviour;
- Once PM4Sand has reached the critical state in the soil it will react as a frictional fluid.

2.6. Conclusion

In this chapter the definition of liquefaction has been given. As well as an explanation of the CSR and CRR, which are often used when talking about liquefaction. The sub-question 'What are the strengths and limitations of the UBCSand model and PM4Sand' has been answered by going into detail about both models. With the answer to this question the similarities and differences between the UBCSand model and PM4Sand were also discussed.

3

Methodology

In this chapter, it is explained how the research is performed. This research uses different methods to assess soil behaviour underneath a breakwater during an earthquake. The research uses a centrifuge test to design the numerical models. The details of this centrifuge test is discussed in chapter 4. A global overview of the research is as follows:

- Calibration of the UBCSand and PM4Sand parameters
  For the numerical models to work properly it is important the correct parameters are used. These parameters are acquired by simulating laboratory tests for the used sands in Plaxis and adjusting the parameters till similar results are found as the results that are found in the laboratory tests.
- Incorporating correct earthquake signal
  This research focuses on a breakwater subjected to an earthquake. Therefore it has to be investigated how the correct earthquake signal is applied in the numerical model. To check the earthquake signal a 1D site investigation is done in Plaxis. Thereafter, it is applied to the breakwater in the numerical model and further improved.
- Generating and assessing results
  Finally, the numerical models will be run and the results for both UBCSand and PM4Sand modelled soils will be generated. The results are focused on the settlements, deformations and excess pore water pressures. These results for UBCSand and PM4Sand are compared in order to find if PM4Sand can be used to model a breakwater subjected an earthquake.

3.1. Calibrating the Plaxis Models

After collecting the required parameters for the Plaxis models, the models have to be calibrated. It is necessary to check if the soil in Plaxis behaves the same way in the modelled laboratory tests as in the laboratory tests from the literature. Since the UBCSand model and PM4Sand are designed to model sand during seismic conditions, the calibration is done with cyclic tests. Possible laboratory tests to use are a Cyclic Triaxial test or Cyclic direct simple shear test. Due to PM4Sand being a 2D model, it cannot replicate a Triaxial test correctly. Therefore the necessary test for calibration of PM4Sand is a CDSS test. The UBCsand model can be calibrated by using both Cyclic Triaxial Tests and Cyclic Direct Simple Shear tests. During the calibration the modelled sand must show the same stress-strain and EPWP as in the laboratory tests. For these calibrations often a CRR vs. the number of cycles diagram is used. An example of this graph is shown in figure 3.1. To calibrate the sample to give the correct EPWP the graph showing the EPWP ratio vs. the number of cycles for liquefaction is used. Figure 3.2 is an example of this. So to calibrate the UBCSand model and PM4Sand, the parameters of the models need to be adjusted so that the curves generated by the models correspond to the curves of the lab tests.

For this research the desired number of cycles to liquefaction is known, as being $N_c = 15$, which represents a standard big earthquake of 7.5Mw (Idriss & Boulanger, 2008). Because this is known, there is no need to use CRR vs. the number of cycles to liquefaction graph to assess the sand behaviour. It is now possible to assess the stress, strain and EPWP at a CRR at $N_c = 15$.

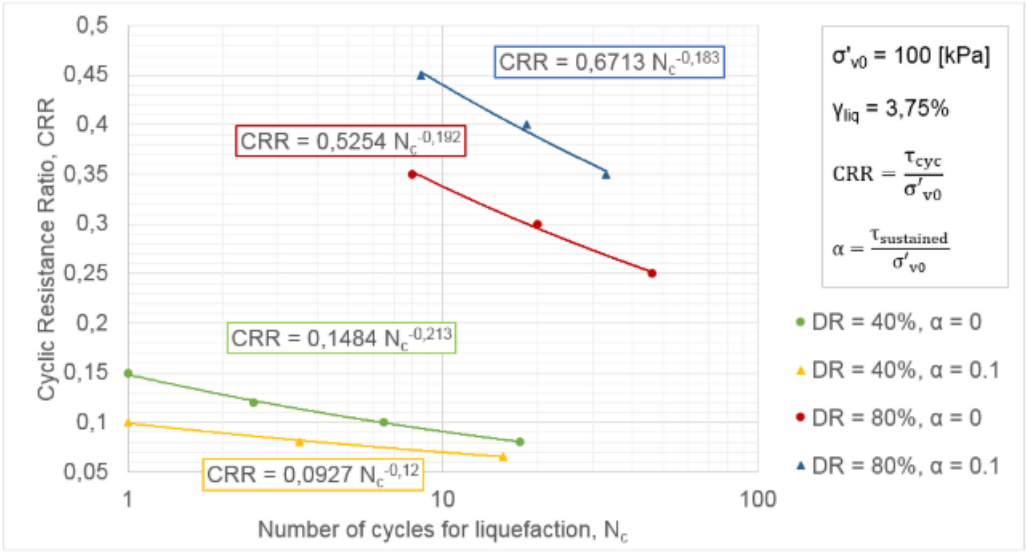

Figure 3.1: Example graph of CRR vs. Nc Toloza (2018)

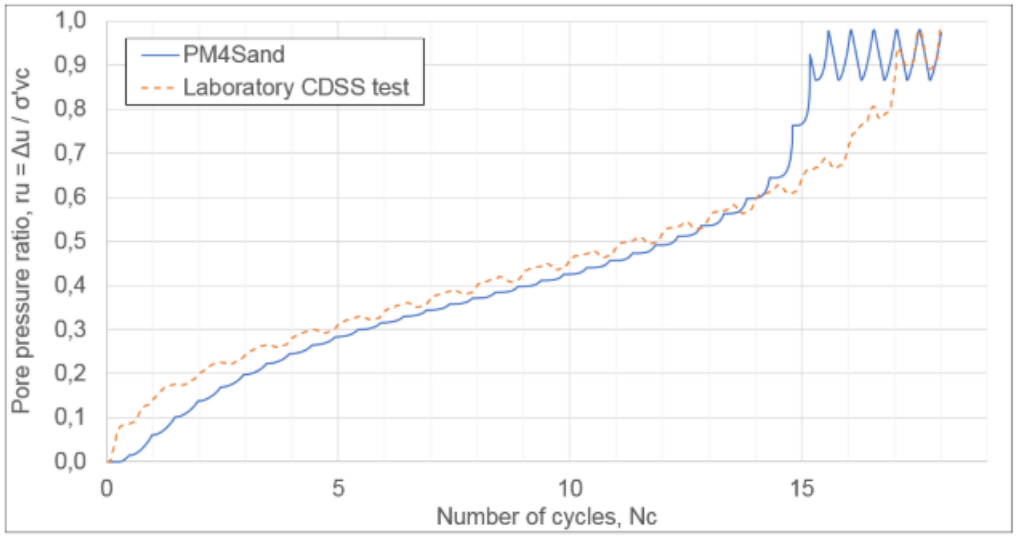

Figure 3.2: Example graph of EPWP ratio vs. Nc Toloza (2018)

3.2. Parameter Determination and Calibration for Modelling the Centrifuge Test in Plaxis

In this section, it will be explained what would be the ideal way to determine PM4Sand parameters. Thereafter, it will be explained how the model calibrations are done for this research. Since the ideal data to determine the PM4Sand parameters were not available, the PM4Sand parameters have been determined by using 2 different methods. Firstly, the UBCSand model has been calibrated with a cyclic triaxial test. With the calibrated UBCSand parameters CDSS tests are simulated to give results to which the PM4Sand parameters can be calibrated. The second method is using a cyclic torsional shear test to calibrate PM4Sand.

3.2.1. Ideal Data for Calibrating PM4Sand

After determining the initial parameters needed for both the UBCSand model and PM4Sand both models will still need to be calibrated to fit the laboratory data. This means that there is no way to calculate the parameters which can immediately be used in the model. However, when looking at chapters 2.3.1 and 2.4.2 there is a preferred method to determine these initial parameters. The preferable option to determine the parameters would be using the corrected clean sand equivalent SPT blow-count measurements ($((N_1)_{60})$) gathered from the project site. Using $((N_1)_{60})$ can be easily put in the previously described formulas and gain the initial needed parameters. Thereafter, the calibrations of the models can be done as described in chapter 3.1. For the UBCSand model, this is ideally done with cyclic triaxial tests and for the PM4Sand model with cyclic direct shear tests. The tests should be done with the testing conditions similar as the in-situ conditions. Therefore it is important to have the relative density and confining pressure resemble the real situation.

3.2.2. How the Models are Calibrated with the Available Data

For this research the ideal data was not available to properly calibrate the numerical models. Therefore the calibrations will be done with three different methods. Firstly, UBCSand parameters will be determined based on the cyclic triaxial test results found in Asadi et al. (2018). The sand used in these triaxial tests is very similar to the used sand in the centrifuge test, because the main properties of both sands are the same. Subsequently, the found UBCSand parameters will be used to simulate a CDSS test. This is done because the PM4Sand parameters cannot be determined from Triaxial test because it is a 3-dimensional test. The results from the with UBCSand parameter simulated CDSS test will be used to calibrate the PM4Sand parameters. Finally, the results of a torsional shear test (Tatsuoka et al., 1982) will also be used to calibrate the PM4Sand parameters.

3.2.3. The UBCSand Parameters Calibration

The UBCSand parameters will be determined with the help of a cyclic triaxial test on Toyoura sand. The Asadi et al. (2018) paper gives graphs of the behaviour of Toyoura sand with a relative density of 50% and 80%. Figure 3.3 shows the behaviour of the Toyoura sand with a relative density of 50% during a cyclic triaxial test. The graphs show that liquefaction occurs after 11 cycles. For this experiment liquefaction is defined as a double axial strain of 5% and the excess pore water pressure reaching close to 100 kPa. Plaxis SoilTesting is used to find the parameters for the UBCSand model that give a similar response as in the experiment of Asadi. First, the parameters are assessed by calculating the SPT-value with formula 2.16 for the different densities of the Toyoura sand. With the SPT-value the values for the elastic shear modulus, elastic-plastic modulus and elastic bulk modulus numbers (K_G^e, K_G^p and K_B^e) are determined with the formulas given in section 2.3.1.

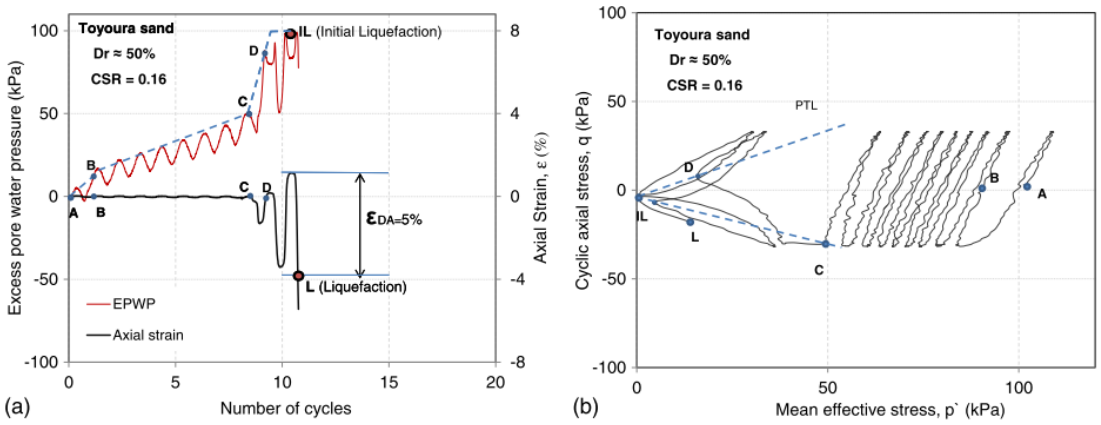

Figure 3.3: Cyclic triaxial test results on Toyoura sand with D_r 50% Asadi et al. (2018)

The predetermined parameters are put in Plaxis and with the SoilTest feature the response of the modelled sand during a cyclic triaxial test is determined. With Plaxis SoilTest it is possible to find graphs that can be compared to the graphs in figure 3.3. Examples of the results from Plaxis SoilTest can be found in figure 3.4 and 3.5. From these figures it becomes clear after how many cycles liquefaction occurs. Figure 3.4 shows that after 10 cycles the strain greatly increases, which suggest liquefaction. A comparison between the p'-q graphs of figures 3.3 and 3.5 can also be made. Although the trajectories of both graphs are quite different, they also show some similar behaviour. Both graphs have to be read from right to left and initially show the cycles response on the soil sample. However, after several cycles the sample fails and the triangular shapes appear. The UBCSand parameters need to be adjusted in such a way that behaviour of the acquired graphs from Plaxis SoilTesting show similar behaviour as the desired sand sample in a lab test shows.

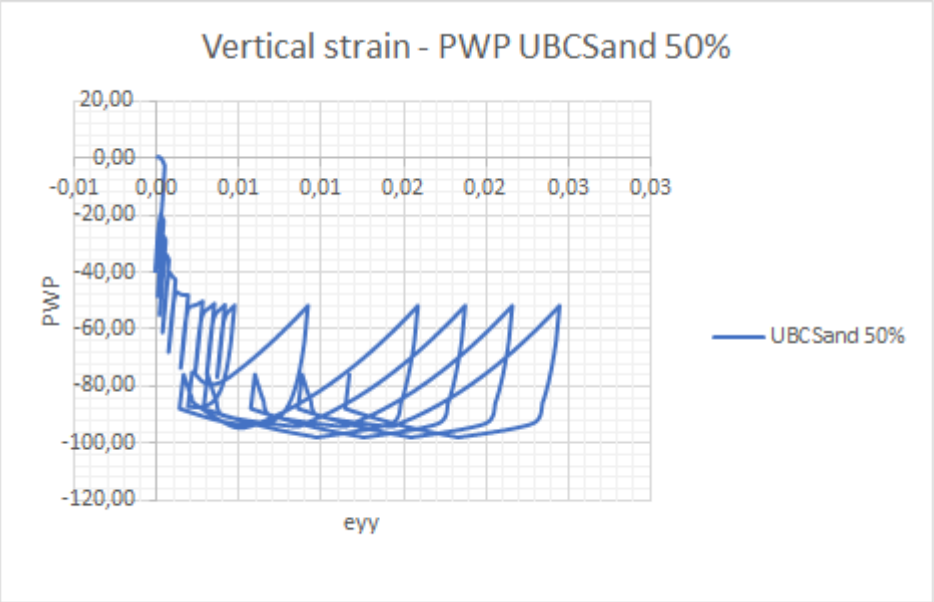

Figure 3.4: Strain versus Excess pore water pressure during cyclic triaxial test UBCsand model for Toyoura sand $D_r = 50\%$

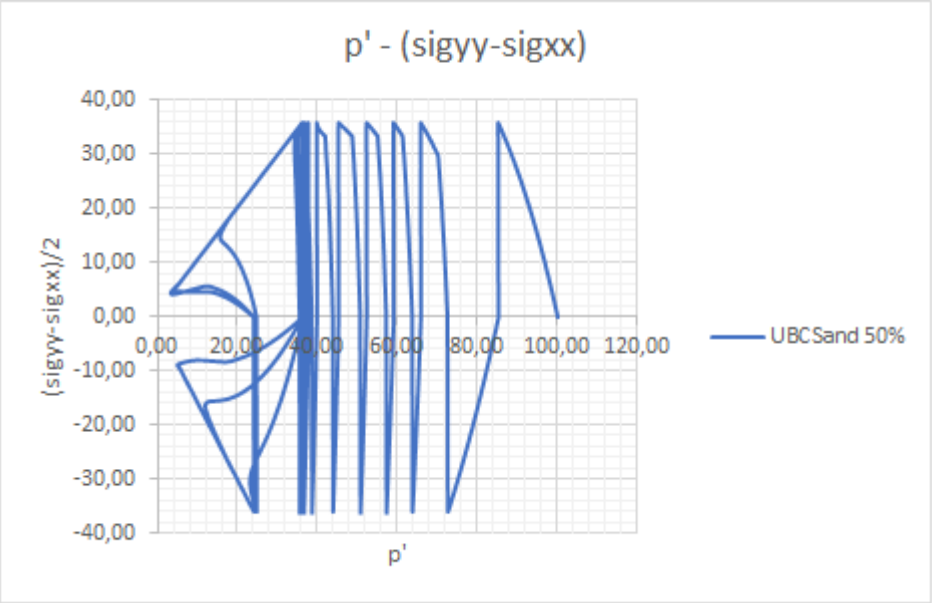

Figure 3.5: Mean effective stress versus deviator stress during cyclic triaxial test UBCsand model for Toyoura sand $D_r = 50\%$

3.2.4. Determining PM4Sand Parameters with Simulated Cyclic DSS Test

The first way the parameters for PM4SAND are determined is with the help of the previously calibrated UBCSand model. With Plaxis SoilTest several cyclic DSS tests are simulated using the UBCSand parameters determined during the previously calibrated Toyoura sand. From these simulated tests graphs for the shear stress, shear strain, stress path, and excess pore water pressure are generated. Just as for the previous calibration method new graphs are generated with Plaxis SoilTest for PM4Sand that are calibrated in such a way that the resulting graphs are similar to the UBCSand model graphs.

3.2.5. PM4Sand Parameters with a Cyclic Torsional Shear Test

The final calibration of PM4Sand is done with a cyclic torsional shear test. This is a test that is performed in an adjusted triaxial test apparatus. The torsional shear apparatus shears a sample by rotating it instead of compressing it like in a normal triaxial compression test. The data that is used for calibrating the PM4Sand parameters with a cyclic torsional shear test comes from a paper written by Tatsuoka et al. (1982). Similar as when calibrating the UBCSand parameters Plaxis SoilTest is used to make sure PM4Sand behaves similar to the sample in the cyclic torsional shear test. Pradhan, Tatsuoka, and Horii (1988) state that the results of a torsional shear test present similar results as a simple shear test. Because a Torsional shear test can not be replicated in Plaxis soilTest, a simple shear test will be used. Since the results are similar for both tests replicating the Torsional Shear Test results with a Simple Shear test will give a similar calibration result. An example of the results of the cyclic torsional shear tests from Tatsuoka are shown in figure 3.6.

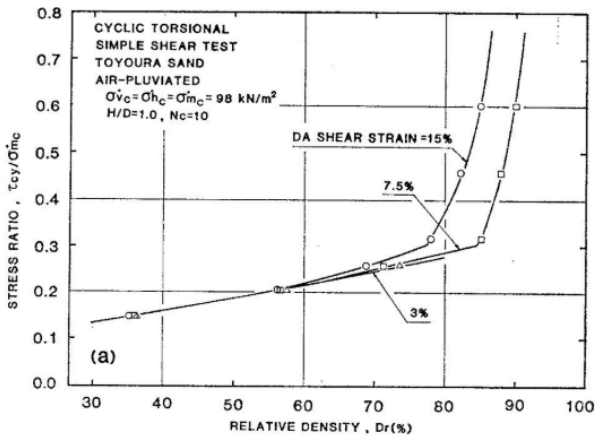

Figure 3.6: Results of cyclic torsional shear tests by Tatsuoka et al. (1982)

The information found from figure 3.6 is different than the results found from the triaxial tests for the UBCSand model. In the case of the torsional shear test the CSR, the N_c and the amount of strain reached in that number of cycles is available. The missing information is how the pore pressure built-up develops over time. It is known that the pore water pressure ratio needs to be close to 1.0 when reaching failure. So for the calibration it will be assumed that this is a requirement that needs to be met. From the way the built-up of the excess pore pressure looks will be assumed to be similar as found for the calibrations of PM4Sand with the simulated UBCSand CDSS tests.

By generating graphs for the shear stress, shear strain, stress path, and excess pore water pressure and assuring these graphs satisfy the results of figure 3.6 the parameters for PM4Sand can be calibrated.

3.3. Conclusion

In the Methodology it is explained how the calibrations of the different data sets has to be done. The UBCSand parameters need to be determined with cyclic triaxial tests from the Asadi et al. (2018) paper.

The PM4Sand parameters need to be determined in two different ways. Firstly, the calibrated UBCSand model are used to simulate CDSS tests. These Simulated CDSS tests are used to calibrate the PM4Sand parameters. The second method is using Cyclic Torsional Shear tests to calibrate the PM4Sand parameters.

4

Scaled Laboratory Test

The scaled laboratory test that will be used for the assessment of PM4Sand is performed by Chaudhary and Hazarika (2018). The performed experiment can be divided into three sections: performance during an earthquake, performance during a tsunami after an earthquake and numerical modelling of the experiment. For this research only the performance during the earthquake and the numerical modelling is interesting. In the following sections, the details of the test will be described.

4.1. Experiment Set-up

The centrifuge model tests were conducted at the Kyoto University, with a centrifuge that can operate up to an acceleration of 50g for dynamic tests (Chaudhary & Hazarika, 2018). The experiments were done with a maximum centrifuge acceleration of 25g, due to the limitations of the tsunami generation device. Next to the normal scaling that comes with using a centrifuge, this experiment is also subjected to a generalised scaling. Generalised scaling is a way to model bigger prototype structures in a centrifuge test, without needing bigger centrifuge equipment. With generalised scaling, an extra scaling (the virtual scaling) is applied and multiplied with the scale factor of the centrifuge to replicate a bigger prototype model. The virtual scaling laws are based on scaling relations in the 1g field (Iai, Tobita, & Nakahara, 2005). In the case of this centrifuge test the virtual scaling is $m = 9$ and the centrifuge scaling $n = 25$. The result of these scaling laws multiplied is the generalized scaling of $N = mn = 9 * 25 = 225$. The generalised scaling method is to make sure the breakwater fits the desired dimensions and still fits in a soil box that fits in the centrifuge.

The soil box used for the centrifuge tests can be found in figure 4.1. Figure 4.2 shows the 3d schematic view of the soilbox and figure 4.3 shows the locations of sensors in the soilbox.

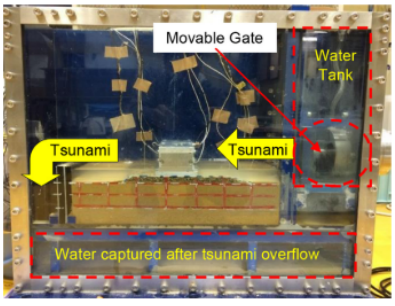

Figure 4.1: The used soil box for the centrifuge tests

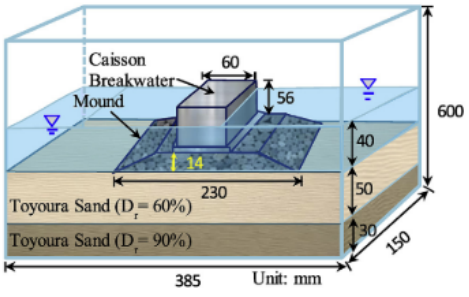

Figure 4.2: 3d schematic view of the soilbox

To limit the imprecision to reality the following measures are taken by Chaudhary and Hazarika (2018) while setting up the soil box:

- The caisson was made of an aluminium box filled with lead balls to get the desired weight and centre of gravity.
- To the side faces of the caisson a lubricant is applied to reduce the amount of friction between the soil box and the caisson.
- Vibration absorbing layers were used on both ends of the soil box to prevent seismic wave reflections during seismic loadings.
- The seabed of the experiment is divided into two layers of Toyoura sands, one with a relative density of $D_r = 90\%$. This dense layer represents the bedrock. While the upper layer has a relative density of $D_r = 60\%$

4.1.1. Instrumentation

The full experimental set-up of the soil box is shown in figure 4.3. Displacement gauges, pore pressure gauges, water pressure gauges and accelerometers were installed in the soil box. With these instruments, the reaction of the caisson and soil to the earthquake was monitored.

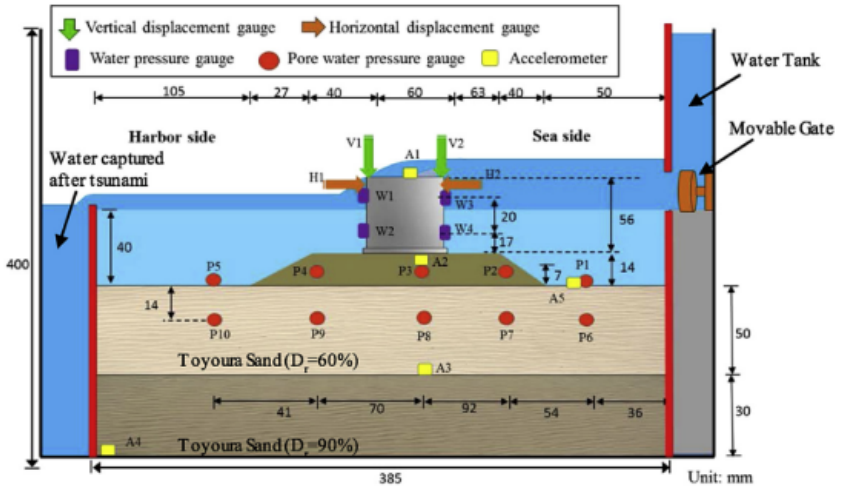

Figure 4.3: Experimental setup up of the soilbox

4.1.2. Earthquake Loading

The part of the experiment with relevance to this research is the reaction of the breakwater to an earthquake. The earthquake is divided into two foreshocks and one mainshock. In table 4.1 the details of the earthquake are shown. Between two shocks a time interval has been added to make sure the pore water pressure could completely dissipate. The earthquake loading has been applied at the bottom of the soil box with a sinusoidal acceleration. The sinusoidal acceleration, frequency and time can also be seen in figure 4.4.

Table 4.1: This table shows the details of the used earthquakes in the experiment

	Centrifuge experiment			Prototype		
	Frequency	Time	Acceleration amplitude	Frequency	Time	Acceleration amplitude
Main shock	83 Hz	1.4 sec	10 g	0.66 Hz	182 sec	0.4 g
First fore shock	83 Hz	1.4 sec	2.5 g	0.66 Hz	182 sec	0.1 g
Second fore shock	83 Hz	1.4 sec	5 g	0.66 Hz	182 sec	0.2 g

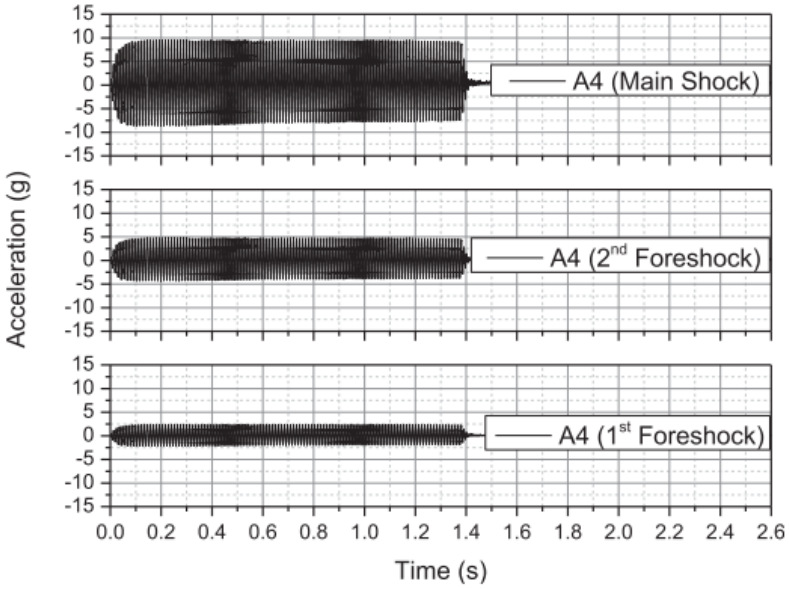

Figure 4.4: In the figure the three different shockwaves are shown

4.2. Parameters of the Used Materials in the Centrifuge Test

For the experiment different materials are used. These materials are Toyoura sand and Crushed stones. The Toyoura Sand is used for the lower and upper layer of the soil on which the breakwater is built. Both layers have different relative densities and therefore will react differently. The Crushed stones are used for the mound that is part of the breakwater. The characteristic of these materials can be found in tables 4.2 and 4.3 (Chaudhary & Hazarika, 2018).

Table 4.2: Properties of the foundation materials used in the experiment (1/2)

Properties	Toyoura sand	Crushed stones
Specific Gravity, ρ_s (g/cm^3)	2.64	2.77
Max. Dry Density (g/cm^3)	1.64	1.78
Min. Dry Density (g/cm^3)	1.34	1.42
Uniformity Coefficient U_c	1.7	1.5
Mean Grain size, D_{50} (mm)	0.16	4.77

Table 4.3: Properties of the foundation materials used in the experiment (2/2)

Properties	Crushed stones	Upper soil layer	Lower soil layer
Unit Weight (γ)	16.2 kN/m^3	15.06 kN/m^3	16.08 kN/m^3
Angle of Internal Friction (ϕ)	45.8 °	35.7 °	43.8 °
Cohesion (c)	0 kN/m^3	0 kN/m^3	0 kN/m^3

4.3. Results of Scaled Centrifuge Test

The results that will be used for this research are related to the excess pore water pressure, the settlement of the caisson and the deformations in the foundation ground reported in the article of Chaudhary and Hazarika (2018).

4.3.1. Excess Pore Water Pressure

Excess pore water pressure is an important result of the experiment since an increase in excess pore water pressure leads to a decrease in strength and can cause liquefaction. In figure 4.5 the excess pore water over time is shown for the three shock waves. It can be clearly seen that the mainshock wave results in the highest excess pore water pressure, this is due to the higher acceleration amplitude of the main shock wave.

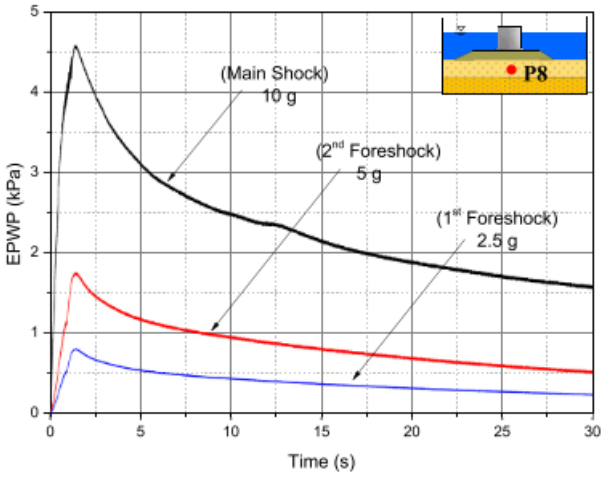

Figure 4.5: The excess pore water pressure measured at p8 during the experiment Chaudhary and Hazarika (2018)

4.3.2. Settlement Of The Caisson

Due to the increase in excess pore water pressure with each shock wave, the shear strength and bearing capacity decrease. This leads to settlement of the caisson. From figures 4.6a and 4.6b it becomes clear the settlement of the second foreshock is two times lager than foreshock one. This corresponds with the increase of amplitude for the earthquake of foreshock two. The difference between the first foreshock and the main shock is 6.5 times for V1 and 6.6 times for V2. This big difference can indicate that liquefaction occurred during the main shock.

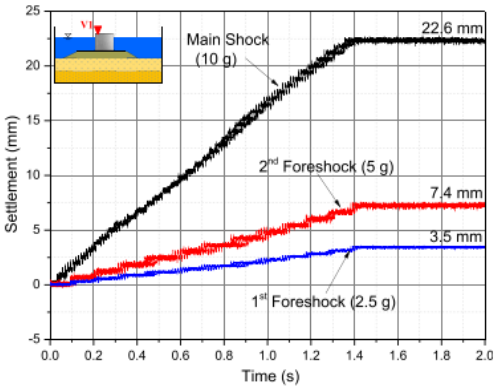

(a) This figure show the settlements over time at V1

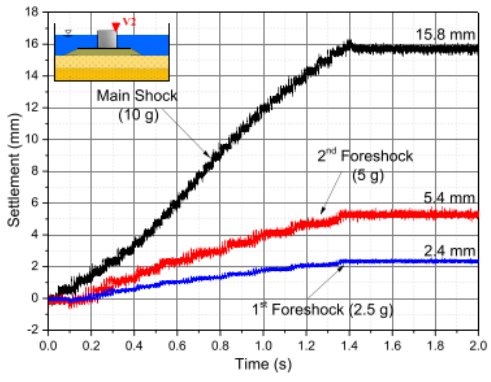

(b) This figure show the settlements over time at V2

Figure 4.6: The settlement of the caisson

4.3.3. Deformation of the Foundation Ground

Figure 4.7 gives a good overview of the effect the earthquake had on the caisson and its foundation. Clearly, the ground deforms more the higher the amplitude of the shock wave is. After the main shock it can be seen that the rubble mound is spread out over the foundation ground. The effect of the earthquake on the foundation soil can best be assessed by comparing the white and red lines in the picture. These lines clearly show a significant settlement underneath the rubble mound, where the seabed soil deformed outward in a lateral direction (Chaudhary & Hazarika, 2018).

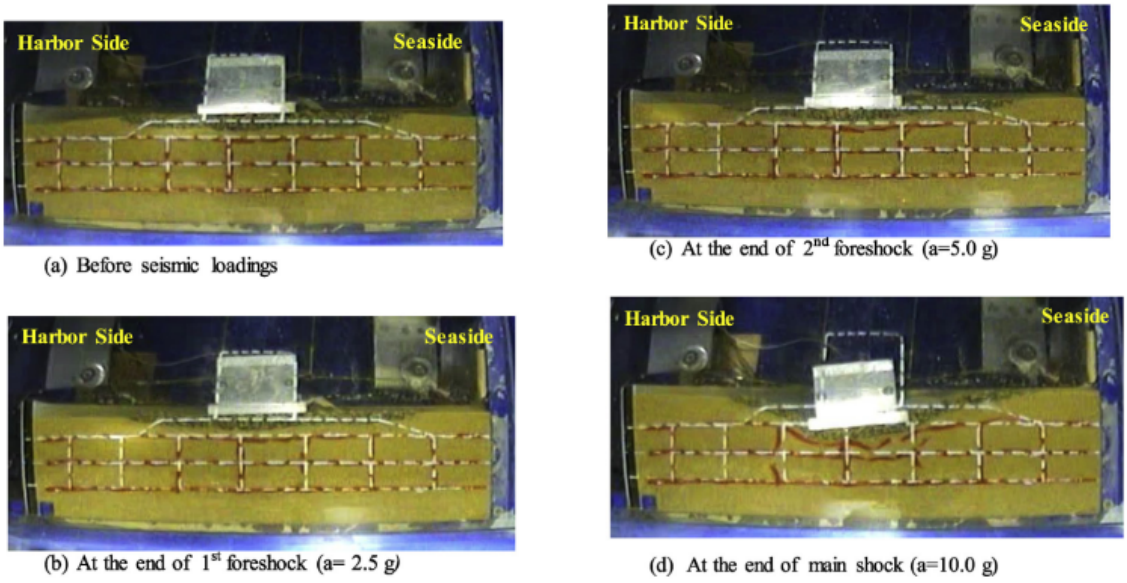

Figure 4.7: Pictures of ground deformation of the foundation

4.4. Numerical Modelling of the Scaled Laboratory Test

To make the mechanism and behaviour of the breakwater and its foundation under the earthquake loadings clear, Chaudhary and Hazarika (2018) also did a numerical simulation. The simulation has been done with the finite difference program FLAC. In the following section, their modelling and results will be discussed.

4.4.1. Model and Boundary Conditions

For the numerical modelling the following model and boundary conditions have been used (Chaudhary & Hazarika, 2018):

- A grid of size 385 mm x 385 mm was generated. The whole grid was discretized into 3025 number of small zones.
- The Toyoura sand was modelled as a cohesionless and homogeneous material with an elasto-plastic response.
- The soil layer exists of two layers of Toyoura sand. The lower layer has a relative density of $D_r = 90\%$ and the upper layer has a $D_r = 60\%$. The lower layer had a height of 30 mm and the upper layer was 50 mm high.
- The rubble mound has been modelled as an elastic material.
- The caisson was also modelled as an elastic material.
- The foundation soils and rubble mound are modelled as fully saturated.
- The effective stress analysis was done with a formula proposed by Byrne (1991). This formula uses an incremental shear-volume coupling equation and incorporates in a cyclic simple shear pore pressure element model.
- At the bottom plane of the model all movements were restrained.
- Free field boundary conditions were applied at the vertical model boundaries during the seismic excitation to avoid wave reflections.
- A damping ratio of 5% was assigned to the model during earthquake loadings.

4.4.2. Numerical Analysis

The built numerical model from Chaudhary and Hazarika (2018) showed similar behaviour as the scaled laboratory test. The excess pore water pressure during the mainshock in the model behaved in the same way as during the experiment. Furthermore, could it be seen that the settlements and deformations after the mainshock in the model were similar to settlements and deformations in the experiment after the mainshock. Figure 4.8 shows the displacement vectors from the modelling of the centrifuge by Chaudhary and Hazarika (2018) after the mainshock.

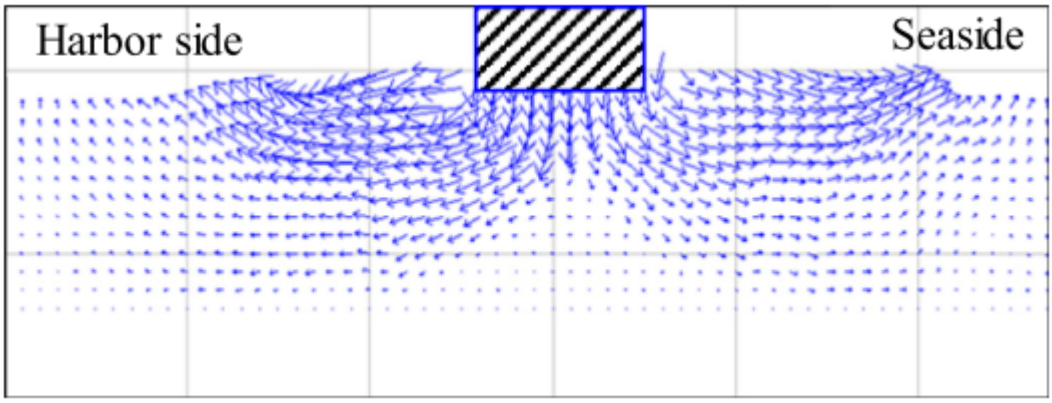

Figure 4.8: Resulting displacement vectors for the model from Chaudhary and Hazarika (2018) at the end of the main shock

To assess the occurrence of liquefaction the pore water pressure ratio over time was investigated. The PWP ratio was determined at a depth of 14 mm beneath the base of the mound and 63 mm distance toward the harbour from the harbourside edge of the caisson. The results can be seen in figure 4.9. It can be seen that during the mainshock a PWP ratio of 0.86 is reached. This is close to a PWP ratio of 1.0, which is needed for full liquefaction. This suggests that liquefaction may occur during the mainshock and could explain the high deformations in the soil.

During the model testing, the influence of the seawater level was also investigated. This has been done by modelling the earthquake with three different sea levels. The results showed that a higher sea level results in a lower settlement. This can be explained by the increase in buoyancy consequential to a higher sea level, This higher buoyancy results in a lower effective weight of the breakwater. Therefore fewer deformations occur in the upper soil layer.

Finally, the effect of the thickness of the upper soil layer on the settlements has been investigated. It could be seen that an increase in the thickness of the upper layer increases settlements.

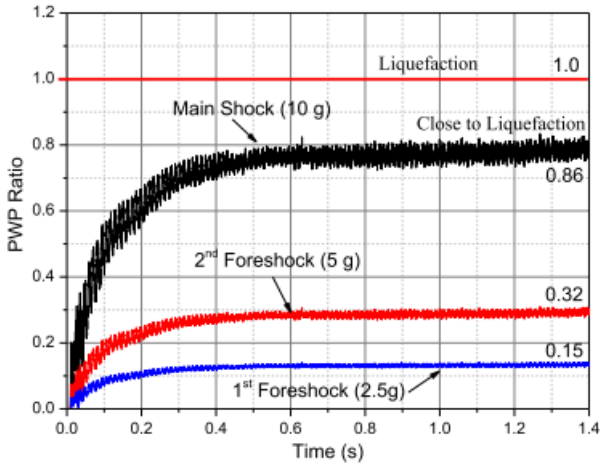

Figure 4.9: Resulting pore water pressure ratio over time during earthquake loadings

4.5. Conclusion

In short, the scaled laboratory test used to evaluate the performance of PM4Sand is executed by Chaudhary and Hazarika (2018). The test was a centrifuge test with an acceleration of 25g. In the test a rubble mound with caisson type breakwater is subjected to an earthquake. The earthquake is an acceleration signal in horizontal direction with a frequency of 83 Hz. The earthquake has a sinusoidal shape and a maximum amplitude of 10g. Results for settlements, deformations and EPWP were found at the end of the tests.

5

Calibrating Numerical Model Parameters

In this chapter, the results of the parameter calibration are presented. In chapter 3 it has been discussed how the parameter determination should be done. Firstly, the parameters acquired from the literature will be discussed as well as the assumed parameters. Thereafter, the calibrated parameters and resultant graphs are shown and discussed. Finally, a qualitative sensitivity analysis has been done.

5.1. Used Literature to Acquire Parameters

The parameters from the Toyoura sand and crushed stones used in the centrifuge experiment have been discussed before and can be found in table 4.2 and table 4.3. The values in table 4.2 and 4.3 for the Toyoura sand have a relative density of 60% for the upper layer and 90% for the lower layer. During the literature study, no laboratory tests and soil properties for Toyoura sand with relative densities of 60% and 90% have been found. Since lab tests and parameters for Toyoura Sand with a relative density of 50% and 80% are available these parameters will be used to model the centrifuge test in Plaxis. The results from the centrifuge tests by Chaudhary and Hazarika (2018) should be similar to the results of the modelled centrifuge tests in Plaxis with a relative density of 50% and 80%.

5.2. Predetermined Parameters

The first step in calibrating the UBCSand and PM4Sand parameters is acquiring the fixed parameters and make estimations for the parameters that need to be calibrated. Table 2.1 and table 2.2 show the parameters needed for modelling the UBCSand and PM4Sand in Plaxis.

5.2.1. Predetermined Parameters for UBCSand

Table 2.1 shows that values for the ϕ_p, ϕ_{cv} and $(N_1)_{60}$ need to be determined. The peak and constant volume friction angles are determined with Equations 2.8 and 2.9. Yoshimine (1996) performed simple shear tests on Toyoura sand with different void ratios. The results of these tests can be found in figure 5.1a. Void ratios 0.660 and 0.784 are equal to a relative density of 83% and 51%. The blue line in figure 5.1a is an example of the M line used for the friction angle calculations. This value corresponds to the peak friction angle for Toyoura sand and therefore is used to calculate this peak friction angle. The constant volume friction angle is determined in the same way, but figure 5.1b is used. The value for $(N1)_{60}$ is determined by rewriting Equation 2.16 to:

$$(N1)_{60} = D_R^2 \cdot C_d \tag{5.1}$$

The calculated fixed parameters are shown in table 5.1.

Table 5.1: Used values for the fixed UBCSand parameters

Parameter	Dr = 50%	Dr = 80%	Unit
ϕ_{cv}	31.33	38	°
ϕ_p	35.30	39.13	°
$(N_1)_{60}$	11.5	29	-

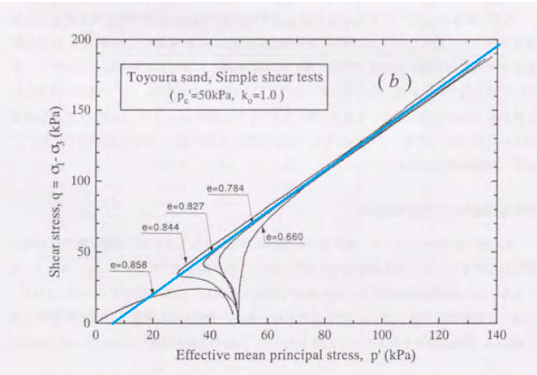

(a) M-line for peak friction angle

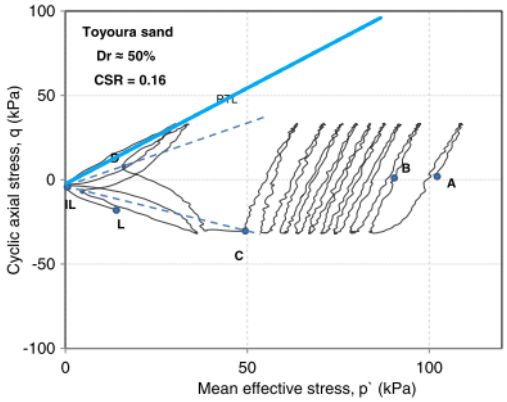

(b) M-line for constant volume friction angle

Figure 5.1: p'-q graphs to determine friction angles. (a) from Yoshimine (1996) and (b) from Asadi et al. (2018)

5.2.2. Predetermined Parameters for PM4Sand

From table 2.2 it can be seen that the values of e_{max}, e_{min} and ϕ_{cv} need to be predetermined. ϕ_{cv} for PM4Sand are the same values as calculated in the previous paragraph for UBCSand. The values for e_{max} and e_{min} are taken from Pestana, Whittle, and Salvati (2002). The taken values are shown in table 5.2.

Table 5.2: Used values for the fixed PM4Sand parameters

Parameter	Dr = 50%	Dr = 80%	Unit
e_{max}	0.98	0.98	-
e_{min}	0.61	0.61	-
ϕ_{cv}	31.33	38	-

5.2.3. Estimation of UBCSand Parameters

For the UBCSand model in Plaxis six parameters can be used to calibrate the model. These parameters have been shown in table 2.1. In Paragraph 2.3.1 the Equations 2.12, 2.13 and 2.14 give a way to estimate these parameters based on $(N_1)_{60}$. Table 5.3 gives the values for the calculated estimation of K_G^e, K_B^e and K_G^p. The parameter values of ne, me and np will have the default values of 0.5 and the parameters will only be adjusted when adjusting K_G^e, K_B^e and K_G^p still does not give accurate curve fits.

Table 5.3: Estimated values for the calibration UBCSand model parameters

Parameter	Dr = 50%	Dr = 80%	Unit
K_G^e	685	932	-
K_B^e	979	1332	-
K_G^p	488	3460	-

5.2.4. Estimation of PM4Sand Parameters

As stated in section 2.4.2 the parameter that is mostly used for calibration is the contraction rate parameter, h_{p0}. Next to this parameter it is possible to change the D_{r0}, G_0, n^b and n^d if changing the h_{p0} does not give the desired curve fit. The apparent relative density, D_{r0}, will have the same value as the relative density of the modelled sand. To determine the shear modulus coefficient, G_0, the D_{r0} and Equation 2.19 are used. Table 5.4 shows the calculated values for PM4Sand. The values for n^b and n^d are taken at there default values of 0.5 and 0.1 and will only be adjusted if calibration of D_{r0}, G_0 and h_p0 does not result in satisfying curve fits.

Table 5.4: Estimated values for the calibration PM4Sand model parameters

Parameter	Dr = 50%	Dr = 60%	Dr = 80%	Unit
D_{r0}	50	60	80	%
G_0	625	729	944	-
K_G^p	0.5	0.5	0.5	-

5.3. Calibration of the Numerical Model Parameters

Following the parameter estimation, the final calibration of the UBCSand model and PM4Sand will be done. Firstly the calibration for the UBCSand model will be presented. Thereafter the final PM4Sand parameters will be presented and discussed. The results of all calibrations and the corresponding parameters can be found in Appendix B.

5.3.1. Calibration of the UBCSand Model Parameters

The calibration of the UBCSand parameters have been chosen so that they are as similar as possible to the test results from Tatsuoka et al. (1982). Figures 5.2, 5.3, 5.4 and 5.5 show the results from Plaxis SoilTest plotted next to the results form the literature.

When looking at the excess pore water plots in figures 5.2 and 5.3 it is clear that the initial excess pore water pressure is higher in the modelled tests, compared to the results from the literature. However, the inclination of both lines, the cyclic behaviour and the number of cycles needed to reach close to a 100 kPa excess pore pressure are very similar.

Looking at the axial strain from the modelled test compared to the axial strain from the literature it can be seen that the number of cycles needed for plastic behaviour to occur is the same. Just like for the EPWP the phase of the cyclic behaviour is also similar. However, it can be seen that the axial strain does not get back to 0% strain or even positive strain after the first plastic cycle occurred. A possible explanation for this is that the test results from Tatsuoka et al. (1982) show double axial strain, while Plaxis shows the axial strain. Therefore it has been chosen to calibrate the UBCSand parameters in such a way that it reaches 2.5% axial strain, which is half the double axial strain presented in the literature tests.

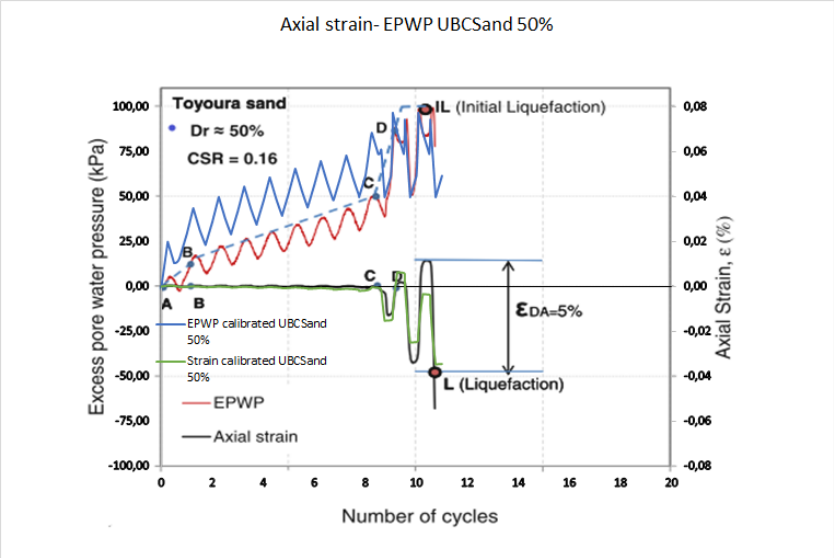

Figure 5.2: Comparison between axial strain and EPWP from the literature and the final calibrated parameter set for UBCSand D_r = 50%

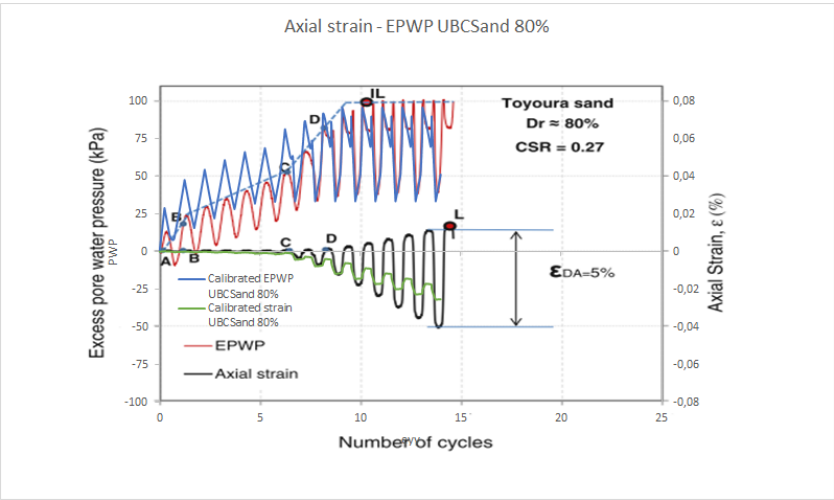

Figure 5.3: Comparison between axial strain and EPWP from the literature and the final calibrated parameter set for UBCSand D_r = 80%

The results of the p'-q plots from the literature and modelled cyclic triaxial tests show some differences and similarities. The change in mean effective stress is much bigger for the modelled UBCSand test than for the results from the literature. This indicates that during the modelled test more initial densification happens. Secondly, the first cycles from the cyclic triaxial test from the literature show an inclined stress path in the p'-q diagram while the modelled test results do not show an inclined stress path in the p'-q diagram. The inclined stress path signifies some anisotropic behaviour in the sample. Finally, the literature data shows it reaches a constant cyclic axial strain before it continues to behave in the cone shape. It is not possible to replicate the results better with the UBCSand model, and therefore it shows some of its limitations.

However, the most important properties of the graph are replicated. The tests start with a similar mean effective stress and reaches similar upper and lower limits of the mean effective stress. Also, the amount of cycles needed to reach the cone-shaped behaviour is the same for both tests. Finally, the inclinations of the cone-shaped behaviour are also similar.

The final used parameters in the UBCSand model are shown in table 5.5 for the sand with $D_r = 50\%$ and table 5.6 for the sand with $D_r = 80\%$.

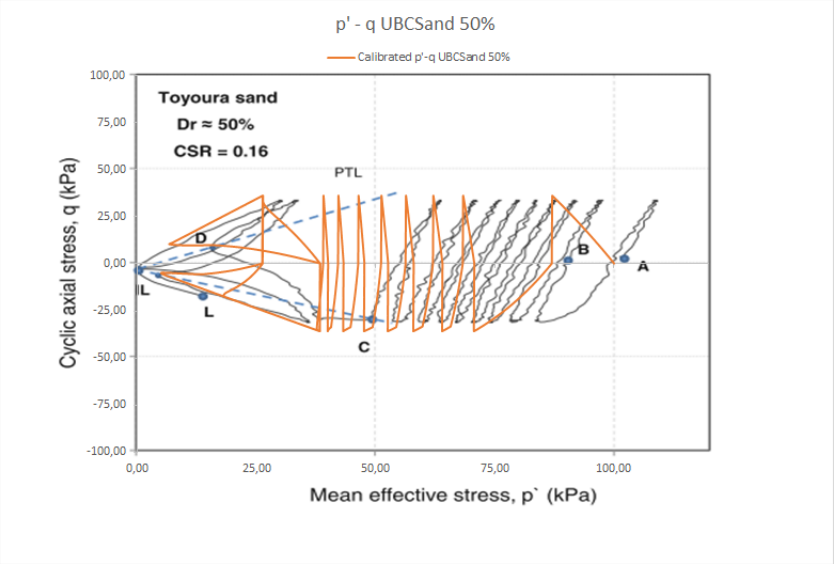

Figure 5.4: Comparison between the p'-q diagram of the literature and the final calibrated parameter set for UBCSand D_r = 50%

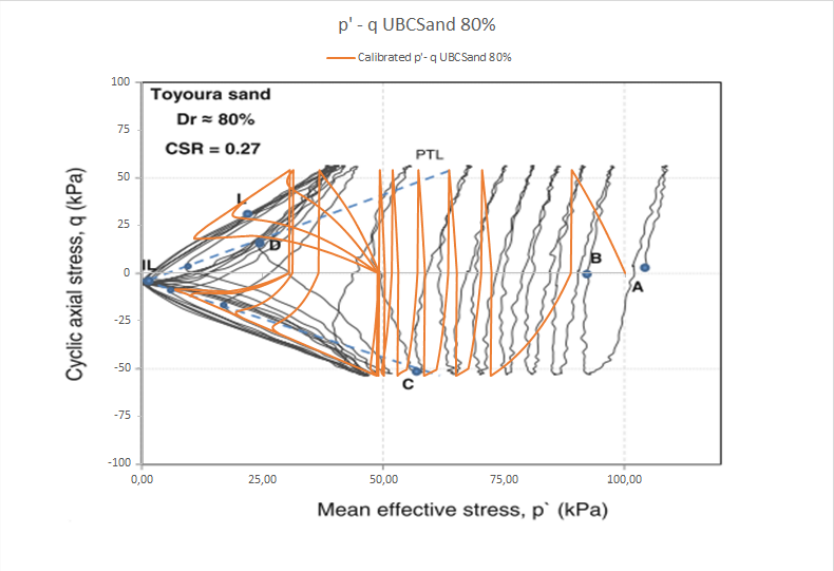

Figure 5.5: Comparison between the p'-q diagram of the literature and the final calibrated parameter set for UBCSand D_r = 80%

Table 5.5: Used parameter values UBCSand model $D_r = 50\%$

K_B^e	685 [-]		f_{dens}	1,00 [-]		c	0,00 kPa
K_G^e	979 [-]		f_{espost}	0,20 [-]		$(N_1)_{60}$	11,50 [-]
K_G^p	612,5 [-]		P_A	100,00 kPa		γ_{unsat}	14,43 kN/m^3
m_e	0,50 [-]		R_f	0,7625 [-]		γ_{sat}	18,77 kN/m^3
n_e	0,50 [-]		ϕ_{cv}	31,33°			
n_p	0,40 [-]		ϕ_p	32,75°			

Table 5.6: Used parameter values UBCSand model $D_r = 80\%$

K_B^e	1350 [-]		f_{dens}	1,00 [-]		c	0,00 kPa
K_G^e	1332 [-]		f_{espost}	0,20 [-]		$(N_1)_{60}$	29 [-]
K_G^p	2550 [-]		P_A	100,00 kPa		γ_{unsat}	15.38 kN/m^3
m_e	0,50 [-]		R_f	0.9 [-]		γ_{sat}	19.36 kN/m^3
n_e	0,50 [-]		ϕ_{cv}	38°			
n_p	0,40 [-]		ϕ_p	41.75°			

5.3.2. Calibration of the PM4Sand Parameters with Simulated Cyclic DSS Test from UBCSand Parameters

The first calibration of PM4Sand parameters has been done by simulating cyclic DSS tests. Instead of performing actual CDSS tests, they have been simulated with Plaxis SoilTets. The simulated CDSS tests are done with the UBCSand parameters that have been determined in section 5.3.1. The results from these simulated tests will be used to calibrate the parameters for the sand modelled with PM4Sand. In Appendix B.1 the results of the simulated CDSS test and the calibrated PM4Sand tests can be found in graphs. The conditions of the CDSS tests and the final PM4Sand parameters are shown in the tables of Appendix B.1. For the calibration it has also been chosen to compare the calibration difference between isotropic and anisotropic tests. This is done because it became clear the built-up of excess pore water pressure for UBCSand and PM4Sand are vastly different when comparing isotropic samples. After investigation it is found that the built-up of EPWP behaves more similar when anisotropic tests are performed, as can be seen when comparing the graphs in figure 5.8 and 5.9 or the graphs in Appendix B.1.

The following observations can be made when comparing the simulated UBCSand tests with the results form the calibration:

- Looking at figure 5.6, which shows the Shear stress - Shear strain comparison between UBCSand and PM4Sand. It can be seen that the UBCSand model reaches the largest strain faster and keeps following the same pattern once the maximum strain is reached. While PM4Sand slowly reaches the desired strain, but the strain will keep increasing with every cycle. There are no significant differences found between the isotropic and anisotropic tests.

- When looking at the stress paths of UBCSand and PM4Sand it becomes clear that the effect of densification is apparent in the UBCSand model, where the change in effective stress becomes smaller after every cycle until failure occurs. This can be seen in figure 5.7. Looking at the difference between the isotropic and anisotropic tests it can be seen that UBCSand shows an initial stiffer response in the anisotropic test. When this is compared to the PM4Sand stress path, it can be seen that PM4Sand also shows the effect of densification. However, this is mainly in the anisotropic tests. For the PM4Sand results, it can also be seen that the loss of effective stress increases during the last few cycles. This is due to the increase in EPWP, which results in the sand losing strength.

- Figures 5.8 and 5.9 show the comparison graphs for the number of cycles- EPWP show a significant difference between the UBCSand model and PM4Sand. UBCSand shows an extreme initial rise in EPWP. When looking at the calibration of the UBCSand parameters in chapter 5.3.1 it suggests that this might be an overestimation of the truth. Looking at EPWP built-up from PM4Sand it looks to almost increase exponentially when ground failure is close. Comparing the results from the anisotropic tests it is clear the EPWP built-up is more similar, although after the initial rise in EPWP, PM4Sand shows a more moderate built-up of EPWP than the UBCSand model.

- Finally, when looking at the number of cycles - strain graph it again can be seen that the UBCSand model reaches the maximum strain faster than PM4Sand and does not increase anymore, while the strain modelled by PM4Sand keeps increasing. This can be seen in figure 5.10

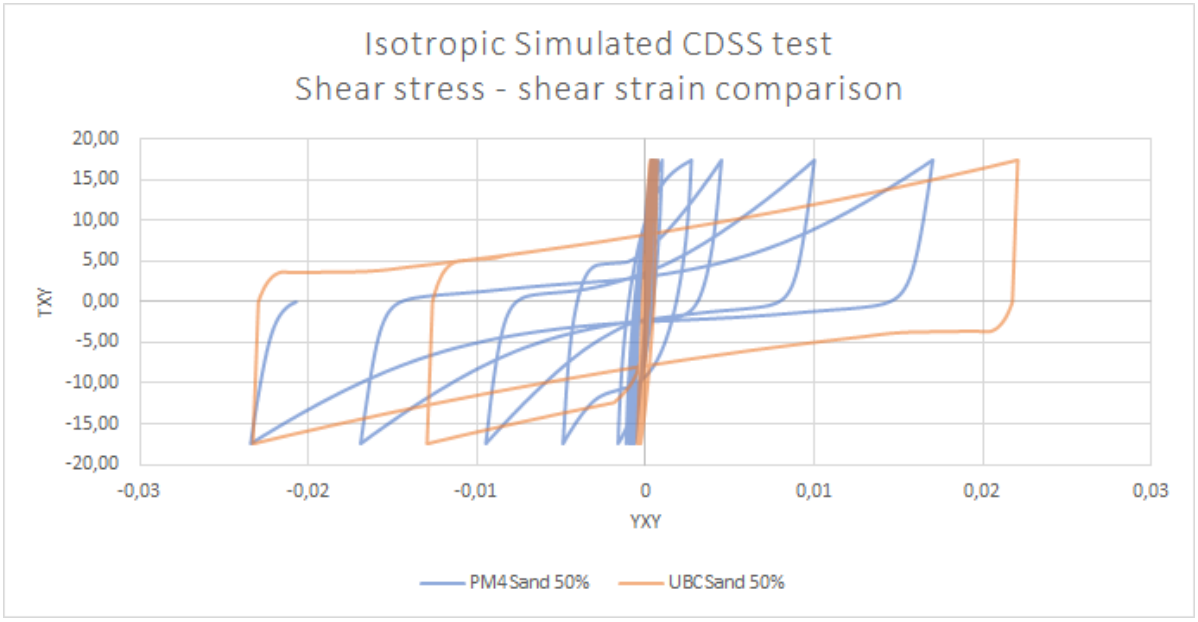

Figure 5.6: Comparison graph showing the shear stress - shear strain relation with UBCSand simulated CDSS test results and the calibrated PM4Sand results for isotropic test with $D_r = 50\%$

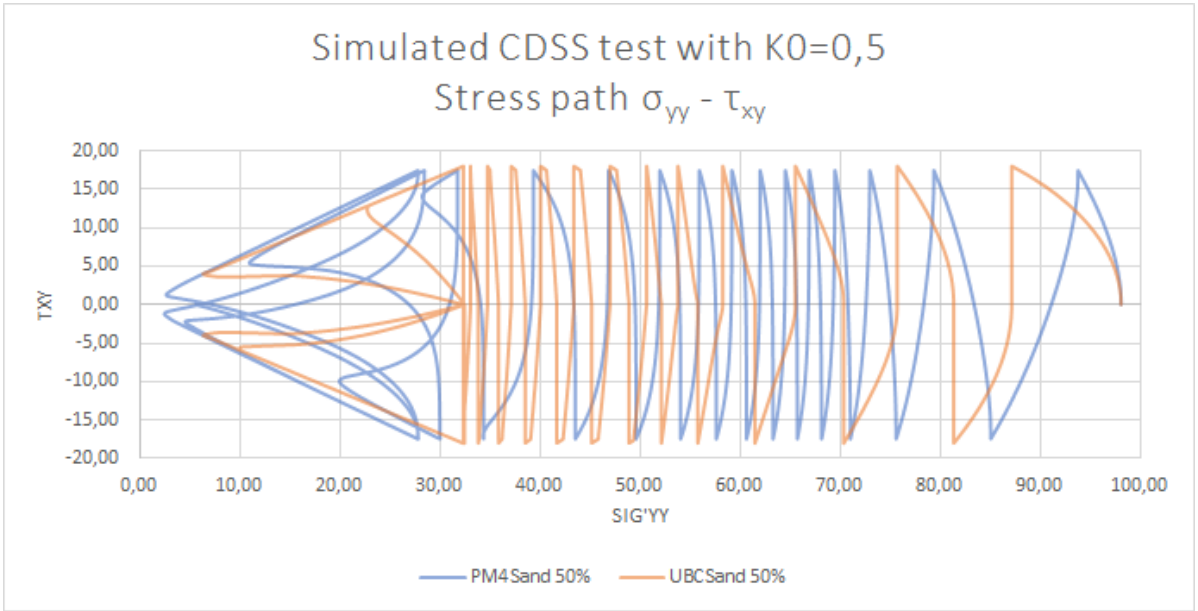

Figure 5.7: Comparison graph showing the stress path with UBCSand simulated CDSS test results and the calibrated PM4Sand results for anisotropic test with $D_r = 50\%$

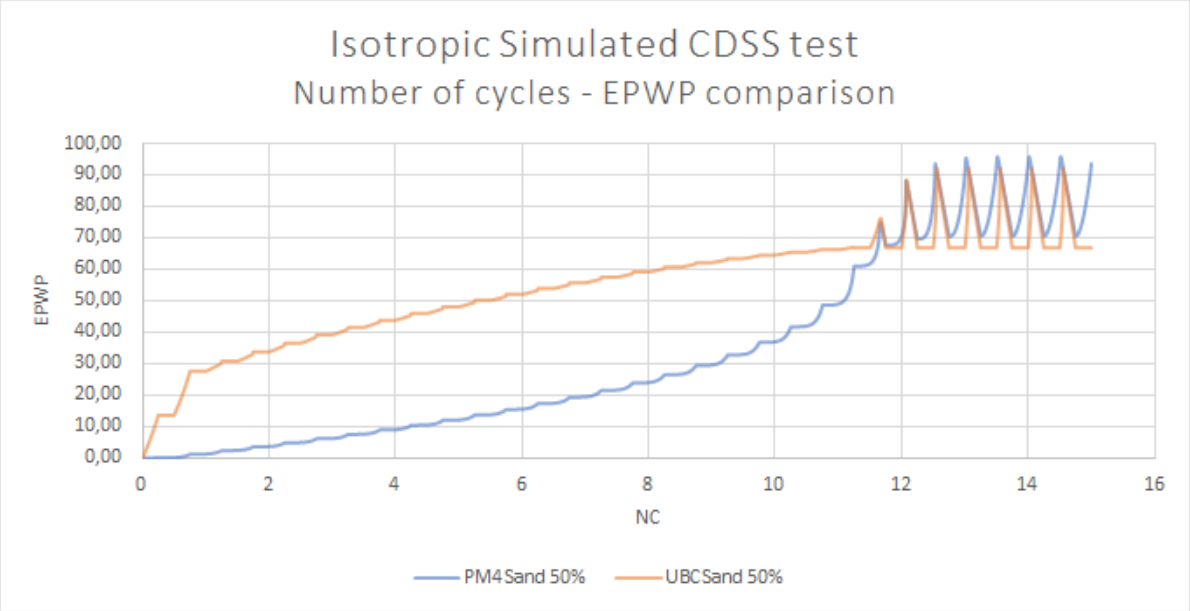

Figure 5.8: Comparison graph showing the number of cycles - excess pore water pressure relation with UBCSand simulated CDSS test results and the calibrated PM4Sand results for isotropic test with $D_r = 50\%$

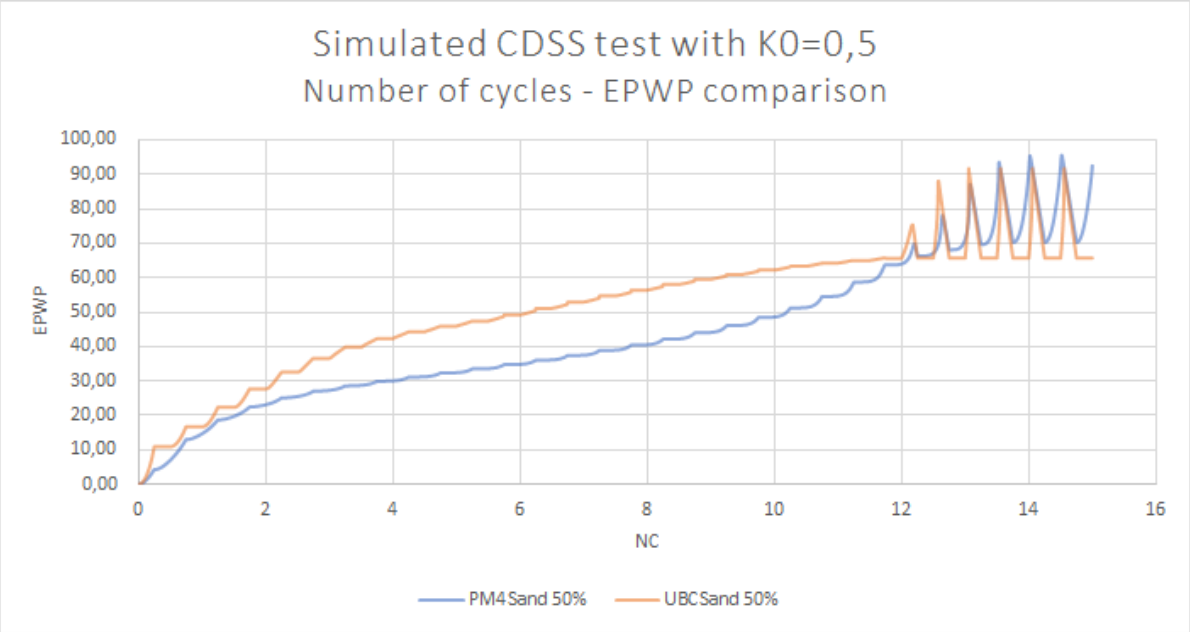

Figure 5.9: Comparison graph showing the number of cycles - excess pore water pressure relation with UBCSand simulated CDSS test results and the calibrated PM4Sand results for anisotropic test with $D_r = 50\%$

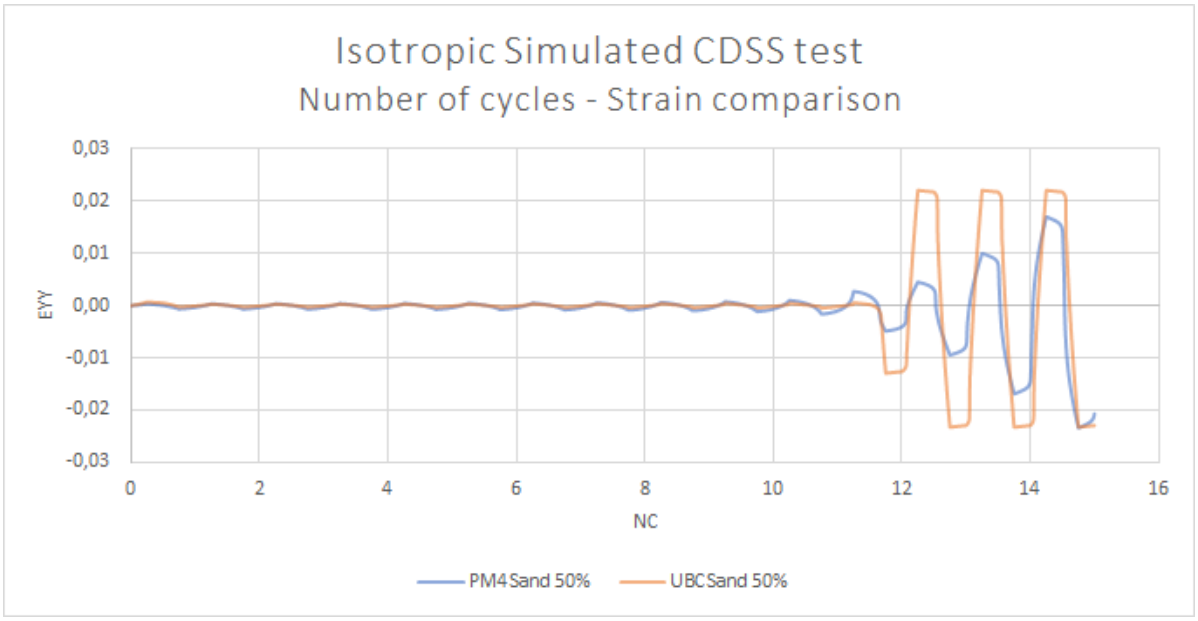

Figure 5.10: Comparison graph showing the number of cycles - strain relation with UBCSand simulated CDSS test results and the calibrated PM4Sand results for isotropic test with $D_r = 50\%$

5.3.3. Calibration of the PM4Sand Parameters with Cyclic Torsional Shear Tests

The calibration of the PM4Sand parameters with the cyclic torsional shear test gives a similar response as can be seen in the previous section 5.3.2. In Appendix B.2 the used test specifications are shown in the tables, as well as the final parameters and the figures that give the response of PM4Sand with the calibrated parameters.

5.4. Sensitivity of PM4Sand Calibrating Parameters

To investigate the sensitivity of the PM4Sand parameters a qualitative sensitivity analysis has been done. For each of the PM4Sand parameters, it has been investigated what happens if a parameter is increased or decreased looking at the same graphs as used for the calibration of the PM4Sand parameters. So for each parameter, their effect on the shear stress, shear strain, stress path, excess pore water pressure and the number of cycles to liquefaction is investigated. The results are put in tables and can be found in the Appendix C. However, the most important observations are as follows:

- The relative density, D_r, influences all investigated behaviour. Therefore the D_r influences the shear stress, shear strain, stress path, excess pore water pressure and the number of cycles to liquefaction.
- The shear modulus coefficient, G_0 only has a significant influence on the strain in the model.
- Similar to the D_r, the contraction rate parameter h_{p0} influences all investigated behaviour. The h_{p0} influences the shear stress, shear strain, stress path, excess pore water pressure and the number of cycles to liquefaction.
- Changing the minimum and maximum void ratios does not show significantly influence to any of the investigated behaviours.
- The bounding and dilatancy surface parameters, n^b and n^d, influences the amount of strain accumulated, the stress path and the number of cycles to liquefaction.

5.5. Conclusion

In the Calibration chapter, the predetermined parameters for UBCSand and PM4Sand are presented. Thereafter the final calibration of the UBCSand model and PM4Sand are given.

It can be seen that the initial EPWP is higher when calibrating the UBCSand parameters and accumulation of strain was found. When looking at the calibrations for the PM4Sand parameters it can be seen the desired strains are reached less quickly compared to the UBCSand parameters. Also the strains keeps increasing with each cycle when using PM4Sand. For both the UBCSand model and PM4Sand densification effects are seen, while PM4Sand also shows a loss of effect stress during the last few cycles due to an increase in EPWP. Comparing the EPWP built-up between the UBCSand model and PM4Sand shows an extreme initial rise in EPWP for the UBCSand model, while the EPWP for PM4Sand rises quickly when it closes failure. When looking at the EPWP for anisotropic soil it can be seen that UBCSand and PM4Sand are more similar.

Finally, a sensitivity analysis has been done for the PM4Sand parameters, showing which adjustment to which parameter results in what kind of behaviour in certain graphs.

6

Details of the Numerical Model

The numerical model used in this research was created in Plaxis. The model has been designed in such a way that it is comparable to the centrifuge test done by Chaudhary and Hazarika (2018). This chapter will go into the details of the numerical model, discussing the dimensions, mesh, boundary conditions and calculation set-up used. The calibration of the soil layers has been done in chapter 5 and the used values for the soil properties can be found in that chapter and Appendix B. For this research one numerical model has been used and only the soil properties have been changed.

6.1. Dimensions of the Numerical Model

The dimensions given to the numerical model resemble the dimensions of the centrifuge test. Figure 6.1 gives the dimensions of the soil box used in the centrifuge test. The dimensions of the rubble mound, caisson, the height of the soil layers and water level in the numerical model have the same values as shown in figure 6.1. Figure 6.2 shows the numerical model in Plaxis. Comparing these figures shows that the soil bed in Plaxis is far wider than the soil bed in the centrifuge test. This is done because the sides of the soil bed will deform when running the simulations. To make sure the deformations do not influence the stability calculations of the breakwater the soil bed has been made wider. Results of these deformations can be seen in Appendix D. It can also be seen that the far outer parts of the soil bed have a different colour. This colour means it is modelled with another sand. To make the model run when the soil is defined by PM4Sand it needs drained soil at its x-axis boundaries, which is done for the numerical models. The dimension of the middle block of the soil bed is the same as in the centrifuge test at 385mm and on both sides, the soil bed is extended with 260mm of soil with the same properties. Finally, a slice of 40mm drained soil has been added to both ends of the soil beds.

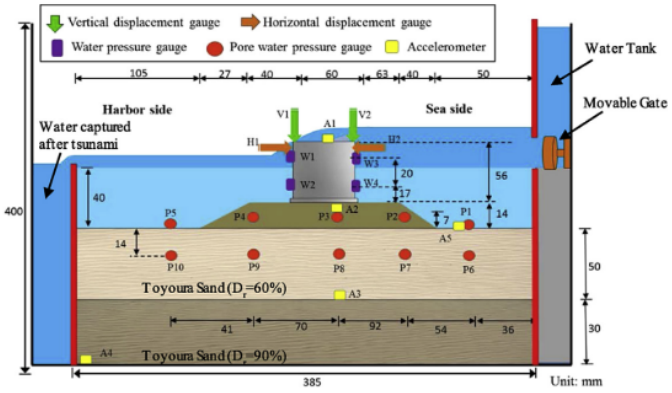

Figure 6.1: An overview of the soilbox dimensions used in the centrifuge test (Chaudhary & Hazarika, 2018)

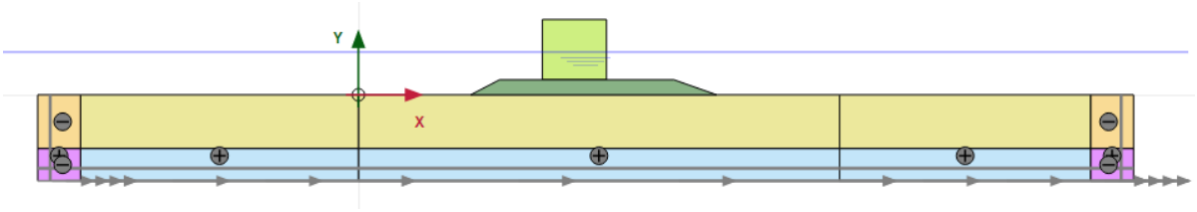

Figure 6.2: Overview of the Numerical model in Plaxis

6.2. Mesh of Numerical Model

The mesh of the numerical model determines the error in the results of the numerical model and the needed calculation time. It is important to find a good ratio between the calculation time and the error in the results. For the earthquake signal, a certain mesh size is needed, which is calculated in section 7.1.1. This value is taken as the maximum size for one element of the mesh.

The mesh used for the numerical model is shown in figure 6.3. A very coarse mesh is used for the caisson and the outer parts of the soil bed. The caisson can have a coarse mesh because it does not deform. The results of deformation in the outer parts of the soil bed are not used in this research and can, therefore, contain an error. A courser mesh at this part of the numerical model results in a quicker calculation time.

Looking at the centre of figure 6.3 it can be seen that the mesh underneath the caisson and rubble mound is the finest and getting more course with increased distance from the center of the model. This is because a small margin of error is desired, while the calculation time is not too much. With an iterative process, this mesh was determined to be the most suitable for the numerical model. The mesh exists of 392 elements and 3392 nodes.

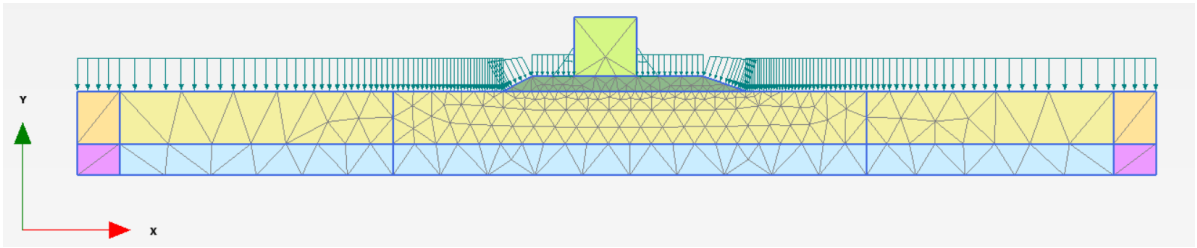

Figure 6.3: The mesh defined in the numerical model

6.3. Calculations Set-up of the Numerical Model

The numerical model in Plaxis has six calculation phases. All phases are shown in figure 6.4. The first three phases are to set-up the structure in the model, by first defining the soil bed, thereafter building the rubble mound on the soil bed and finally building the caisson on top of that. The last three phases are the different earthquakes the breakwater is subjected to. These three earthquakes are modelled as if no prior forces are exerted on the breakwater.

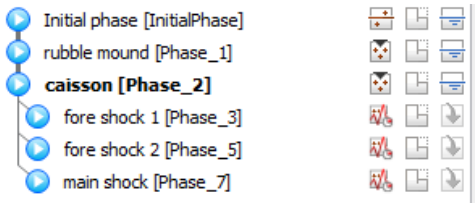

Figure 6.4: The six calculation phases used in Plaxis

Mainly the default calculation settings of Plaxis are used. Table 6.1 shows the adjusted settings for different phases. The weight has been adjusted to model the 25g of the centrifuge test. The time interval has been adjusted to the input signal for the earthquakes as well as the max time steps. The number of sub steps have been set equal to the suggested number of sub steps by Plaxis.

Table 6.1: Calculation settings used for the numerical model in Plaxis

Phase/setting	*Calculation type/value*
Initial phase	K0 procedure
$\sum M_{weight}$	25.0
Rubble mound & caisson	Plastic
$\sum M_{weight}$	25.0
Fore shock 1, 2 & main shock	Dynamic with consolidation
Dynamic time interval	1,375 s
Reset displacement to zero	On
Reset small strain	On
Max time steps	913
Number of sub steps	419
In case PM4Sand is used	cavitation cut-off on & cavitation stress at 100 kN/m^2

6.4. Boundary Conditions of the Numerical Model

In the numerical model also some boundary conditions have been changed. The following conditions are different from the default or worth noting:

- deformation X boundary: normally fixed. The sides of the soil box are static and therefore should be modelled similar;
- deformation Ymin boundary: fully fixed. The bottom of the soil box cannot deform, so this boundary has to be fixed;
- dynamic X boundary: Free-field. Reflection of the earthquake signal at the sides of the model is not desired, therefore the free field boundary condition has been chosen;
- dynamic Ymin boundary: compliant base. This is the best way to model the dynamic Ymin boundary. It limits reflection at the bottom of the model;
- dynamic Ymax boundary: none;
- groundwater flow: Ymax open, Ymin and X boundary closed. These boundary conditions are chosen because water can only escape through the top of the soil.

6.5. Conclusion

In this chapter the details of the numerical model have been given. The chosen dimensions of the numerical model as well as the reason why the soil bed has been widened. The chosen mesh has been discussed, as well as the calculation set-up and the boundary conditions

7

Incorporating Earthquake Signal in Plaxis

In this section, it is explained which earthquake signal is used for modelling the centrifuge test and how this signal is checked to be correct. Firstly, details and problems of adding the signal to Plaxis will be discussed. Next, the generation of the mesh and step selection will be reviewed. Finally, it will be explained how the signal is checked for correctness with the help of a 1D site response analysis. The step by step assessment of the 1D site response analysis can be found in Appendix A.

7.1. Input of the Earthquake Signal in Plaxis

As shown in table 4.1 and figure 4.4 the earthquake signal used in the centrifuge test is an acceleration as a sinusoidal function. Where the amplitude of the signal is given by the acceleration and the period is given by time in seconds. Two different ways of modelling the earthquake signal have been investigated. Making the Plaxis input signal as an acceleration signal and modelling the earthquake as a displacement signal.

The problem with using an acceleration input signal is that after being exposed to the earthquake the displacement of the structure does not revert to zero, but the whole structure ended up being moved out of place. This is an undesired outcome because in the centrifuge test the final displacement is zero. Plaxis has a function called 'drift correction' to adjust for this phenomenon, but it alters the signal and is therefore not desirable. That is why an attempt was made to convert the signal to a displacement signal. With the proper integration the displacement signal should result in the desired acceleration signal. This did not work because the internal integration in Plaxis was too complicated. Plaxis uses an implicit time integration of Newmark, which is difficult to use and convert analytically. Therefore the choice was made to use an acceleration signal as input for the earthquake in Plaxis. This means that the drift correction from Plaxis is used.

The input signals for Plaxis are inserted with tables. These tables consist of the points relating to the sinusoidal function. One sine wave is divided into 8 points and has the described attributes from table 4.1. Because the time steps are very small, the final point can't end precisely on 1,4 seconds. Therefore the centrifuge test earthquake signal of 83Hz has a length of 1,375 seconds and the prototype earthquake signal of 0.66Hz has a length of 187,5 seconds.

To properly model the earthquake signal it is necessary to make use of a gradual increase of the earthquake signal from the start. Increasing the acceleration bit by bit until the desired amplitude is reached. An example of this can be seen in the first 0.2 seconds of the earthquake signal in figure 7.1.

7.1.1. Number of Steps and Mesh Size for Generating a Earthquake Signal

In Plaxis two important things need to be done to make sure an earthquake signal travels correctly through the system. The mesh size and the max steps assigned in the numerical control parameters need to be chosen correctly. Kuhlmeyer, R.L., Lysmer (1973) suggest to assume a size less than or equal to one-eight of the wavelength associated with the maximum frequency component f_{max} of the input wave (Laera & Brinkgreve, 2015). The formula for the average element size is as follows:

$$AverageElementSize \leq \frac{\lambda}{8} = \frac{V_{s,min}}{8 f_{max}} \tag{7.1}$$

With $V_{s,min}$ is the lowest wave velocity and f_{max} is the maximum frequency component from the Fourier spectrum.

The values used for the calculations of the average element size and the results are shown in table 7.1.

Table 7.1: Used values to calculate the average element size of the Plaxis mesh

D_r	$V_{s,min}$	f_{max} 83 Hz earthquake	f_{max} 0,66 Hz earthquake	Average element size 83 Hz	Average element size 0,66 Hz
80%	250	83	0.66	0.38 m	47,35 m
50%	140	83	0.66	0.21 m	26,52 m

The values chosen for the max steps assigned in the numerical control parameters are straight forward, but very important. The input of the earthquake signal is a table created with values for the time versus the amplitude. The value that needs to be chosen for the max step is the number of input rows minus one. If another value is chosen, Plaxis will not take the time steps suggested from the data, but interpolate between the given data to match it own chosen data.

7.2. 1D Site Response Analysis for the Earthquake Signal

To check if the desired earthquake signal converted in the desired way to Plaxis a 1D site response analysis has been done. For this site response analysis, a small column of soil is created in Plaxis so that the horizontal length coincides with the required element length and the vertical dimension is equal to the thickness of the soil deposit (Laera & Brinkgreve, 2015).

The complexity of the numerical model for this 1D column is increased step by step until the desired earthquake signal is modelled. The full workout of this process can be found in Appendix A. Following are the most important steps taken:

- model the soil as linear elastic;
- model the 1D column with a compliant base boundary;
- increase the number of data points in the earthquake signal;
- model the soils with UBCSand and PM4Sand;
- add damping to the soil properties;
- check response with the drift correction function.

An example of the results of an earthquake signal through the 1D column is shown in figure 7.1. This graph shows the final earthquake signal throughout the 1D soil column modelled with PM4Sand, a compliant base boundary at the bottom of the column and damping incorporated in the soil properties. Each coloured line is the behaviour of the earthquake at a different point in the 1D column.

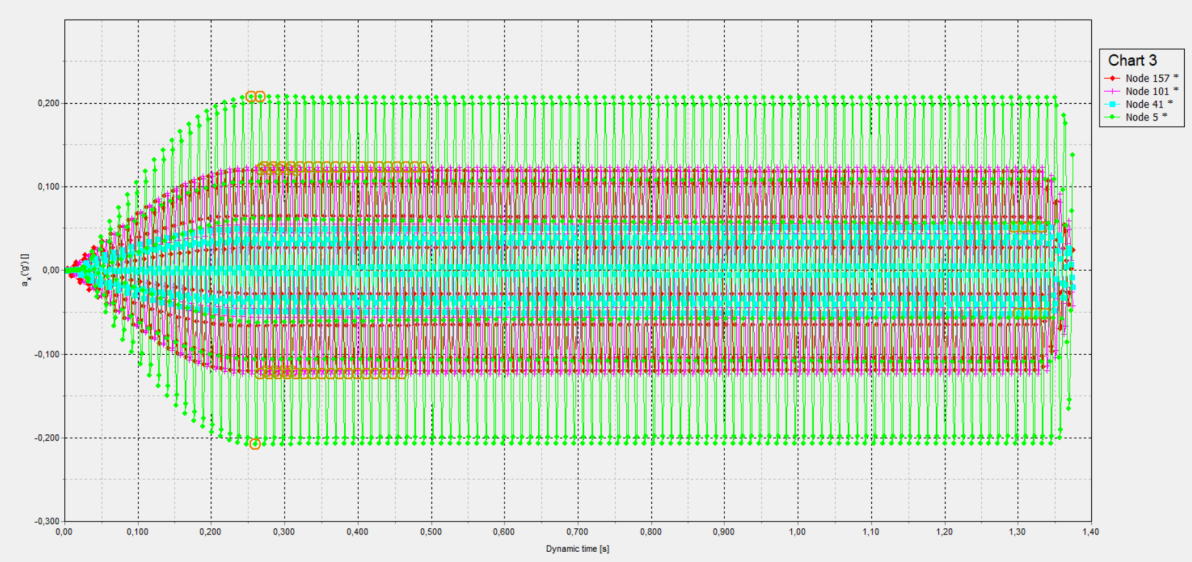

Figure 7.1: Earthquake signal through the 1D column for a two layered column modelled with PM4Sand, damping and a compliant base boundary (3/3)

During the research, the following outcomes have been found:

- In the 1D soil column, the acceleration of the signal becomes smaller at 2/3 the length of the column and increases at the top of the column
- The compliant base boundary results in an earthquake signal through the 1D column with less interference. The signal throughout the column looks more like the starting signal.
- The earthquake signal with more input points gives the signal a lower amplitude at the bottom of the column and a higher amplitude at the top of the 1D column. The shape is the same.
- Using no damping and no compliant base boundary combined with a UBCSand soil gives an interference in the earthquake signal and results in the earthquake signal that diverges from the input signal
- Throughout the tests it became clear that the earthquake signal through the 1D column has a higher amplitude than the input signal, except at 1/3 of the column.
- Adding damping to the UBCSand soil resulted in an earthquake signal with a lower amplitude.
- The use of no compliant base boundary combined with PM4Sand resulted in an incorrect transfer of the earthquake signal, where a signal with almost no amplitude travels through the 1D column.
- Using damping and a compliant base boundary for a 1D column with a PM4Sand modelled soil column results in a similar earthquake signal through the column as when modelled with UBC-Sand. Only the amplitude of the signal is higher, in the final situation around 25% higher.
- Using the drift correction function from Plaxis results in a very small shape change that does not look to be significant.

7.3. Earthquake with Consolidation

After running some simulations of the centrifuge test in Plaxis a problem arose. The resulting excess pore water pressure from the Plaxis simulations gave unexpected results. As can be seen in figure 7.2 a spotty behaviour was shown with high positive and negative EPWP. This does not give a clear representation of reality. To solve this, dynamic calculations with consolidation are done in Plaxis when applying an earthquake load on the soil body. This means that the soil can consolidate when the earthquake is happening. Using this calculation method resulted in more gradual changes of EPWP through the soil body as can be seen in figure 7.3

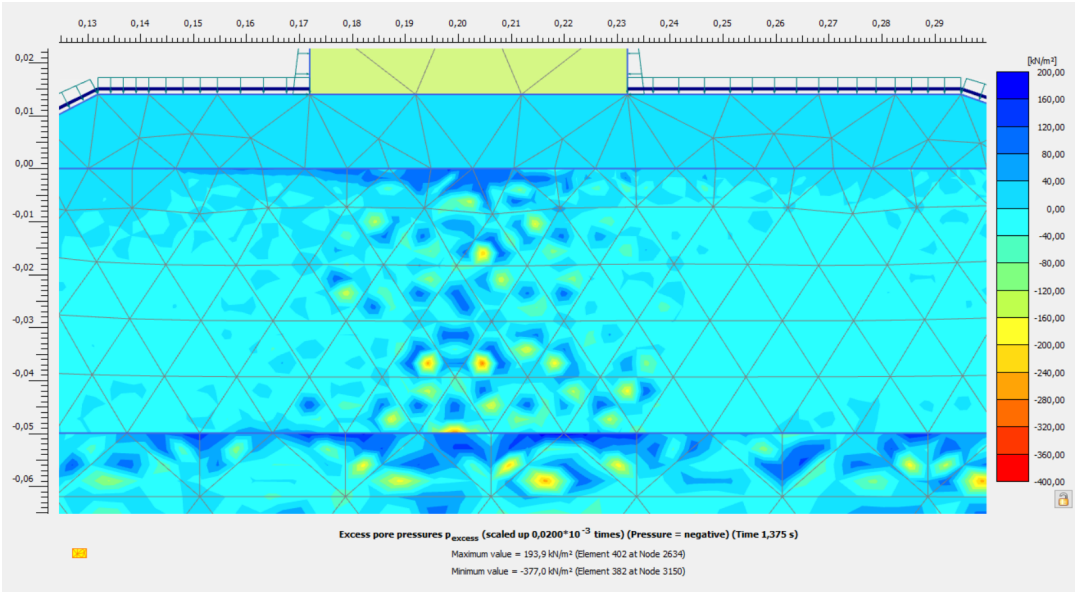

Figure 7.2: EPWP under the caisson after a dynamic calculation generated with Plaxis for a sand with a relative density of 60% and modelled with PM4Sand

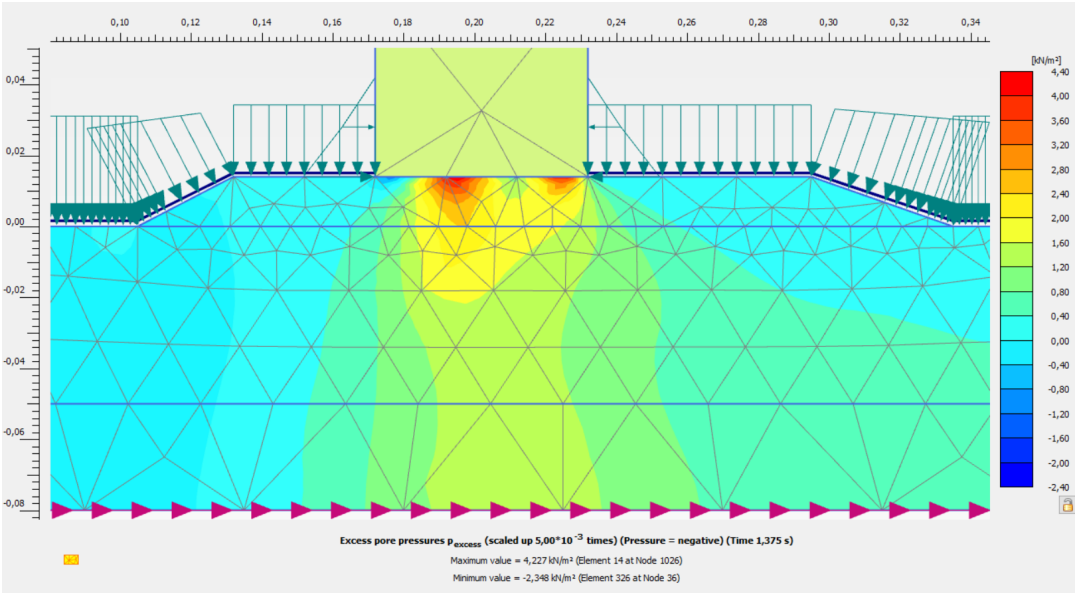

Figure 7.3: EPWP under the caisson after a dynamic with consolidation calculation generated with Plaxis for a sand with a relative density of 60% and modelled with PM4Sand

When using the dynamic with consolidation calculation type it is necessary to know the permeability of the Toyoura Sand. From Ishikawa and Yasuda (2012) a value of $3.0 * 10^{-4}$ m/s for the permeability has been taken. Figure 7.4 shows the results found for the EPWP and consolidation in during the centrifuge testing. It can be seen that for all three shock waves the EPWP after 30 seconds is around 1/3 of the maximum EPWP value. Using the permeability found by Ishikawa and Yasuda (2012) almost immediately results in the dissipation of the EPWP after the earthquake ended. With an iterative process, it was found that a permeability of $1.76 * 10^{-8}$ m/s gives a dissipation of EPWP that resembles quite well. Due to time constraints, further iteration of the permeability value has not been done. An example of the EPWP dissipation is shown in figure 7.5. This figure shows the cyclic behaviour when the earthquake is happing. After the earthquake stops it can be seen the EPWP keeps slightly rising, before it starts dissipating. This rise could occur because there are still forces or movement in the ground that built up EPWP.

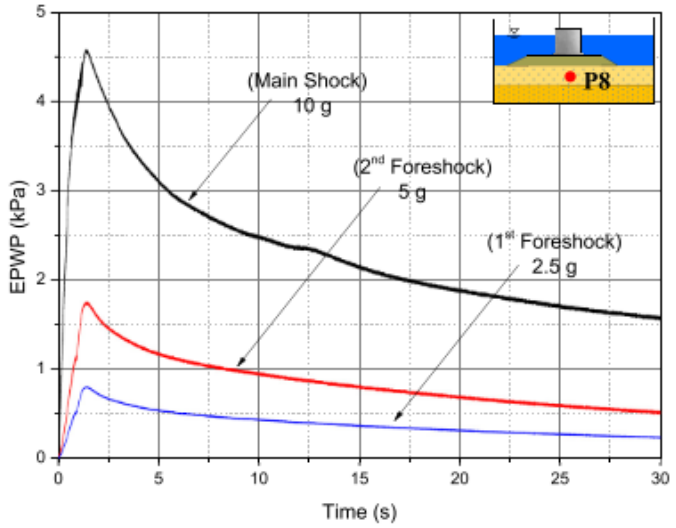

Figure 7.4: EPWP under the caisson for each shock wave during the centrifuge experiment

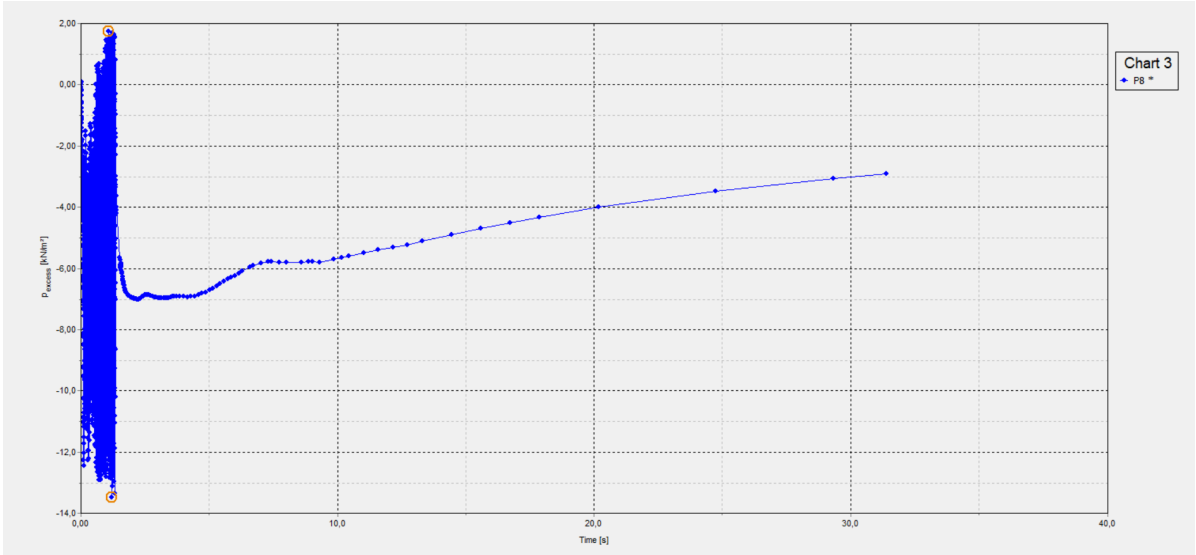

Figure 7.5: EPWP under the caisson for sand with a relative density of 50% and modelled with UBCSand

7.4. Rayleigh Damping

All plasticity models can generate irreversible (plastic) strains which may cause damping. However, this damping may not be enough to realistically portray the damping characteristics of the soil. When additional damping is needed in dynamic calculations this can be done by applying Rayleigh damping (Technology & Jose, 2008). In Plaxis a damping ratio (ξ) and two target frequencies are used to calculate the Rayleigh parameters α and β. It is suggested to choose the first target frequency as the first natural frequency of the soil deposit and the second target frequency as the closest odd integer number of the predominant frequency of the input motion (Technology & Jose, 2008). The natural frequency of the soil deposit can be calculated with the following formula:

$$f_1 = \frac{v_s}{4H} \tag{7.2}$$

with v_s = shear wave velocity in the deposit and H = the thickness of the soil deposit. The natural frequency for the Toyoura sand with a relative density of 50% is 3.11 Hz and for 80% is 9.26 Hz.

The predominant frequency can be found by looking at the Fourier spectrum. Since the earthquake signal only consists of one frequency, this is the frequency from the Fourier spectrum. In this case it is 83 Hz on centrifuge scale and 0.66 Hz on prototype scale. As mentioned in chapter 4.4 the damping used by Chaudhary and Hazarika (2018) for numerical modelling was 5%. Using this damping ratio resulted in a much larger settlement of the caisson than found with the centrifuge test. Therefore the damping ratio was adjusted and a damping ratio of 10% gave a settlement similar as found with the centrifuge test.

7.5. Conclusion

To determine the right input earthquake signal, a 1D site response analysis is done. It is found the amplitude of the signal should be slowly increased, till the desired amplitude to get a correct earthquake signal. Also, the use of the compliant base boundary and Rayleigh damping improves the behaviour of the earthquake signal. It is also found that using the drift correction function does not significantly influence the earthquake signal.

When assessing the excess pore water pressure in the final Plaxis models a spotty behaviour became visible. To give a smoother EPWP result the dynamic calculation phase is changed to dynamic with the consolidation phase.

Finally, the determination of the Rayleigh damping has been discussed, which showed the frequency from the Fourier spectrum should be 83 Hz on centrifuge scale.

8

Validation of PM4Sand for Liquefaction under Breakwaters

In this chapter, the results of the numerical models will be discussed. Firstly, the results for numerical models with centrifuge dimensions are analysed and thereafter the results for the numerical models at prototype dimension. For both dimensions, the results of the numerical models contain deformations of the total system, the settlements of the caisson and the EPWP in the sand underneath the caisson. Figures of all results can be found in Appendix D.

8.1. Numerical Model Results with Centrifuge Dimensions

In the numerical models on centrifuge scale the gravity is set at 25g. This makes the numerical model behave similarly as in the centrifuge tests. The results of this numerical model will be discussed, focusing on the settlements, deformations and EPWP.

8.1.1. Settlement Results

A summary of the settlements from each run numerical model can be found in table 8.1. As explained in chapter 5 the soils are calibrated with different methods and for different relative densities. To separate the different modelled soils they have been given abbreviations. Where the 50, 60 or 80 determines the relative density of the sand layer. For the PM4Sand models an indication is given for which calibrated parameter set is used. CDSS means the parameters from the calibration based on the simulated UBCSand CDSS test are used. TST means the parameters from the calibration based on the Torsional Shear Test are used. Finally, Iso means the isotropic calibrations are used, while Aniso means the anisotropic calibrations are used. V1 is positioned at the top left of the caisson and V2 is positioned at the top right of the caisson. The given settlements are the downward displacements of V1 and V2, so u_y.

Table 8.1: Settlement results of the executed Plaxis models

Settlement results of Models				UBCSand		PM4Sand						
Measurement position	Earthquake type	Unit	Centrifuge tests	UBC50	UBC80	CDSS 50 iso	CDSS 80 iso	CDSS 50 Aniso	CDSS 80 Aniso	TST 50	TST 60	TST 80
V1	1st foreshock	mm	3,5	5,3	4,1	2,9	0,75	3,1	0,8	2,5	3,8	1,2
	2nd foreshock	mm	7,4	10	9,4	13	11	19	10	15	19	4,3
	Main shock	mm	22,6	25	21	22	24	28	23	30	27	26
V2	1st foreshock	mm	2,4	5,8	5,3	2,4	0,75	3,4	0,8	3,4	3,5	1,2
	2nd foreshock	mm	5,4	8,7	8,9	9,9	5,1	9,7	6	5,2	1,3	2,7
	Main shock	mm	15,8	21	20	14	3,3	14	5,8	10	24	11

When looking at the results it can be seen that the settlements are of the same magnitude as the found results of the centrifuge tests, however, some specific settlements can be up to more or less 100%. The results from the UBCSand simulations show the settlements are similar to the found settlements in the centrifuge test. However, during the centrifuge test, the caisson seems to tilt more compared to the UBCSand simulations.

The results from the numerical models that used PM4Sand to model the Toyoura Sand give diverse results. This is understandable since different methods have been used for the calibrations. Firstly, modelling with PM4Sand seems to simulate the final tilt of the caisson after the main earthquake shock better than UBCSand. When looking at all results the simulation with a sand of relative density 50% and modelled with PM4sand parameters calibrated by the simulated CDSS test are closest to the results found during the centrifuge test. Because CDSS tests are the preferred way of simulating the PM4Sand parameters this makes sense. The settlements occurring with anisotropic PM4Sand calculations are higher compared to the isotropic PM4Sand calculations. This can be explained by looking back at chapter 5, where was found that the anisotropic calibrations resulted in less densification and higher initial EPWP. The results of the numerical models that run with the parameters calibrated with the Torsional shear test seem to give a higher displacement than found with the centrifuge tests. While the tilt of the caisson differs depending on the relative density of the sand.

8.1.2. Excess Pore Water Pressure Results

The results found for the EPWP built-up in the soil bodies during the Plaxis simulations are different from the results of the centrifuge test. The results from the centrifuge test are shown in figure 8.1, which shows a steady, almost linear built-up of EPWP till the end of the shock wave after 1,4 seconds. When looking at figure 8.2 a very distorted signal can be seen, with some small EPWP built-up in the first 0.15 seconds where after the EPWP bounces between a positive and negative value. This behaviour is not expected and does not represent the behaviour that occurs in real-life situations.

To find a better EPWP response several changes to the model have been made with different results. They are listed below:

- The mesh has been changed from fine to very fine. This resulted in extreme long calculation times and larger displacement but did not significantly improve the EPWP response.
- The mass matrix has been set to 1 instead of zero. This resulted in increased calculation times, larger displacements and a more unstable earthquake signal throughout the system. However, the behaviour of the EPWP built-up did not change significantly.
- Applying numerical damping to the model made the earthquake signal more stable, but did not improve the EPWP built-up.
- Increasing the number of input points for the earthquake signal resulted in a higher displacement and higher EPWP, but not a better EPWP built-up.
- Decreasing the earthquake amplitude by a factor 10 gives a better EPWP built-up through the soil body. The result of EPWP built-up in the sand underneath the caisson for an earthquake with an amplitude of 0.25g is shown in figure 8.3. This figure is showing an EPWP built-up more similar to the centrifuge results. However, there are almost no displacements in the model when using an earthquake with this amplitude.

It is clear the EPWP behaviour from the Plaxis models does not give the correct response and further investigation is needed.

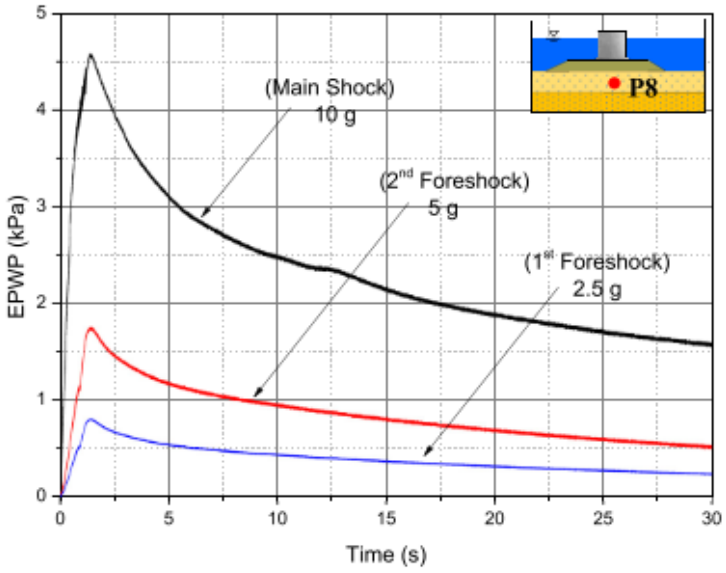

Figure 8.1: EPWP under the caisson for each shock wave during the centrifuge experiment

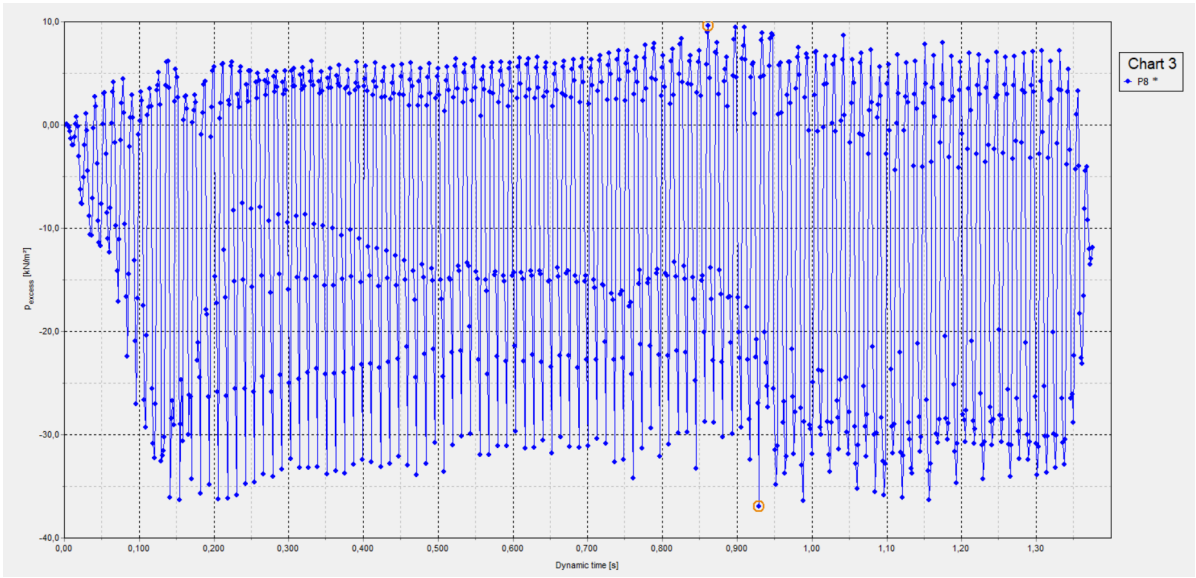

Figure 8.2: EPWP built-up during the main earthquake shock, an amplitude of 10g, in the soil body modelled with UBCSand at a relative density of 50%

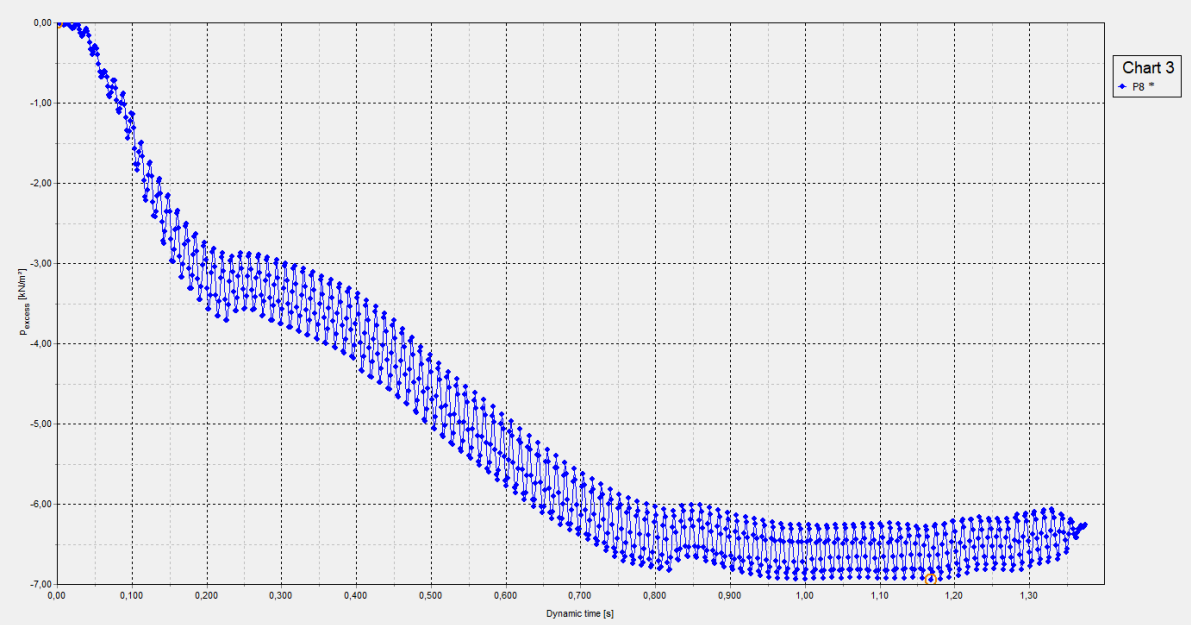

Figure 8.3: EPWP built-up in the soil underneath the caisson modelled with UBCSand, $D_r = 50\%$ and the maximum amplitude of the input earthquake at 0.25g.

8.2. Numerical models with prototype dimensions

In an attempt to gain more insight about the difference between modelling sandy soils with UBCSand and PM4Sand several numerical models with prototype dimensions were created and run. The same calibrated soils parameters are used for the centrifuge dimension, except for the Rayleigh damping. The Rayleigh damping is different because the earthquake signal and dimensions are different and therefore the Rayleigh damping parameters have been adjusted.

When looking at the deformation and settlements results in Appendix D.2 it is clear that the breakwater modelled with UBCSand fails. However, the breakwater modelled with PM4Sand seems to behave stiffer than the results found at centrifuge scale. This suggest that the parameters calibrated for PM4Sand are less affected by the amount of initial stress chosen during laboratory tests than for UBCSand. Since the initial stress of the breakwater is far higher with prototype dimensions it could be that the laboratory tests need to be adjusted to get proper calibrations. Another option is that the initial static shear stress in the model was too big, which resulted in the UBCSand model underestimating the CRR and resulted in extreme deformations.

The EPWP results from Appendix D.2 show a spike in the first 30 seconds of the simulation. After that the built-up of EPWP slowly increases. For the breakwater modelled with PM4Sand, the EPWP built-ups for foreshock 1 and foreshock 2 give positive EPWP, which would suggest suction. Similar to the EPWP built-up for the Plaxis models with centrifuge dimensions the behaviour does not seem correct and needs further investigation.

8.3. Conclusion

The results found in this section make it difficult to validate the use of PM4Sand as a model for calculating the behaviour of sandy soil up to liquefaction under breakwaters. We can see that PM4Sand gives comparable findings for the deformation and settlement of the breakwater. These results are closer to the outcome from the centrifuge test than the results from the Plaxis models with UBCSand. However, the behaviour of EPWP built-up modelled with UBCSand or PM4Sand does not corresponds to the expected results from the centrifuge test.

9 Discussion

During this research, several limitations are found and some assumptions have been made. In this chapter, these limitations and assumptions are presented. Furthermore, some points of discussion are included to take into account when continuing with this research.

9.1. Limitations

Some of the limitations encountered during this research are as follows:

- The amount of available data on liquefaction under breakwaters due to earthquakes is very limited.
- There was no CDSS data available for Toyoura Sand at the time, which matched the properties of the Toyoura Sand used in the scaled laboratory test.
- To scale the centrifuge test to the desired dimensions, Chaudhary and Hazarika (2018) used a method called virtual scaling. This makes scaling of the centrifuge results back to prototype scale a complicated process. More information is needed concerning the assumptions made in order to properly calculate the dimensions and soil properties at prototype scale.
- The used earthquake signal in the centrifuge test looks very different from common earthquake signals encountered in the field.
- Measuring EPWP at the exact desired location is very difficult.
- The calculation time of dynamic calculations in numerical models can become very time-consuming.

9.2. Assumptions

During this research the following assumptions are made:

- The rubble mound can be modelled in Plaxis with the Mohr-Coulomb model as a drained material.
- Laboratory results of Cyclic Triaxial Tests can be converted to Cyclic Direct Simple Shear tests with Plaxis Soil Test
- The results from a cyclic Torsional Shear Test are comparable with a Cyclic Direct Simple Shear tests.
- The initial static shear stress in models did have a major effect on the outcome of the used constitutive models models.

9.3. Points of Discussion

Some aspects of this research need to be discussed. In this section, some of the most important points of discussion are elaborated on.

9.3.1. Available Literature

When searching for literature covering cases of failing breakwaters due to earthquakes with enough available data on displacements and EPWP built-ups in the ground to model it in a numerical model, none have been found. Therefore, literature about scaled laboratory tests on failing breakwaters during earthquakes has been used. When looking for these scaled laboratory tests only a few results have been found. However, those results lack information on soil properties, deformations or EPWP to accurately model the tests with PM4Sand in a numerical model.

This resulted in the need to creatively acquire similar data as described in the literature. Therefore Cyclic Triaxial test and Cyclic Torsional Shear tests were taken from other literature sources to be able to calibrate the parameters for the numerical modelling. Ideally, a centrifuge laboratory test would be designed and executed with modelling the results in a numerical model in mind. This would result in the possibility to get all needed data of the soil and conditions accurately and properly comparing the centrifuge test results to the numerical model results.

9.3.2. Dynamic Calculation Times

In search of the correct modelling of the breakwater subjected to an earthquake a lot of variations to the numerical models have been tested. That has been stated before, but some examples are: using dynamic calculations, dynamic with consolidation calculations, changing boundary conditions, adjusting earthquake signals, changing the mesh, changing the step sizes and more. Because the calculation times for the designed numerical models are already very long, the final numerical model calculation time is up to two days. Therefore, choices have been made to reduce the amount of calculation time where possible. Most notably are adjusting the mesh size and number of sub-steps for the calculation. Decreasing the mesh size at the boundaries of the model to coarse and limiting the area of fine mesh reduces the calculation time significantly. Furthermore, increasing the number of sub-steps results in smaller error margins. However, this also exponentially increases the calculation time. Since no more time was available the optimal solution between time and error margin has been chosen. None the less changing these values may improve on the accuracy of the results.

9.3.3. Excess Pore Water Pressure

The results found for the EPWP built-up in the soil underneath the breakwater does not correspond with the found results for the centrifuge test. The cyclic behaviour found in the EPWP of the numerical models bouncing between an EPWP of 10kPa and -40kPa compared to a liniar increase of EPWP to 4,5kPa in the centrifuge test is a significant difference. As mentioned before a lot of adjustments have been made to the model to see if the results would improve. Only decreasing the amplitude of the earthquake resulted in EPWP build-up comparable to the EPWP found in the centrifuge test. In this case the EPWP steadily increased to an EPWP of 7kPa. This suggest that amplitude and the earthquake signal are incorporated in the EPWP results found with the numerical models. This leads to the question: why is there not a big cyclic response visible in the results from the centrifuge test? It could be that the results are filtered from the earthquake signal, however this cannot be concluded from the paper.

It could be worthwhile to further investigate how to optimize calibrating the parameters, so the EPWP in the soil during an earthquake underneath a breakwater is better simulated. If UBCSand and PM4Sand parameters are very sensitive when looking at the EPWP an insufficient calibration could be a reason why the EPWP behaviour is that much different from the centrifuge test results.

Finally, the influence of the initial static shear stress on the EPWP can be investigated. Since both UBCSand and PM4Sand do not give optimal results when initial static shear is present, further investigation could be useful.

10

Conclusion

In this chapter, the conclusions of the report are given. First, the sub-questions are answered. After that, the answer to the main research question will give he overall conclusion of this report.

1. *What are the strengths and limitations of the UBCSand model and PM4Sand?*
   The UBCSand model is a model that allows for static liquefaction, accumulates plastic strains upon cyclic loading, as well as pore water pressure in undrained cyclic loading, which may eventually lead to liquefaction. UBCSand uses the critical state friction angle as a direct input parameter. UBCSand underestimates the strength of the soil at higher overburden pressures and when static shear stresses increase UBCSand underestimates the cyclic resistance ratio of the soil.

   PM4Sand follows a critical state soil mechanics framework, with the relative state parameter index as the difference between the current relative density and the relative density at the critical state. Once the critical state is reached because of shearing, the soil will flow as a frictional fluid. PM4Sand will accumulate pore pressures during undrained loading. It makes use of three main parameters, from which the contraction rate parameter h_{p0} always needs to be calibrated. For confining stress higher than 1 atm PM4Sand underestimates the cyclic resistance ratio.

   The UBCSand model and PM4Sand are similar in the following points:

   - both models make use of a critical state;
   - in both models pore water pressure will be accumulated during undrained cyclic loading;
   - both models are not ideal for situations with initial static shear stress, however, UBCSand seems to diverge more.

   The differences between UBCSand and PM4Sand are:

   - the calibration of the UBCSand parameters should be done with cyclic triaxial data, while the calibration of the PM4Sand parameters should be done with Cyclic Direct Simple Shear tests;
   - PM4Sand is designed to mainly change one parameter during calibration, while UBCSand has a lot more parameters that need to be adjusted for proper calibration;
   - UBCSand uses a critical state friction parameter as input, while PM4Sand uses a relative state parameter;
   - the UBCSand model will show elastic behaviour till the shear stress is zero and thereafter the behaviour will be elastoplastic. Where PM4Sand will show more immediate elastoplastic behaviour;
   - once PM4Sand has reached the critical state in the soil it will react as a frictional fluid.

2. *How does liquefaction occur in scaled laboratory tests?*
   The used scaled laboratory test that is used for the assessment of PM4Sand is the centrifuge test performed by Chaudhary and Hazarika (2018). This is an experiment where a breakwater consisting of a rubble mound and a caisson is subjected to an earthquake. The experiment is conducted at 25g. The earthquake consists of 3 shock waves, for each the amplitude of this signal increases, while the rest of shock wave properties is the same. During the experiment, the deformation, settlement of the caisson and the EPWP in the soil underneath the caisson is recorded for each shock wave. This data will be used to create the same experiment in Plaxis and compare the results for soil modelled with UBCSand and PM4Sand with the results from the centrifuge test.

3. *How does the breakwater react during an earthquake modelled by the UBCSand model and PM4Sand?*
   The results of Plaxis models with soil layers modelled by UBCSand show that the settlement of the caisson is getting overestimated by 2,4mm, approximately 10%. Also, the tilt of the caisson is not as big as the results of the centrifuge test show. When looking at the EPWP it is clear this does not give the similar results as found in the centrifuge test. The results at prototype scale show that the Plaxis model with UBCSand generates extreme deformations. This could be due to the calibration of parameters not scaling properly from centrifuge scale to prototype scale. The parameter might need to be recalibrated with the proper initial stress in a new cyclic triaxial test. Another reason can be that there is too much initial shear stress, which results in UBCSand underestimating the cyclic resistance ratio.

   The results of the Plaxis models with soil layers modelled with PM4Sand vary depending on which calibration method is used. The results for PM4Sand calibrated with the simulated cyclic DSS tests are close to results found from the centrifuge test. The difference is about 1,6mm or approximately 7,5%. The settlement and tilt of the caisson only vary a bit from the centrifuge test results. But when looking at the EPWP, similar to the UBCSand results, it is clear these results do not correspond with the result from the centrifuge test. The deformations occurring at prototype scale are less than expected.

4. *How do the results of the UBCSand and PM4Sand model compare?*
   When comparing the results from the UBCSand model and PM4Sand, it is clear that PM4Sand comes closer to the deformation results of the centrifuge test if the right calibration method is chosen. Both models do not give a proper EPWP response.

By summing up all conclusions the research question will be answered: *'How does PM4Sand compare to the UBCSand model when used to calculate the stability of a breakwater on a sandy soil in Plaxis that can withstand an earthquake which can induce liquefaction?'* When looking at deformations and settlements of the caisson PM4Sand replicates the results from the centrifuge test better than the results from the UBCSand model. The result run at prototype scale make it clear PM4Sand gives a displacement and settlement that are different from the results of the centrifuge test, but do not extremely deviate. While the results of the UBCSand model at the prototype scale show total failure. However, with both models, it was not possible to get an EPWP build-up that behaves similar to the one found in the centrifuge test.

11

Recommendations

After completing this research it can be concluded that the research question cannot yet be properly answered. Although PM4Sand looks to give a better estimation of the deformation and settlements occurring when a breakwater is subjected to an earthquake than the UBCSand model, no conclusions can be made about the EPWP behaviour. Therefore, this research can be expanded on and it is recommended to take the following into account:

- It is recommended that further research is done to understand how the EPWP underneath the breakwater subjected to an earthquake should be modelled. Firstly, investigate what role the high amplitude of an earthquake signal has on the EPWP build-up. Secondly, the role of the initial shear stress plays when modelling the EPWP build-up should be investigated.
- When performing expanding research on this subject it is also recommended to model the numerical models on prototype scale. Although the gravity in a model can be adjusted with the material weight proportion, this adjustment does not account for the water in the model. This can be a cause of the wrongly found EPWP.
- Decide from the beginning of a project if numerical modelling with PM4Sand is an option. If so, it should be made sure all needed parameters can be determined properly and CDSS tests are done on the sand at the project site. This is necessary for the proper calibration of PM4Sand.

In case more research will be done on this subject, it would be recommended to design the research the following way. Firstly, it is advised to create data on a real breakwater subjected to an earthquake. If it is not possible to create this data, built an experiment with an as big as possible breakwater, without using a centrifuge test to get the results. Next to this, it is advised to also perform a new centrifuge test on a breakwater subjected to an earthquake. With both tests results available it is possible to investigate the effects of scaling in the numerical model. When designing the laboratory tests it is important to take into account what boundary conditions are chosen for the numerical modelling. For example, making sure the earthquake signal does not reflect on the soil box walls is important as well as creating a proper bedrock.

It is advised to use a common sand with a lot of information available on it. Toyoura Sand is a commonly used sand for laboratory tests in Japan, but other sands are more often used in other parts of the world. The sand should be tested with CDSS tests, so calibration can be done properly. Secondly, it is important to know the permeability rate of the used sand if a dynamic calculation with consolidation will be done. When using a centrifuge test it is also important to have the right information available to calculate the permeability when the gravity is higher than 1g.

Finally, it can also be worthwhile to check how different types of breakwaters subjected to an earthquake are reacting to being modelled with PM4Sand. As mentioned before the initial static shear stress can be a problem when modelling with PM4Sand. In case of a conventional rubble mound, this would be higher, which can lead to inaccurate modelling. Comparing the results different breakwater types can be insightful.

A

Appendix Earthquake Signal Analysis

In this appendix the used earthquake signal in the Plaxis models will be analysed. This will be done by analysing the earthquake signal in with a 1D site response analysis. Where the earthquake signal will travel through a 1D column with properties comparable to the centrifuge test. The testing will be done in steps to see what effect changing the soil properties and model boundary conditions have. The steps will be:

- Model the soil as linear elastic
- Model the 1D column with a compliant base boundary
- Increase the amount of data points in the earthquake signal
- Model the soils with UBCSand and PM4Sand
- Add damping to the soil properties
- Check response with the drift correction function

To give a clear overview how the earthquake signal behaves in the 1D column graphs will be shown of the amplitude versus time at different positions in the 1D column. These positions are called nodes and are shown in Figure A.1. Node 7 is at the bottom left of the soil column and shows the input signal. In later figures node 9 in the graphs is at the position of node 7, so at the left bottom of the column. However it shows how the input earthquake signal is transferred onto the soil.

The input signal for every test is the same as shown in Figure A.2. A signal that slowly builds up to a amplitude of 0.1 g and lasts for 1.375 seconds.

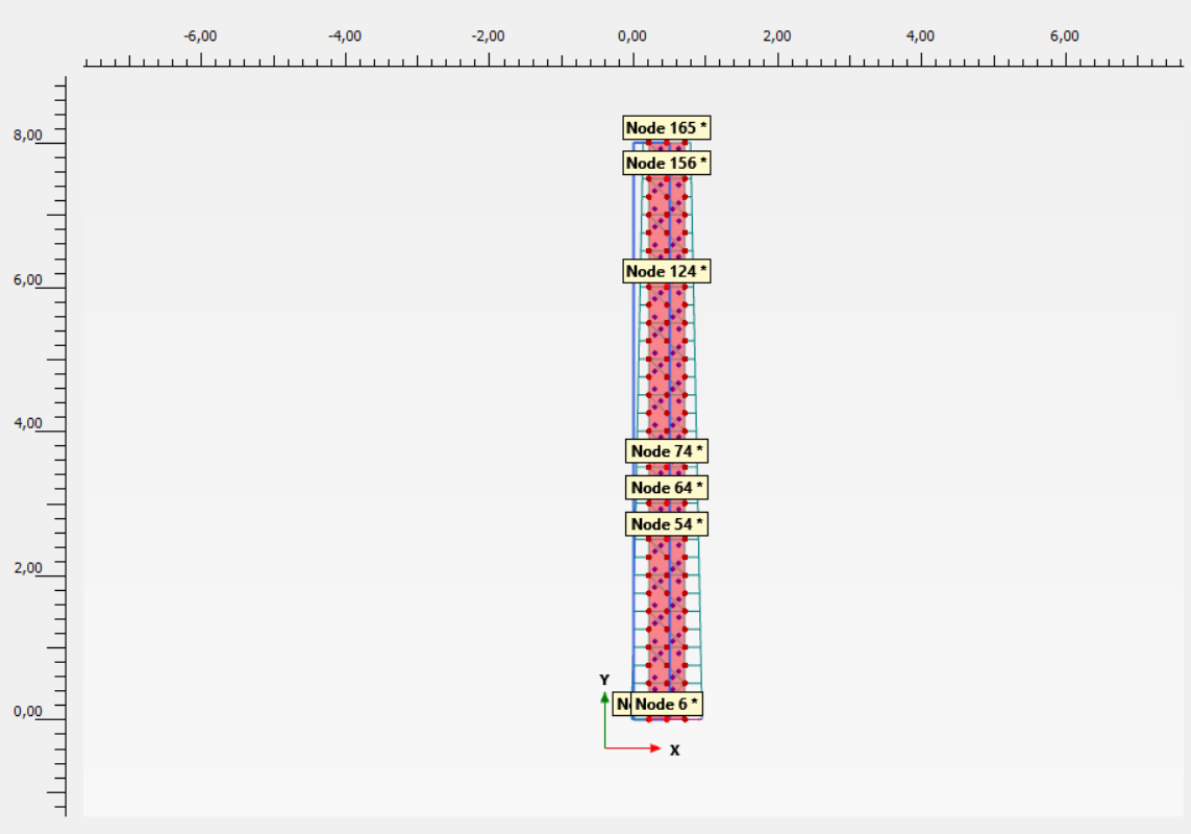

Figure A.1: Position of the nodes in the 1D column with linear elastic soil

A.1. Earthquake signal in a linear elastic soil

The first situation that is assessed, is a 1D column with a linear elastic soil. The amount of elasticity also determines how the signal travels through the 1D column. Firstly, the soil is modelled as extremely elastic. This would mean the earthquake signal should be the same throughout the 1D column. In the following Figure A.2 it can be seen that is indeed the case. In Figure A.2 three signals are plotted, however only 1 clear plot can be seen. This means that the three plots overlay each other and therefore are identical.

Next the 1D soil column was modelled with a linear elastic material that resembles the properties of concrete. The results are shown in Figure A.3. It becomes clear the signal is much more disrupted than the original blue input signal at node 9. Also the amplitude of the signal throughout the 1D column seems to increase.

After reducing the elastic behaviour of the 1D column the effect of a compliant base boundary at the bottom of the soil column is assessed. Figure A.4 shows the results of adding a compliant base boundary. It looks as this removes all the disruptions found in the previous case and the earthquake signal has again a similar shape as the input signal. This indicates that the disruptions of the case without a compliant base boundary can be assigned to the reflection of the earthquake signal at the bottom. It is clear that amplitude throughout the sample still increases.

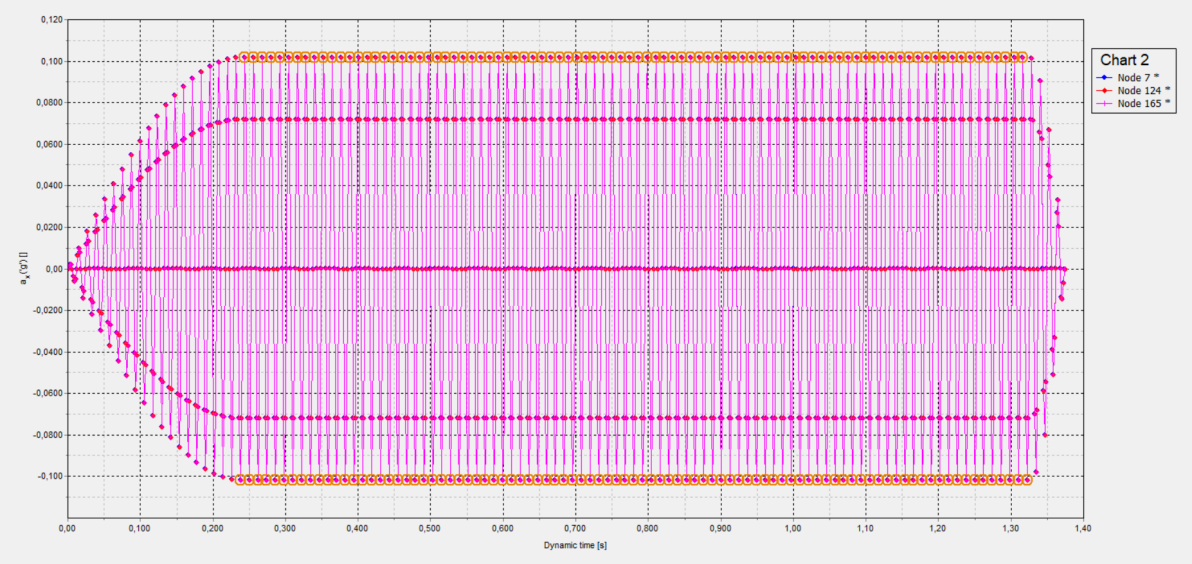

Figure A.2: Earthquake signal through the an extremely elastic 1D column

The final assessment done for a linear elastic soil column is increasing the number of input points given for the earthquake signal. Instead of the previously used 8 input points per phase of the signal, 40 input points are used. The results are shown in three graphs, because putting all plots in one graph makes it hard to read. The graphs are shown in Figure A.5, Figure A.6 and Figure A.7. Figure A.5 shows that the amplitude of the earthquake signal at the bottom of the column is already a bit lower than the input signal. Here it is 0.07 g, while the input signal has an amplitude of 0.1 g. Looking at Figure A.6 and A.7 it can be seen that the amplitude of the earthquake signal increases while travelling through the 1D column and at the top becomes a bit higher than could be seen for the example with linear elastic soil and a compliant base boundary. This shows that a higher amount of input data will give a more accurate earthquake signal. However, it also means an significant increase in calculation time.

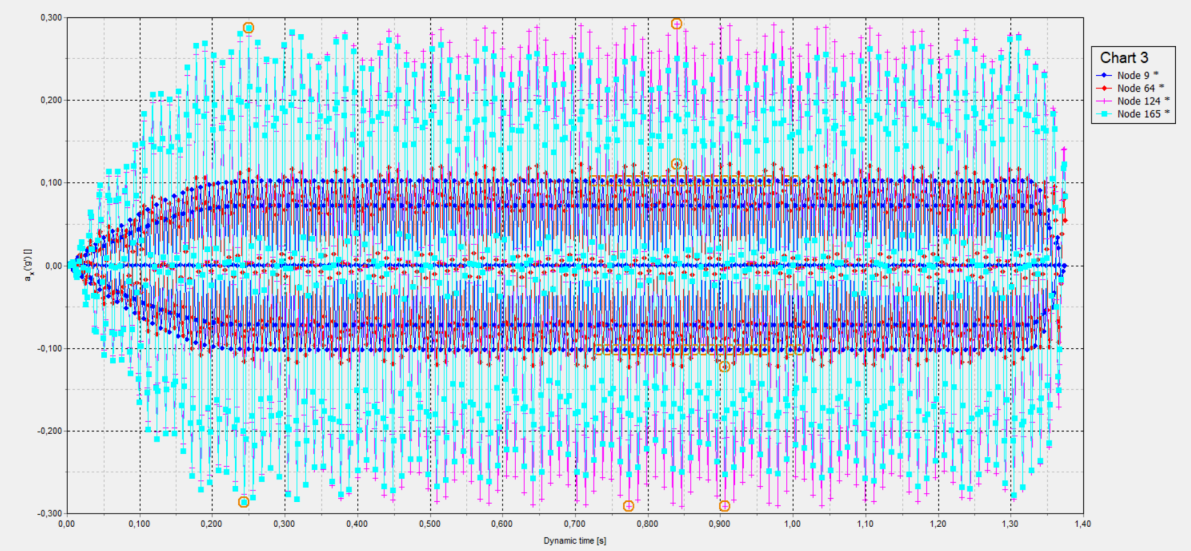

Figure A.3: Earthquake signal through the 1D column of elastic modelled concrete

A.2. Earthquake signal with two sand layers

To get the 1D column more comparable to the soil that was used in the centrifuge tests and that will be modelled in Plaxis it is now split in two. This column will first be assessed with soil modelled with UBCSand and thereafter the soil will be modelled with PM4Sand.

The node distribution through the 1D column is a bit different from the 1D column modelled with a linear elastic soil. The node distribution for this assessment is shown in Figure A.8. Node 157 and 167 are located at the left bottom of the soil column. And node 157 shows how the input earthquake signal is transferred onto the soil.

A.2.1. 1D soil column modelled with UBCSand

Firstly, the 1D column is assessed without damping or a compliant base boundary. The results are shown in Figures A.9, A.10 and A.11

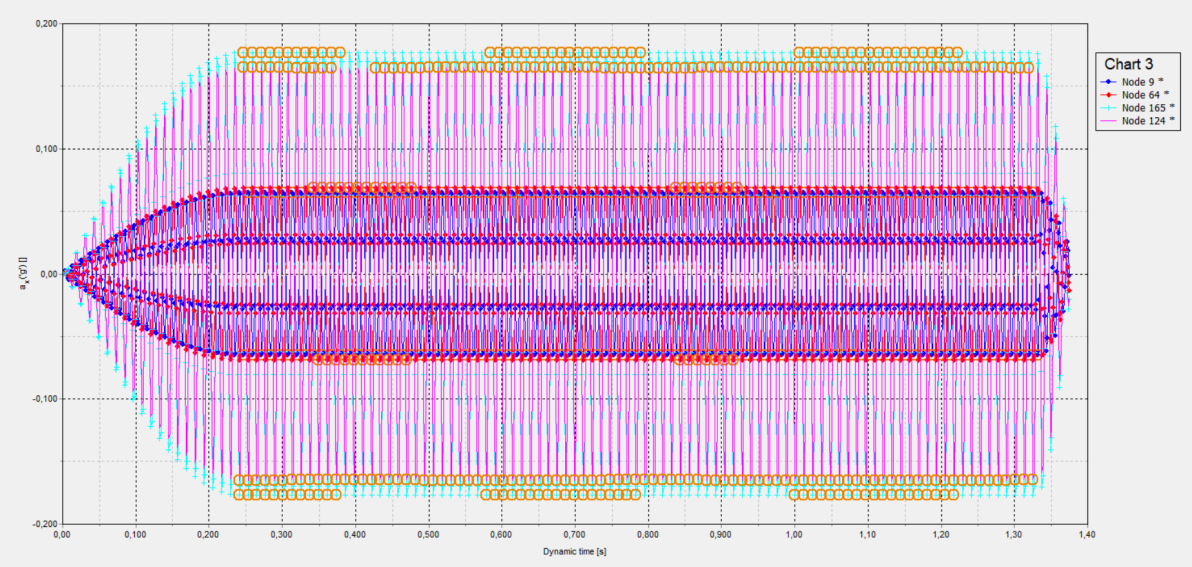

Figure A.4: Earthquake signal through the 1D column of elastic modelled concrete with a compliant base

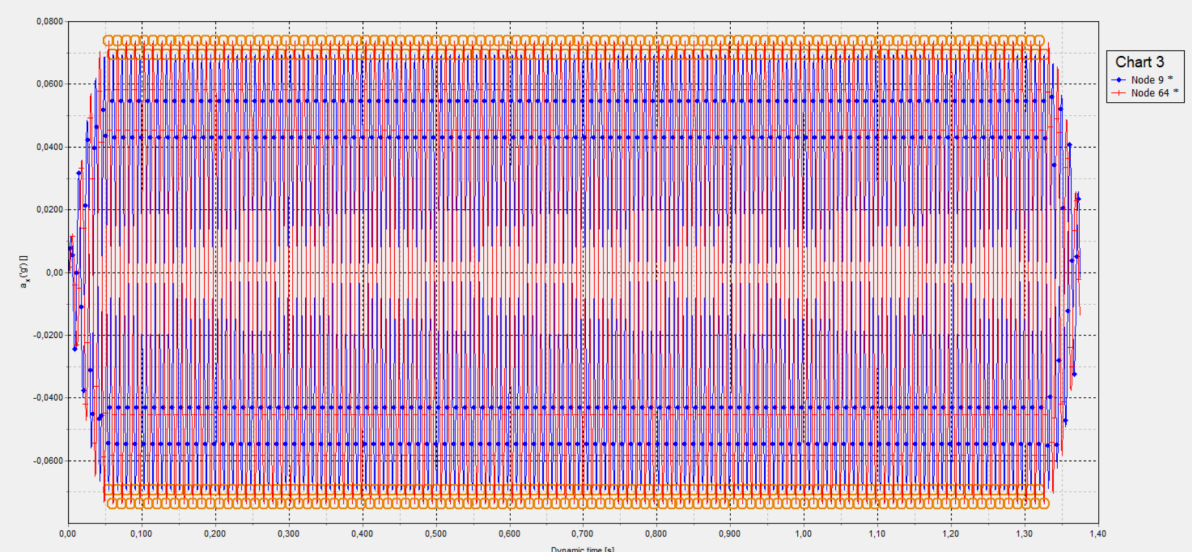

Figure A.5: Earthquake signal through the 1D column of elastic modelled concrete

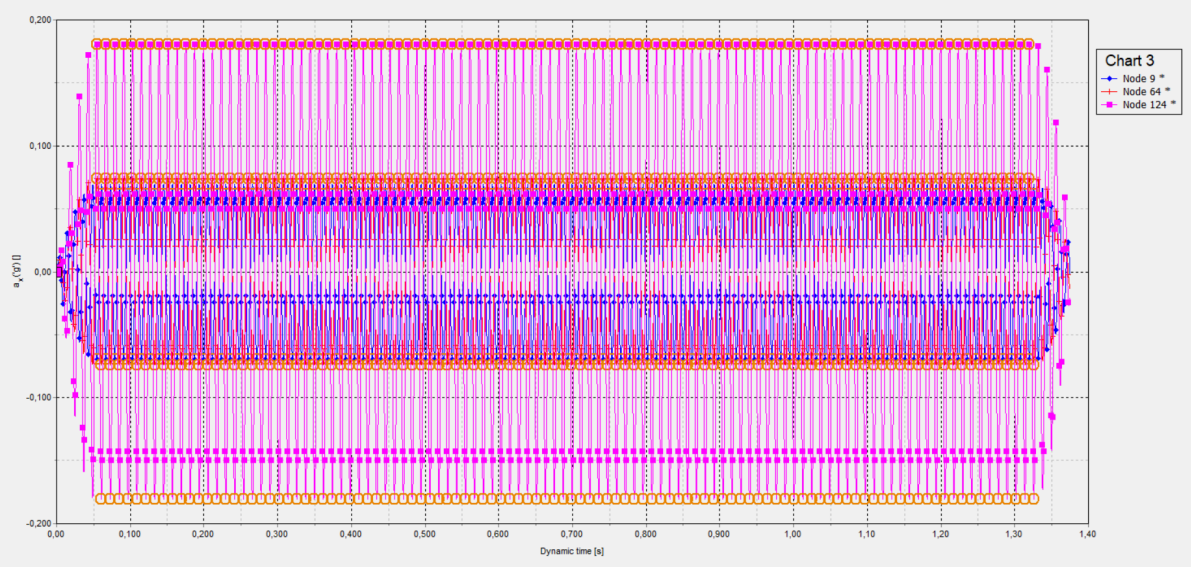

Figure A.6: Earthquake signal through the 1D column of elastic modelled concrete

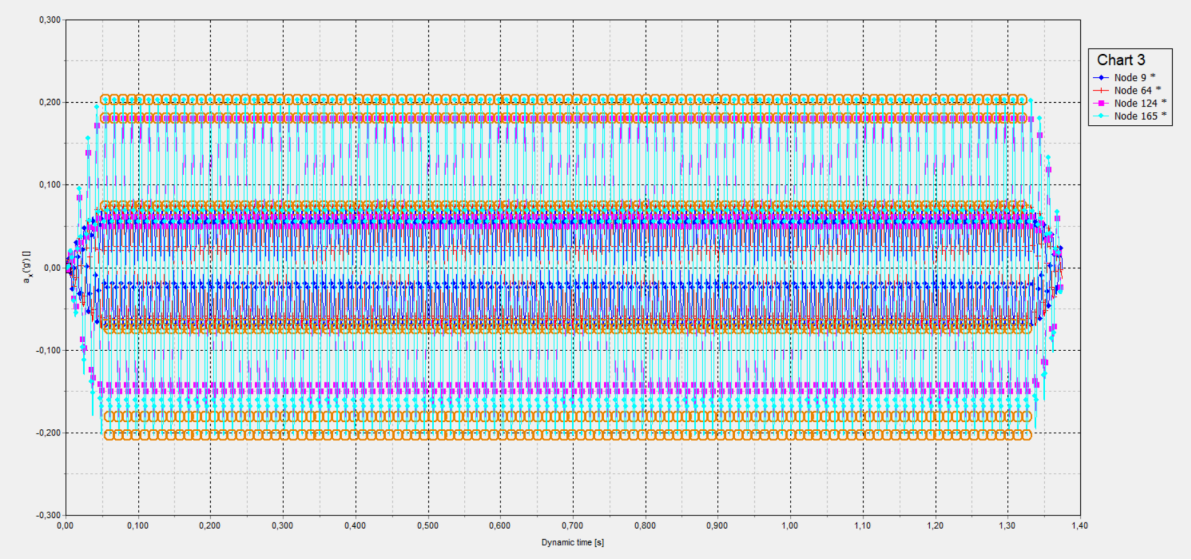

Figure A.7: Earthquake signal through the 1D column of elastic modelled concrete

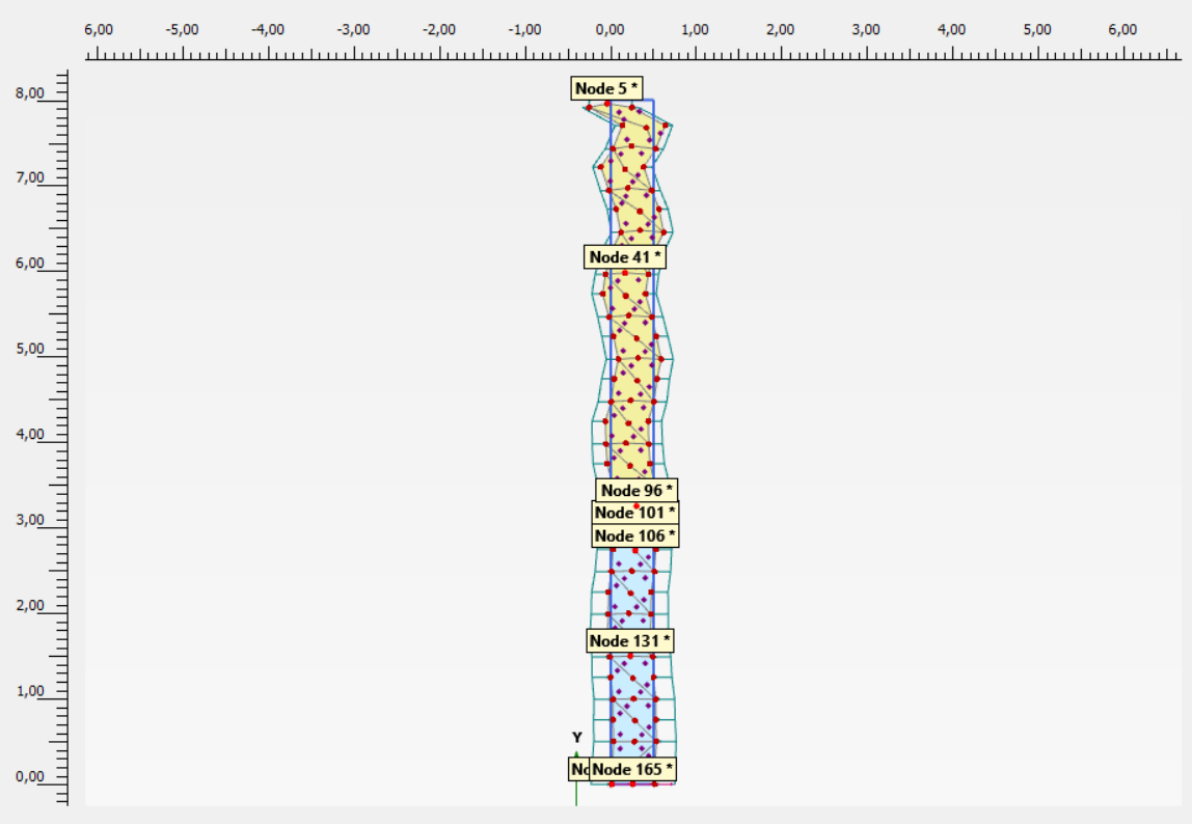

Figure A.8: The node distribution for the assessment of the soils modelled with UBCSand and PM4Sand

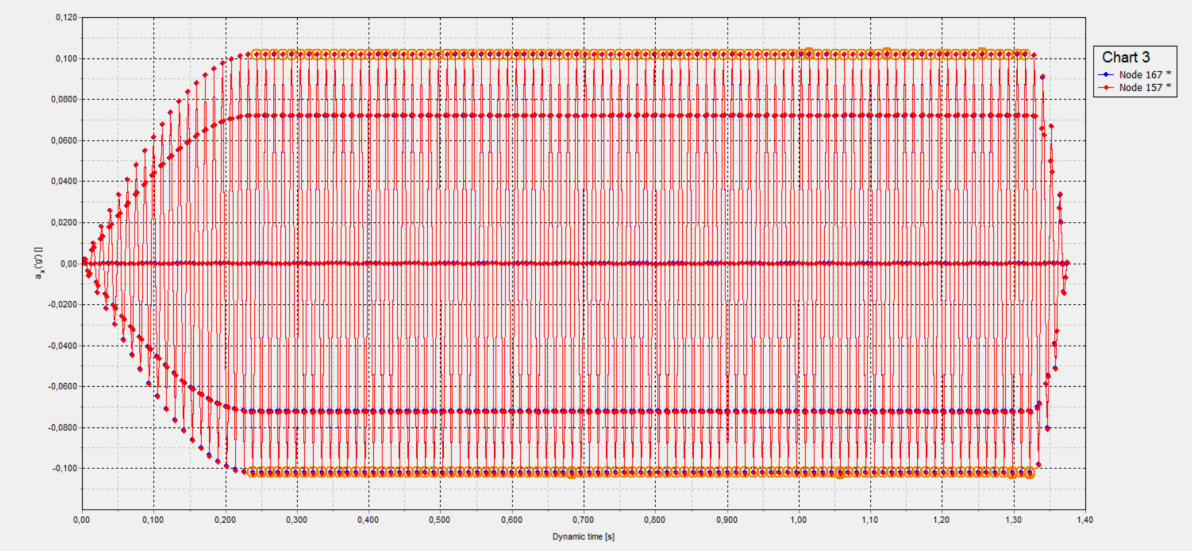

Figure A.9: Graph of the transmission of the input earthquake signal to bottom of the 1D column for a two layered column with UBCSand and no damping or compliant base boundary

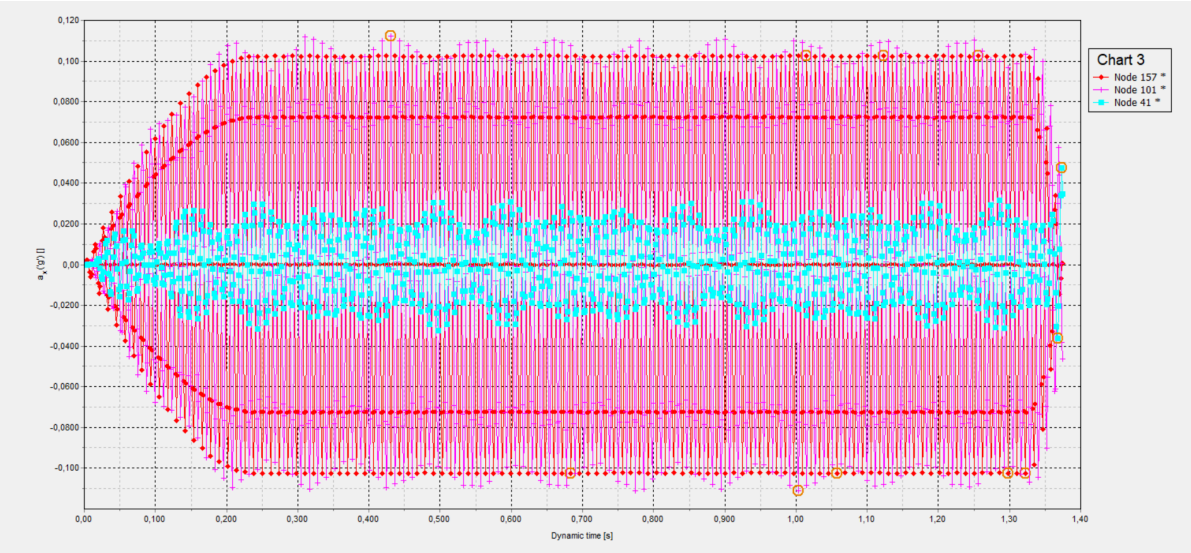

Figure A.10: Earthquake signal through the 1D column for a two layered column modelled with UBCSand and no damping or compliant base boundary

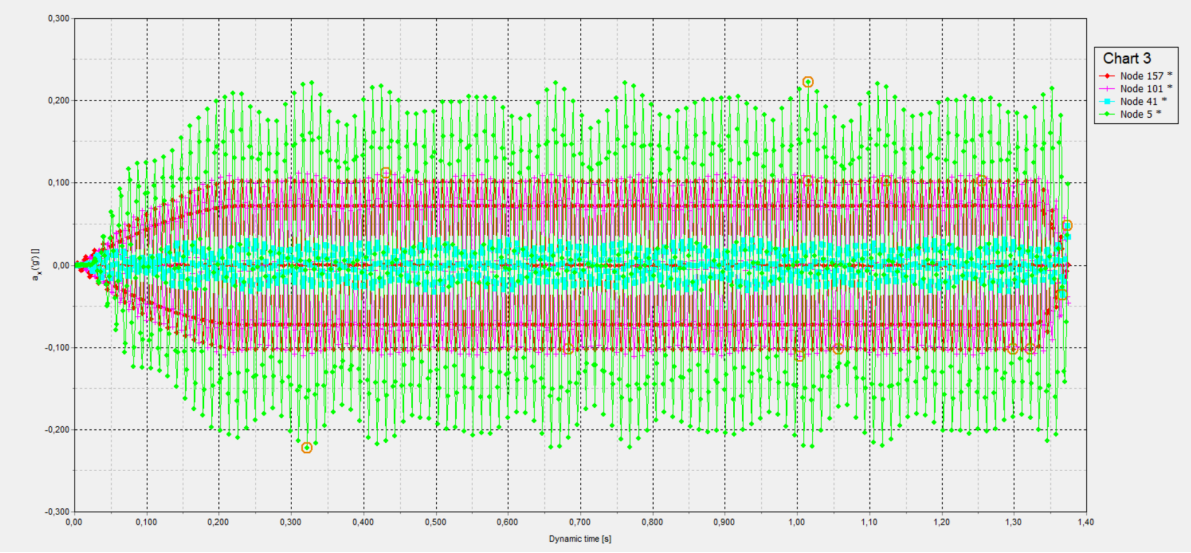

Figure A.11: Earthquake signal through the 1D column for a two layered column modelled with UBCSand and no damping or compliant base boundary

Next, damping is taken into account while assessing the earthquake signal. A similar effect as applying a compliant base boundary on the linear elastic column can be seen. The disturbance in earthquake signal throughout the is column is disappeared and the earthquake signal look like the input signal throughout the 1D column. Figures A.12, A.13 and A.14 show the earthquake signal throughout the 1D column.

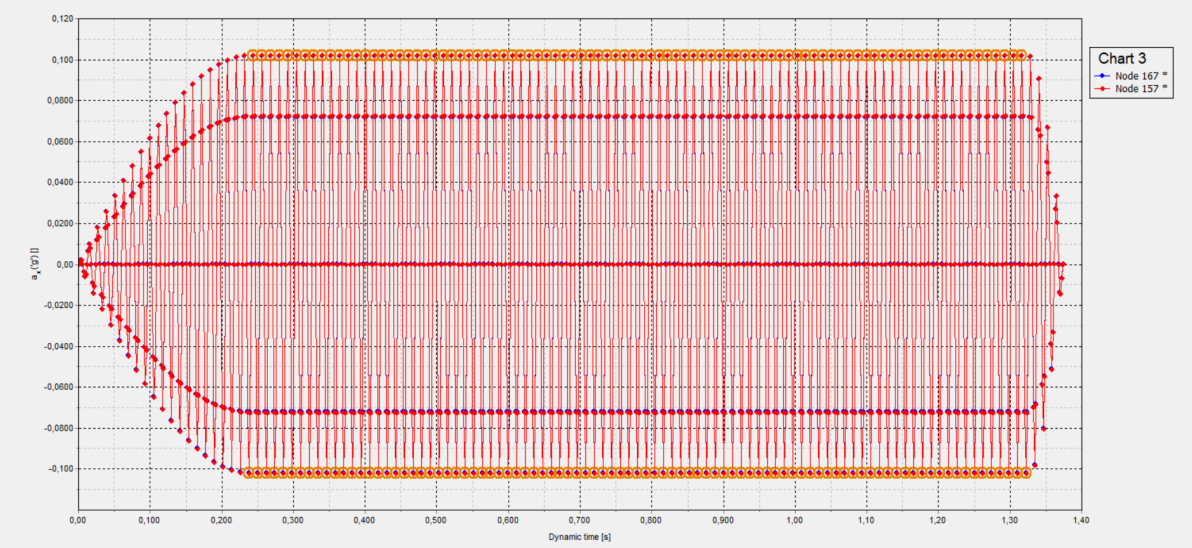

Figure A.12: Earthquake signal through the 1D column for a two layered column modelled with UBCSand, with damping and no compliant base boundary (1/3)

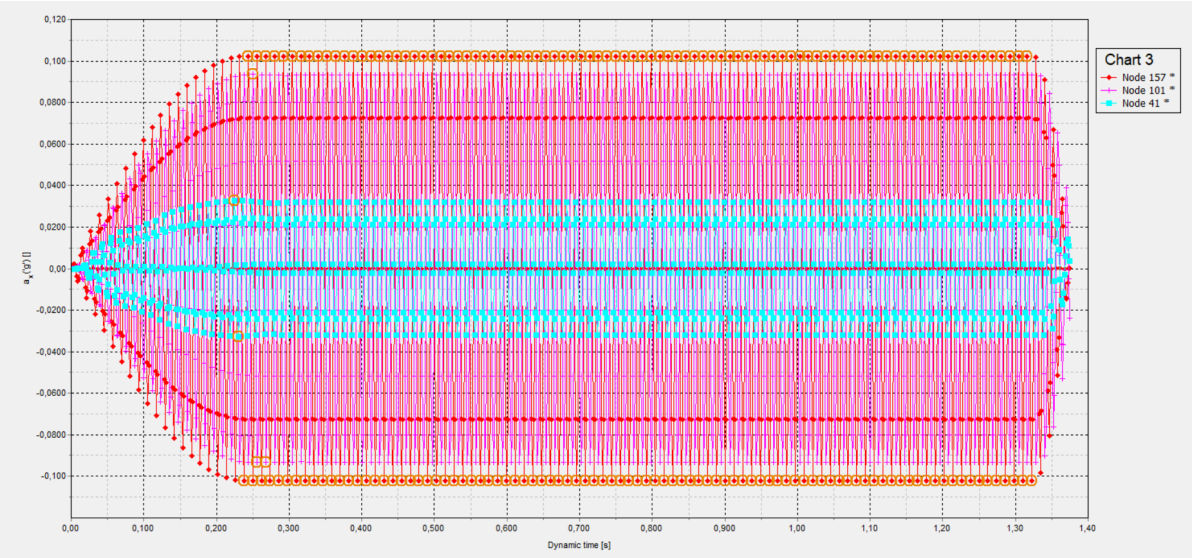

Figure A.13: Earthquake signal through the 1D column for a two layered column modelled with UBCSand, with damping and no compliant base boundary (2/3)

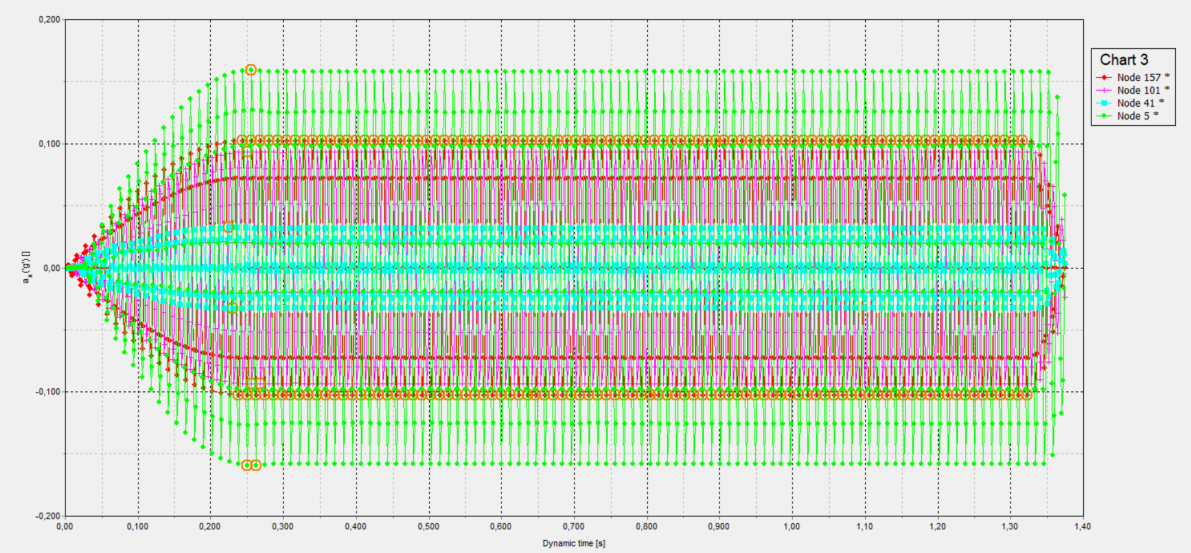

Figure A.14: Earthquake signal through the 1D column for a two layered column modelled with UBCSand, with damping and no compliant base boundary (3/3)

The final assessment for the earthquake signal through the 1D colum with UBCSand modelled sand is adding a compliant base boundary. The results are very similar to the case without a compliant base boundary. Therefore only the final graph is shown with Figure A.15. Comparing this figure with Figure A.14, shows that adding the compliant base boundary results in higher amplitude.

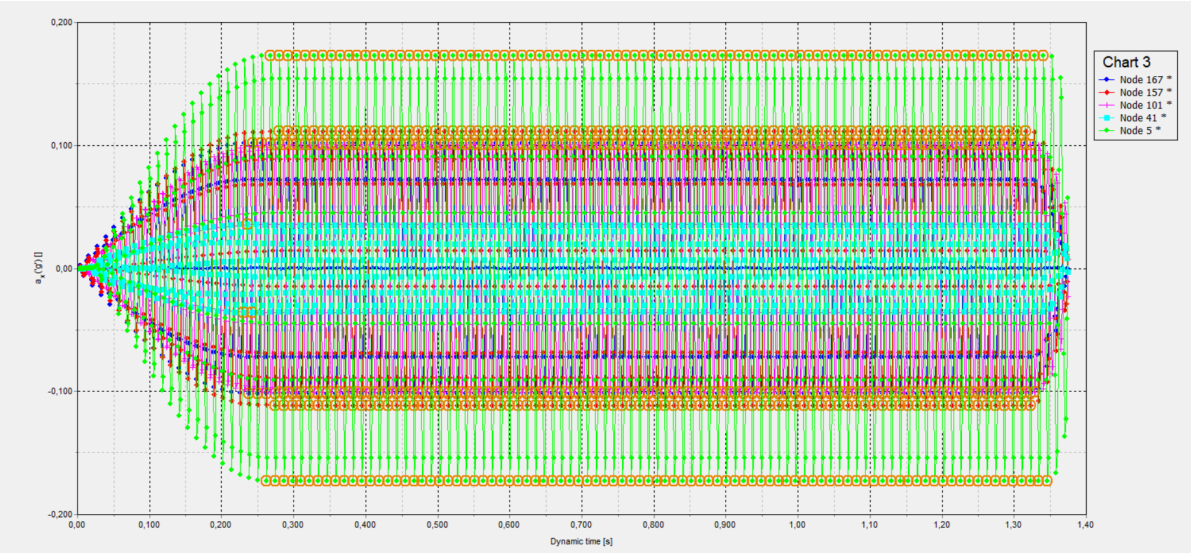

Figure A.15: Earthquake signal through the 1D column for a two layered column modelled with UBCSand, damping and a compliant base boundary

A.2.2. 1D Soil Column Modelled with PM4Sand

The first step in assessing the behaviour of an earthquake signal through a 1D soil column modelled with PM4Sand has been done in a similar wasy as for the UBCSand 1D column. The earthquake signal is applied to the bottom of the column and the earthquake signal throughout the column are shown in graphs. Figures A.16 and A.17 show the results. It can be seen that the input signal is not properly transferred to the soil column.

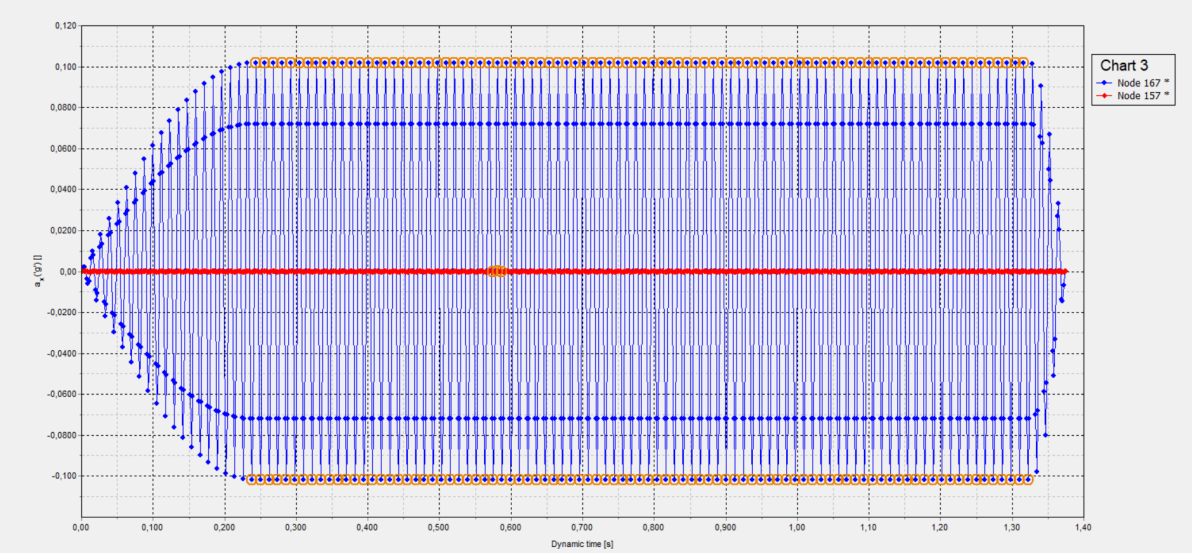

Figure A.16: Earthquake signal through the 1D column for a two layered column modelled with PM4Sand, without damping or a compliant base boundary (1/2)

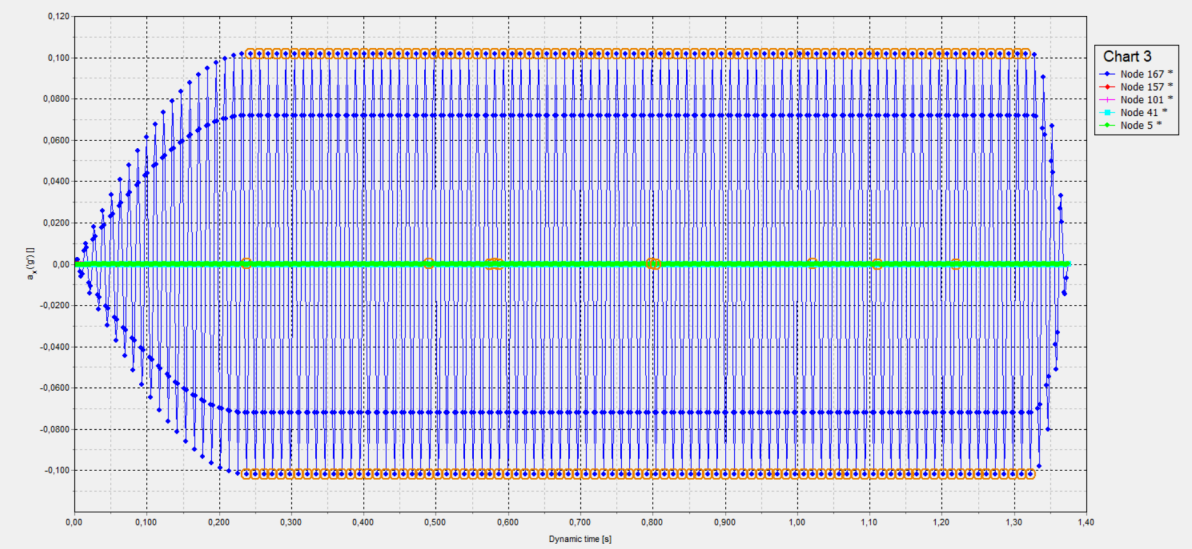

Figure A.17: Earthquake signal through the 1D column for a two layered column modelled with PM4Sand, without damping or a compliant base boundary (2/2)

When adding the compliant base boundary to the 1D column a the signal is indeed getting transferred to the 1D column. In Figures A.18, A.19 and A.20 it can be seen that although the shape of the input signal and the earthquake signal in the column are similar, the amplitude of the signal in the 1D column is significantly higher.

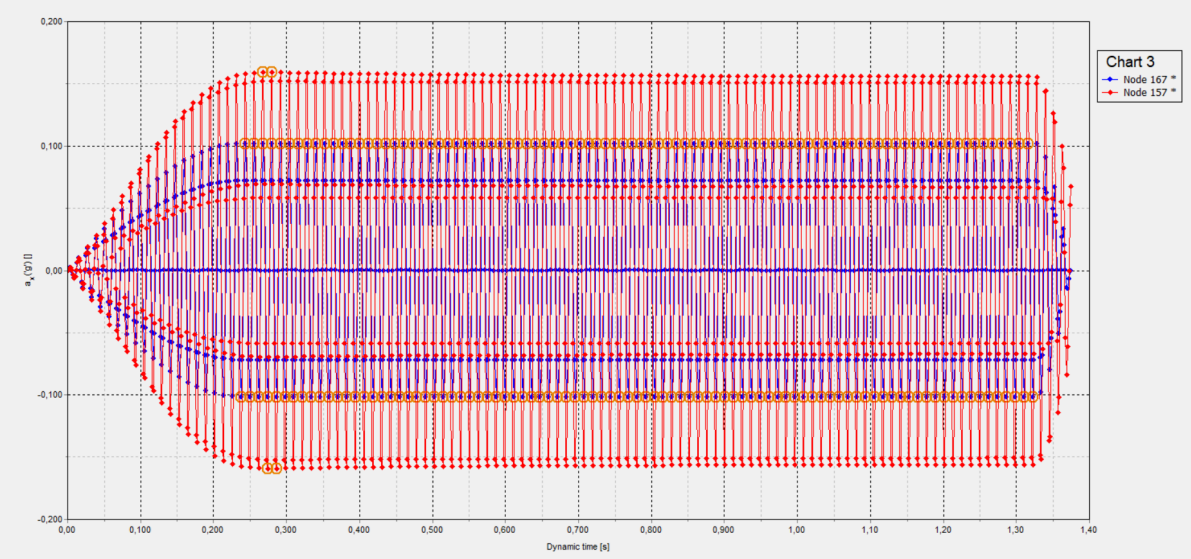

Figure A.18: Earthquake signal through the 1D column for a two layered column modelled with PM4Sand, without damping, but with a compliant base boundary (1/3)

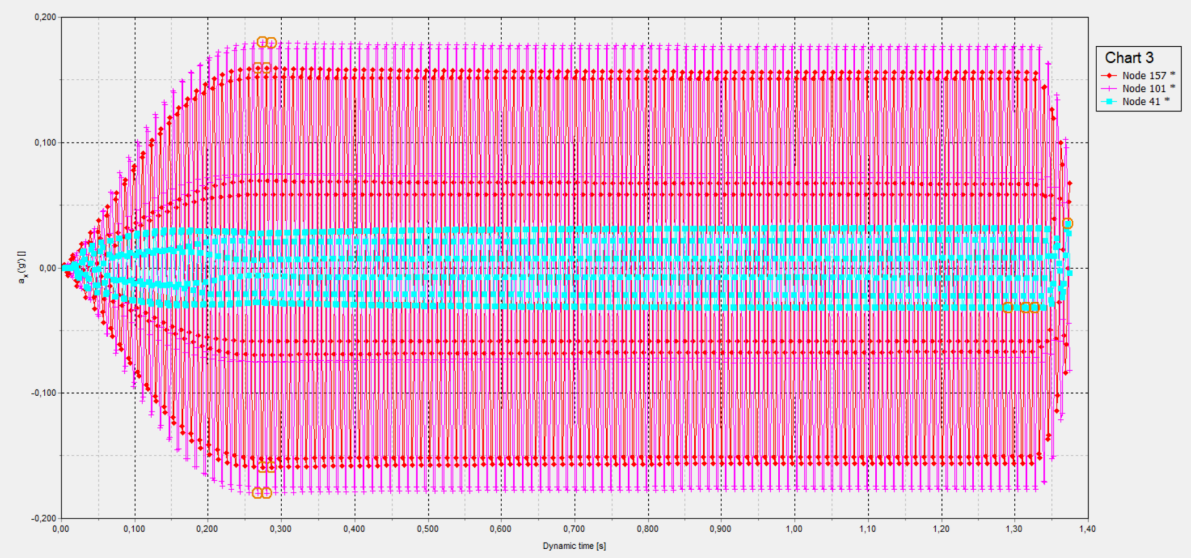

Figure A.19: Earthquake signal through the 1D column for a two layered column modelled with PM4Sand, without damping, but with a compliant base boundary (2/3)

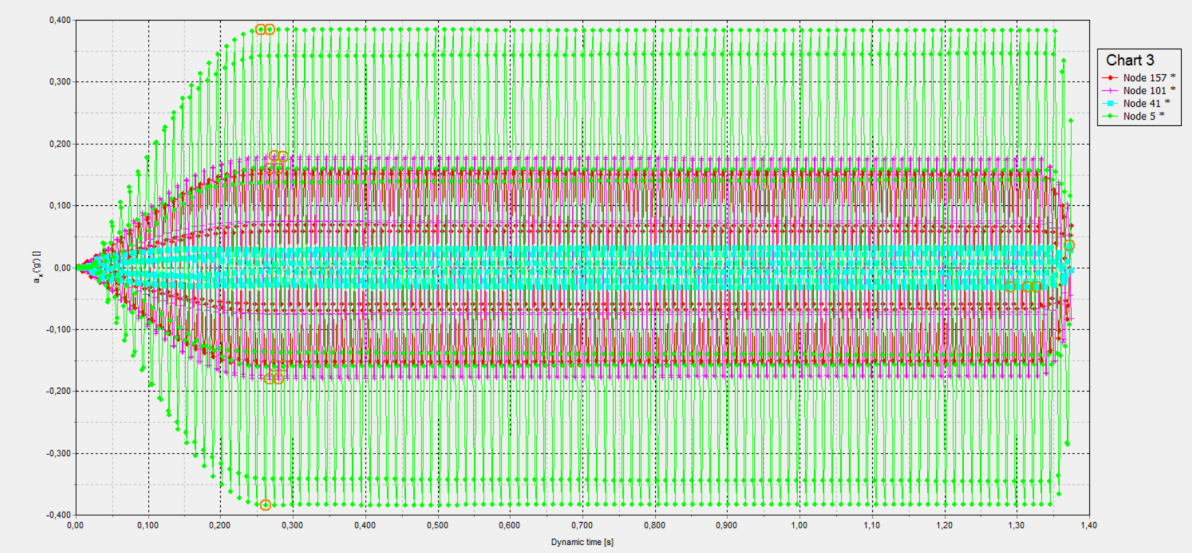

Figure A.20: Earthquake signal through the 1D column for a two layered column modelled with PM4Sand, without damping, but with a compliant base boundary (3/3)

Finally with adding damping to the 1D soil column properties the increase of amplitude seen i the previous assessment is now significantly decreased. Figures A.21, A.22 and A.23.

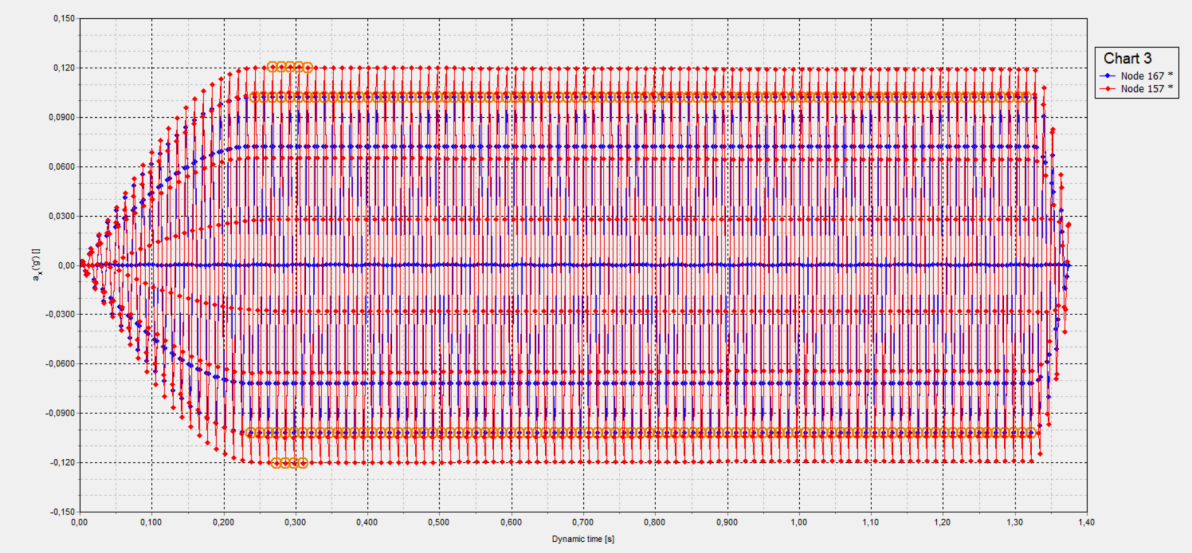

Figure A.21: Earthquake signal through the 1D column for a two layered column modelled with PM4Sand, damping and a compliant base boundary (1/3)

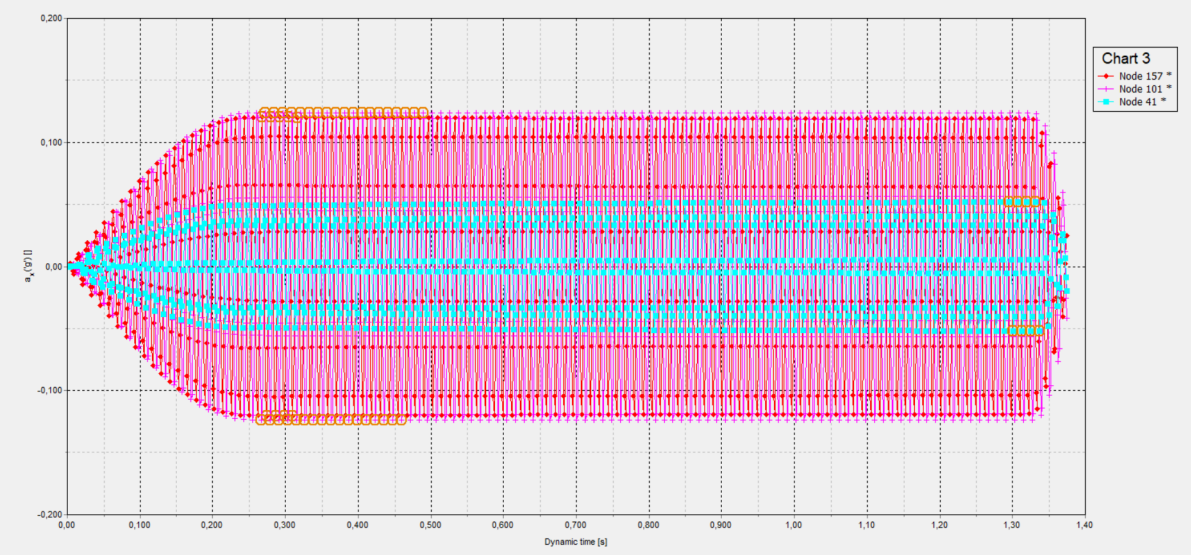

Figure A.22: Earthquake signal through the 1D column for a two layered column modelled with PM4Sand, damping and a compliant base boundary (2/3)

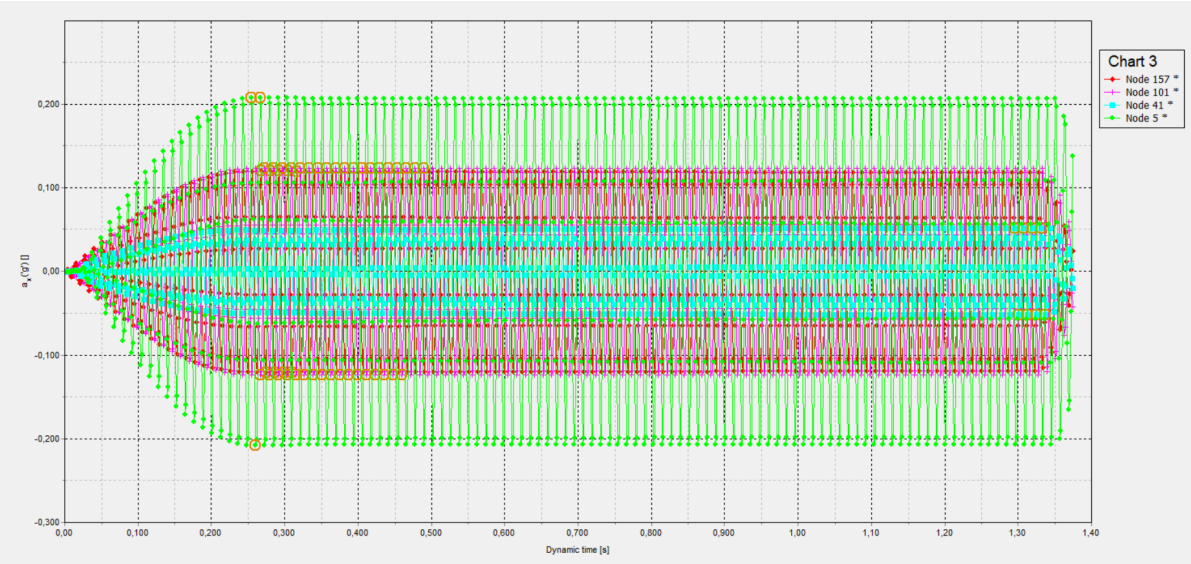

Figure A.23: Earthquake signal through the 1D column for a two layered column modelled with PM4Sand, damping and a compliant base boundary (3/3)

A.3. The Effect of the Drift Correction Function

In Plaxis it is possible to choose a box called 'drift correction' when adding an acceleration earthquake signal. This function corrects the displacement that occurs during the calculations and makes sure the model again stops at zero. The displacement signal throughout the 1D column without a drift correction is shown in Figures A.24 and A.25. When comparing these graphs with the graphs from Figures A.26 and A.27 that show the displacement signal with the drift correction graphs look very similar. The only difference that can be seen is the final point of the earthquake signal does not end at zero and a small curve along the maximum points of the graphs when the drift correction is used can be found.

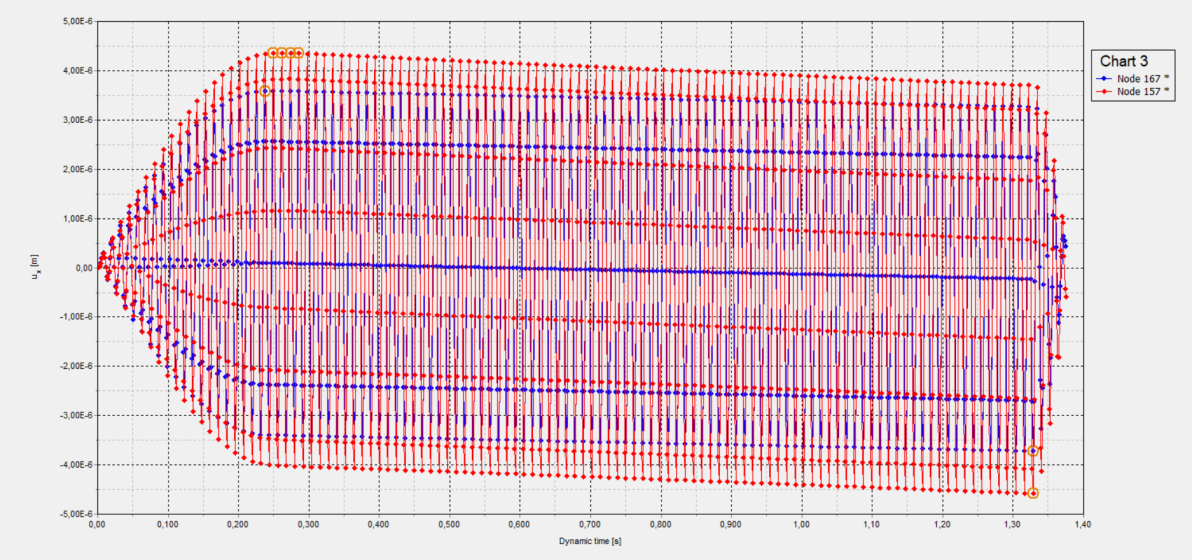

Figure A.24: Displacement signal through the 1D column for a two layered column modelled with PM4Sand, damping, a compliant base boundary and no drift correction (1/2)

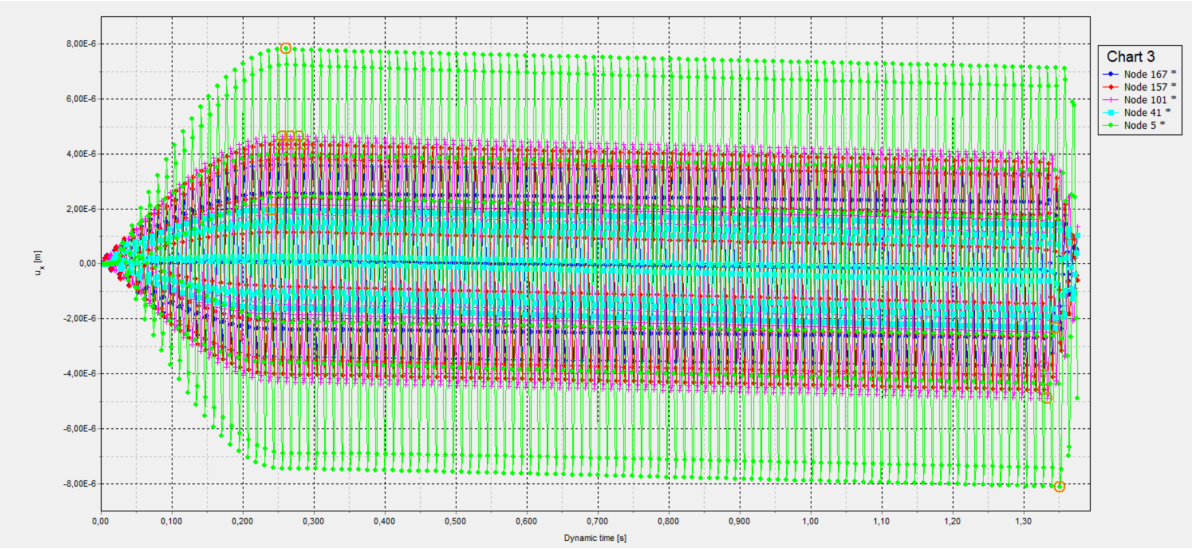

Figure A.25: Displacement signal through the 1D column for a two layered column modelled with PM4Sand, damping, a compliant base boundary and no drift correction (1/2)

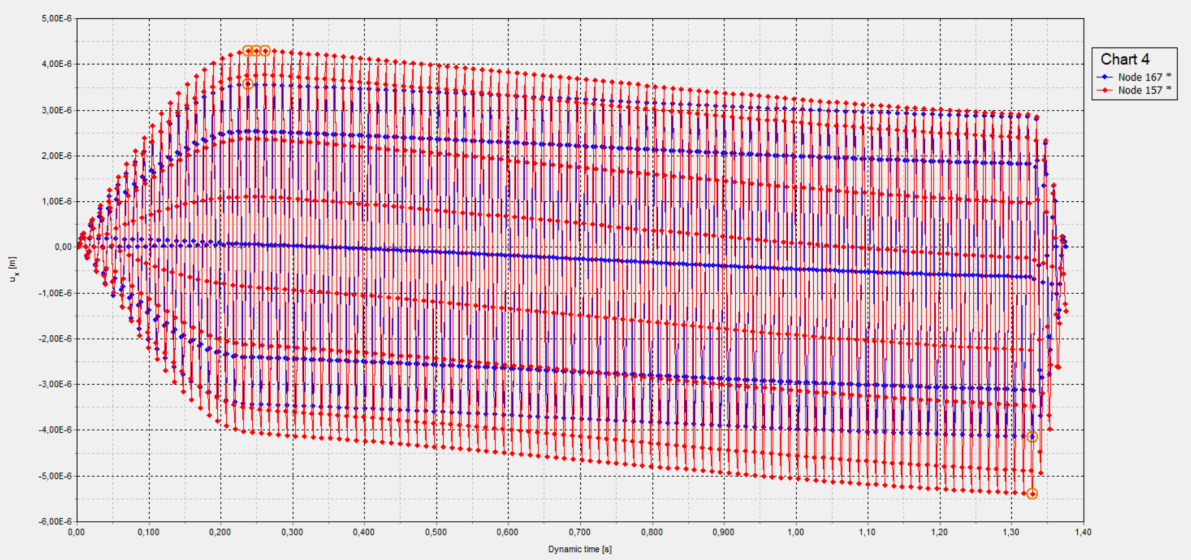

Figure A.26: Displacement signal through the 1D column for a two layered column modelled with PM4Sand, damping, a compliant base boundary and drift correction (1/2)

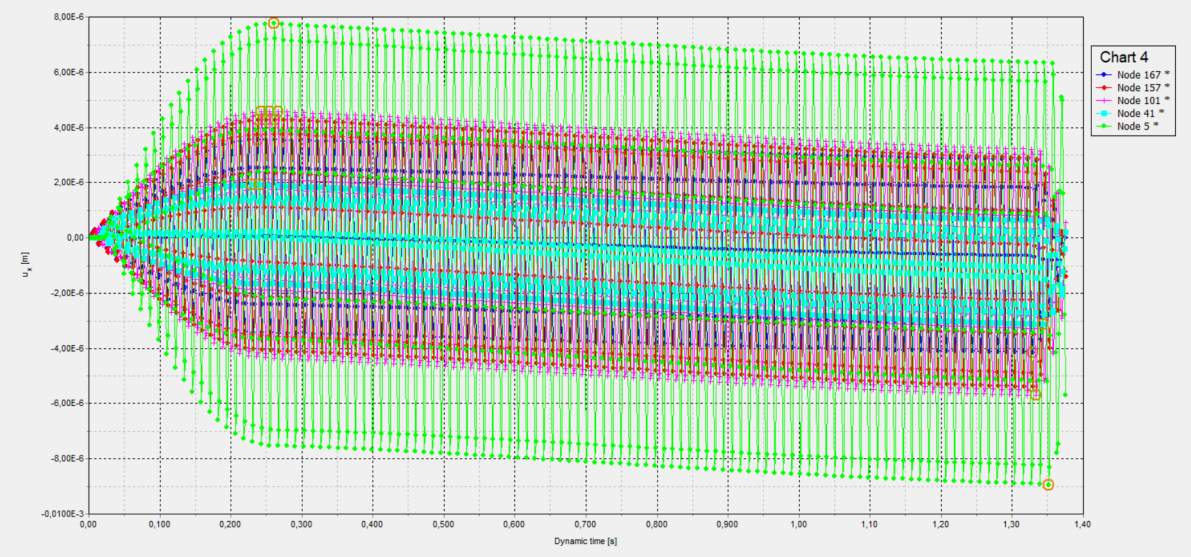

Figure A.27: Displacement signal through the 1D column for a two layered column modelled with PM4Sand, damping, a compliant base boundary and drift correction (2/2)

B

Appendix Calibration

In this Appendix the Tables with final parameter values for the used PM4Sand parameters are shown. As well as the resulting graphs from the calibration process. First the PM4Sand calibration with the simulated Cyclic DSS test will be shown and thereafter the graphs for the Torsional shear tests. For the simulated CDSS test Toyoura sands with relative density of 50% and 80% are calibrated, both sands have been calibrated with an isotropic state and anisotropic state. For the Cyclic Torsional shear test the relative density of 50%, 60% and 80% have been taken. Only the sand with relative density 50% has also results for an anisotropic stress state.

B.1. PM4Sand calibration with simulated CDSS test

B.1.1. PM4Sand with isotropic conditions and D_r = 50%

Table B.1: Test properties calibrated with CDSS from UBCSand model for isotropic PM4Sand parameters with $D_r = 50\%$

Test properties calibrated with CDSS from UBCSand model		
Initial stress σ_{yy}	98	kN/m^2
CSR	0,178	
τ_{xy}	17,444	kN/m^2
N_c	15	cycles
Isotropic test		

Table B.2: Used parameter values PM4Sand $D_r = 50\%$ isotropic

D_{r0}	0,525		e_{max}	0,98		ϕ_{cv}	31,33
G_0	960		e_{min}	0,61		ν	0,3
h_{p0}	0,42		n^b	0,65		q	10
P_A	101,3		n^d	0,1		R	1,5
Postshake	0						

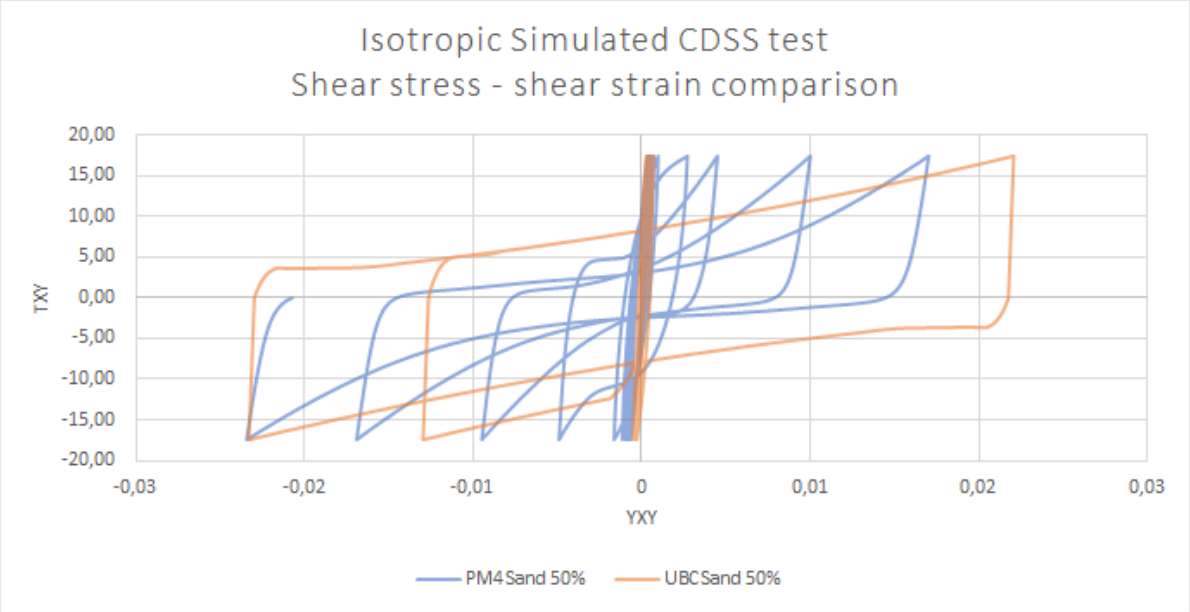

Figure B.1: Comparison graph showing the shear stress - shear strain relation with UBCSand simulated CDSS test results and the calibrated PM4Sand results for isotropic test with $D_r = 50\%$

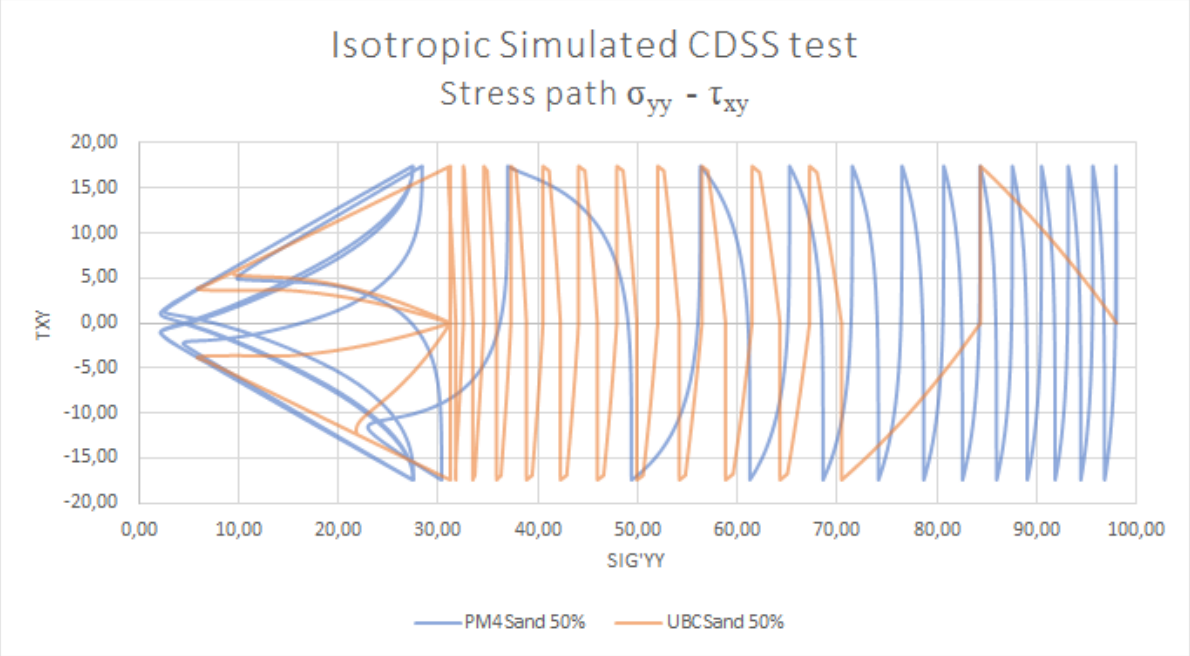

Figure B.2: Comparison graph showing the stress path with UBCSand simulated CDSS test results and the calibrated PM4Sand results for isotropic test with $D_r = 50\%$

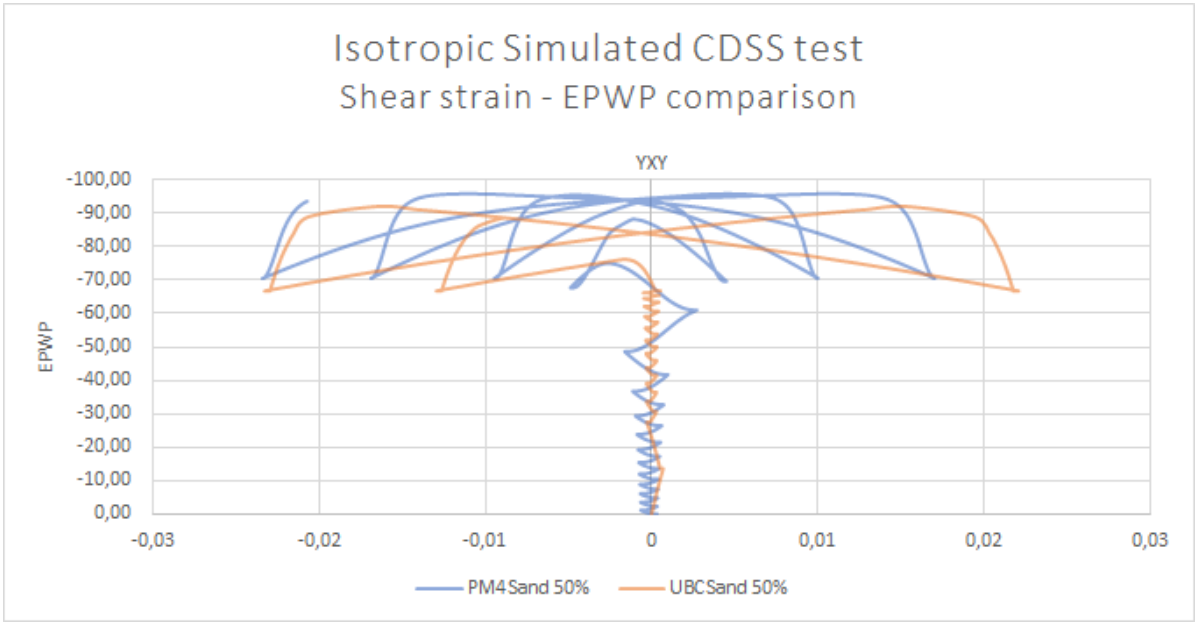

Figure B.3: Comparison graph showing the shear strain - excess pore water pressure relation with UBCSand simulated CDSS test results and the calibrated PM4Sand results for isotropic test with $D_r = 50\%$

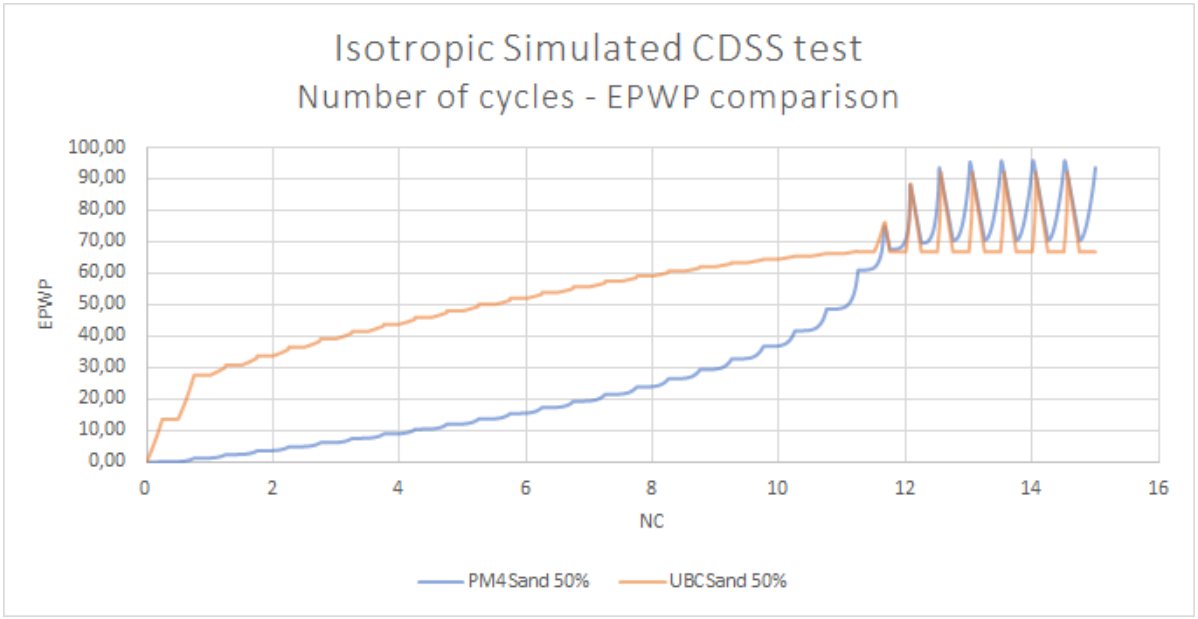

Figure B.4: Comparison graph showing the number of cycles - excess pore water pressure relation with UBCSand simulated CDSS test results and the calibrated PM4Sand results for isotropic test with $D_r = 50\%$

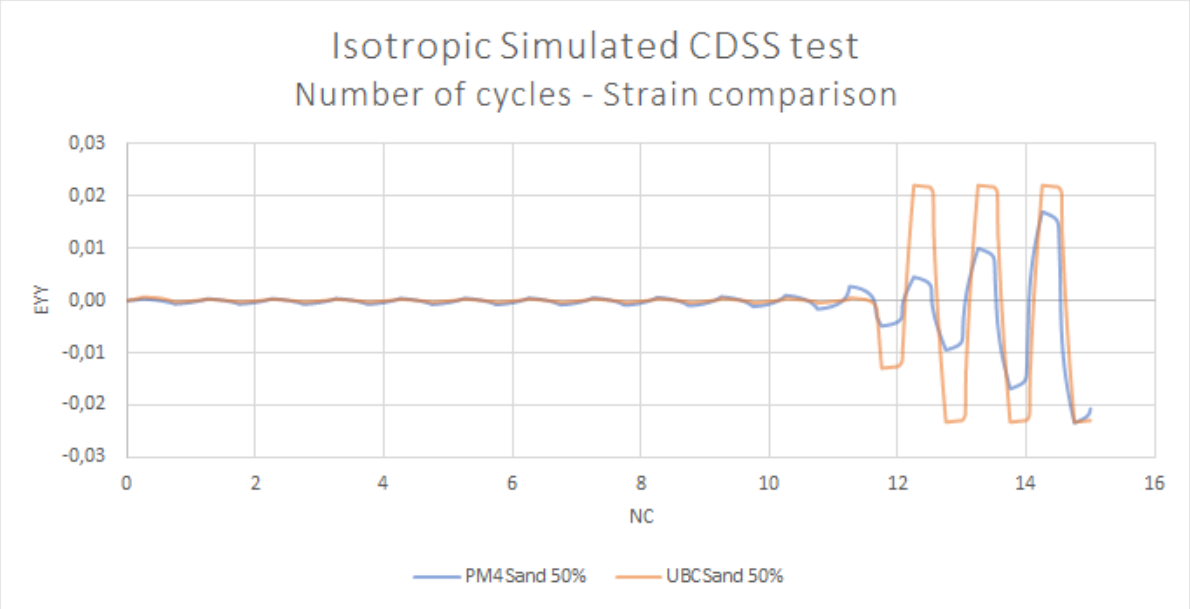

Figure B.5: Comparison graph showing the number of cycles - strain relation with UBCSand simulated CDSS test results and the calibrated PM4Sand results for isotropic test with $D_r = 50\%$

B.1.2. PM4Sand with K_0 = 0.5 and D_r = 50%

Table B.3: Test properties calibrated with CDSS from UBCSand model for anisotropic PM4Sand parameters with $D_r = 50\%$

Test properties calibrated with CDSS from UBCSand model		
Initial stress σ_{yy}	98	kN/m^2
CSR	0,178	
τ_{xy}	17,444	kN/m^2
N_c	15	cycles
$K_0 = 0.5$		

Table B.4: Used parameter values PM4Sand $D_r = 50\%$ and anisotropic

D_{r0}	0.6		e_{max}	0,98		ϕ_{cv}	31,33
G_0	805		e_{min}	0,61		ν	0,3
h_{p0}	0,42		n^b	0,65		q	10
P_A	101,3		n^d	0,1		R	1,5
Postshake	0						

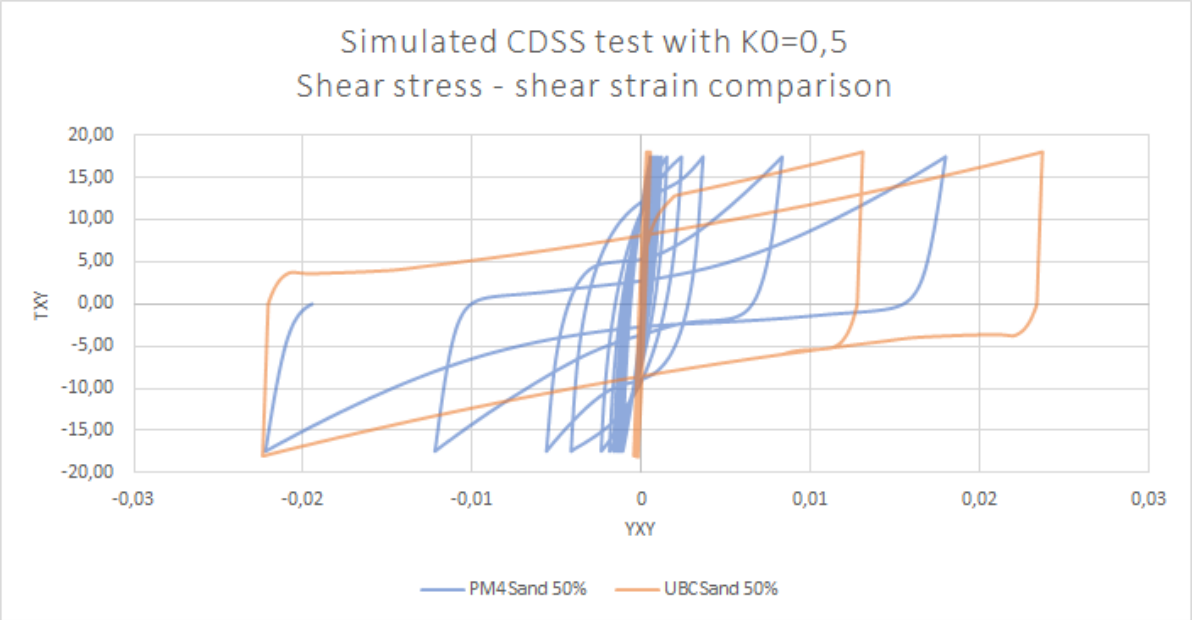

Figure B.6: Comparison graph showing the shear stress - shear strain relation with UBCSand simulated CDSS test results and the calibrated PM4Sand results for anisotropic test with $D_r = 50\%$

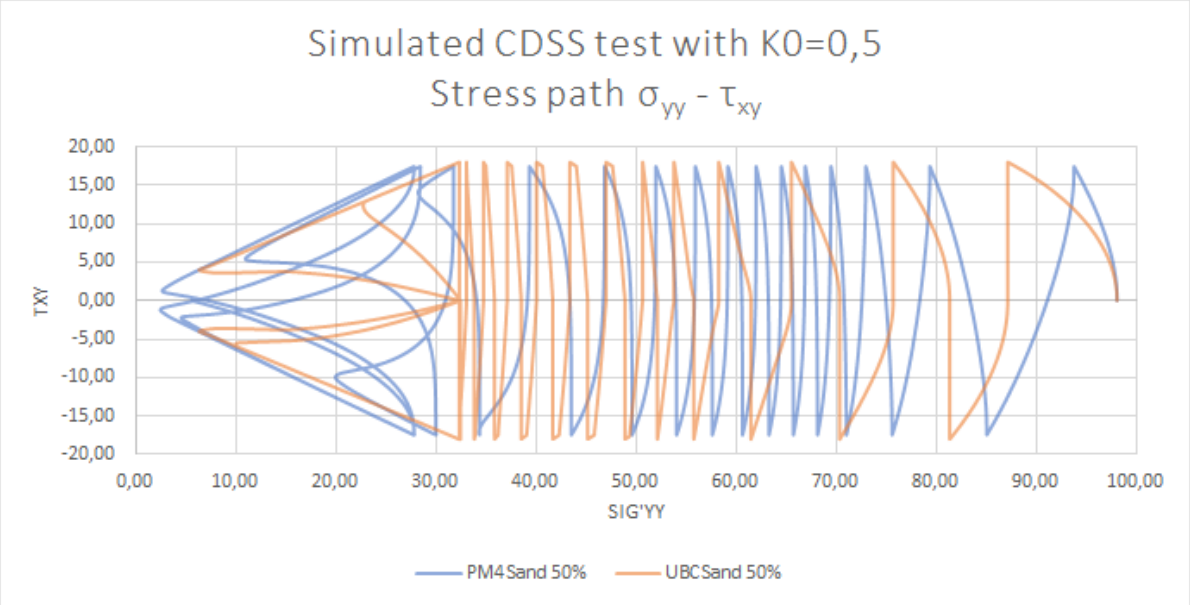

Figure B.7: Comparison graph showing the stress path with UBCSand simulated CDSS test results and the calibrated PM4Sand results for anisotropic test with $D_r = 50\%$

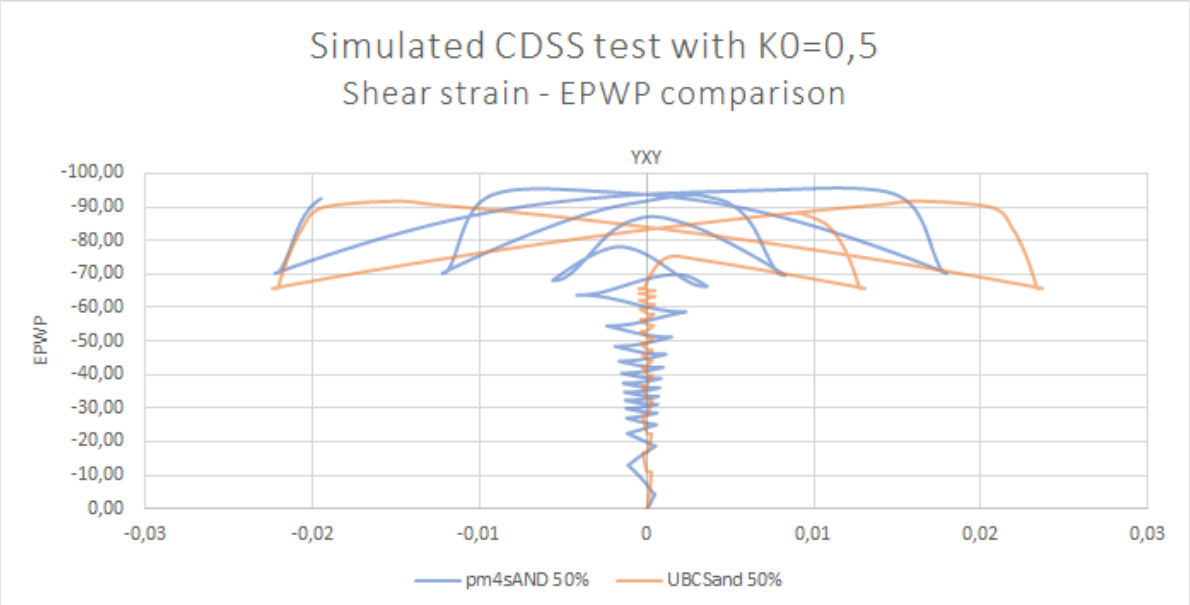

Figure B.8: Comparison graph showing the shear strain - excess pore water pressure relation with UBCSand simulated CDSS test results and the calibrated PM4Sand results for anisotropic test with $D_r = 50\%$

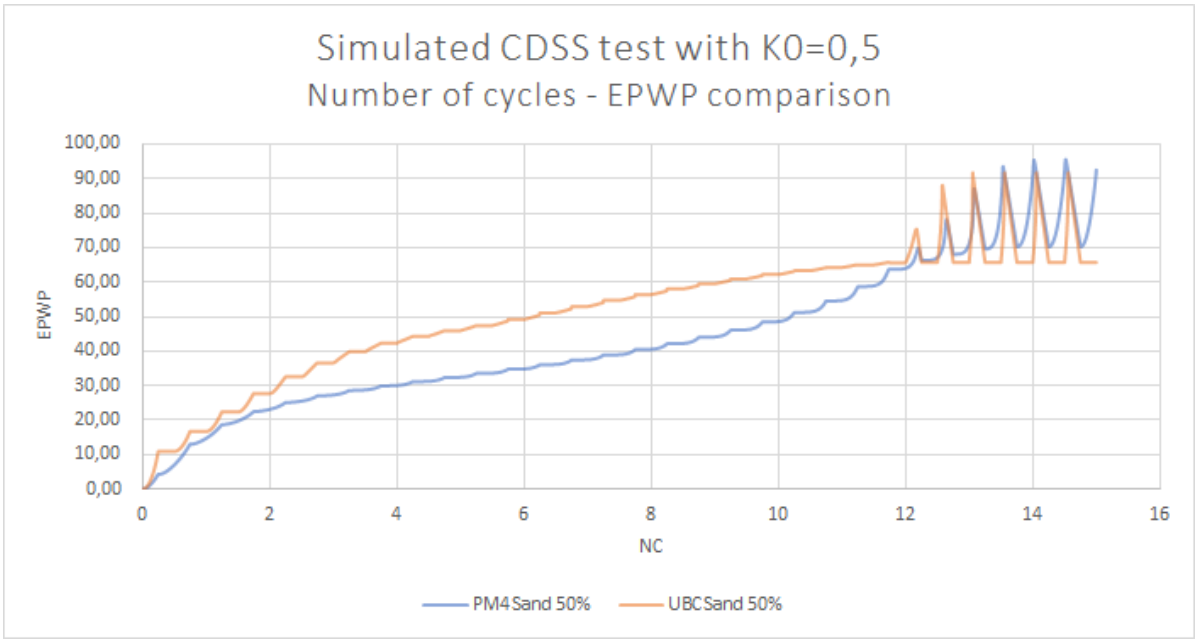

Figure B.9: Comparison graph showing the number of cycles - excess pore water pressure relation with UBCSand simulated CDSS test results and the calibrated PM4Sand results for anisotropic test with $D_r = 50\%$

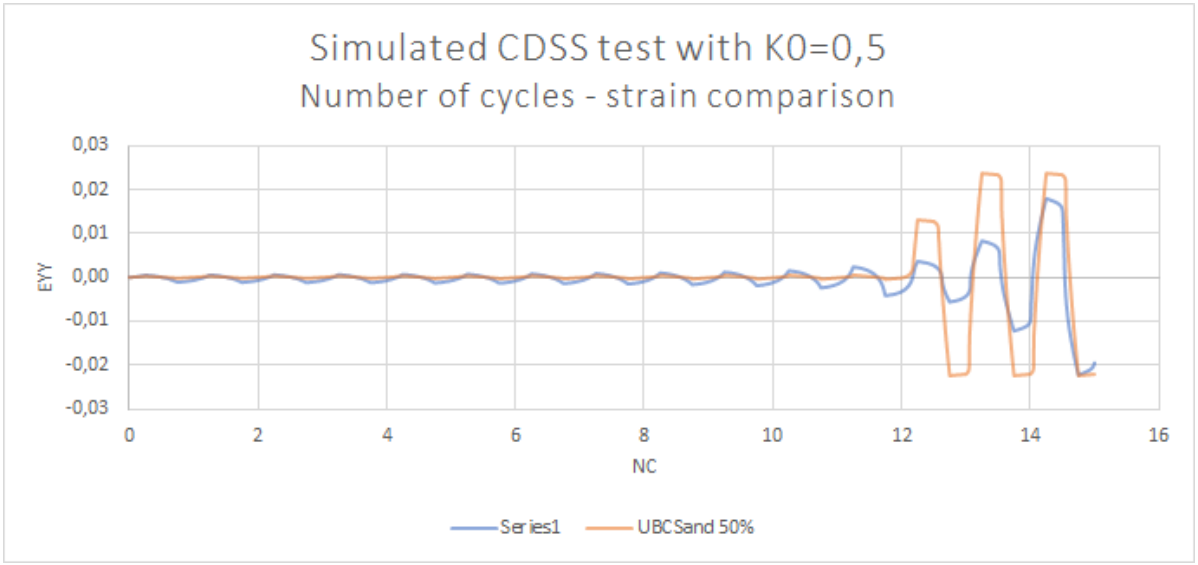

Figure B.10: Comparison graph showing the number of cycles - strain relation with UBCSand simulated CDSS test results and the calibrated PM4Sand results for anisotropic test with $D_r = 50\%$

Table B.5: Test properties calibrated with CDSS from UBCSand model for isotropic PM4Sand parameters with $D_r = 80\%$

Test properties calibrated with CDSS from UBCSand model		
Initial stress σ_{yy}	98	kN/m^2
CSR	0.270	
τ_{xy}	26.5	kN/m^2
N_c	15	cycles
Isotropic test		

B.1.3. PM4Sand with isotropic conditions and D_r = 80%

Table B.6: Used parameter values PM4Sand $D_r = 80\%$ isotropic

D_{r0}	0.725		e_{max}	0,98		ϕ_{cv}	38
G_0	1950		e_{min}	0,61		ν	0,3
h_{p0}	0.165		n^b	0.45		q	10
P_A	101,3		n^d	0,1		R	1,5
Postshake	0						

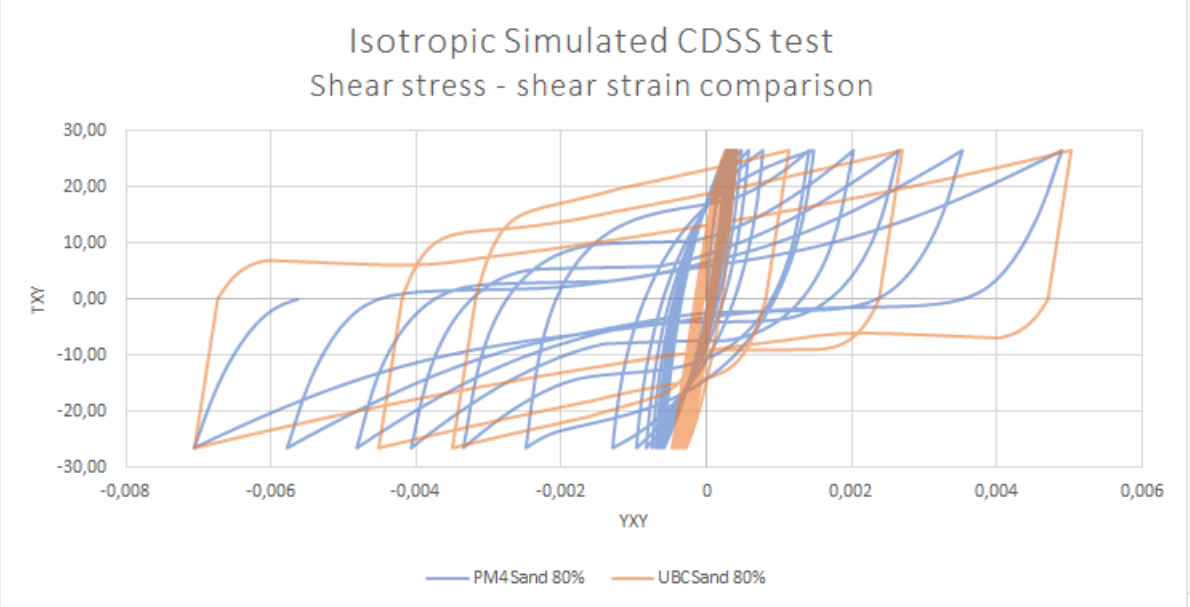

Figure B.11: Comparison graph showing the shear stress - shear strain relation with UBCSand simulated CDSS test results and the calibrated PM4Sand results for isotropic test with $D_r = 80\%$

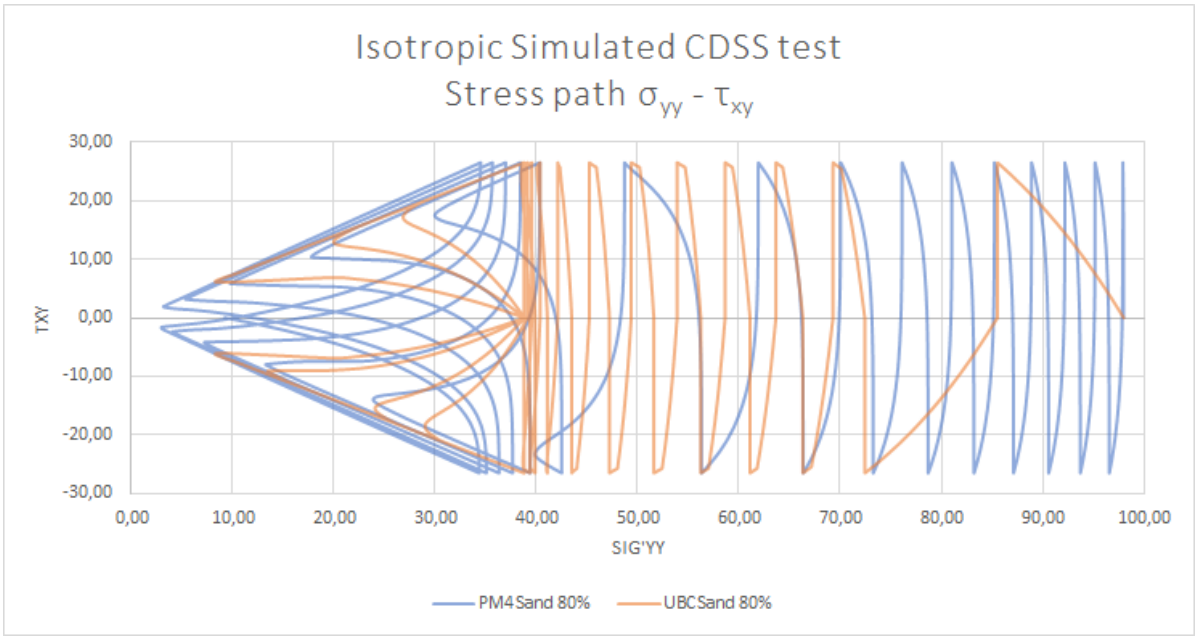

Figure B.12: Comparison graph showing the stress path with UBCSand simulated CDSS test results and the calibrated PM4Sand results for isotropic test with $D_r = 80\%$

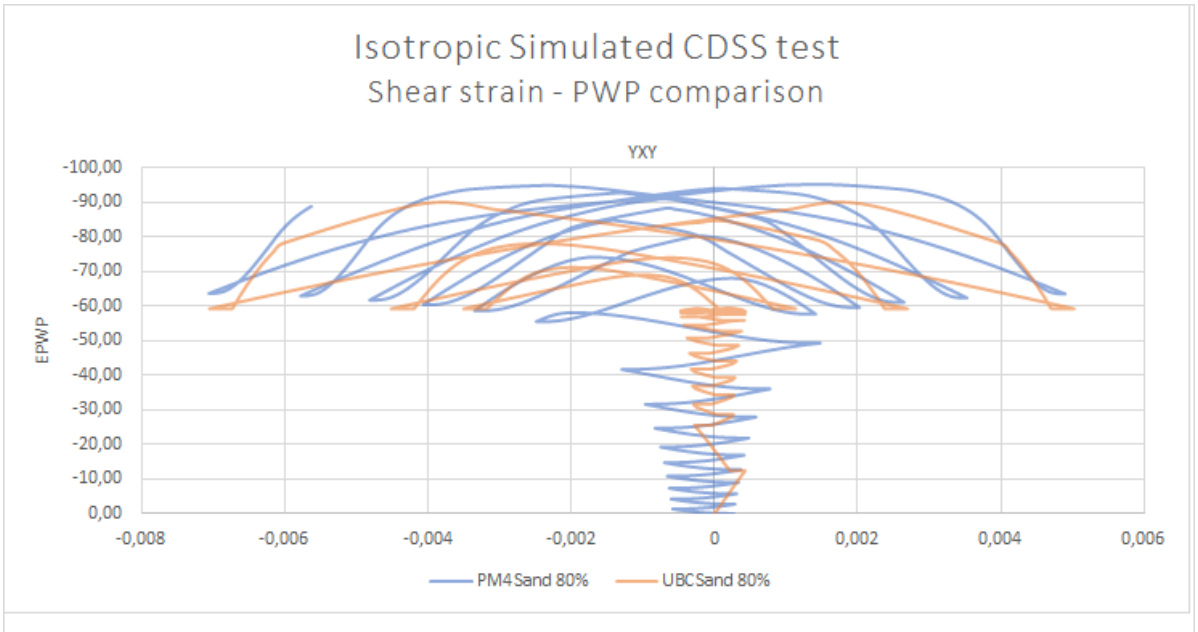

Figure B.13: Comparison graph showing the shear strain - excess pore water pressure relation with UBCSand simulated CDSS test results and the calibrated PM4Sand results for isotropic test with $D_r = 80\%$

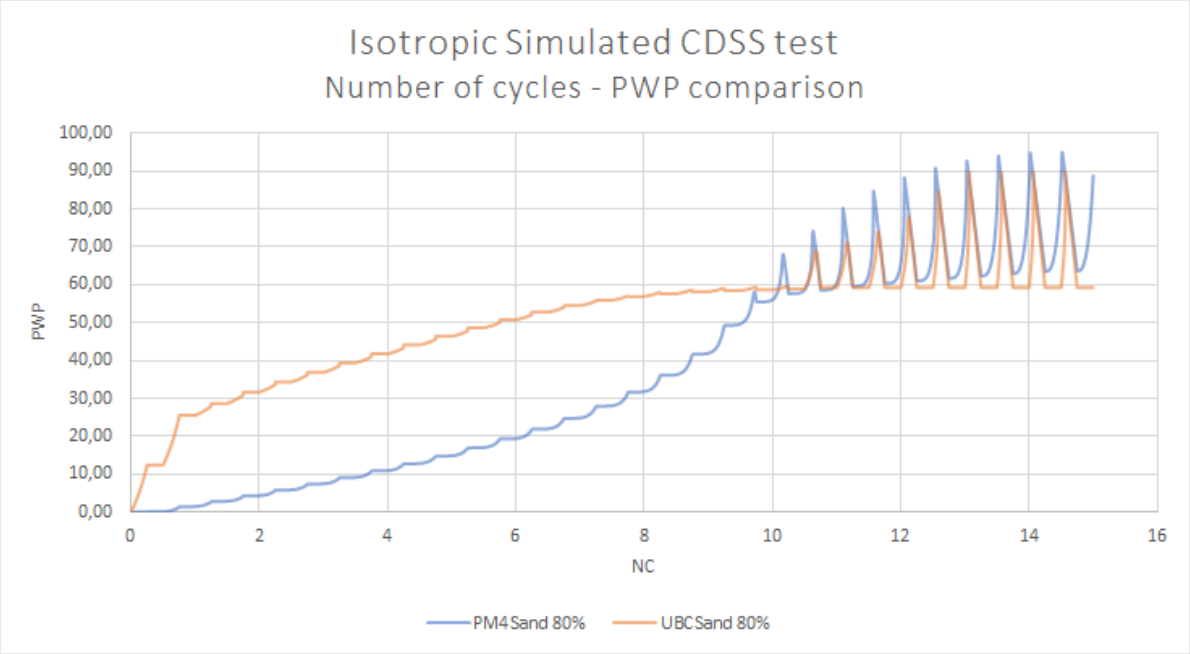

Figure B.14: Comparison graph showing the number of cycles - excess pore water pressure relation with UBCSand simulated CDSS test results and the calibrated PM4Sand results for isotropic test with $D_r = 80\%$

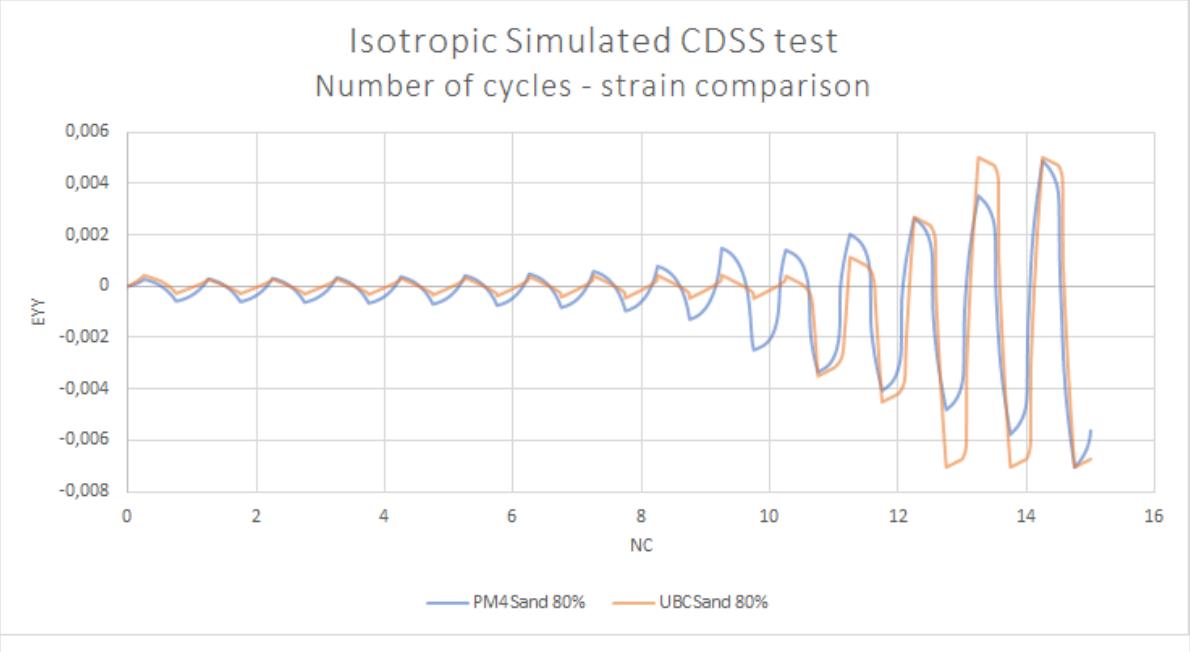

Figure B.15: Comparison graph showing the number of cycles - strain relation with UBCSand simulated CDSS test results and the calibrated PM4Sand results for isotropic test with $D_r = 80\%$

B.1.4. PM4Sand with K_0 = 0.5 and D_r = 80%

Table B.7: Test properties calibrated with CDSS from UBCSand model for anisotropic PM4Sand parameters with $D_r = 80\%$

Test properties calibrated with CDSS from UBCSand model		
Initial stress σ_{yy}	98	kN/m^2
CSR	0.270	
τ_{xy}	26.5	kN/m^2
N_c	15	cycles
$K_0 = 0.5$		

Table B.8: Used parameter values PM4Sand $D_r = 80\%$ and anisotropic

D_{r0}	0.76		e_{max}	0,98		ϕ_{cv}	38
G_0	1935		e_{min}	0,61		ν	0,3
h_{p0}	0.225		n^b	0.35		q	10
P_A	101,3		n^d	0,1		R	1,5
Postshake	0						

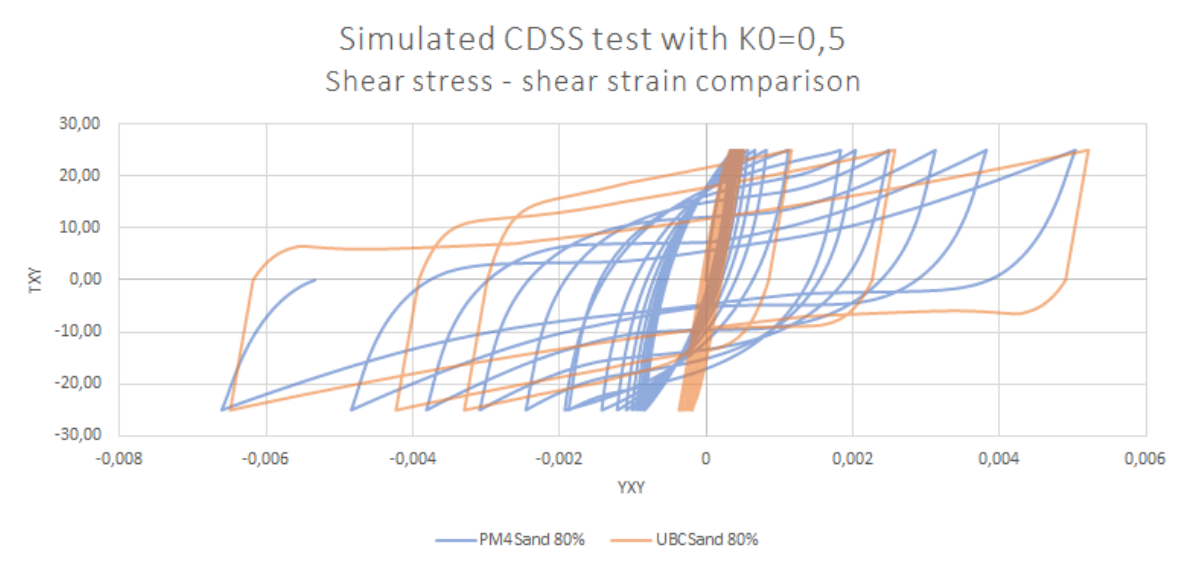

Figure B.16: Comparison graph showing the shear stress - shear strain relation with UBCSand simulated CDSS test results and the calibrated PM4Sand results for anisotropic test with $D_r = 80\%$

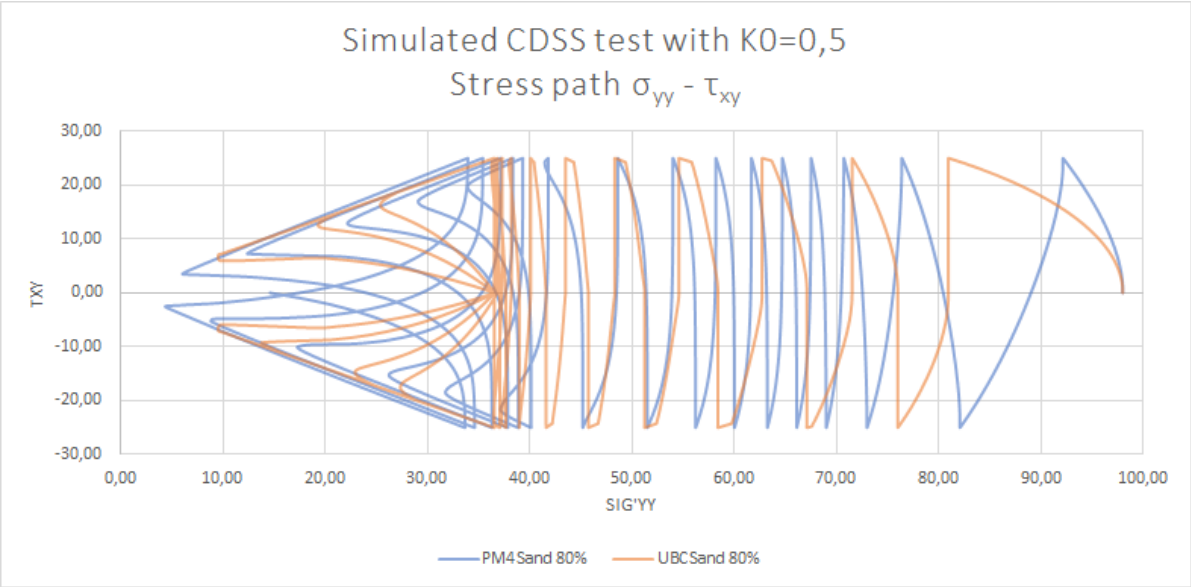

Figure B.17: Comparison graph showing the stress path with UBCSand simulated CDSS test results and the calibrated PM4Sand results for anisotropic test with $D_r = 80\%$

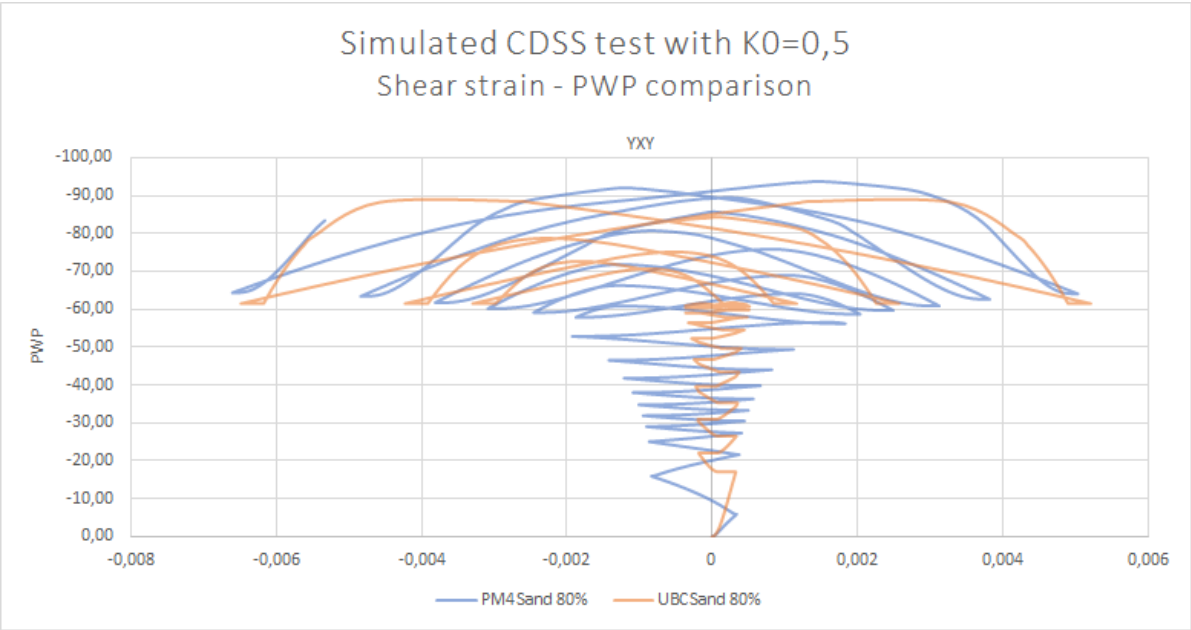

Figure B.18: Comparison graph showing the shear strain - excess pore water pressure relation with UBCSand simulated CDSS test results and the calibrated PM4Sand results for anisotropic test with $D_r = 80\%$

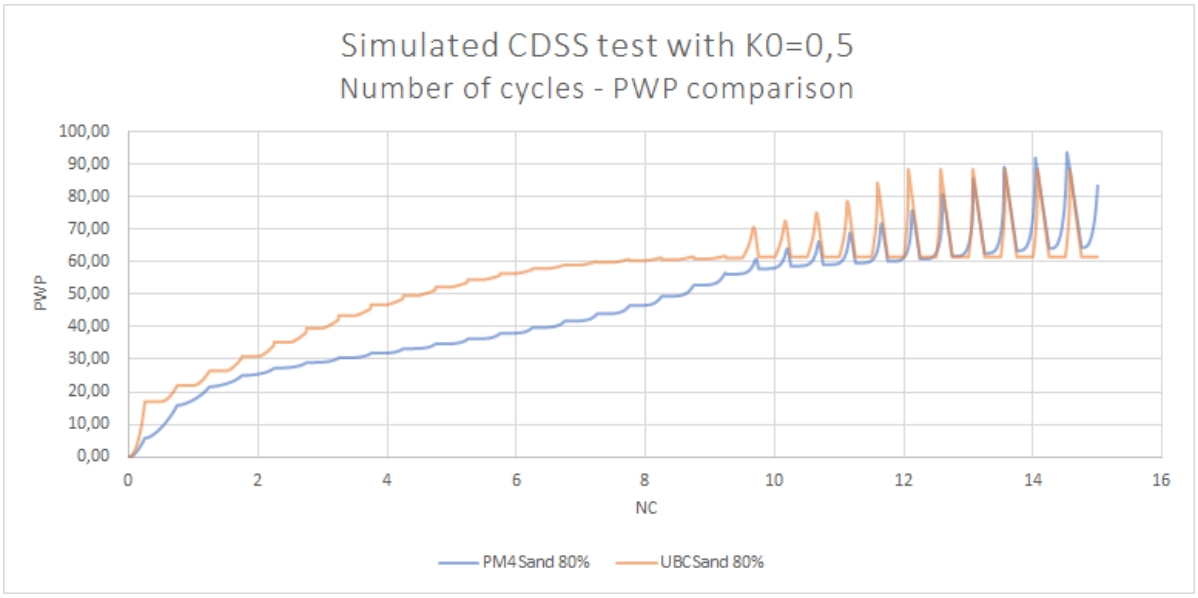

Figure B.19: Comparison graph showing the number of cycles - excess pore water pressure relation with UBCSand simulated CDSS test results and the calibrated PM4Sand results for anisotropic test with $D_r = 80\%$

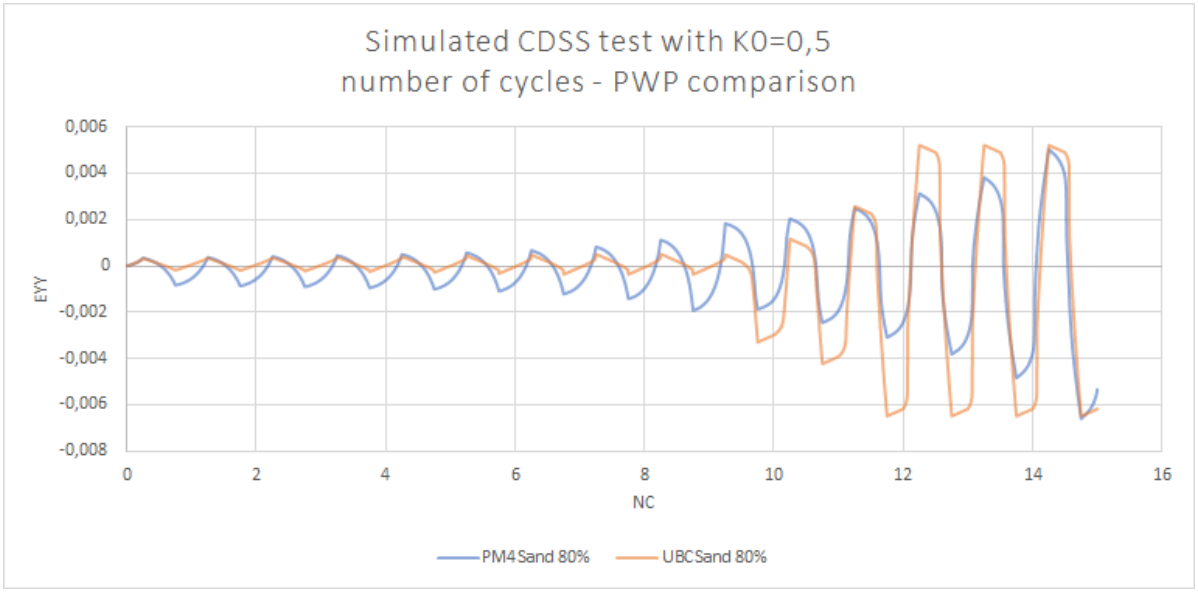

Figure B.20: Comparison graph showing the number of cycles - strain relation with UBCSand simulated CDSS test results and the calibrated PM4Sand results for anisotropic test with $D_r = 80\%$

B.2. PM4Sand calibration with Cyclic Torsional shear test

B.2.1. PM4Sand with isotropic conditions and D_r = 50%

Table B.9: Test properties calibrated with cyclic Torsional shear test for isotropic PM4Sand parameters with $D_r = 50\%$

Test properties calibrated with CTST		
Initial stress σ_{yy}	98	kN/m^2
CSR	0.1875	
τ_{xy}	18.375	kN/m^2
Reach 3% DA strain in	10	cycles
Isotropic test		

Table B.10: Used parameter values PM4Sand $D_r = 50\%$ isotropic from cyclic torsional shear test

D_{r0}	0.5		e_{max}	0,98		ϕ_{cv}	31.33
G_0	965		e_{min}	0,61		ν	0,3
h_{p0}	0.44		n^b	0.8		q	10
P_A	101,3		n^d	0,1		R	1,5
Postshake	0						

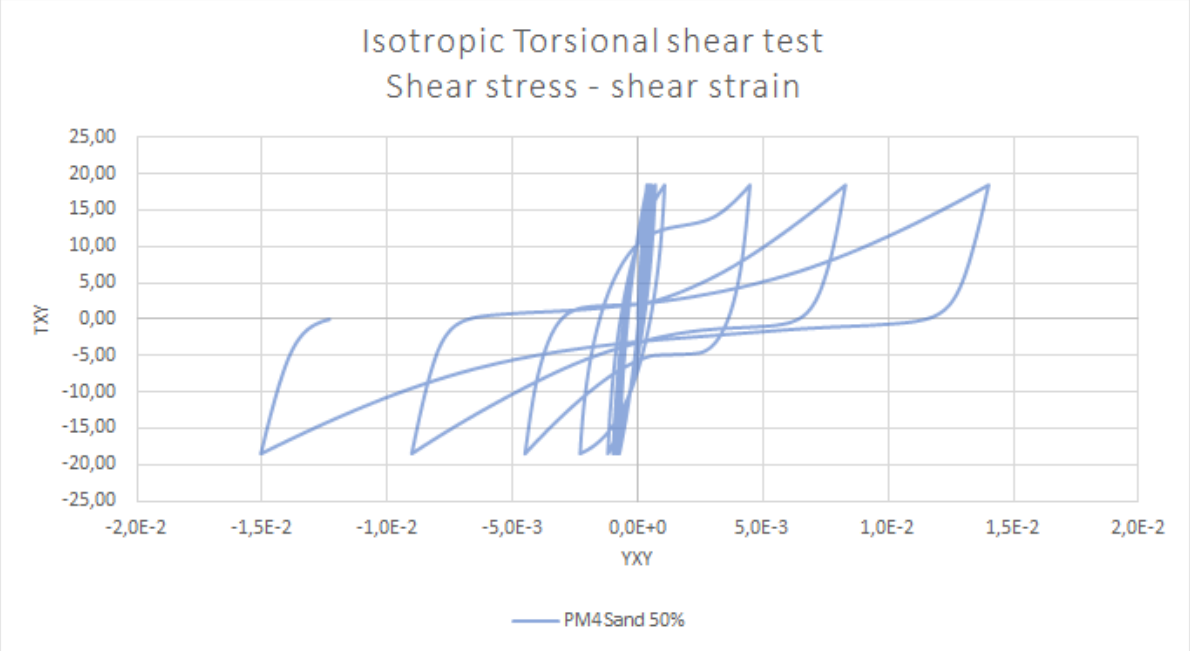

Figure B.21: Graph showing the shear stress - shear strain relation test results for the calibrated PM4Sand results of an isotropic CTST test with $D_r = 50\%$

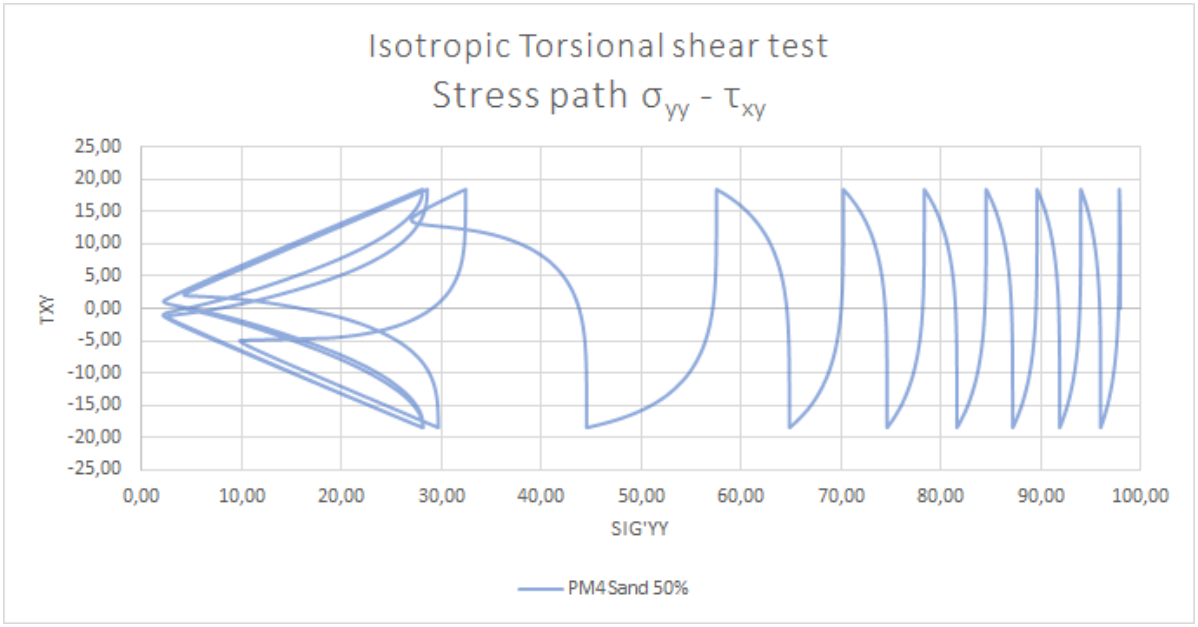

Figure B.22: Graph showing the stress path test results for the calibrated PM4Sand results of an isotropic CTST test with $D_r = 50\%$

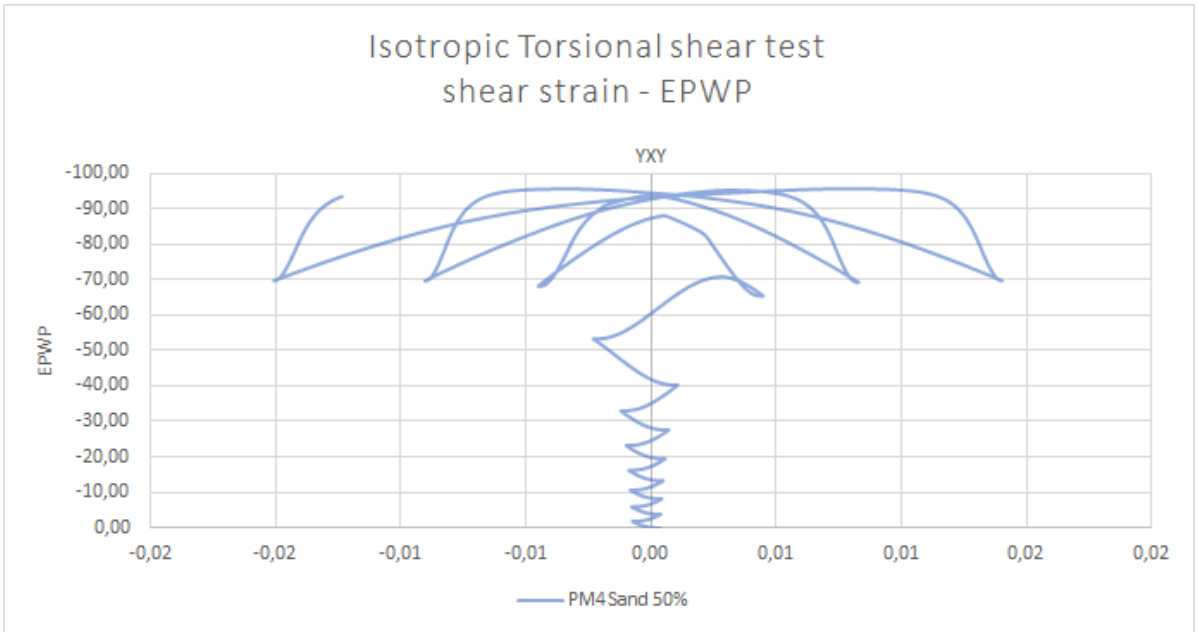

Figure B.23: Graph showing the strain - excess pore water pressure relation test results for the calibrated PM4Sand results of an isotropic CTST test with $D_r = 50\%$

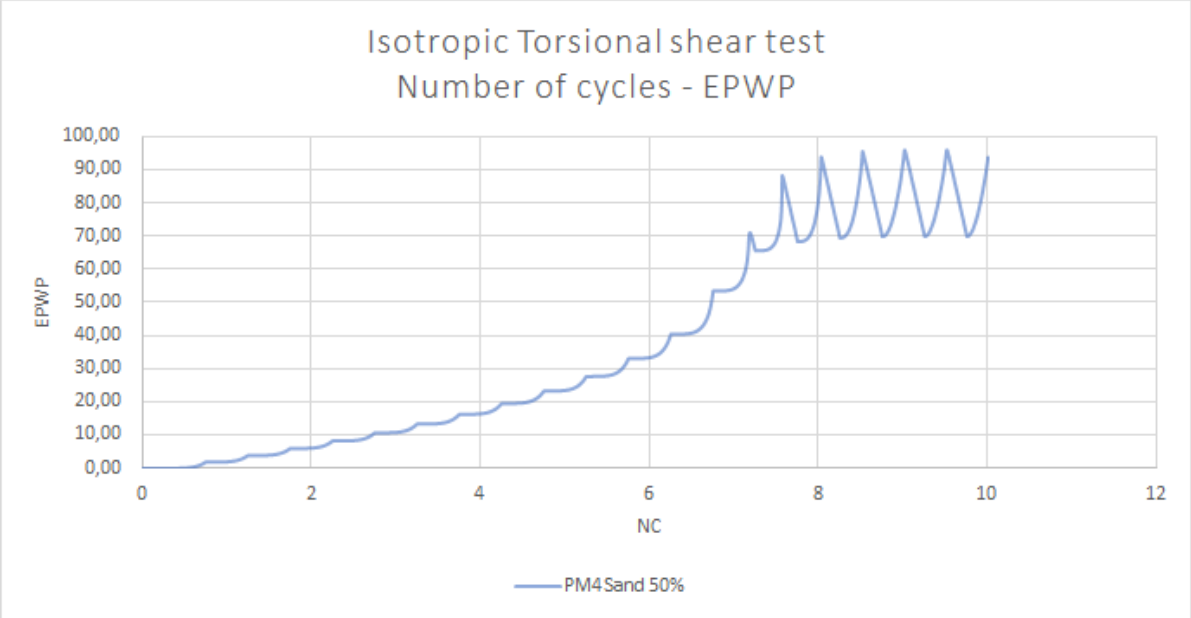

Figure B.24: Graph showing the number of cycles - excess pore water pressure relation test results for the calibrated PM4Sand results of an isotropic CTST test with $D_r = 50\%$

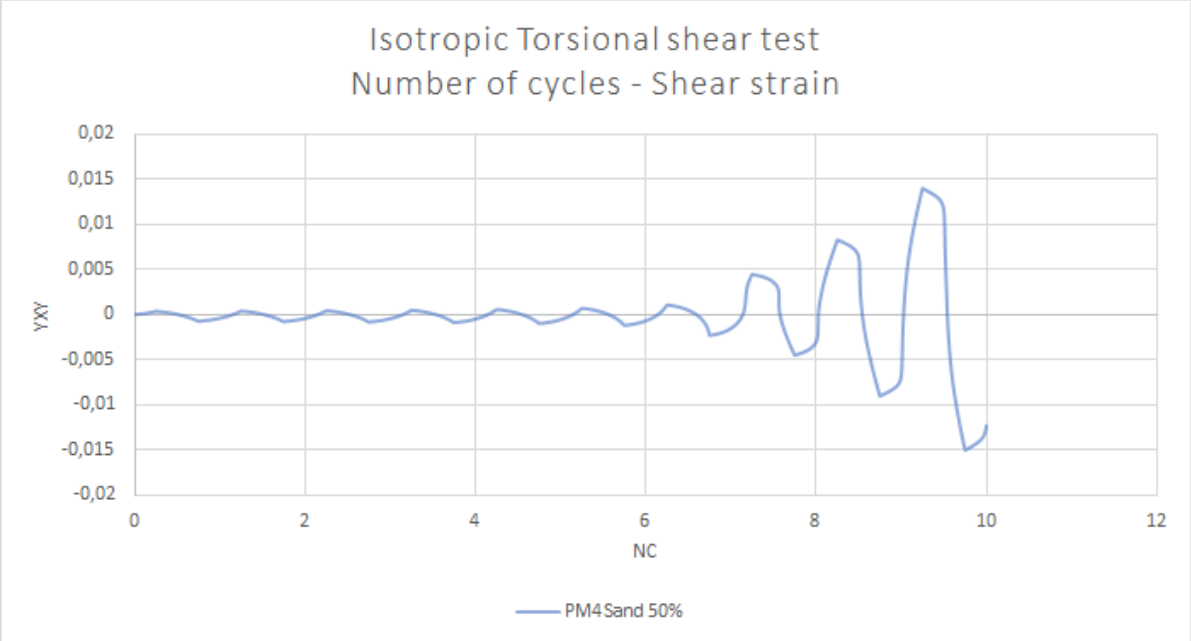

Figure B.25: Graph showing the number of cycles - strain relation test results for the calibrated PM4Sand results of an isotropic CTST test with $D_r = 50\%$

B.2.2. PM4Sand with anisotropic conditions and D_r = 50%

Table B.11: Test properties calibrated with cyclic Torsional shear test for anisotropic PM4Sand parameters with $D_r = 50\%$

Test properties calibrated with CTST		
Initial stress σ_{yy}	98	kN/m^2
CSR	0.1875	
τ_{xy}	18.375	kN/m^2
Reach 3% DA strain in	10	cycles
anisotropic test		

Table B.12: Used parameter values PM4Sand $D_r = 50\%$ anisotropic from cyclic torsional shear test

D_{r0}	0.5		e_{max}	0,98		ϕ_{cv}	31.33
G_0	965		e_{min}	0,61		ν	0,3
h_{p0}	0.44		n^b	0.8		q	10
P_A	101,3		n^d	0,1		R	1,5
Postshake	0						

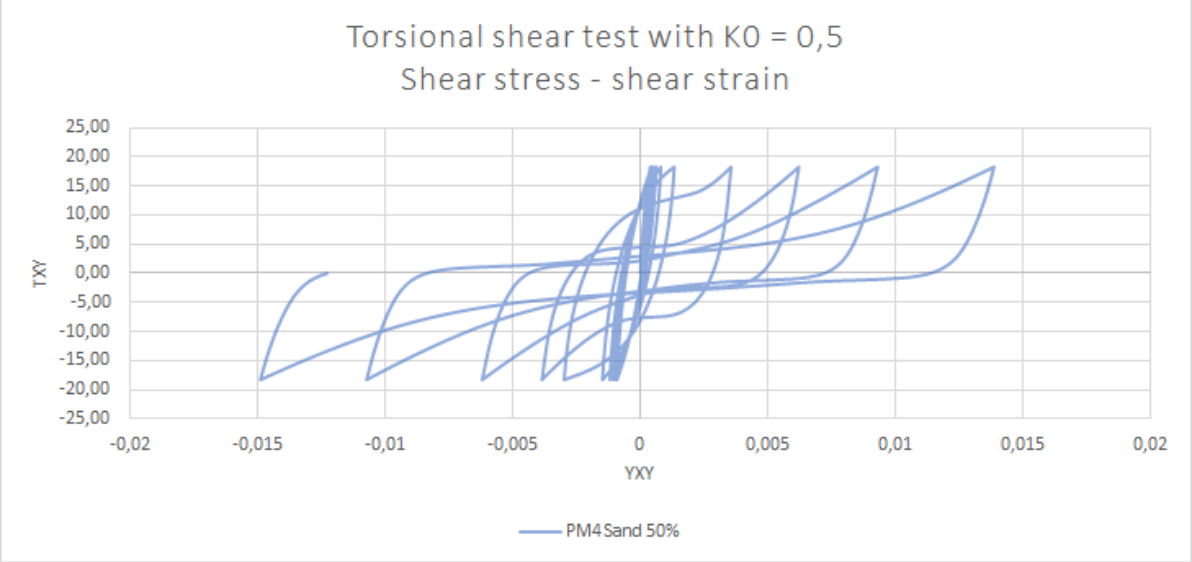

Figure B.26: Graph showing the shear stress - shear strain relation test results for the calibrated PM4Sand results of an anisotropic CTST test with $D_r = 50\%$

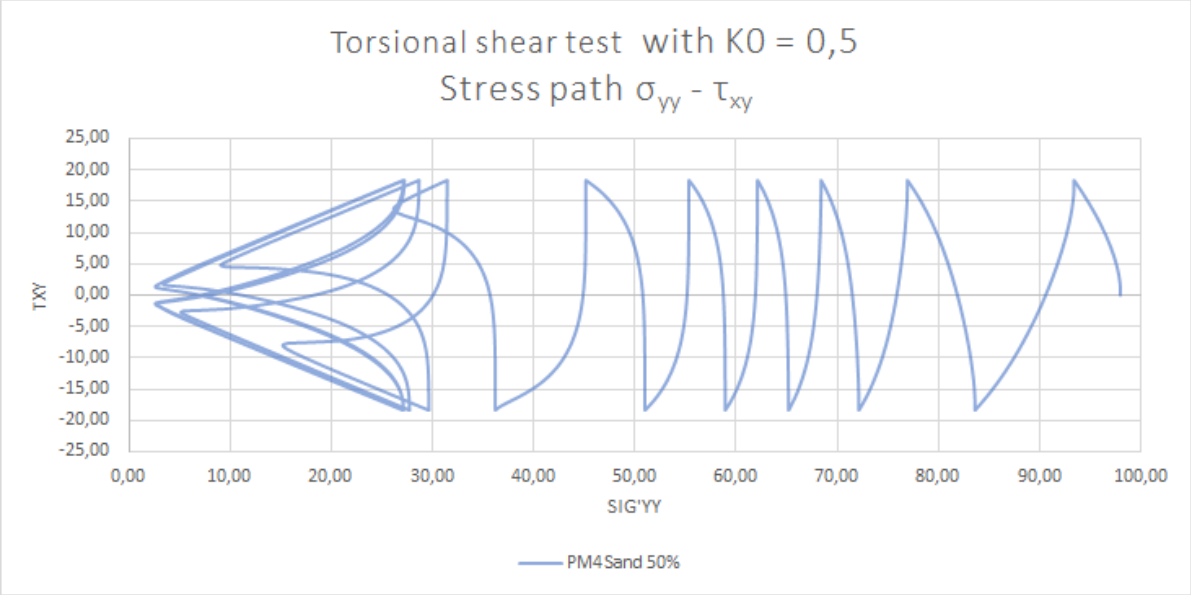

Figure B.27: Graph showing the stress path test results for the calibrated PM4Sand results of an anisotropic CTST test with $D_r = 50\%$

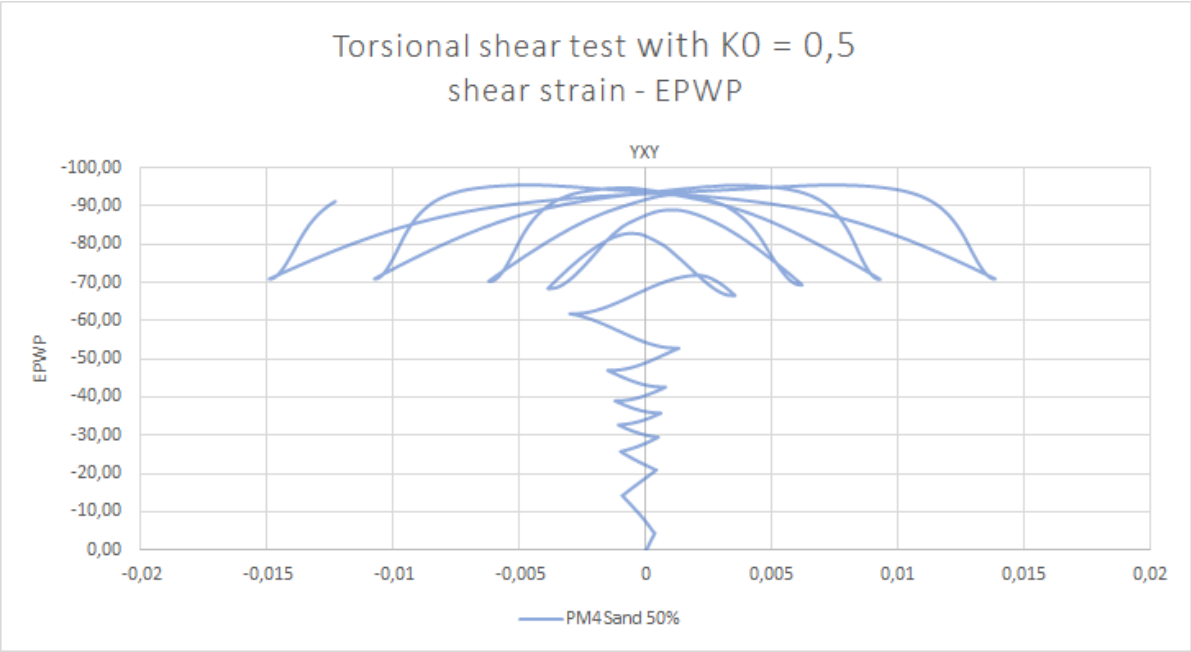

Figure B.28: Graph showing the strain - excess pore water pressure relation test results for the calibrated PM4Sand results of an anisotropic CTST test with $D_r = 50\%$

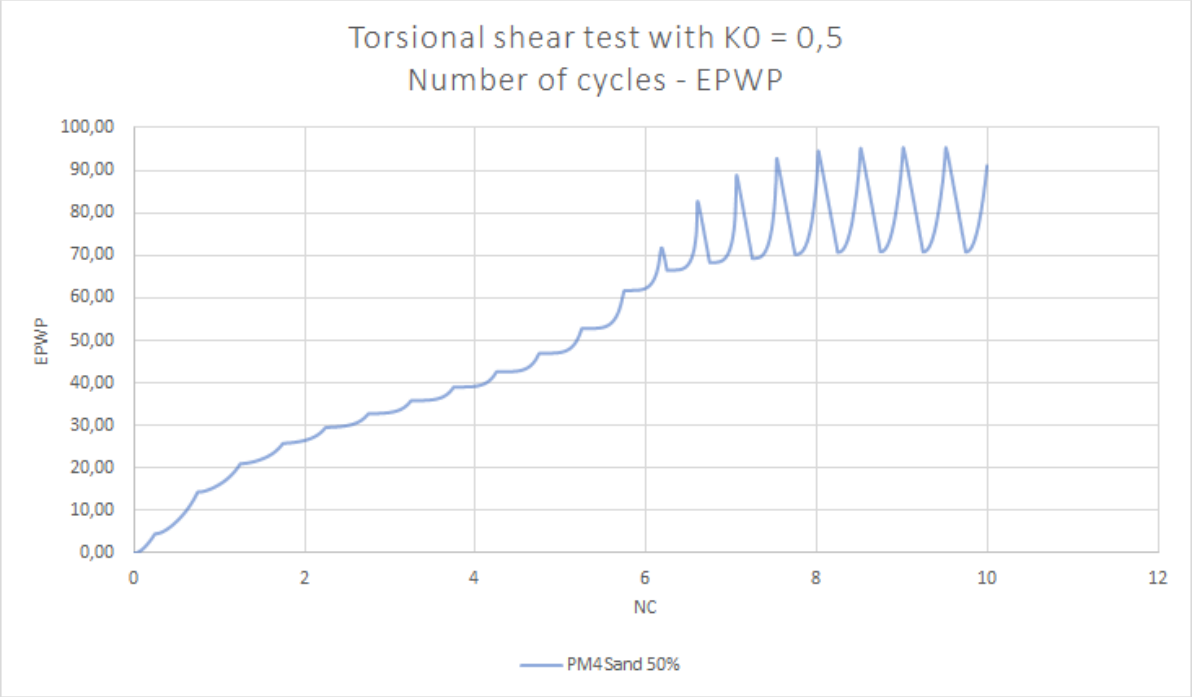

Figure B.29: Graph showing the number of cycles - excess pore water pressure relation test results for the calibrated PM4Sand results of an anisotropic CTST test with $D_r = 50\%$

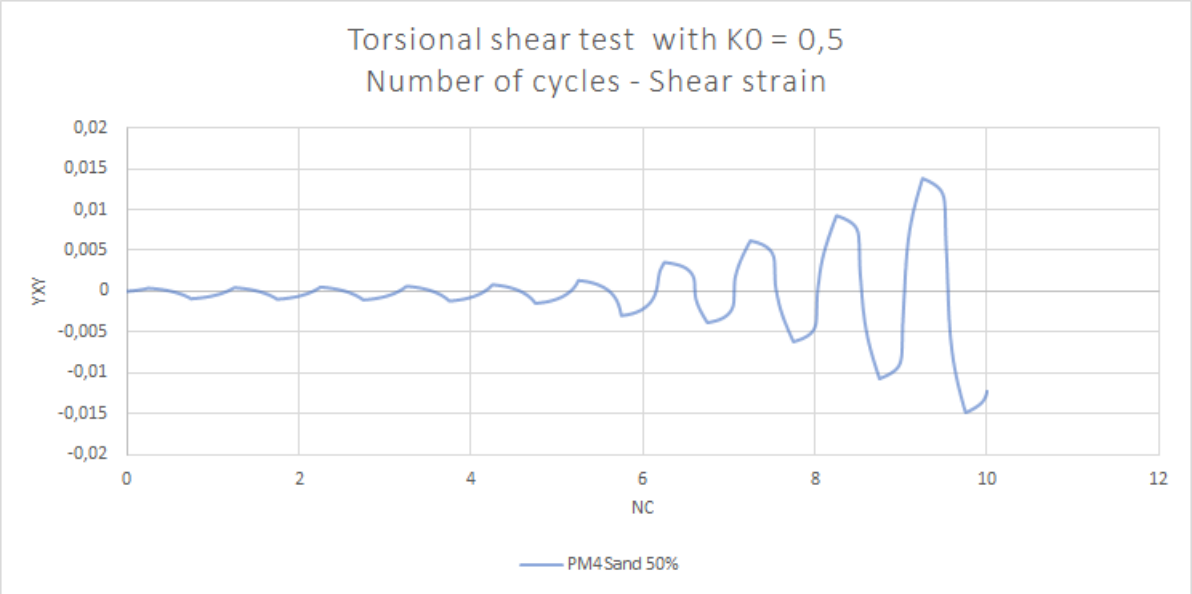

Figure B.30: Graph showing the number of cycles - strain relation test results for the calibrated PM4Sand results of an anisotropic CTST test with $D_r = 50\%$

B.2.3. PM4Sand with isotropic conditions and D_r = 60%

Table B.13: Test properties calibrated with cyclic Torsional shear test for isotropic PM4Sand parameters with $D_r = 60\%$

Test properties calibrated with CTST		
Initial stress σ_{yy}	98	kN/m^2
CSR	0.209	
τ_{xy}	20.44	kN/m^2
Reach 3% DA strain in	15	cycles
Isotropic test		

Table B.14: Used parameter values PM4Sand $D_r = 60\%$ isotropic from cyclic torsional shear test

D_{r0}	0.6		e_{max}	0,98		ϕ_{cv}	33
G_0	729		e_{min}	0,61		ν	0,3
h_{p0}	0.82		n^b	0.5		q	10
P_A	101,3		n^d	0,1		R	1,5
Postshake	0						

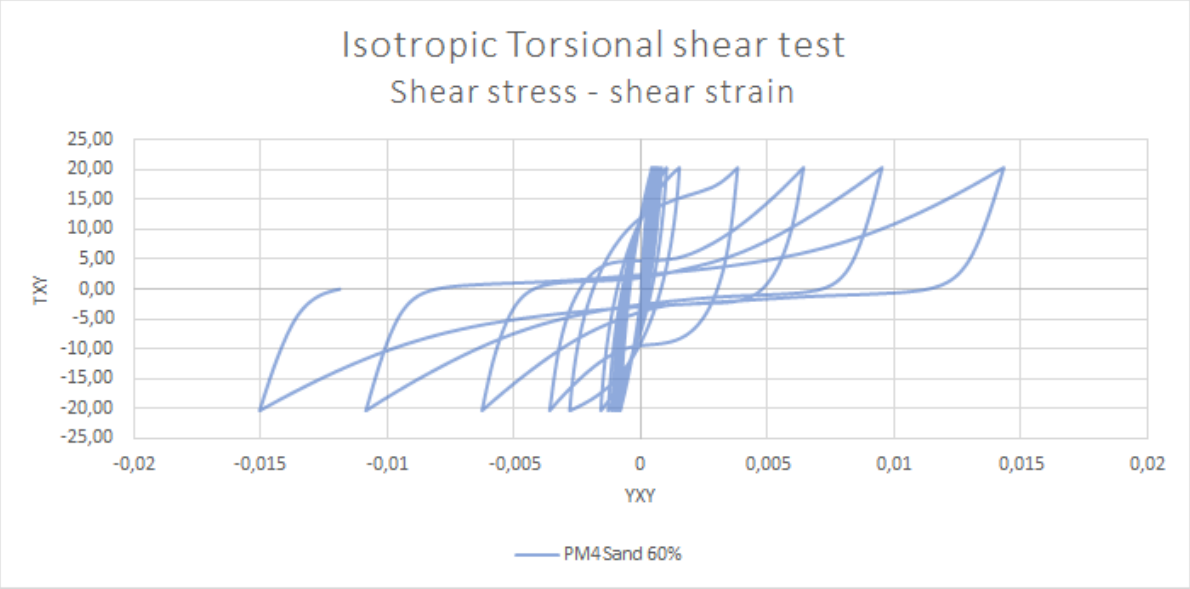

Figure B.31: Graph showing the shear stress - shear strain relation test results for the calibrated PM4Sand results of an isotropic CTST test with $D_r = 60\%$

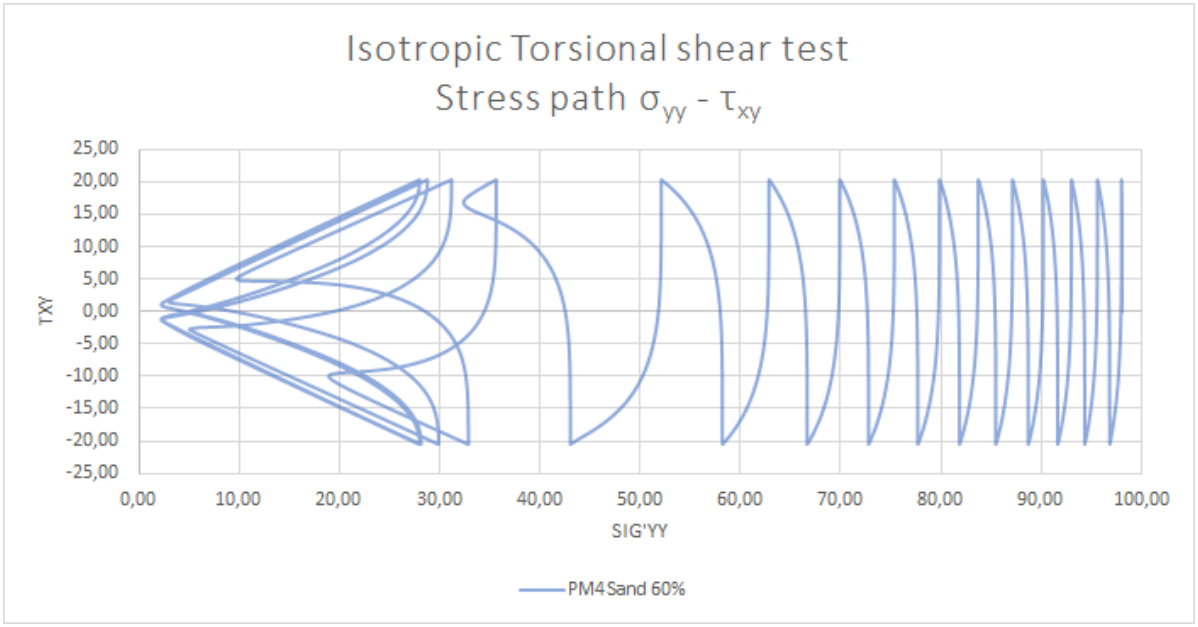

Figure B.32: Graph showing the stress path test results for the calibrated PM4Sand results of an isotropic CTST test with $D_r = 60\%$

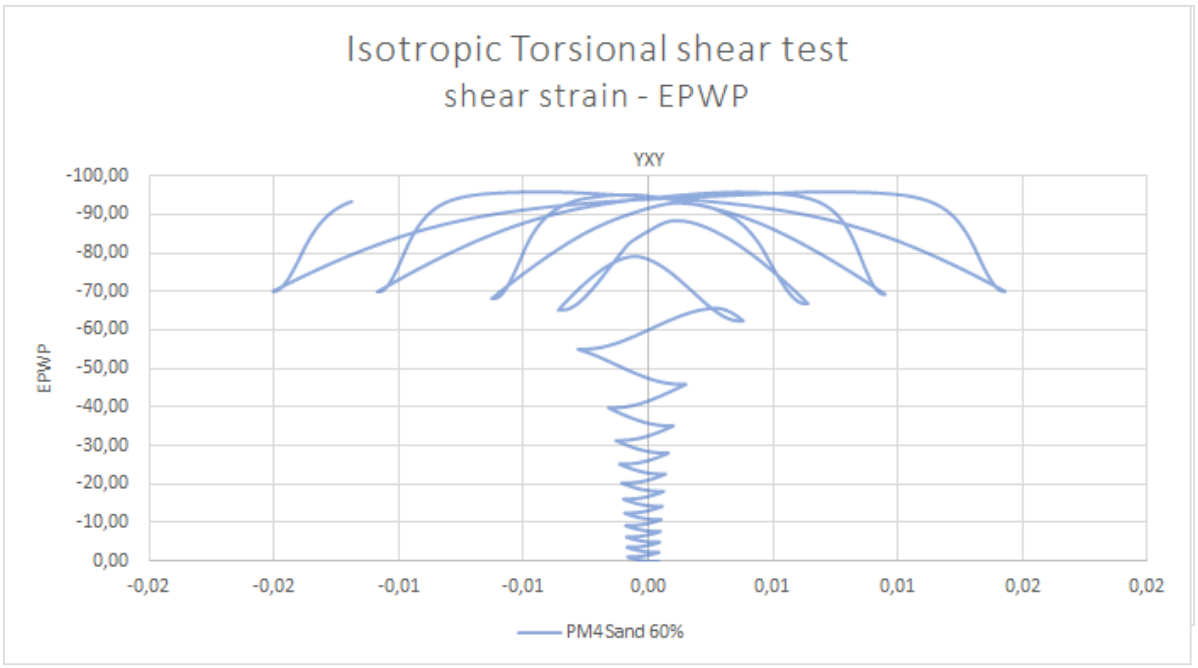

Figure B.33: Graph showing the strain - excess pore water pressure relation test results for the calibrated PM4Sand results of an isotropic CTST test with $D_r = 60\%$

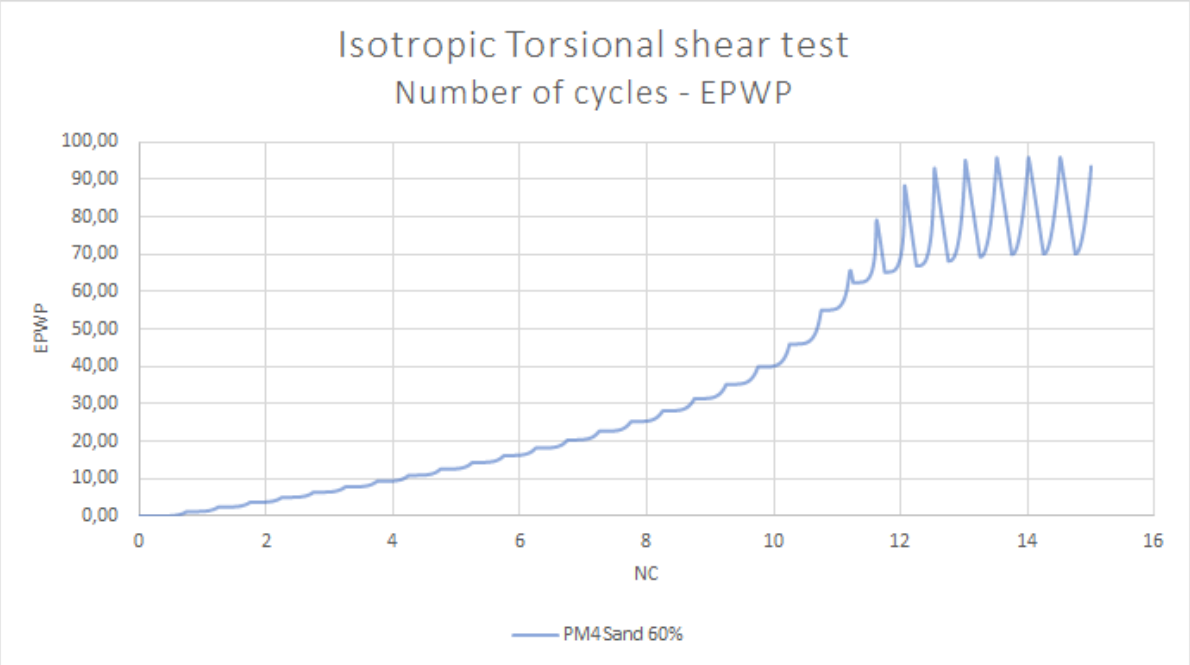

Figure B.34: Graph showing the number of cycles - excess pore water pressure relation test results for the calibrated PM4Sand results of an isotropic CTST test with $D_r = 60\%$

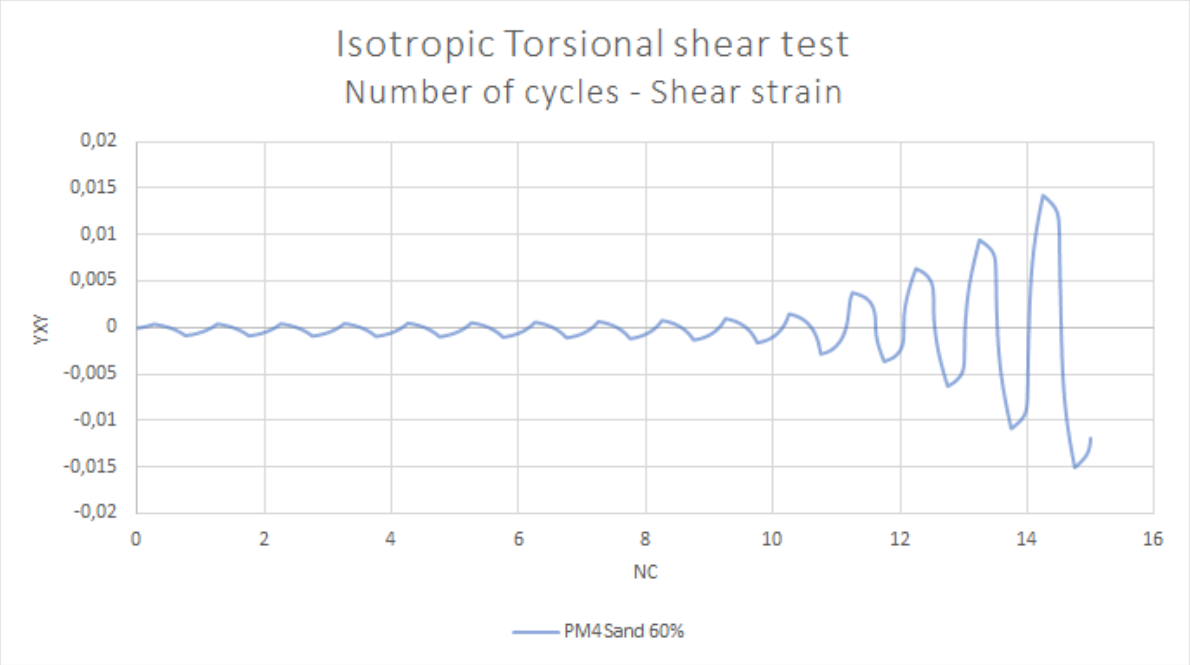

Figure B.35: Graph showing the number of cycles - strain relation test results for the calibrated PM4Sand results of an isotropic CTST test with $D_r = 60\%$

B.2.4. PM4Sand with isotropic conditions and D_r = 80%

Table B.15: Test properties calibrated with cyclic Torsional shear test for isotropic PM4Sand parameters with $D_r = 80\%$

Test properties calibrated with CTST		
Initial stress σ_{yy}	98	kN/m^2
CSR	0.267	
τ_{xy}	26.17	kN/m^2
Reach 3% DA strain in	15	cycles
Isotropic test		

Table B.16: Used parameter values PM4Sand $D_r = 80\%$ isotropic from cyclic torsional shear test

D_{r0}	0.7		e_{max}	0,98		ϕ_{cv}	38
G_0	1075		e_{min}	0,61		ν	0,3
h_{p0}	0.255		n^b	0.55		q	10
P_A	101,3		n^d	0,1		R	1,5
Postshake	0						

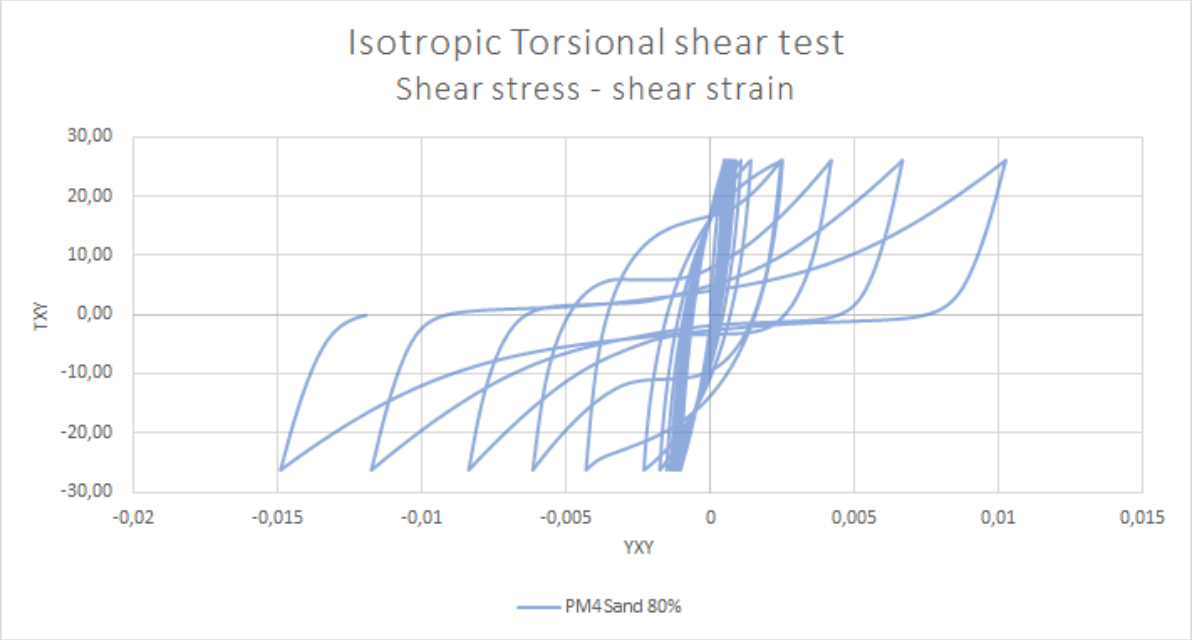

Figure B.36: Graph showing the shear stress - shear strain relation test results for the calibrated PM4Sand results of an isotropic CTST test with $D_r = 80\%$

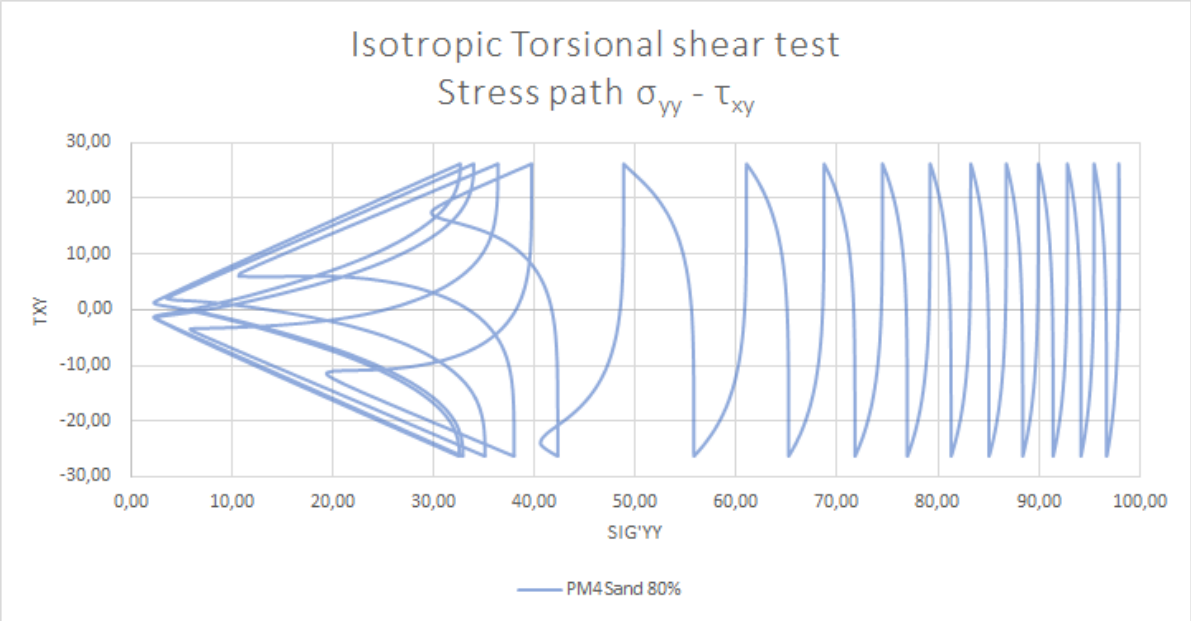

Figure B.37: Graph showing the stress path test results for the calibrated PM4Sand results of an isotropic CTST test with $D_r = 80\%$

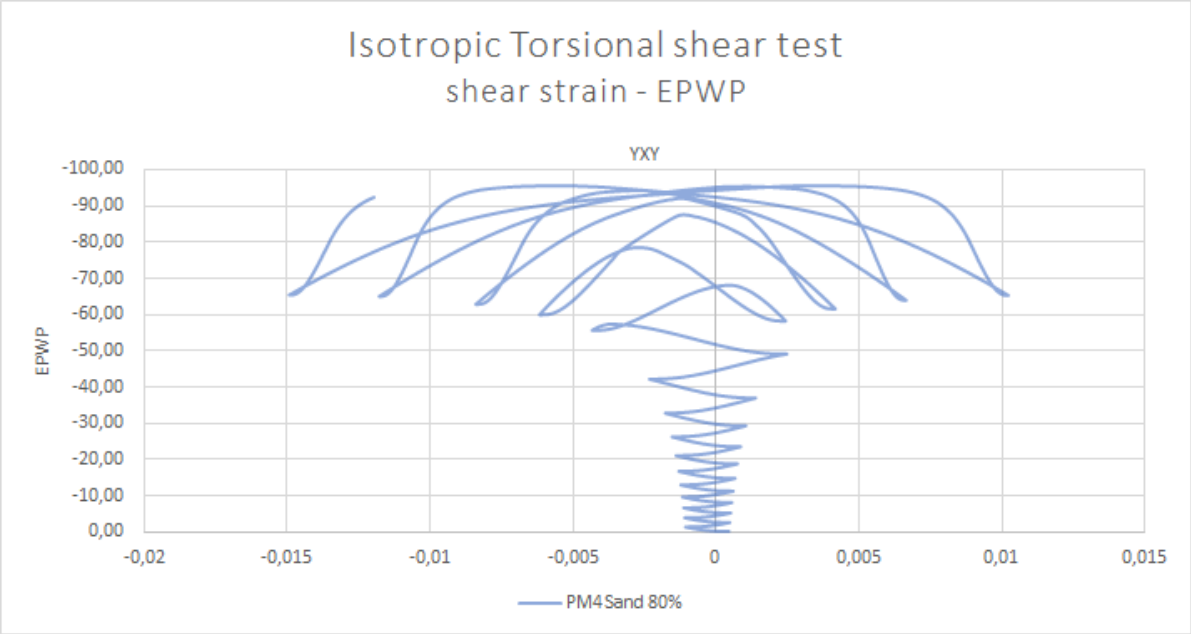

Figure B.38: Graph showing the strain - excess pore water pressure relation test results for the calibrated PM4Sand results of an isotropic CTST test with $D_r = 80\%$

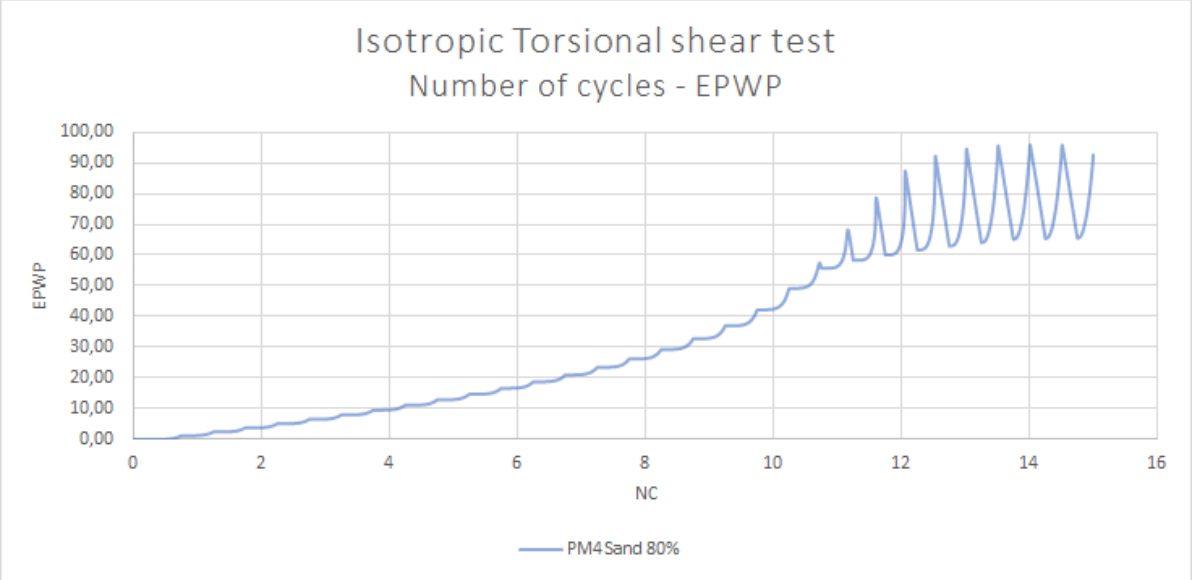

Figure B.39: Graph showing the number of cycles - excess pore water pressure relation test results for the calibrated PM4Sand results of an isotropic CTST test with $D_r = 80\%$

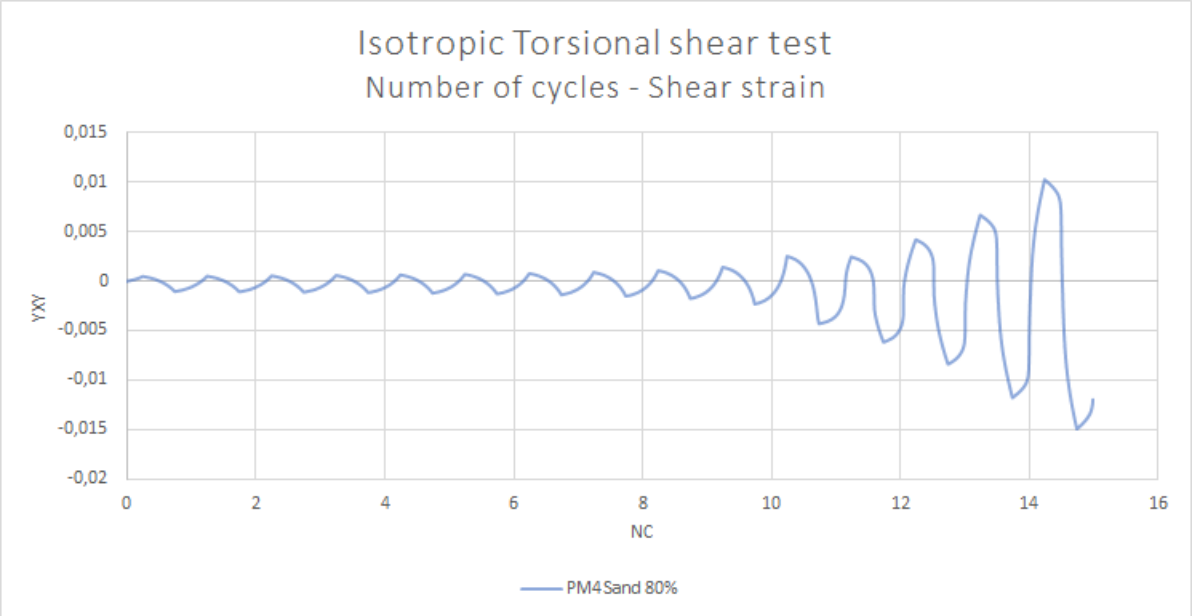

Figure B.40: Graph showing the number of cycles - strain relation test results for the calibrated PM4Sand results of an isotropic CTST test with $D_r = 80\%$

C

Appendix Sensitivity of PM4Sand

In the following tables the results of the sensitivity analysis can be found. The PM4Sand parameters have been changed and the effect on the different graphs are reported.

Table C.1: Shear stress - shear strain comparison plot

Shear stress - shear strain comparison plot					
	lower value	result lower value	Base parameter set	higher value	result higher value
Parameters					
Dr_0	0,5	Increase in total strain Increase in the amount of cycles not around zero Decrease in skewness of the graph	0,525	0,535	Decrease in total strain Decrease in amount of cycles not around zero
G_0	800	Increse in total strain Distance between cycles with increased strain are increased	960	1150	Decrease in total strain Distance between cycles with increased strain are decreased
h_{p0}	0,35	Increase in total strain Distance between cycles with increased strain are increased	0,42	0,5	Decrease in total strain Decrease in amount of cycles not around zero
P_A			101,3		
e_{max}	0,9	No significant noticeable changes	0,98	0,99	No significant noticeable changes
e_{min}	0,5	No significant noticeable changes	0,61	0,75	No significant noticeable changes
n^b	0,45	Increase in total strain First two cycles not around zero are closer together, last two cycles not around zero look similar	0,65		Decrease in total strain
n^d	0,05	Increase in total strain Increase in amount of cycles not around zero Graph is less skewed	0,1	0,2	Decrease in total strain Decrease in amount of cycles not around zero
ϕ'_{cv}	27	Small increase in total strain	31,33	35	Decrease in total strain Increase in amount of cycles not around zero
ν	0,275	Decrease in total strain Decrease in amount of cycles not around zero	0,3	0,325	Increase in total strain Increase in amount of cycles not around zero
Q	9,5	Increase in total strain Increase in amount of cycles not around zero	10	10,5	Decrease in total strain Decrease in amount of cycles not around zero
R	1,4	Decrease in total strain Decrease in amount of cycles not around zero	1,5	1,6	Increase in total strain Increase in amount of cycles not around zero
Postshake			0		

Table C.2: Horizontal stress - shear stress comparison plot

Horizontal stress- shear stress comparison plot					
	lower value	result lower value	Base parameter set	higher value	result higher value
Parameters					
Dr_0	0,5	Fewer cycles needed before reaching cone-shaped behaviour Distance between cycles up to the cone-shaped behaviour increased	0,525	0,535	More cycles needed before reaching cone-shaped behaviour Distance between cycles upto the cone-shaped behaviour decreased
G_0	800	No significant noticeable changes	960	1150	No significant noticeable changes
h_{p0}	0,35	Fewer cycles needed before reaching cone-shaped behaviour Distance between cycles up to the cone-shaped behaviour increased	0,42	0,5	More cycles needed before reaching cone-shaped behaviour Distance between cycles up to the cone-shaped behaviour decreased
P_A			101,3		
e_{max}	0,9	No significant noticeable changes	0,98	0,99	No significant noticeable changes
e_{min}	0,5	No significant noticeable changes	0,61	0,75	No significant noticeable changes
n^b	0,45	Last cycle before reaching cone-shaped behaviour flipped upside down. Looks like the graph before the cone-shaped behaviour changed half a phase	0,65	0,85	No significant noticeable changes
n^d	0,05	Last cycle before reaching cone-shaped behaviour flipped upside down. Looks like the graph before the cone-shaped behaviour changed half a phase	0,1	0,2	More cycles needed before reaching cone-shaped behaviour Distance between cycles up to the cone-shaped behaviour decreased
ϕ'_{cv}	27	Last cycle before reaching cone-shaped behaviour flipped upside down. Looks like the graph before the cone-shaped behaviour changed half a phase	31,33	35	A small wrinkle in the last cycle before the cone-shaped behaviour occurred
ν	0,275	A small wrinkle in the last cycle before the cone-shaped behaviour occurred	0,3	0,325	Last cycle before reaching cone-shaped behaviour flipped upside down. Looks like the graph before the cone-shaped behaviour changed half a phase
Q	9,5	Last cycle before reaching cone-shaped behaviour flipped upside down. Looks like the graph before the cone-shaped behaviour changed half a phase	10	10,5	More cycles needed before reaching cone-shaped behaviour Distance between cycles up to the cone-shaped behaviour decreased
R	1,4	More cycles needed before reaching cone-shaped behaviour Distance between cycles up to the cone-shaped behaviour decreased	1,5	1,6	Fewer cycles needed before reaching cone-shaped behaviour Distance between cycles up to the cone-shaped behaviour increased
Postshake			0		

Table C.3: Shear strain - EPWP comparison plot

Shear strain - EPWP comparison plot					
	lower value	result lower value	Base parameter set	higher value	result higher value
Parameters					
Dr_0	0,5	Increase in total strain More Cycles at highest EPWP	0,525	0,535	Decrease in total strain Less cycles at the highest EPWP
G_0	800	Increase in total strain	960	1150	Decrease in total strain Less cycles at the highest EPWP
h_{p0}	0,35	Increase in total strain More Cycles at highest EPWP	0,42	0,5	Decrease in total strain Less cycles at the highest EPWP
P_A			101,3		
e_{max}	0,9	No significant noticeable changes	0,98	0,99	No significant noticeable changes
e_{min}	0,5	No significant noticeable changes	0,61	0,75	No significant noticeable changes
n^b	0,45	Increase in total strain	0,65	0,85	Decrease in total strain
n^d	0,05	Increase in total strain More Cycles at highest EPWP	0,1	0,2	Decrease in total strain Less cycles at the highest EPWP
ϕ'_{cv}	27	Increase in total strain	31,33	35	Decrease in total strain More cycles at the highest EPWP
ν	0,275	Decrease in total strain Less cycles at the highest EPWP	0,3	0,325	Increase in total strain More Cycles at highest EPWP
Q	9,5	Increase in total strain More Cycles at highest EPWP	10	10,5	Decrease in total strain Less cycles at the higherst EPWP
R	1,4	Decrease in total strain Less cycles at the highest EPWP	1,5	1,6	Increase in total strain More Cycles at highest EPWP
postshake			0		

Table C.4: Number of cyles - EPWP comparison plot

Number of cyles - EPWP comparison plot					
	lower value	result lower value	Base parameter set	higher value	result higher value
Parameters					
Dr_0	0,5	Fewer cycles needed to reach the highest EPWP conditions Steeper inclination first part of the graph	0,525	0,535	More cycles needed to reach the highest EPWP conditions
G_0	800	No significant noticeable changes	960	1150	No significant noticeable changes
h_{p0}	0,35	Fewer cycles needed to reach the highest EPWP conditions Steeper inclination first part of the graph	0,42	0,5	More cycles needed to reach the highest EPWP conditions
P_A			101,3		
e_{max}	0,9	No significant noticeable changes	0,98	0,99	No significant noticeable changes
e_{min}	0,5	No significant noticeable changes	0,61	0,75	No significant noticeable changes
n^b	0,45	First EPWP peak increased	0,65	0,85	No significant noticeable changes
n^d	0,05	Fewer cycles needed to reach the highest EPWP conditions Steeper inclination first part of the graph	0,1	0,2	More cycles needed to reach the highest EPWP conditions
ϕ'_{cv}	27	No significant noticeable changes	31,33	35	Fewer cycles needed to reach the highest EPWP conditions Steeper inclination first part of the graph
ν	0,275	More cycles needed to reach the highest EPWP conditions	0,3	0,325	Fewer cycles needed to reach the highest EPWP conditions Steeper inclination first part of the graph
Q	9,5	Fewer cycles needed to reach the highest EPWP conditions Steeper inclination first part of the graph	10	10,5	More cycles needed to reach the highest EPWP conditions
R	1,4	More cycles needed to reach the highest EPWP conditions	1,5	1,6	Fewer cycles needed to reach the highest EPWP conditions Steeper inclination first part of the graph
Postshake			0		

Table C.5: Shear stress - shear strain comparison plot

Shear stress - shear strain comparison plot					
	lower value	result lower value	Base parameter set	higher value	result higher value
Parameters					
Dr_0	0,5	Increase in total strain Fewer cycles needed before strain increase occurs	0,525	0,535	Decrease in total strain More cycles needed before strain increase occurs
G_0	800	Increase in total strain	960	1150	Decrease in total strain
h_{p0}	0,35	Increase in total strain Less cycles needed before strain increase occurs	0,42	0,5	Decrease in total strain More cycles needed before strain increase occurs
P_A			101,3		
e_{max}	0,9	No significant noticeable changes	0,98	0,99	No significant noticeable changes
e_{min}	0,5	No significant noticeable changes	0,61	0,75	No significant noticeable changes
n^b	0,45	No significant noticeable changes	0,65	0,85	No significant noticeable changes
n^d	0,05	Increase in total strain Fewer cycles needed before strain increase occurs	0,1	0,2	Decrease in total strain More cycles needed before strain increase occurs
ϕ'_{cv}	27	No significant noticeable changes	31,33	35	Decrease in total strain Initial increase in strain is, once strain increase occurs is larger
ν	0,275	Decrease in total strain More cycles needed before strain increase occurs	0,3	0,325	Increase in total strain Less cycles needed before strain increase occurs
Q	9,5	Increase in total strain Fewer cycles needed before strain increase occurs	10	10,5	Decrease in total strain More cycles needed before strain increase occurs
R	1,4	Decrease in total strain More cycles needed before strain increase occurs	1,5	1,6	Increase in total strain Less cycles needed before strain increase occurs
postshake			0		

D

Appendix Plaxis model results

D.1. Results for Plaxis models of the centrifuge test

D.1.1. UBCSand $D_r = 50\%$

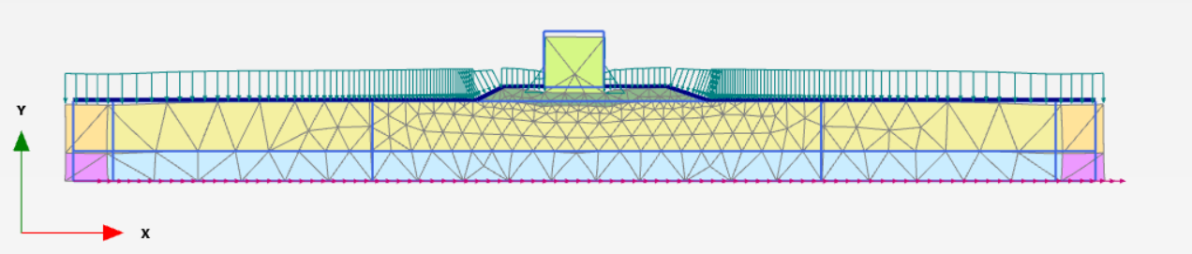

Figure D.1: Deformation underneath the breakwater after foreshock 1 for a top sand layer modelled with UBCSand and a $D_r = 50\%$

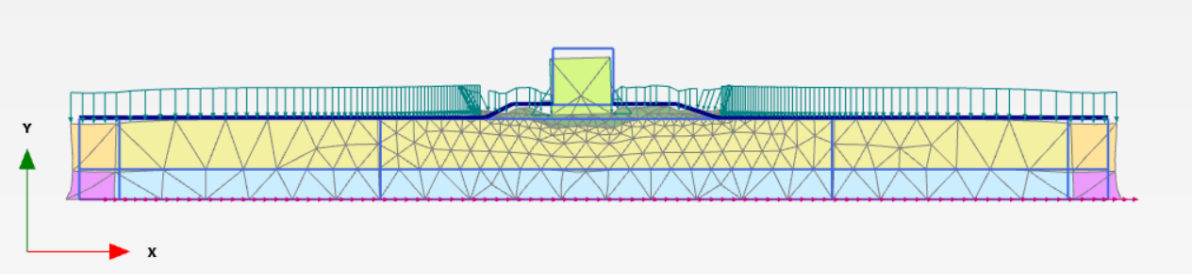

Figure D.2: Deformation underneath the breakwater after foreshock 2 for a top sand layer modelled with UBCSand and a $D_r = 50\%$

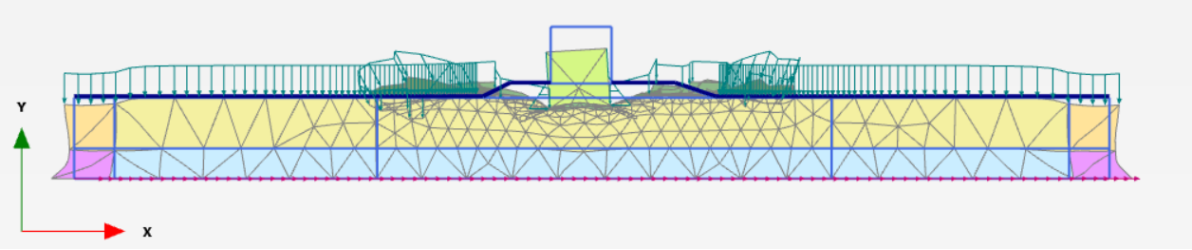

Figure D.3: Deformation underneath the breakwater after main shock for a top sand layer modelled with UBCSand and a $D_r = 50\%$

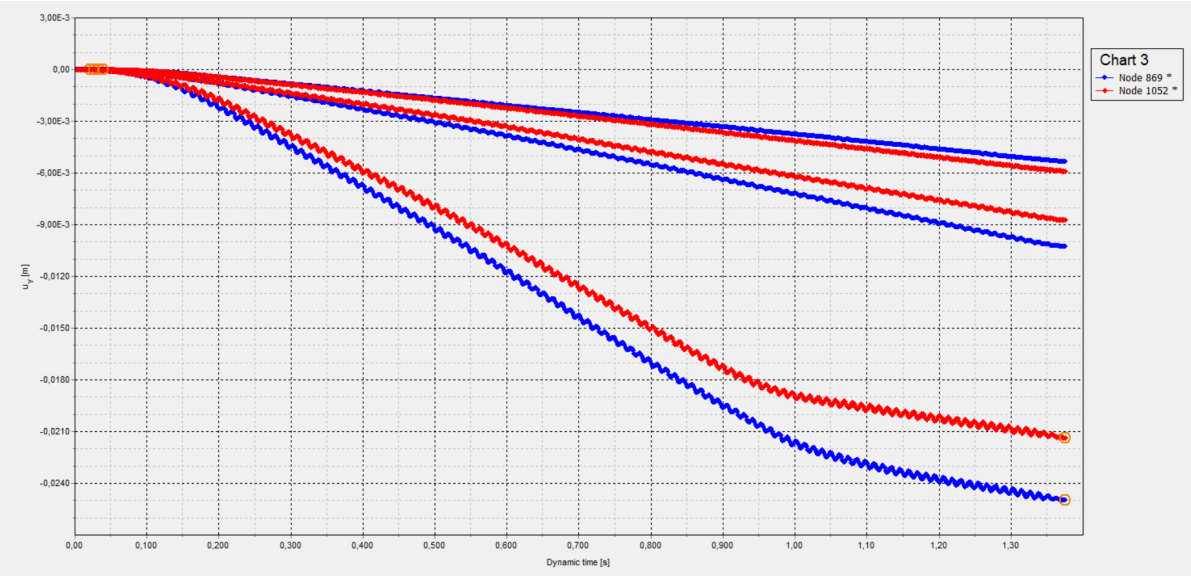

Figure D.4: Settlement graph of the caisson for a top sand layer modelled with UBCSand and a $D_r = 50\%$

Figure D.5: EPWP underneath the breakwater for a top sand layer modelled with UBCSand and a $D_r = 50\%$

D.1.2. UBCSand $D_r = 80\%$

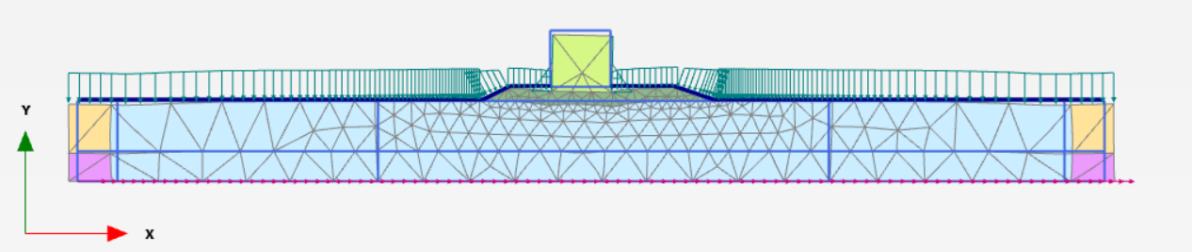

Figure D.6: Deformation underneath the breakwater after foreshock 1 for a top sand layer modelled with UBCSand and a $D_r = 80\%$

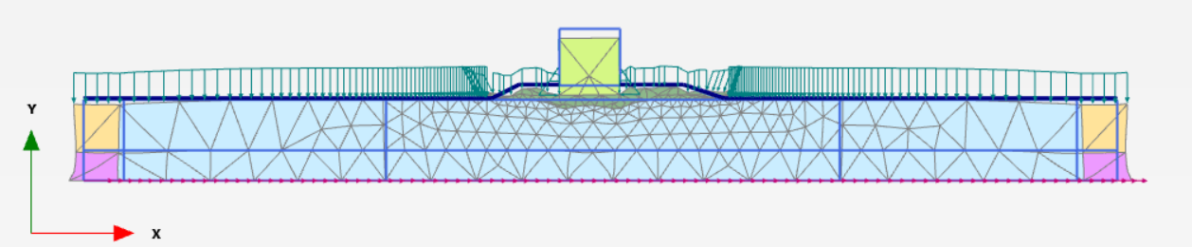

Figure D.7: Deformation underneath the breakwater after foreshock 2 for a top sand layer modelled with UBCSand and a $D_r = 80\%$

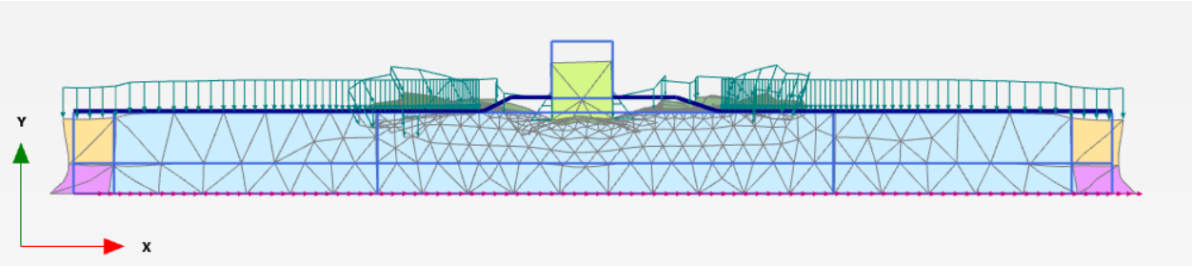

Figure D.8: Deformation underneath the breakwater after main shock for a top sand layer modelled with UBCSand and a $D_r = 80\%$

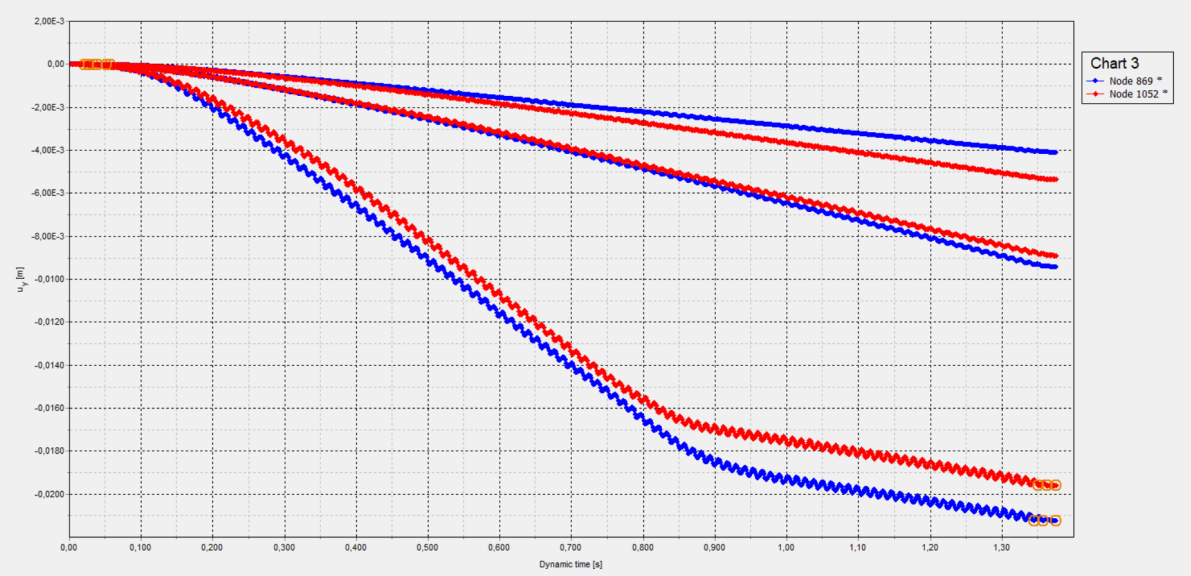

Figure D.9: Settlement graph of the caisson for a top sand layer modelled with UBCSand and a $D_r = 80\%$

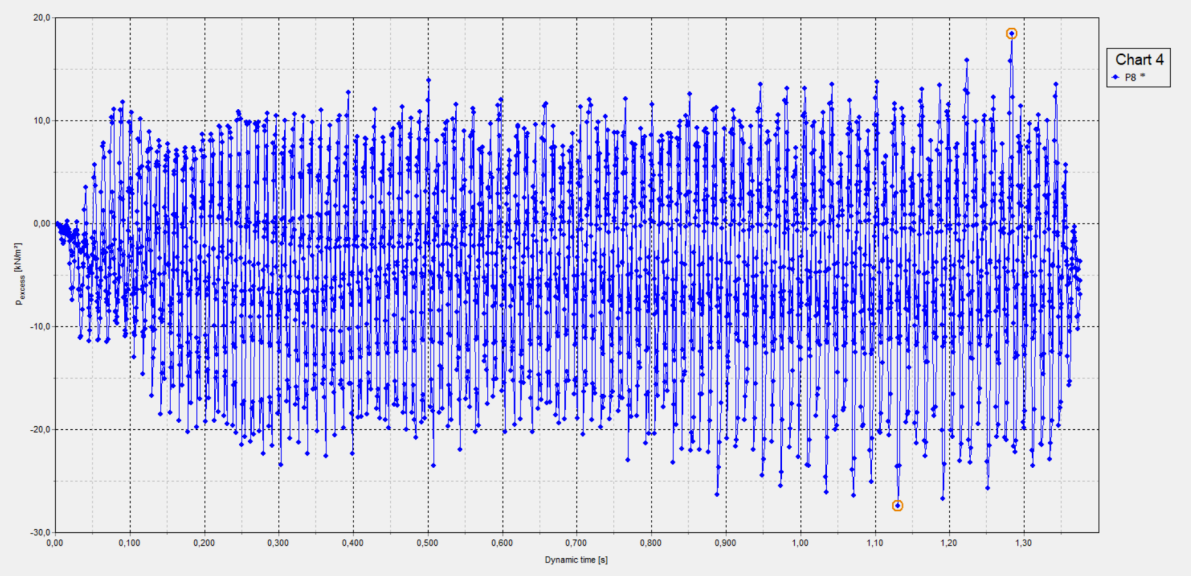

Figure D.10: EPWP underneath the breakwater for a top sand layer modelled with UBCSand and a $D_r = 80\%$

D.1.3. PM4Sand simulated CDSS isotropic $D_r = 50\%$

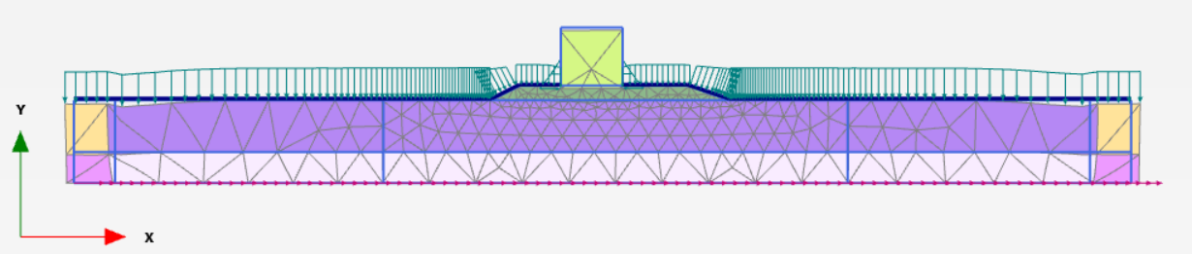

Figure D.11: Deformation underneath the breakwater after foreshock 1 for an isotropic top sand layer modelled with PM4Sand calibrated with a CDSS test and a $D_r = 50\%$

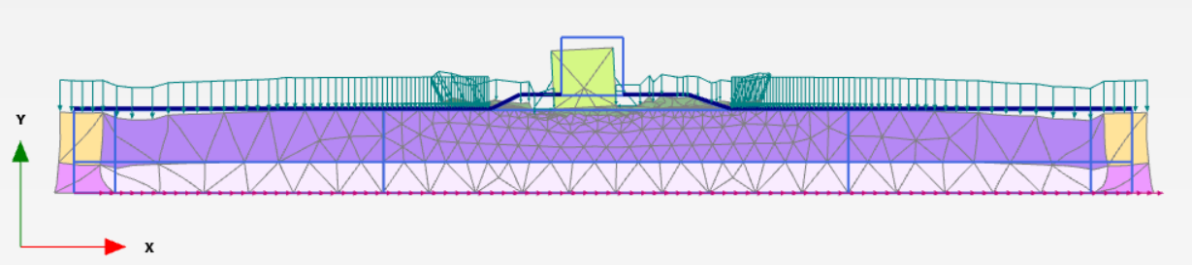

Figure D.12: Deformation underneath the breakwater after foreshock 2 for an isotropic top sand layer modelled with PM4Sand calibrated with a CDSS test and a $D_r = 50\%$

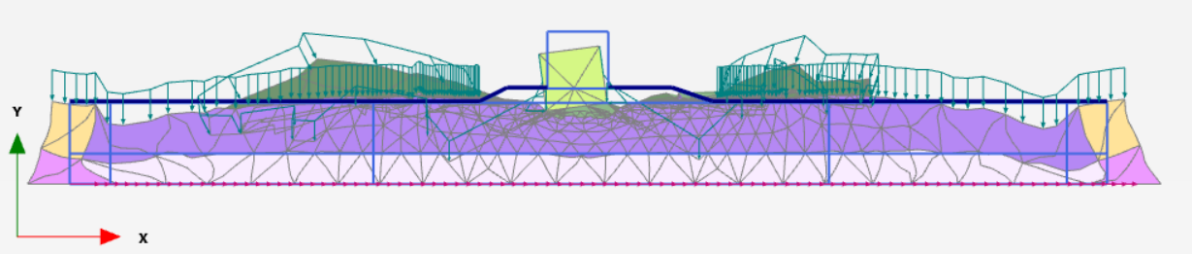

Figure D.13: Deformation underneath the breakwater after the main shock for an isotropic top sand layer modelled with PM4Sand calibrated with a CDSS test and a $D_r = 50\%$

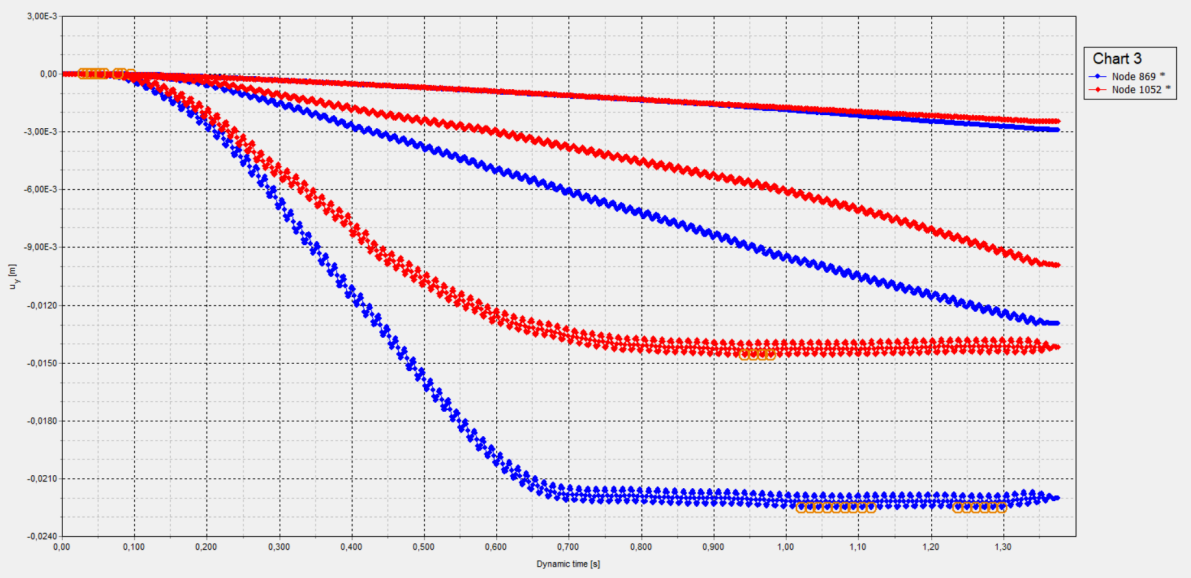

Figure D.14: Settlement graph of the caisson for an isotropic top sand layer modelled with PM4Sand, calibrated with a CDSS test and a $D_r = 50\%$

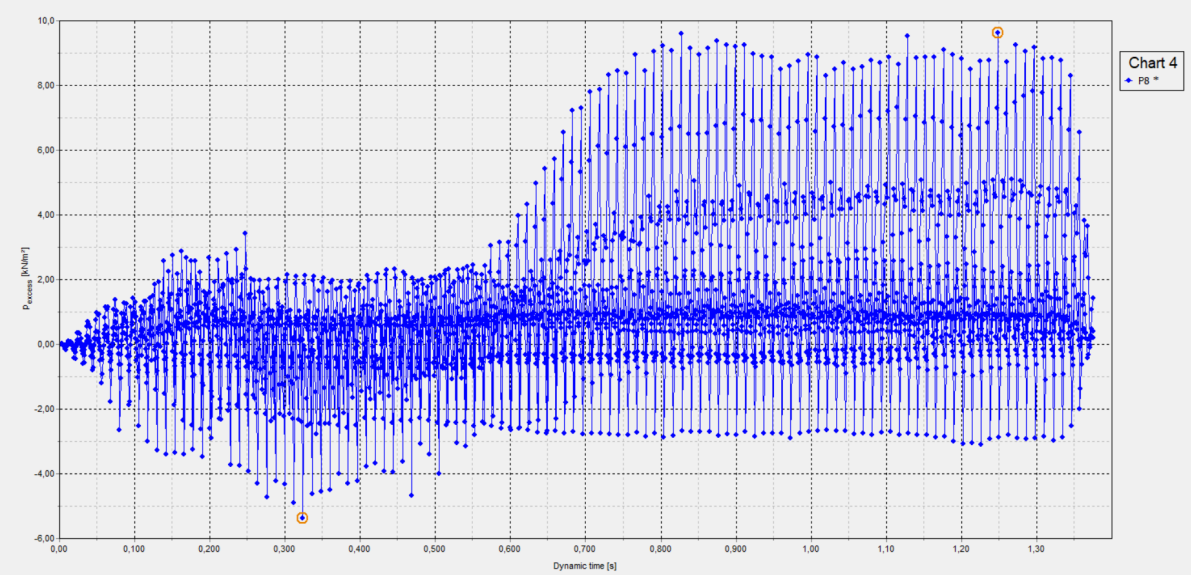

Figure D.15: EPWP underneath the breakwater for an isotropic top sand layer modelled with PM4Sand, calibrated with a CDSS test and a $D_r = 50\%$

D.1.4. PM4Sand simulated CDSS isotropic $D_r = 80\%$

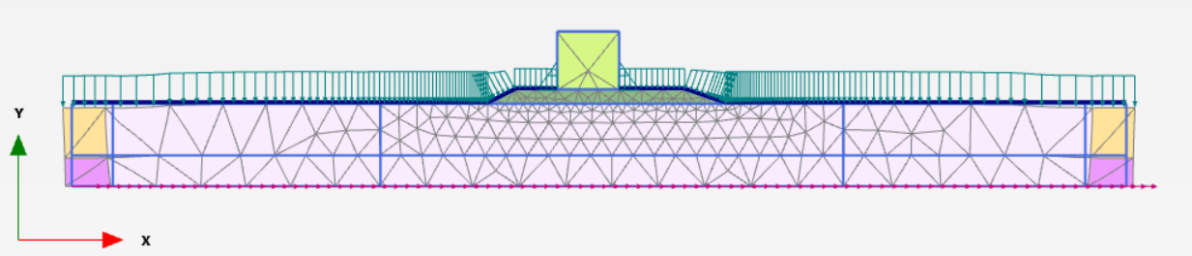

Figure D.16: Deformation underneath the breakwater after foreshock 1 for an isotropic top sand layer modelled with PM4Sand calibrated with a CDSS test and a $D_r = 80\%$

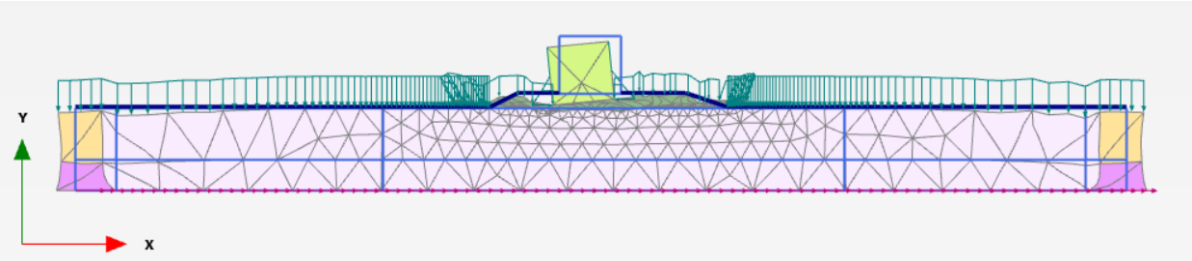

Figure D.17: Deformation underneath the breakwater after foreshock 2 for an isotropic top sand layer modelled with PM4Sand calibrated with a CDSS test and a $D_r = 80\%$

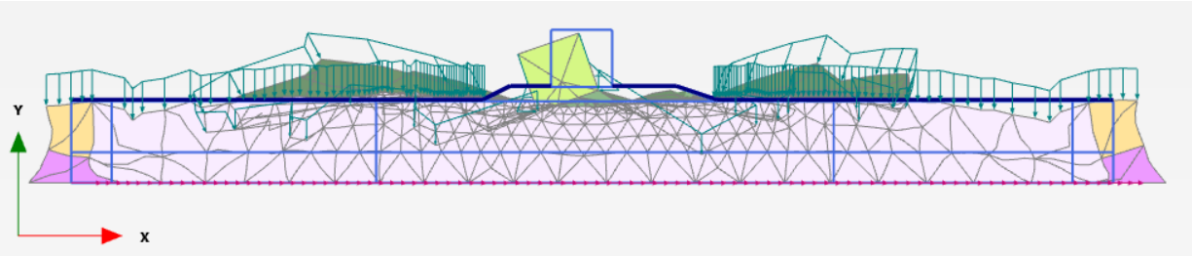

Figure D.18: Deformation underneath the breakwater after the main shock for an isotropic top sand layer modelled with PM4Sand calibrated with a CDSS test and a $D_r = 80\%$

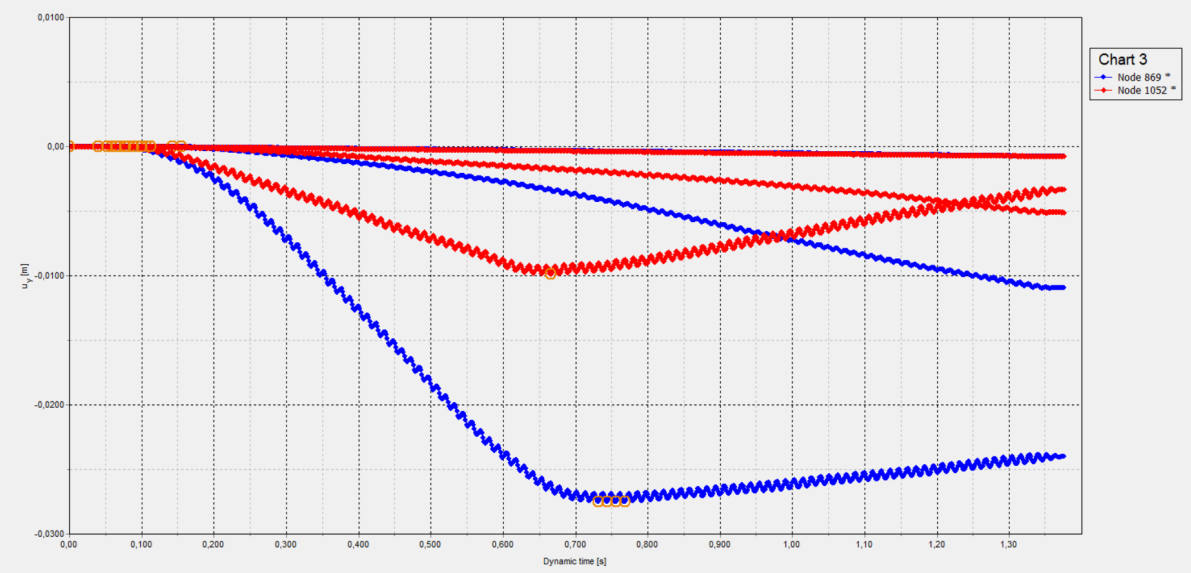

Figure D.19: Settlement graph of the caisson for an isotropic top sand layer modelled with PM4Sand, calibrated with a CDSS test and a $D_r = 80\%$

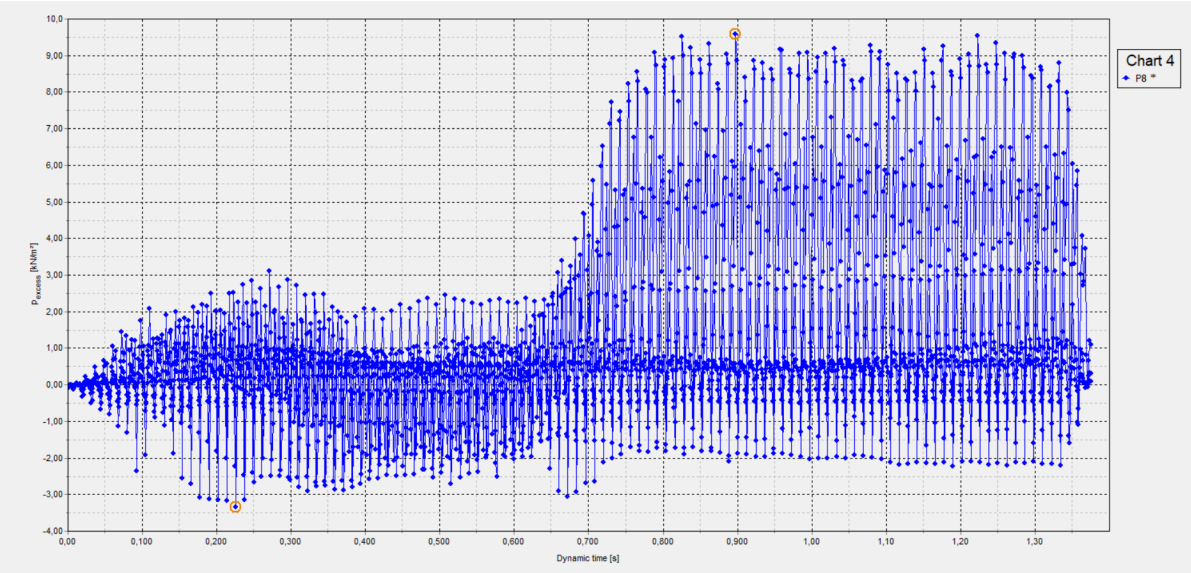

Figure D.20: EPWP underneath the breakwater for an isotropic top sand layer modelled with PM4Sand, calibrated with a CDSS test and a $D_r = 80\%$

D.1.5. PM4Sand simulated CDSS Anisotropic $D_r = 50\%$

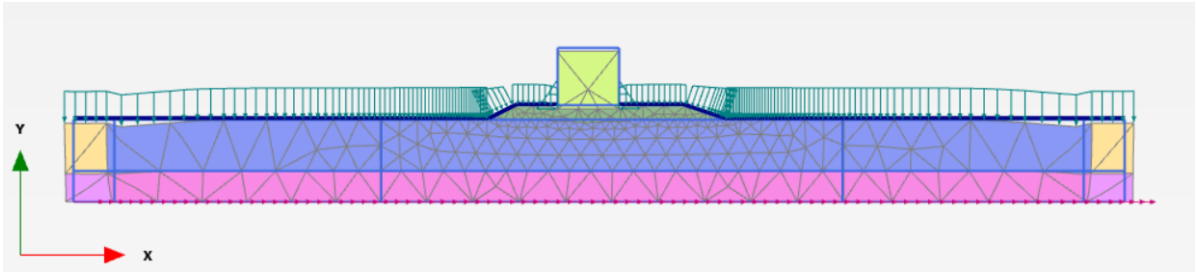

Figure D.21: Deformation underneath the breakwater after foreshock 1 for an anisotropic top sand layer modelled with PM4Sand calibrated with a CDSS test and a $D_r = 50\%$

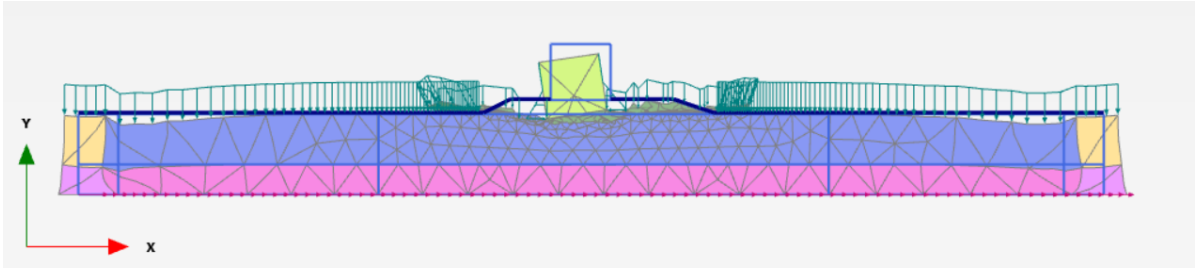

Figure D.22: Deformation underneath the breakwater after foreshock 2 for an anisotropic top sand layer modelled with PM4Sand calibrated with a CDSS test and a $D_r = 50\%$

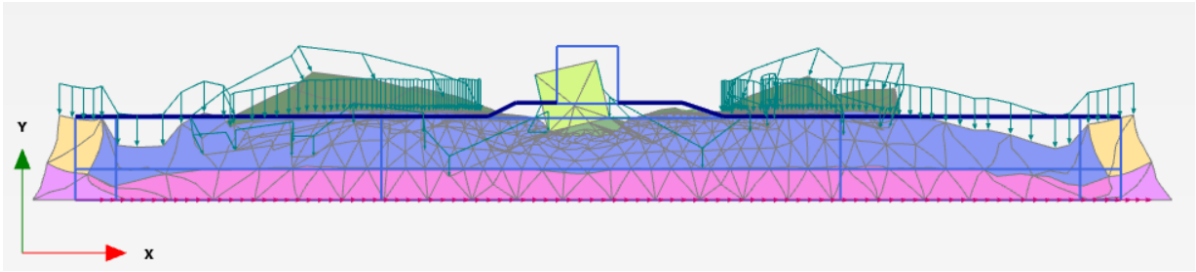

Figure D.23: Deformation underneath the breakwater after the main shock for an anisotropic top sand layer modelled with PM4Sand calibrated with a CDSS test and a $D_r = 50\%$

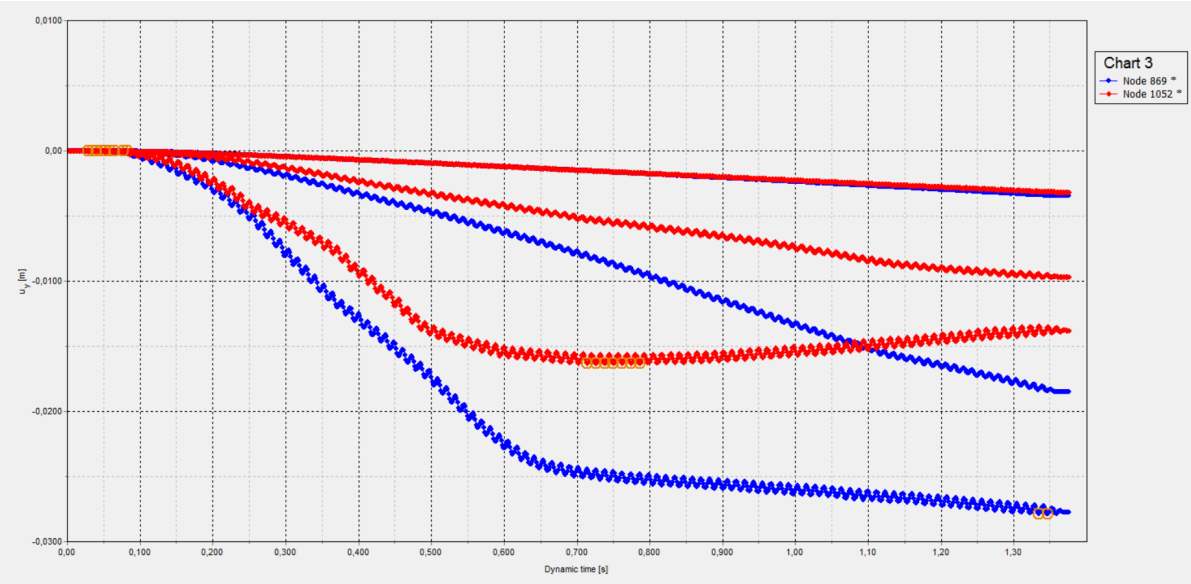

Figure D.24: Settlement graph of the caisson for an anisotropic top sand layer modelled with PM4Sand, calibrated with a CDSS test and a $D_r = 50\%$

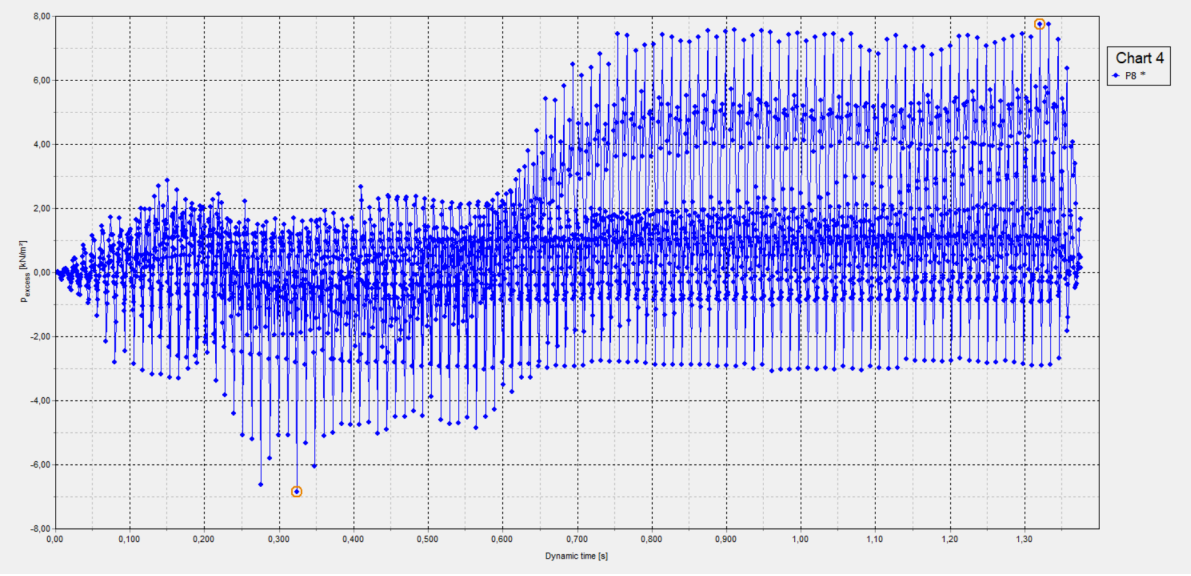

Figure D.25: EPWP underneath the breakwater for an anisotropic top sand layer modelled with PM4Sand, calibrated with a CDSS test and a $D_r = 50\%$

D.1.6. PM4Sand simulated CDSS Anisotropic $D_r = 80\%$

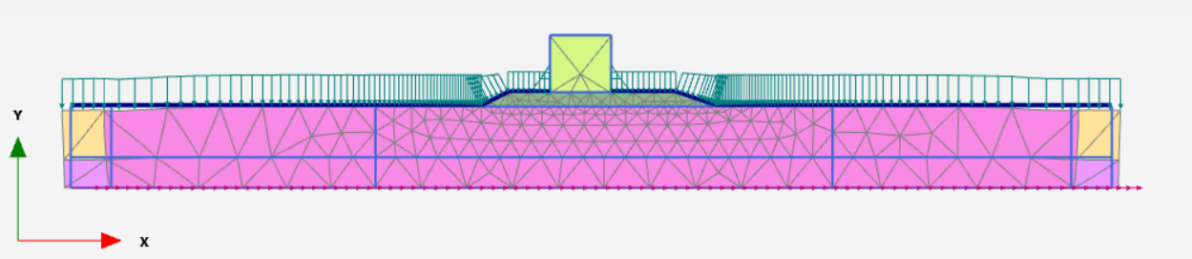

Figure D.26: Deformation underneath the breakwater after foreshock 1 for an anisotropic top sand layer modelled with PM4Sand calibrated with a CDSS test and a $D_r = 80\%$

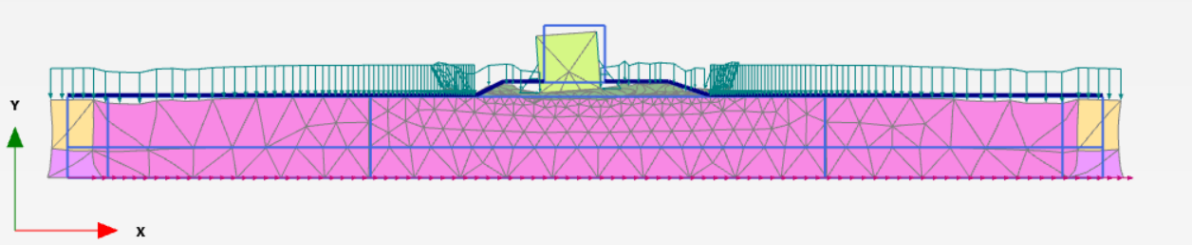

Figure D.27: Deformation underneath the breakwater after foreshock 2 for an anisotropic top sand layer modelled with PM4Sand calibrated with a CDSS test and a $D_r = 80\%$

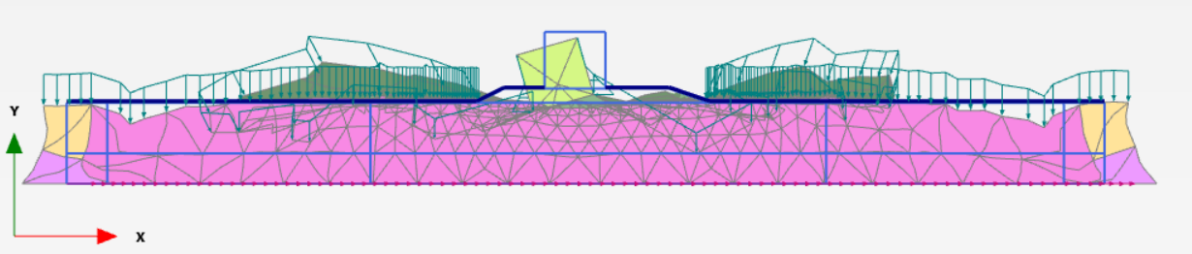

Figure D.28: Deformation underneath the breakwater after the main shock for an anisotropic top sand layer modelled with PM4Sand calibrated with a CDSS test and a $D_r = 80\%$

Figure D.29: Settlement graph of the caisson for an anisotropic top sand layer modelled with PM4Sand, calibrated with a CDSS test and a $D_r = 80\%$

Figure D.30: EPWP underneath the breakwater for an anisotropic top sand layer modelled with PM4Sand, calibrated with a CDSS test and a $D_r = 80\%$

D.1.7. PM4Sand simulated TST $D_r = 50\%$

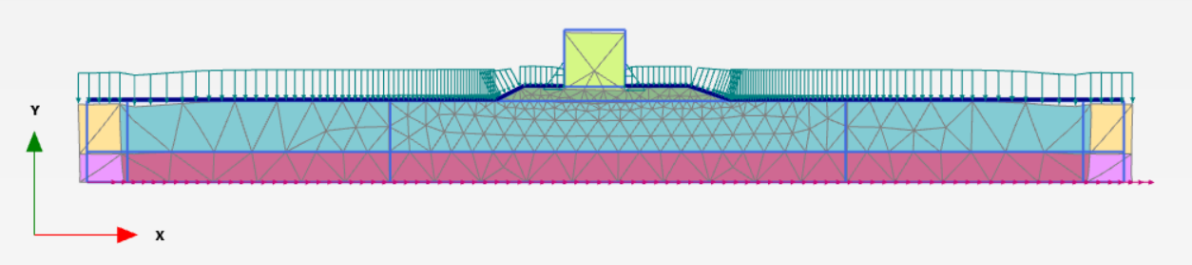

Figure D.31: Deformation underneath the breakwater after foreshock 1 for a top sand layer modelled with PM4Sand calibrated with a TST and a $D_r = 50\%$

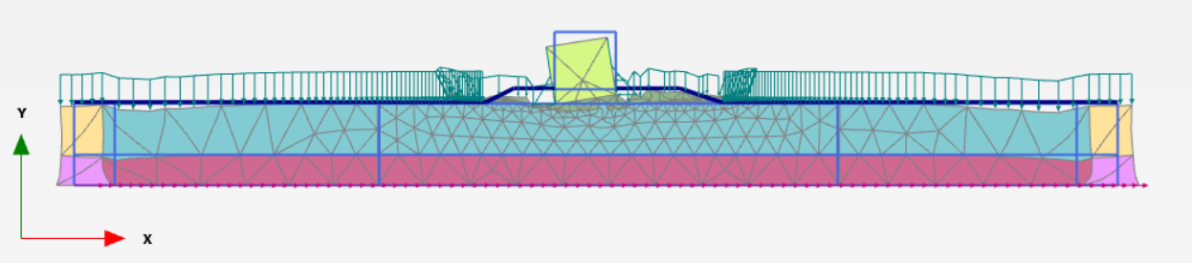

Figure D.32: Deformation underneath the breakwater after foreshock 2 for a top sand layer modelled with PM4Sand calibrated with a TST and a $D_r = 50\%$

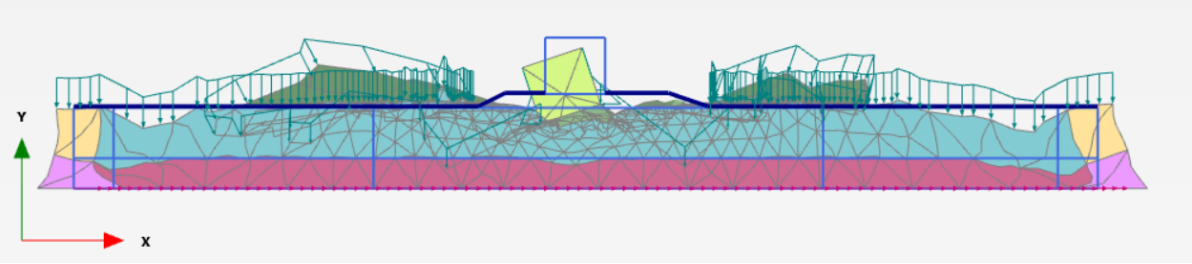

Figure D.33: Deformation underneath the breakwater after the main shock for a top sand layer modelled with PM4Sand calibrated with a TST and a $D_r = 50\%$

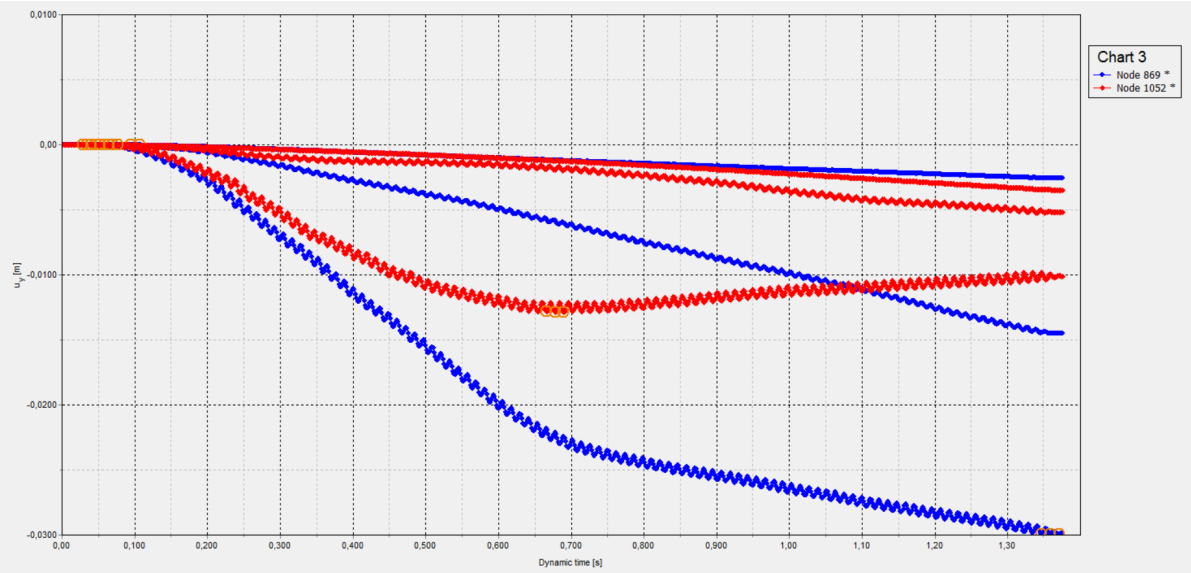

Figure D.34: Settlement graph of the caisson for a top sand layer modelled with PM4Sand, calibrated with a TST test and a $D_r = 50\%$

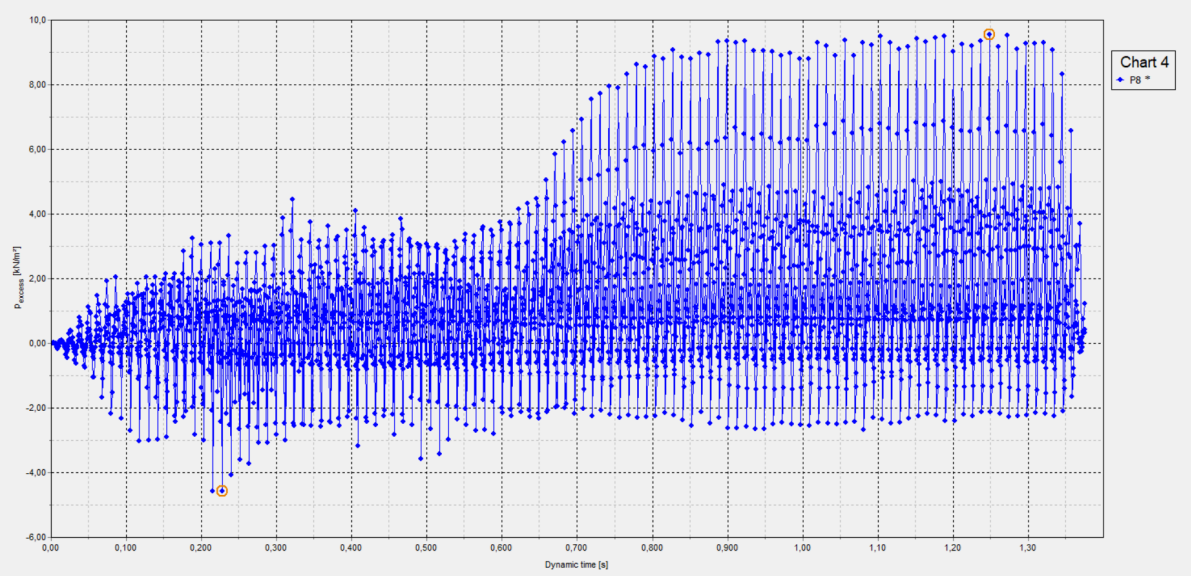

Figure D.35: EPWP underneath the breakwater for a top sand layer modelled with PM4Sand, calibrated with a TST test and a $D_r = 50\%$

D.1.8. PM4Sand simulated TST $D_r = 60\%$

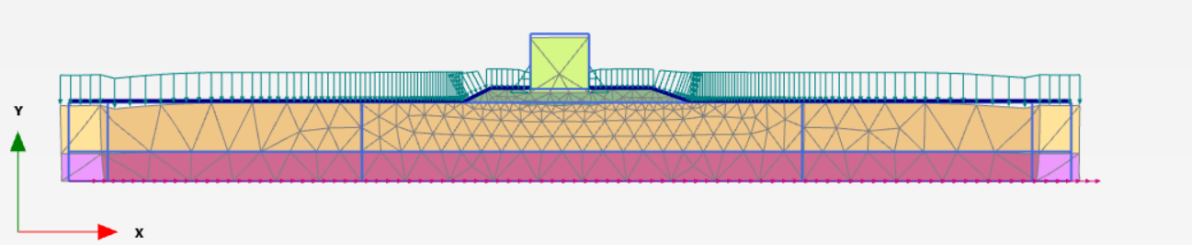

Figure D.36: Deformation underneath the breakwater after foreshock 1 for a top sand layer modelled with PM4Sand calibrated with a TST and a $D_r = 60\%$

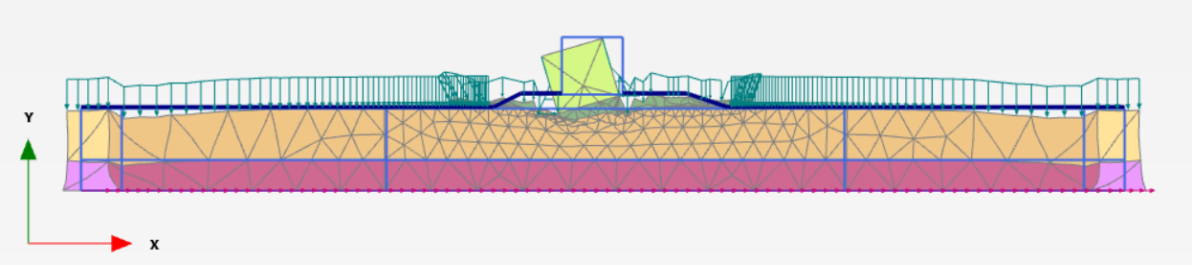

Figure D.37: Deformation underneath the breakwater after foreshock 2 for a top sand layer modelled with PM4Sand calibrated with a TST and a $D_r = 60\%$

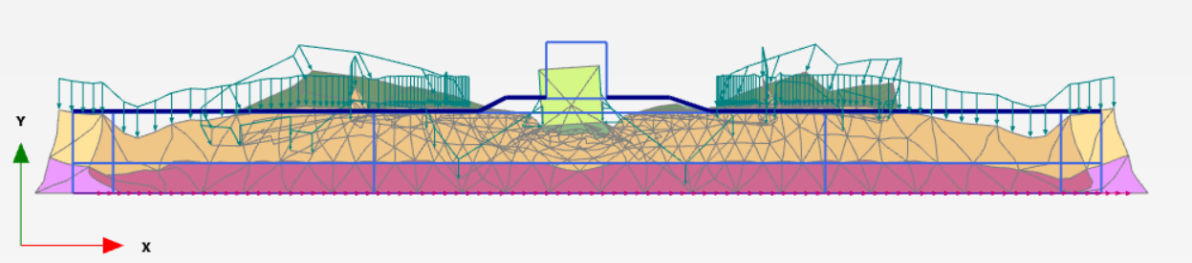

Figure D.38: Deformation underneath the breakwater after the main shock for a top sand layer modelled with PM4Sand calibrated with a TST and a $D_r = 60\%$

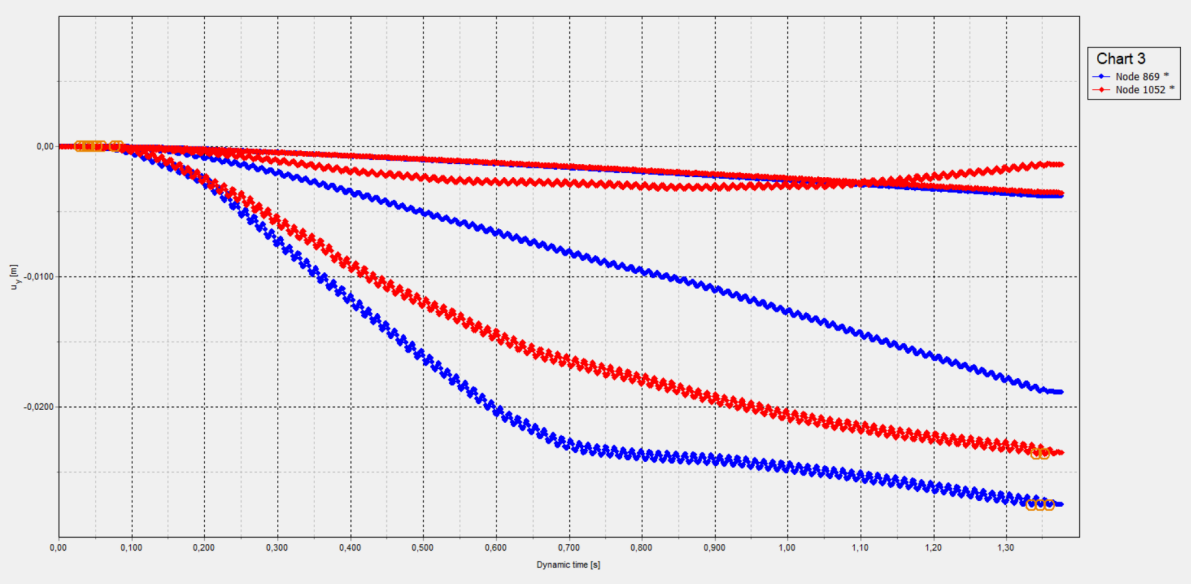

Figure D.39: Settlement graph of the caisson for a top sand layer modelled with PM4Sand, calibrated with a TST test and a $D_r = 60\%$

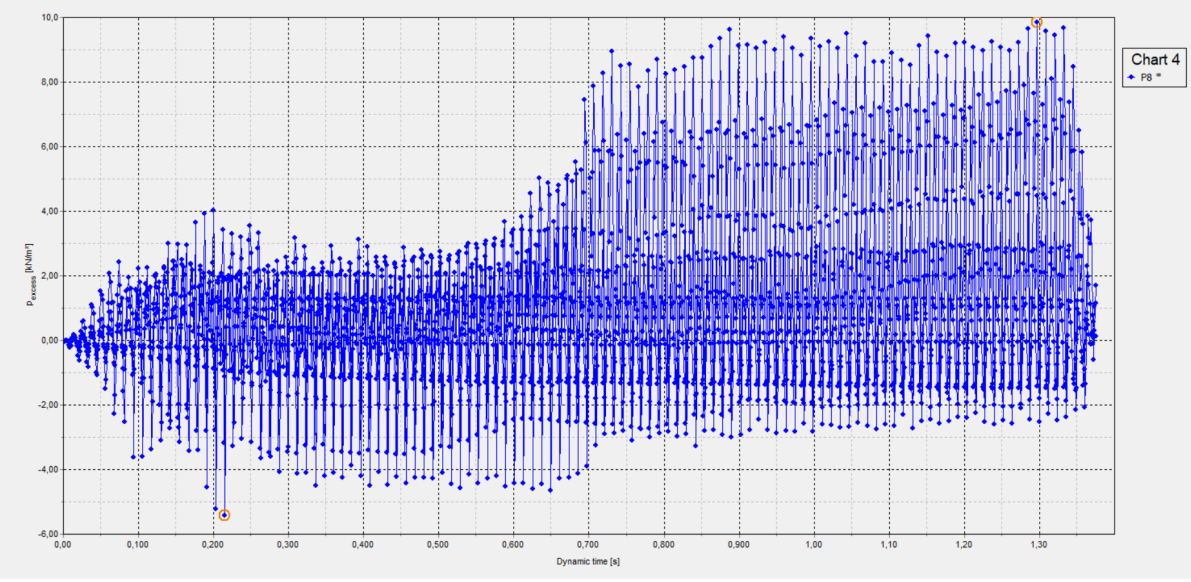

Figure D.40: EPWP underneath the breakwater for a top sand layer modelled with PM4Sand, calibrated with a TST test and a $D_r = 60\%$

D.1.9. PM4Sand simulated TST $D_r = 80\%$

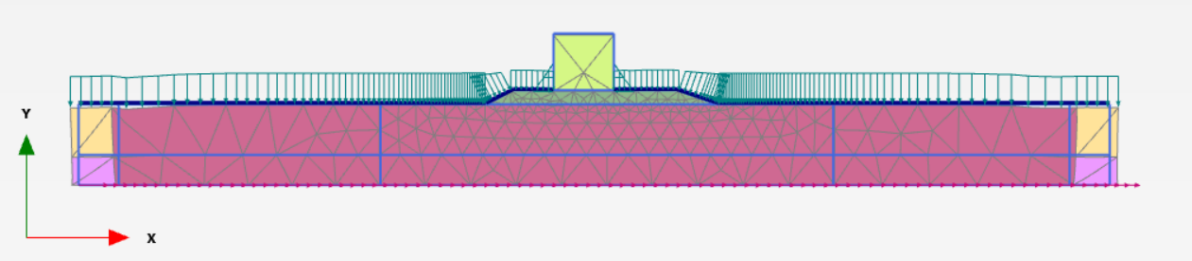

Figure D.41: Deformation underneath the breakwater after foreshock 1 for a top sand layer modelled with PM4Sand calibrated with a TST and a $D_r = 80\%$

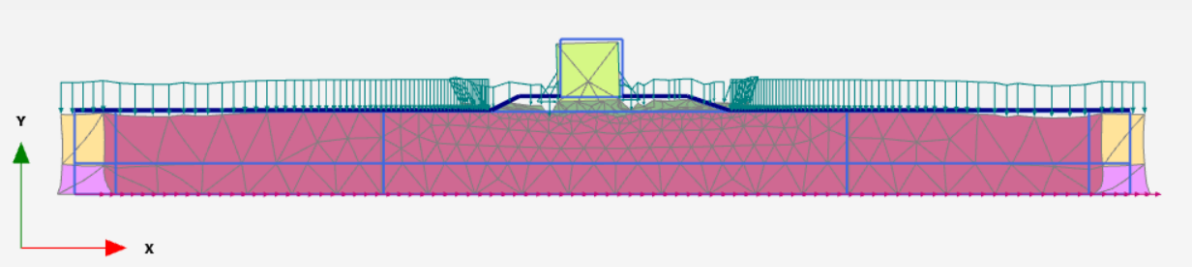

Figure D.42: Deformation underneath the breakwater after foreshock 2 for a top sand layer modelled with PM4Sand calibrated with a TST and a $D_r = 80\%$

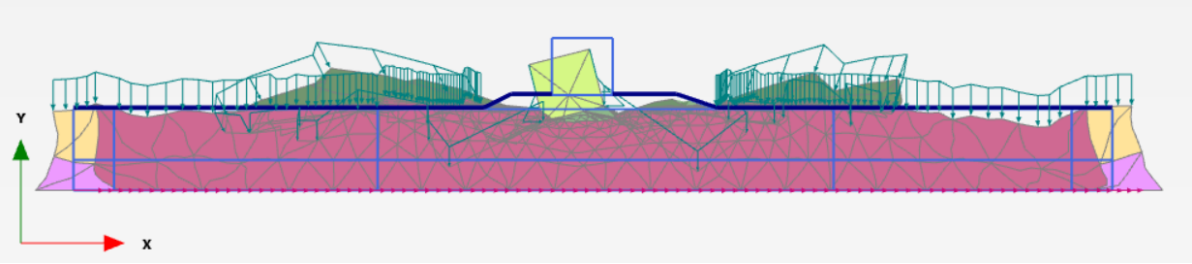

Figure D.43: Deformation underneath the breakwater after the main shock for a top sand layer modelled with PM4Sand calibrated with a TST and a $D_r = 80\%$

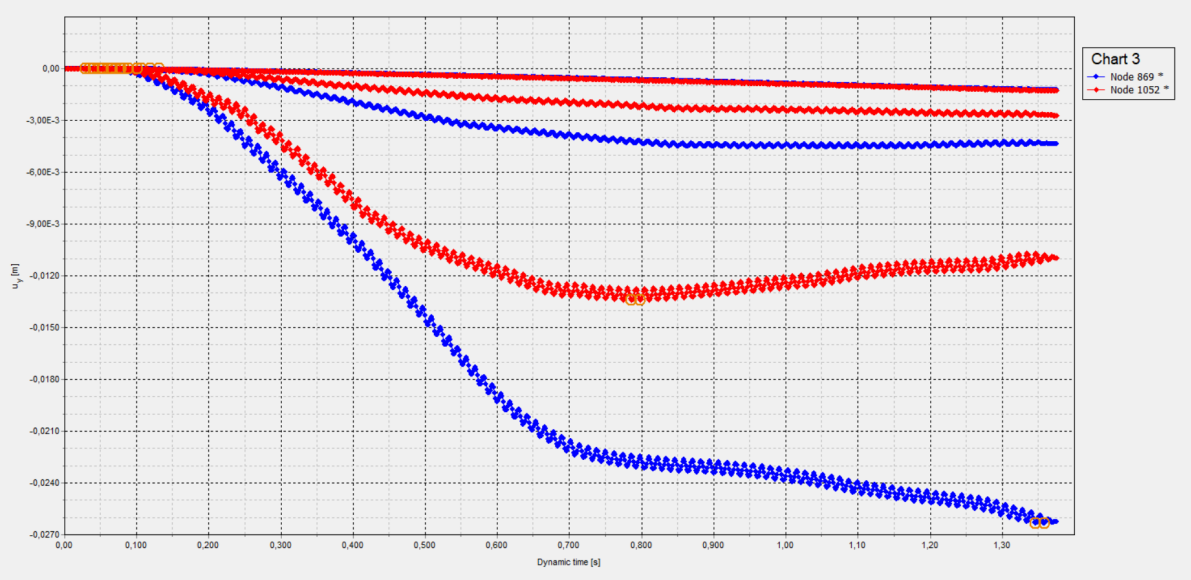

Figure D.44: Settlement graph of the caisson for a top sand layer modelled with PM4Sand, calibrated with a TST test and a $D_r = 80\%$

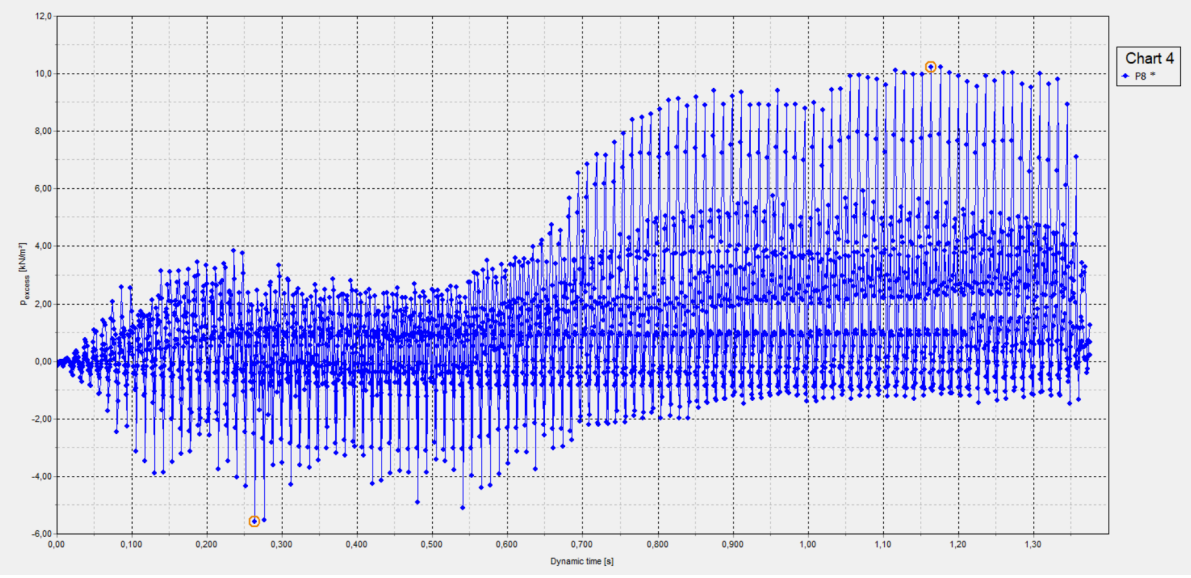

Figure D.45: EPWP underneath the breakwater for a top sand layer modelled with PM4Sand, calibrated with a TST test and a $D_r = 80\%$

D.2. Results for Plaxis models with prototype dimension

D.2.1. UBCSand $D_r = 50\%$

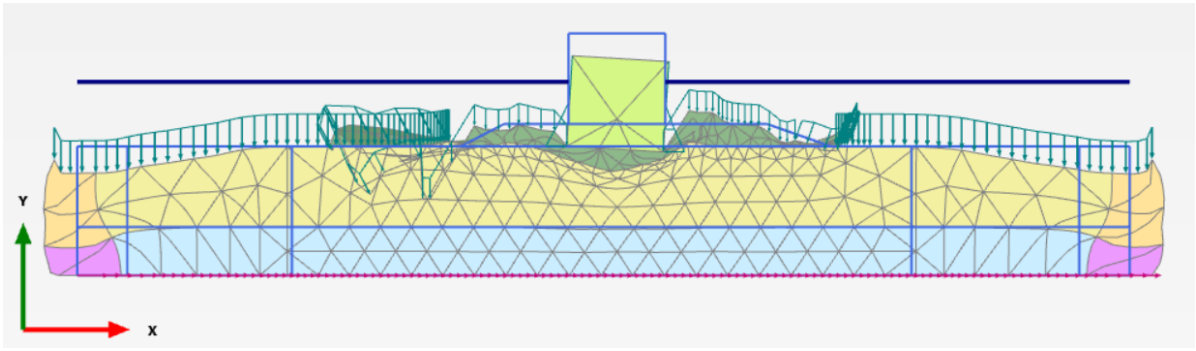

Figure D.46: Deformation underneath the breakwater after foreshock 1 for a top sand layer modelled with UBCSand and a $D_r = 50\%$

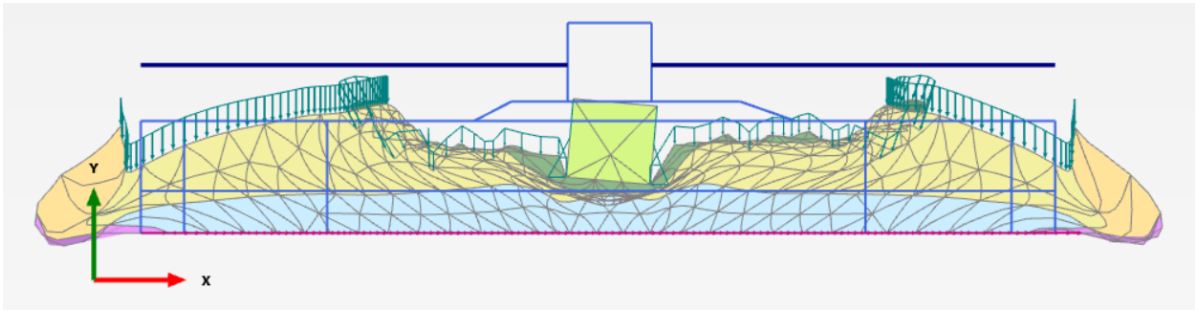

Figure D.47: Deformation underneath the breakwater after main shock for a top sand layer modelled with UBCSand and a $D_r = 50\%$

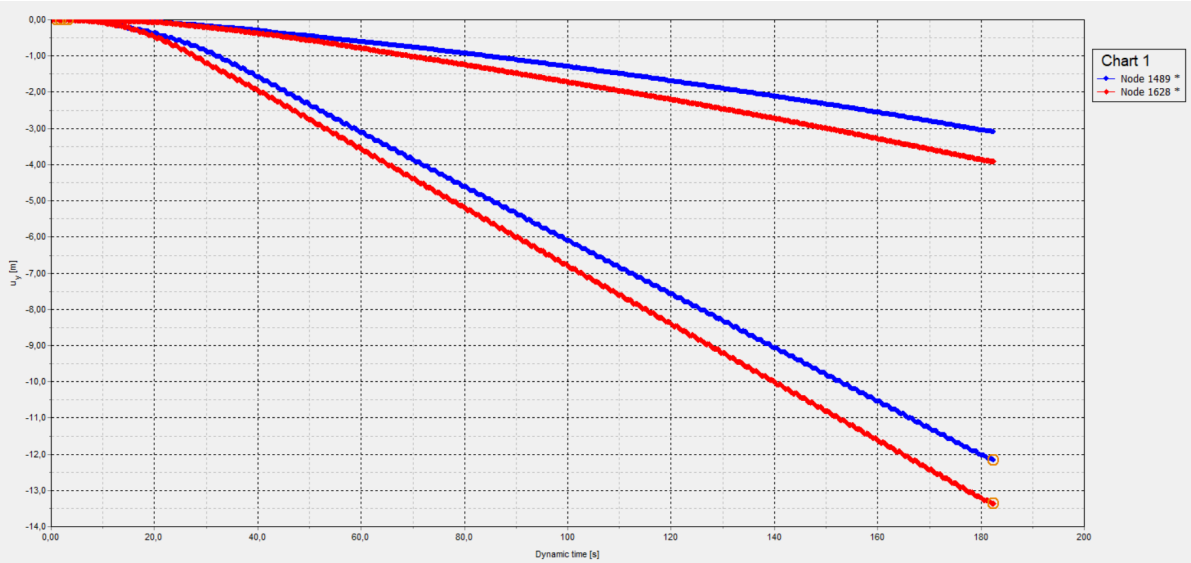

Figure D.48: Settlement graph of the caisson for a top sand layer modelled with UBCSand and a $D_r = 50\%$

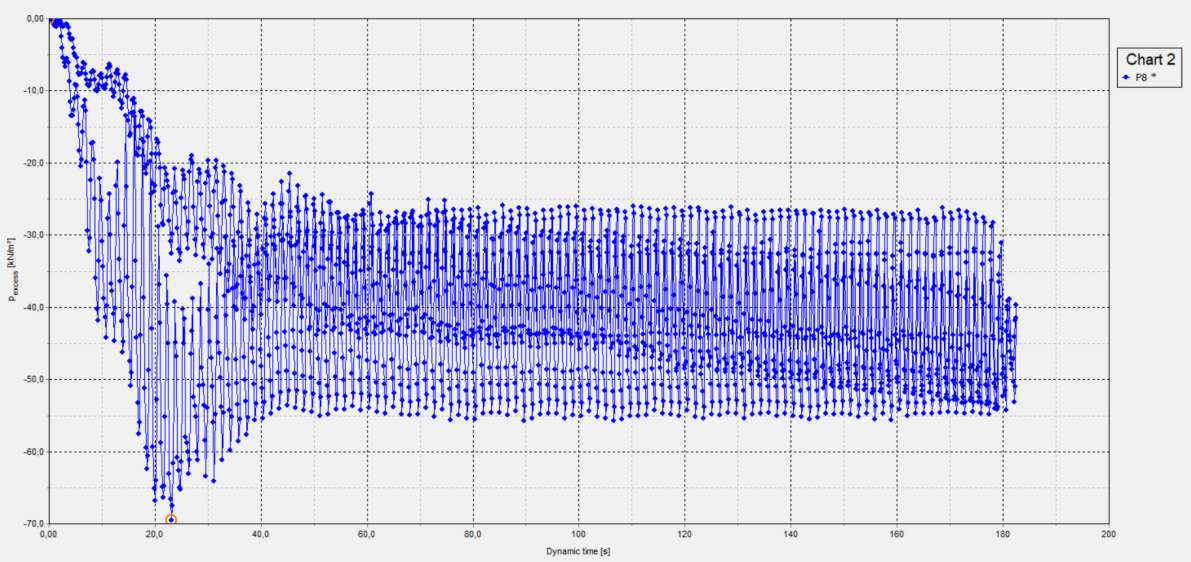

Figure D.49: EPWP underneath the breakwater for a top sand layer modelled with UBCSand and a $D_r = 50\%$

D.2.2. PM4Sand simulated TST $D_r = 60\%$

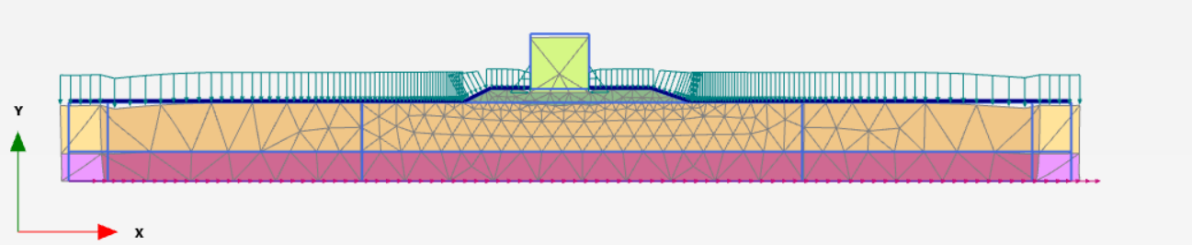

Figure D.50: Deformation underneath the breakwater after foreshock 1 for a top sand layer modelled with PM4Sand calibrated with a TST and a $D_r = 60\%$

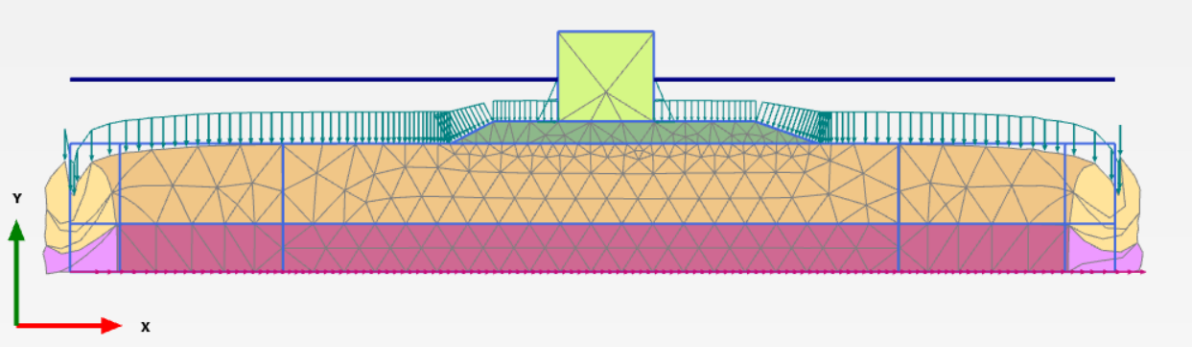

Figure D.51: Deformation underneath the breakwater after foreshock 2 for a top sand layer modelled with PM4Sand calibrated with a TST and a $D_r = 60\%$

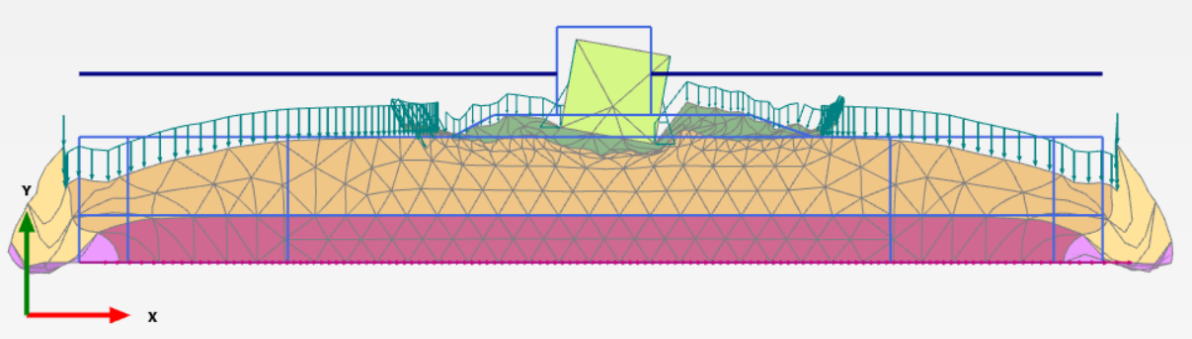

Figure D.52: Deformation underneath the breakwater after the main shock for a top sand layer modelled with PM4Sand calibrated with a TST and a $D_r = 60\%$

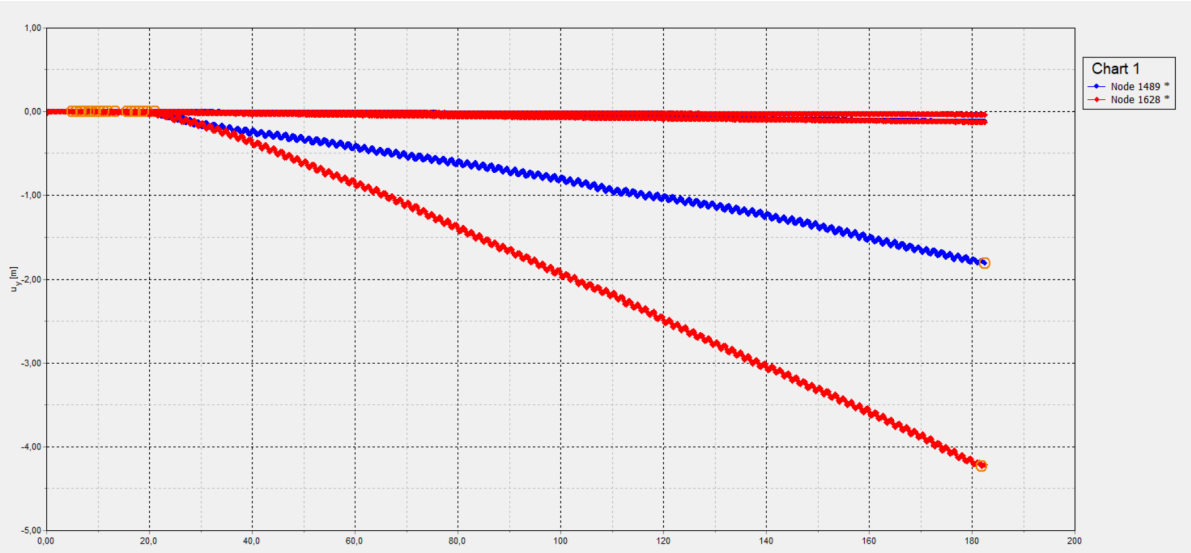

Figure D.53: Settlement graph of the caisson for a top sand layer modelled with PM4Sand, calibrated with a TST test and a $D_r = 60\%$

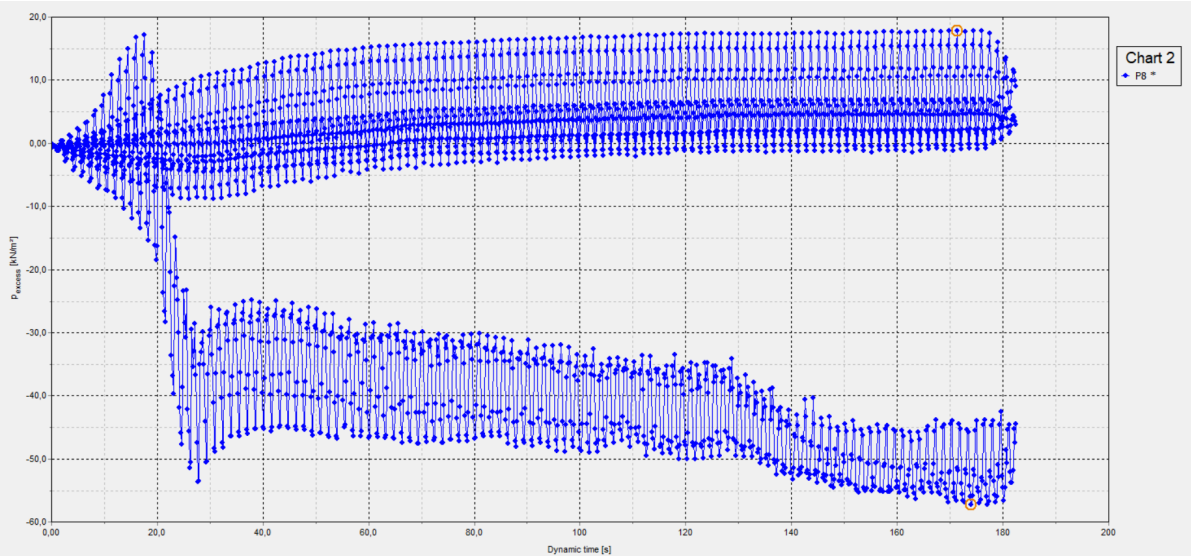

Figure D.54: EPWP underneath the breakwater for a top sand layer modelled with PM4Sand, calibrated with a TST test and a $D_r = 60\%$

References

Asadi, M. S., Asadi, M. B., Orense, R. P., & Pender, M. J. (2018). Undrained Cyclic Behavior of Reconstituted Natural Pumiceous Sands. *Journal of Geotechnical and Geoenvironmental Engineering*, *144*(8), 1–12.

Boulanger, R. W., & Ziotopoulou, K. (2015). *A Sand Plasticity Model for Earthquake Engineering Applications PM4SAND (Version 3):* (Tech. Rep. No. March). University of California at Davis.

Brinkgreve, R. (2019). *17 - Lecture - UBCSand.* TU Delft. Retrieved from `https://brightspace.tudelft.nl/d2l/le/content/125719/viewContent/1156308/View`

Byrne, P. M. (1991). A cyclic shear-volume coupling and pore pressure model for sand. *International conference on recent advances in geotechnical engineering and soil dynamics*, *1*, 47–55. Retrieved from `https://scholarsmine.mst.edu/icrageesd/02icrageesd/session01/1`

Chaudhary, B., & Hazarika, H. (2018). Centrifuge modelling for stability evaluation of a breakwater foundation subjected to an earthquake and a tsunami. *Ocean Engineering*, *148*(June 2017), 169–181.

Dafalias, Y. F., & Manzari, M. T. (2004). Critical submergence for a rectangular intake. *Journal of engineering mechanics*, *130*, 266–634.

Galavi, V., & Petalas, A. (2013). *Plaxis Liquefaction Model Ubc3D-Plm* (Tech. Rep.). Delft: Plaxis bv.

Iai, S., Tobita, T., & Nakahara, T. (2005). Generalised scaling relations for dynamic centrifuge tests. *Géotechnique*, *55*(5), 355–362.

Idriss, I. M., & Boulanger, R. W. (2008). *Soil Liquefaction during earthquakes* (D. Becker, Ed.). Oakland: Earthquake Engineering Research Institute.

Ishihara, K., Yamazaki, A., & Haga, K. (1985). Liquefaction of K0-consoidated Sand under cyclic rotation of principal stress direction with lateral constraint. *Soils and Foundations*, *25*(4), 63–74.

Ishikawa, K., & Yasuda, S. (2012). Study of Sand Boiling Characteristics Along Tokyo Bay During the 2011 Tohoku-Pacific Ocean Earthquake. *Journal of Japan Society of Civil Engineers, Ser. A1 (Structural Engineering & Earthquake Engineering (SE/EE))*, *68*(4), I_274–I_281. doi: 10.2208/jscejseee.68.i_274

Kuhlmeyer, R.L., Lysmer, J. (1973). Finite element method accuracy for wave propagation problems. *Journal of Soil Mechanics & Foundations Div*, *99*, 421–427.

Laera, A., & Brinkgreve, R. B. J. (2015). *Site response analysis and liquefaction evaluation.* Delft: Plaxis bv.

Makra, A. (2013). *Evaluation of the UBC3D-PLM constitutive model for prediction of earthquake induced liquefaction on embankement dams* (MSc thesis). Delft University of Technology.

Pestana, J. M., Whittle, A. J., & Salvati, L. A. (2002). Evaluation of a constitutive model for clays and sands: Part I - Sand behaviour. *International Journal for Numerical and Analytical Methods in Geomechanics*, *26*(11), 1097–1121.

PLAXIS Material Models. (2015). *Plaxis Handbook*.

Pradhan, T., Tatsuoka, F., & Horii, N. (1988). Simple shear testing on sand in a torsional shear apparatus. *Soils and Foundations*, *28*(2), 95–112.

Seed, H. B. (1983). Earthquake-resistant design of earth dams. In (pp. 41–64). University of California, Berkeley, CA.

Somasundaram, S. (2004). *Cyclic loading response of Fraser river sand for validation of numerical models simulating centrifuge tests* (MSc thesis). The university of British Columbia.

Tatsuoka, F., Maramatsu, M., & Sasaki, T. (1982). Cyclic undrained stress-strain behavior of dense sands by torsional simple shear test. *Soils and Foundations*, *22*(2), 55–70.

Technology, S., & Jose, S. (2008). Reference Manual Reference Manual. *Technology*, *1*(November).

Toloza, P. V. (2018). *Liquefaction Modelling using the PM4Sand Constitutive Model in PLAXIS 2D* (MSc thesis). Delft University of Technology.

Vilhar, G., Brinkgreve, R. B. J., & Zampich, L. (2018). *PLAXIS The PM4Sand model 2018 (Manual).* Delft: Plaxis bv.

Vilhar, G. ; Laera, A. ; Foria, F. ; Gupta, A. ; Brinkgreve, R. (2018). Implementation, validation and application of PM4Sand model in PLAXIS. *Geotechnical Special Publication*, *292*(June), 200–211.

Yoshimine, M. (1996). *Undrained flow deformation of saturated sand under monotonic loading conditions* (Unpublished doctoral dissertation). University of Tokyo.